

AFWAL-TR-86-3003
Volume III

12

AD-A170 989



**ASSESSMENT OF DAMAGE TOLERANCE REQUIREMENTS
AND ANALYSES**

Volume III - Analytical Predictions and Correlations

M. LEVY

Fairchild Industries
Fairchild Republic Company
Farmingdale, N.Y. 11735

MARCH 1986

Final Technical Report for Period September 1982 - July 1985

DTIC FILE COPY

Approved for public release; distribution is unlimited

DTIC
ELECTE
AUG 18 1986
S E D

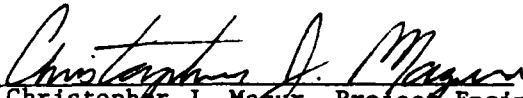
FLIGHT DYNAMICS LABORATORY
AIR FORCE WRIGHT AERONAUTICAL LABORATORIES
AIR FORCE SYSTEMS COMMAND
WRIGHT-PATTERSON AIR FORCE BASE, OHIO 45433-6553

NOTICE

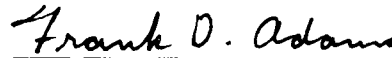
When Government drawings, specifications, or other data are used for any purpose other than in connection with a definitely related Government procurement operation, the United States Government thereby incurs no responsibility nor any obligation whatsoever; and the fact that the government may have formulated, furnished, or in any way supplied the said drawings, specifications, or other data, is not to be regarded by implication or otherwise as in any manner licensing the holder or any other person or corporation, or conveying any rights or permission to manufacture use, or sell any patented invention that may in any way be related thereto.

This report has been reviewed by the Office of Public Affairs (ASD/PA) and is releasable to the National Technical Information Service (NTIS). At NTIS, it will be available to the general public, including foreign nations.

This technical report has been reviewed and is approved for publication.

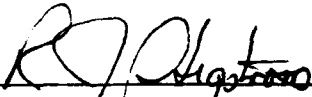


Lt Christopher J. Mazur, Project Engineer
Fatigue, Fracture & Reliability Group
Structural Integrity Branch



Frank D. Adams, Chief
Structural Integrity Branch
Structures & Dynamics Division

FOR THE COMMANDER



ROGER J. HEGSTROM, Colonel, USAF
Chief, Structures and Dynamics Division

"If your address has changed, if you wish to be removed from our mailing list, or if the addressee is no longer employed by your organization please notify AFWAL/FIBE, W-PAFB, OH 45433 to help us maintain a current mailing list".

Copies of this report should not be returned unless return is required by security considerations, contractual obligations, or notice on a specific document.

UNCLASSIFIED

SECURITY CLASSIFICATION OF THIS PAGE

REPORT DOCUMENTATION PAGE

1a. REPORT SECURITY CLASSIFICATION Unclassified		1b. RESTRICTIVE MARKINGS	
2a. SECURITY CLASSIFICATION AUTHORITY		3. DISTRIBUTION/AVAILABILITY OF REPORT Approved for public release; distribution unlimited.	
2b. DECLASSIFICATION/DOWNGRADING SCHEDULE			
4. PERFORMING ORGANIZATION REPORT NUMBER(S)		5. MONITORING ORGANIZATION REPORT NUMBER(S) AFWAL-TR-86-3003, Vol III	
6a. NAME OF PERFORMING ORGANIZATION Fairchild Industries Fairchild Republic Co.	6b. OFFICE SYMBOL (If applicable)	7a. NAME OF MONITORING ORGANIZATION Flight Dynamics Laboratory (AFWAL/FIBEC)	
6c. ADDRESS (City, State and ZIP Code) Farmingdale NY 11735		7b. ADDRESS (City, State and ZIP Code) Wright-Patterson Air Force Base Ohio, 45433-6553	
8a. NAME OF FUNDING/SPONSORING ORGANIZATION AFWAL	8b. OFFICE SYMBOL (If applicable) FIBEC	9. PROCUREMENT INSTRUMENT IDENTIFICATION NUMBER F33615-82-C-3215	
8c. ADDRESS (City, State and ZIP Code) Wright-Patterson Air Force Base Dayton, Ohio 45433		10. SOURCE OF FUNDING NOS.	
11. TITLE (Include Security Classification) See Reverse		PROGRAM ELEMENT NO. 62201F	TASK NO. 01
		PROJECT NO. 2401	WORK UNIT NO. 61
12. PERSONAL AUTHOR(S) Meir Levy			
13a. TYPE OF REPORT Final	13b. TIME COVERED FROM Sep 82 TO Mar 86	14. DATE OF REPORT (Yr., Mo., Day) 31 March 1986	15. PAGE COUNT 143
16. SUPPLEMENTARY NOTATION			
17. COSATI CODES		18. SUBJECT TERMS (Continue on reverse if necessary and identify by block number)	
FIELD	GROUP	SUB. GR.	
13	13		
13	05		
		Crack growth correlation, crack growth predictions, specimens crack growth results, 2024-T3XX, lap-joint specimens, stringer-reinforced specimens.	
19. ABSTRACT (Continue on reverse if necessary and identify by block number)			
<p>Structural test program of typical aircraft structural configuration was conducted to assess the current Air Force damage tolerance design requirements defined in MIL-A-83444. The specimens, made of 2024-T3XX and 7075-T6XX, were subjected to randomized flight-by-flight spectra, representative of fighter/trainer and bomber/cargo type loading spectra, respectively, and to constant amplitude loading spectrum. A total of seventy-two (72) specimens were tested. The test results were correlated with analytical predictions using crack growth and crack initiation methods. As a result of this study, recommendation is provided to the validity of MIL-A-83444, to develop guidelines for selection of critical crack locations, and to assess the state-of-the-art analytical capabilities in prediction crack growth and crack initiation time.</p> <p>This volume, Volume III, of a five volume report presents the analytical to experimental correlations.</p>			
20. DISTRIBUTION/AVAILABILITY OF ABSTRACT UNCLASSIFIED/UNLIMITED <input checked="" type="checkbox"/> SAME AS RPT. <input type="checkbox"/> DTIC USERS <input type="checkbox"/>		21. ABSTRACT SECURITY CLASSIFICATION Unclassified	
22a. NAME OF RESPONSIBLE INDIVIDUAL Lt Christopher Mazur		22b. TELEPHONE NUMBER (Include Area Code) (513) 255-6104	22c. OFFICE SYMBOL AFWAL/FIBEC

DD FORM 1473, 83 APR

EDITION OF 1 JAN 73 IS OBSOLETE.

Unclassified

SECURITY CLASSIFICATION OF THIS PAGE

Unclassified

SECURITY CLASSIFICATION OF THIS PAGE

11. TITLE (Include Security Classification)

Assessment of Damage Tolerance Requirements and Analyses Volume III - Analytical Predictions and Correlations

Unclassified

SECURITY CLASSIFICATION OF THIS PAGE

FOREWORD

This report is prepared by Fairchild Industries, Fairchild Republic Company for the United States Air Force under a research and development program entitled "Assessment of Damage Tolerance Requirements and Analyses," Contract No. 33615-82-C-3215. This program is being administered by the Flight Dynamics Laboratory, Air Force Wright Aeronautical Laboratories, Air Force Systems Command, Wright-Patterson Air Force Base, Ohio. Mr James L. Rudd (AFWAL/FIBEC) was the Air Force project engineer through December 1985. Subsequently, Mr Rudd was replaced by Lt Christopher Mazur. A. Kuo was the Program Manager and Principal Investigator through March 1985. Subsequently, Mr Kuo was replaced by Meir Levy for the completion of the program. The structural test program has been performed at the University of Dayton Research Lab under the supervision of George Roth.

Accession For	
NTIS GRA&I	<input checked="" type="checkbox"/>
DTIC TAB	<input type="checkbox"/>
Unannounced	<input type="checkbox"/>
Justification	
By _____	
Distribution/ _____	
Availability Codes	
Dist	Avail and/or Special
A-1	



TABLE OF CONTENTS

<u>Section</u>	<u>Title</u>	<u>Page</u>
1.0	INTRODUCTION	1
2.0	ANALYTICAL METHODS	3
2.1	MATERIAL PROPERTIES	4
2.2	APPLIED LOADING SPECTRA	4
3.0	BASIC ALLOWABLES TEST PROGRAM	6
3.1	TENSILE TEST PROGRAM	6
3.2	CRACK INITIATION TEST PROGRAM	7
3.3	FRACTURE TOUGHNESS TEST PROGRAM	10
3.3.1	Data Reduction	10
3.4	CONSTANT AMPLITUDE CRACK GROWTH RATE TEST PROGRAM	17
4.0	STRUCTURAL TEST PROGRAM	36
4.1	LAP-JOINT TEST PROGRAM	37
4.1.1	Single-Shear Lap-Joint Test Program	37
4.1.2	Double-Shear Lap-Joint Test Program	62
4.2	STRINGER-REINFORCED SPECIMENS	85
4.2.1	Test Results and Analytical Predictions	85
4.2.2	Experimental vs. Analytical Predictions of Specimens Subjected to Constant Amplitude Loading Spectrum	85
4.2.3	Experimental vs. Analytical Predictions of Specimens Subjected to A-10A Loading Spectrum	86
4.2.4	Experimental vs. Analytical Predictions of Specimens Subjected to AMAVS Loading Spectrum	87
	APPENDIX A	A-1
A-1	A-10A ANALYTICAL LOADING SPECTRUM	A-1
A-2	AMAVS ANALYTICAL LOADING SPECTRUM	A-1

LIST OF FIGURES

<u>Figure</u>	<u>Title</u>	<u>Page</u>
2-1	Fracture Surface of 7075-T651 Aluminum Alloy Subjected to AMAVS Loading Spectrum	5
3.3-1	R Curve for 2024-T3 Sheet (W = 12.0 in.)	12
3.3-2	R Curve for 2024-T3 Sheet (W = 18.0 in.)	12
3.3-3	R Curve for 2024-T351 Plate (W = 8.0 in.)	13
3.3-4	R Curve for 2024-T3511 Tee Extrusion (W = 2.75 in.)	13
3.3-5	R Curve for 2024-T3511 Angle Extrusion (W = 2.25 in.)	14
3.3-6	R Curve for 7075-T651 Plate (W = 3.0 in., t = 0.324)	14
3.3-7	R Curve for 7075-T651 Plate (W = 3.0 in., t = 0.406)	15
3.3-8	R Curve for 7075-T6 Sheet (W = 12.0 in.)	15
3.3-9	R Curve for 7075-T6511 Tee Extrusion (W = 2.75 in.)	16
3.3-10	R Curve for 7075-T6511 Angle Extrusion (W = 2.75 in.)	16
3.4-1	Constant Amplitude Crack Growth Rate for 2024-T3 Sheet $R \geq 0$	20
3.4-2	Constant Amplitude Crack Growth Rate for 2024-T351 Plate $R \geq 0$	21
3.4-3	Constant Amplitude Crack Growth Rate for 2024-T3511 Tee $R \geq 0$	22
3.4-4	Constant Amplitude Crack Growth Rate for 2024-T3511 Angle $R \geq 0$	23
3.4-5	Constant Amplitude Crack Growth Rate for 7075-T6 Sheet $R \geq 0$	24
3.4-6	Constant Amplitude Crack Growth Rate for 7075-T651 Plate $R \geq 0$	25
3.4-7	Constant Amplitude Crack Growth Rate for 7075-T6511 Tee $R \geq 0$	26
3.4-8	Constant Amplitude Crack Growth Rate for 7075-T6511 Angle $R \geq 0$	27
3.4-9	Constant Amplitude Crack Growth Rate for 2024-T3 Sheet $R < 0$	28
3.4-10	Constant Amplitude Crack Growth Rate for 2024-T351 Plate $R < 0$	29
3.4-11	Constant Amplitude Crack Growth Rate for 2024-T3511 Tee $R < 0$	30
3.4-12	Constant Amplitude Crack Growth Rate for 2024-T3511 Angle $R < 0$	31
3.4-13	Constant Amplitude Crack Growth Rate for 7075-T6 Sheet $R < 0$	32
3.4-14	Constant Amplitude Crack Growth Rate for 7075-T651 Plate $R < 0$	33
3.4-15	Constant Amplitude Crack Growth Rate for 7075-T6511 Tee $R < 0$	34
3.4-16	Constant Amplitude Crack Growth Rate for 7075-T6511 Angle $R < 0$	35
4.1.1-1	Photo of Single-Shear Lap-Joint Specimen Subsequent to Failure	43
4.1.1-2	Crack Growth Diagram for Single-Shear Lap-Joint Specimen LJ-1	44

LIST OF FIGURES (Continued)

<u>Figure</u>	<u>Title</u>	<u>Page</u>
4.1.1-3	Crack Growth Diagram for Single-Shear Lap-Joint Specimen LJ-2	45
4.1.1-4	Crack Growth Diagram for Single-Shear Lap-Joint Specimen LJ-3	46
4.1.1-5	Crack Growth Diagram for Single-Shear Lap-Joint Specimen LJ-4	47
4.1.1-6	Crack Growth Diagram for Single-Shear Lap-Joint Specimen LJ-5	48
4.1.1-7	Crack Growth Diagram for Single-Shear Lap-Joint Specimen LJ-6	49
4.1.1-8	Crack Growth Diagram for Single-Shear Lap-Joint Specimen LJ-7	50
4.1.1-9	Crack Growth Diagram for Single-Shear Lap-Joint Specimen LJ-8	51
4.1.1-10	Crack Growth Diagram for Single-Shear Lap-Joint Specimen LJ-9	52
4.1.1-11	Crack Growth Diagram for Single-Shear Lap-Joint Specimen LJ-10	53
4.1.1-12	Crack Growth Diagram for Single-Shear Lap-Joint Specimen LJ-11	54
4.1.1-13	Crack Growth Diagram for Single-Shear Lap-Joint Specimen LJ-12	55
4.1.1-14	Crack Growth Diagram for Single-Shear Lap-Joint Specimen LJ-25	56
4.1.1-15	Crack Growth Diagram for Single-Shear Lap-Joint Specimen LJ-26	57
4.1.1-16	Crack Growth Diagram for Single-Shear Lap-Joint Specimen LJ-27	58
4.1.1-17	Crack Growth Diagram for Single-Shear Lap-Joint Specimen LJ-28	59
4.1.1-18	Crack Growth Diagram for Single-Shear Lap-Joint Specimen LJ-29	60
4.1.1-19	Crack Growth Diagram for Single-Shear Lap-Joint Specimen LJ-30	61
4.1.2-1	Photo of Double-Shear Lap-Joint Specimen	66
4.1.2-2	Crack Growth Diagram for Double-Shear Lap-Joint Specimen LJ-13	67
4.1.2-3	Crack Growth Diagram for Double-Shear Lap-Joint Specimen LJ-14	68
4.1.2-4	Crack Growth Diagram for Double-Shear Lap-Joint Specimen LJ-15	69
4.1.2-5	Crack Growth Diagram for Double-Shear Lap-Joint Specimen LJ-16	70
4.1.2-6	Crack Growth Diagram for Double-Shear Lap-Joint Specimen LJ-17	71
4.1.2-7	Crack Growth Diagram for Double-Shear Lap-Joint Specimen LJ-18	72
4.1.2-8	Crack Growth Diagram for Double-Shear Lap-Joint Specimen LJ-19	73
4.1.2-9	Crack Growth Diagram for Double-Shear Lap-Joint Specimen LJ-20	74
4.1.2-10	Crack Growth Diagram for Double-Shear Lap-Joint Specimen LJ-21	75
4.1.2-11	Crack Growth Diagram for Double-Shear Lap-Joint Specimen LJ-22	76
4.1.2-12	Crack Growth Diagram for Double-Shear Lap-Joint Specimen LJ-23	77
4.1.2-13	Crack Growth Diagram for Double-Shear Lap-Joint Specimen LJ-24	78

LIST OF FIGURES (Continued)

<u>Figure</u>	<u>Title</u>	<u>Page</u>
4.1.2-14	Crack Growth Diagram for Double-Shear Lap-Joint Specimen LJ-31	79
4.1.2-15	Crack Growth Diagram for Double-Shear Lap-Joint Specimen LJ-32	80
4.1.2-16	Crack Growth Diagram for Double-Shear Lap-Joint Specimen LJ-33	81
4.1.2-17	Crack Growth Diagram for Double-Shear Lap-Joint Specimen LJ-34	82
4.1.2-18	Crack Growth Diagram for Double-Shear Lap-Joint Specimen LJ-35	83
4.1.2-19	Crack Growth Diagram for Double-Shear Lap-Joint Specimen LJ-36	84
4.2-1	Stringer Reinforced Specimen Center 'TEE' Split Skin	91
4.2-2	Stringer Reinforced Specimen Edge 'L' Stringer Continuous Skin	92
4.2-3	Stringer Reinforced Specimen Installed on MTS Machine	93
4.2-4	Crack Growth Diagram for Stringer-Reinforced Specimen No. 37 (-1A) Subjected to C.A. Loading Spectra	94
4.2-5	Crack Growth Diagram for Stringer-Reinforced Specimen No. 38 (-1A) Subjected to C.A. Loading Spectra	95
4.2-6	Crack Growth Diagram for Stringer-Reinforced Specimen No. 39 (-1A) Subjected to A-10A Loading Spectra	96
4.2-7	Crack Growth Diagram for Stringer-Reinforced Specimen No. 40 (-1A) Subjected to A-10A Loading Spectra	97
4.2-8	Crack Growth Diagram for Stringer-Reinforced Specimen No. 41 (-1B) Subjected to C.A. Loading Spectra	98
4.2-9	Crack Growth Diagram for Stringer-Reinforced Specimen No. 42 (-1B) Subjected to C.A. Loading Spectra	99
4.2-10	Crack Growth Diagram for Stringer-Reinforced Specimen No. 43 (-1B) Subjected to A-10A Loading Spectra	100
4.2-11	Crack Growth Diagram for Stringer-Reinforced Specimen No. 44 (-1B) Subjected to A-10A Loading Spectra	101
4.2-12	Crack Growth Diagram for Stringer-Reinforced Specimen No. 45 (-3A) Subjected to C.A. Loading Spectra	102
4.2-13	Crack Growth Diagram for Stringer-Reinforced Specimen No. 46 (-3A) Subjected to C.A. Loading Spectra	103

LIST OF FIGURES (Continued)

<u>Figure</u>	<u>Title</u>	<u>Page</u>
4.2-14	Crack Growth Diagram for Stringer-Reinforced Specimen No. 47 (-3A) Subjected to A-10A Loading Spectra	104
4.2-15	Crack Growth Diagram for Stringer-Reinforced Specimen No. 48 (-3A) Subjected to A-10A Loading Spectra	105
4.2-16	Crack Growth Diagram for Stringer-Reinforced Specimen No. 49 (-3B) Subjected to C.A. Loading Spectra	106
4.2-17	Crack Growth Diagram for Stringer-Reinforced Specimen No. 50 (-3B) Subjected to A-10A Loading Spectra	107
4.2-18	Crack Growth Diagram for Stringer-Reinforced Specimen No. 51 (-3B) Subjected to C.A. Loading Spectra	108
4.2-19	Crack Growth Diagram for Stringer-Reinforced Specimen No. 52 (-3B) Subjected to A-10A Loading Spectra	109
4.2-20	Crack Growth Diagram for Stringer-Reinforced Specimen No. 53 (-5A) Subjected to C.A. Loading Spectra	110
4.2-21	Crack Growth Diagram for Stringer-Reinforced Specimen No. 54 (-5A) Subjected to C.A. Loading Spectra	111
4.2-22	Crack Growth Diagram for Stringer-Reinforced Specimen No. 55 (-5A) Subjected to A-10A Loading Spectra	112
4.2-23	Crack Growth Diagram for Stringer-Reinforced Specimen No. 56 (-5A) Subjected to A-10A Loading Spectra	113
4.2-24	Crack Growth Diagram for Stringer-Reinforced Specimen No. 57 (-5B) Subjected to C.A. Loading Spectra	114
4.2-25	Crack Growth Diagram for Stringer-Reinforced Specimen No. 58 (-5B) Subjected to C.A. Loading Spectra	115
4.2-26	Crack Growth Diagram for Stringer-Reinforced Specimen No. 59 (-5B) Subjected to A-10A Loading Spectra	116
4.2-27	Crack Growth Diagram for Stringer-Reinforced Specimen No. 60 (-5B) Subjected to A-10A Loading Spectra	117
4.2-28	Crack Growth Diagram for Stringer-Reinforced Specimen No. 61 (-7A) Subjected to AMAVS Loading Spectra	118

LIST OF FIGURES (Continued)

<u>Figure</u>	<u>Title</u>	<u>Page</u>
4.2-29	Crack Growth Diagram for Stringer-Reinforced Specimen No. 62 (-7A) Subjected to AMAVS Loading Spectra	119
4.2-30	Crack Growth Diagram for Stringer-Reinforced Specimen No. 63 (-7B) Subjected to AMAVS Loading Spectra	120
4.2-31	Crack Growth Diagram for Stringer-Reinforced Specimen No. 64 (-7B) Subjected to AMAVS Loading Spectra	121
4.2-32	Crack Growth Diagram for Stringer-Reinforced Specimen No. 65 (-9A) Subjected to AMAVS Loading Spectra	122
4.2-33	Crack Growth Diagram for Stringer-Reinforced Specimen No. 66 (-9A) Subjected to AMAVS Loading Spectra	123
4.2-34	Crack Growth Diagram for Stringer-Reinforced Specimen No. 67 (-9B) Subjected to AMAVS Loading Spectra	124
4.2-35	Crack Growth Diagram for Stringer-Reinforced Specimen No. 68 (-9B) Subjected to AMAVS Loading Spectra	125
4.2-36	Crack Growth Diagram for Stringer-Reinforced Specimen No. 69 (-11A) Subjected to AMAVS Loading Spectra	126
4.2-37	Crack Growth Diagram for Stringer-Reinforced Specimen No. 70 (-11A) Subjected to AMAVS Loading Spectra	127
4.2-38	Crack Growth Diagram for Stringer-Reinforced Specimen No. 71 (-11B) Subjected to AMAVS Loading Spectra	128
4.2-39	Crack Growth Diagram for Stringer-Reinforced Specimen No. 72 (-11B) Subjected to AMAVS Loading Spectra	129

LIST OF TABLES

<u>Table</u>	<u>Title</u>	<u>Page</u>
3.1-1	Average Tensile Properties	7
3.2-1	Damage Index " d_f "	9
3.3-1	Average Fracture Toughness Properties	11
3.4-1	Modified Walker's Equation Coefficients	19
4-1	Structural Test Program	36
4.1.1-1	Single-Shear Lap Joint Specimen Test Program	40
4.1.1-2	Analytical vs. Experimental Crack Growth Life for Single-Shear Lap-Joint Specimens Subjected to Constant Amplitude Loading Spectrum	41
4.1.1-3	Analytical vs. Experimental Crack Growth Life for Single-Shear Lap-Joint Specimens Subjected to A-10A Loading Spectrum	41
4.1.1-4	Analytical vs. Experimental Crack Growth Life for Single-Shear Lap-Joint Specimens Subjected to AMAVS Loading Spectrum	42
4.1.2-1	Double-Shear Lap-Joint Specimens Test Program	62
4.1.2-2	Analytical vs. Experimental Crack Growth for Double-Shear Lap-Joint Specimens Subjected to Constant Amplitude Loading Spectrum	64
4.1.2-3	Analytical vs. Experimental Crack Growth for Double-Shear Lap-Joint Specimens Subjected to A-10A Loading Spectrum	65
4.1.2-4	Analytical vs. Experimental Crack Growth for Double-Shear Lap-Joint Specimens Subjected to AMAVS Loading Spectrum	65
4.2-1	Test Matrix for Stringer-Reinforced Specimens	88
4.2-2	Experimental vs. Predicted Life for Stringer-Reinforced Specimens Subjected to Constant Amplitude Loading Spectrum	89
4.2-3	Experimental vs. Predicted Life for Stringer-Reinforced Specimens Subjected to A-10A Loading Spectrum	89
4.2-4	Experimental vs. Predicted Life for Stringer-Reinforced Specimens Subjected to AMAVS Loading Spectrum	90
A-1	A-10A Analytical Loading Spectrum	A-2
A-2	AMAVS Analytical Loading Spectrum	A-4

1.0 INTRODUCTION

The eight major tasks listed below have been planned to achieve the program objectives. Namely, (a) assessing the validity of, and recommending improvements to MIL-A-83444, (b) developing guidelines for identifying the most critical initial primary damage locations for typical aircraft structures, and (c) assessing and improving the state-of-the-art analytical methods to satisfy the requirements of MIL-A-83444.

- Task I: Analytical Methods
- Task II: Basic Tests
- Task III: Analytical Predictions
- Task IV: Structural Tests
- Task V: Analytical/Experimental Correlations
- Task VI: Assessment of and Recommended Improvements to MIL-A-83444
- Task VII: Guidelines for Selecting Most Critical Initial Primary Damage Location
- Task VIII: Assessment of and Improvements to Damage Tolerance Analyses

The material presented in this report includes the results of the structural specimen tests conducted under Tasks II and IV, and the analytical crack growth predictions and lives associated with them. This program began in September 1982 and completed in May 1986.

This report presents the analytical predictions and the test results of the Structural Test Program; it also presents a summary of the Basic Test Program conducted prior to the Structural Testing. The predictions were correlated with the experimental data to show the effectiveness of the analytical methods for predicting crack growth and crack initiation. The analytical methods used are documented in Volume II of the report, and include Crack Growth Method "Method 1" and Combined Method "Method 2". A short description of "Method 1" and "Method 2" is provided in Section 2.0.

The structural test program included thirty-six (36) lap-joint specimens representing structural splice configurations often found in airframe construction, and thirty-six (36) stringer-reinforced subcomponent specimens to represent typical stringer to skin panel configuration. The crack growth life of each specimen was predicted using the computer program "DAMGRO" (Ref. DAMGRO User Manual). The computer program and the analytical parameters and techniques associated with it have been developed during Phase 1 of the program.

The Basic Test Program was conducted to obtain static and fatigue allowables used during the structural test program. It included sixty (60) tensile specimens to establish basic static allowables, eighty (80) crack initiation specimens to establish fatigue initiation parameters, twenty (20) fracture toughness specimens to establish critical fracture toughness allowables and sixty-four (64) constant amplitude crack growth rates specimens to establish da/dN vs K_{max} curves.

The materials selected for the entire test program were 7075-T6XX and 2024-T3XX to represent typical bomber and fighter lower wing skin materials, respectively. The loading spectra chosen were the 'AMAVS' randomized loading spectrum to represent a bomber/cargo type aircraft and the 'A-10A' loading spectrum to represent a fighter/trainer type aircraft. An additional loading spectrum was a constant amplitude loading. The loading conditions for AMAVS and A-10A spectra are presented in Volume IV of the report. The analytical predictions, however, were done using condensed loading spectra as shown in Appendix A. The analytical formulations as well as the symbols used in this report are defined in Volume II.

2.0 ANALYTICAL METHODS

The analytical methods and the material allowables used in predicting the crack growth life of the structural test specimens, were established under Task I and Task II of the program. Task I included the derivation of the stress intensity and stress severity factors for various structural configurations. It also included the development of a computer program "DAMGRO", which provides an automative means of predicting crack growth and crack initiation of structural elements. Task II, included coupon testing to establish the basic material allowables such as constant amplitude crack growth rates, critical fracture toughness, crack initiation allowables, and tensile properties.

The analytical predictions were performed using two methods:

a) Crack Growth Method, "Method 1";

This method is consistent with the current initial flaw requirement defined in MIL-A-83444. In addition to the primary flaw of 0.050 inch, secondary flaws of 0.005 inch are assumed to exist at the edge of adjacent holes. All cracks are grown simultaneously under the application of spectrum loading.

b) Combined Method, "Method 2";

This method combines crack growth with crack initiation. Rather than assumed secondary flaws, a prediction of crack initiation is done. The initiation was postulated to depend on the strain energy density ($S = 0.5 (\sigma K)^2 / E$) at the edge of the holes. A damage index 'd₁' was derived for every loading spectra to determine the time of crack initiation.

The analytical parameters associated with both methods are given in Volume II of the report, and in the "DAMGRO" user manual.

Since the test specimens were subjected to randomized flight-by-flight loading spectra, a load interaction model had to be used. The model used was the Modified Willenborg retardation model, with shut-off value of 2.3 (for aluminum alloys). The model is described in Volume II of the report.

2.1 MATERIAL PROPERTIES

The basic material properties for 2024-T3XX and 7075-T6XX were established during Task II of the program and are provided in Section 3.0; they include crack initiation parameters, fracture toughness data, crack growth rates, and tensile properties. The crack growth rates were presented using the Modified Walker Equation, da/dN vs. K_{max} . The equation has the form;

$$da/dN = c ((1-R)^m K_{max})^n$$

where c , m , n are Walker constants summarized in Section 3.4. R and K_{max} are the stress ratio and maximum stress intensity factor.

2.2 APPLIED LOADING SPECTRA

During the structural test program, three distinct loading spectra were applied. They include the following:

- a) Constant amplitude loading spectrum. The loading spectrum contained repeated cycles with equal load amplitude. The majority of the specimens were tested at a maximum stress level of 17.0 Ksi and stress ratio of $R = 0.10$.
- b) The A-10A flight-by-flight loading spectrum. The spectrum represents fighter/trainer type maneuvers. The cycles were randomized flight-by-flight, including take-off and landing cycles. Twenty-five (25) repeated identical loading blocks were applied to represent one life time

on the A-10A aircraft (=6000 hours). Each block contained approximately 7416 cycles. The cycle by cycle loading spectrum is given in Volume IV of the report. A Condensed Loading Spectrum was used during the Analytical Prediction as shown in Appendix A. It contained 204 stress layers for every 4% of life (Ref. App. A).

- c) The AMAVS flight-by-flight loading spectrum. The spectrum represents typical bomber/cargo type maneuvers. Approximately, 128 repeated Spectrum Blocks represent one life (= 13,500 hours). Each Spectrum Block contains 11245 cycles. In performing the Analytical Predictions a condensed stress spectrum was used containing 112 stress layers (Ref. App. A).

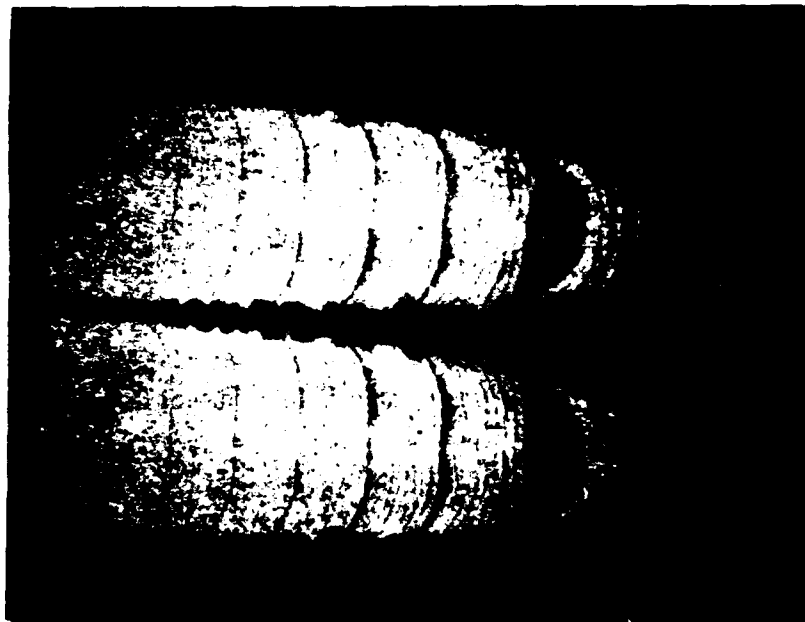


Figure 2-1. Fracture Surface of 7075-T651 Aluminum Alloy Subjected to AMAVS Loading Spectrum

3.0 BASIC ALLOWABLES TEST PROGRAM

The purpose of the basic test program was to establish static and fatigue allowables for the product form used during the structural test program. A total of two hundred twenty four (224) specimens were tested, including the following:

- o Sixty (60) tensile coupon tests
- o Eighty (80) crack initiation coupon tests
- o Twenty (20) fracture toughness coupon tests
- o Sixty-four (64) constant amplitude crack growth rates coupon tests

In addition, one (1) specimen was subjected to the AMAVS randomized spectrum for the purpose of establishing marker band verification. The basic test program is described in detail in Volume III of the report.

The specimens were made of 2024-T3XX and 7075-T6XX Aluminum Alloys, similar to that used during the Structural Test Program.

3.1 TENSILE TEST PROGRAM

The purpose of the tensile test program was to establish the material acceptability and to provide the static allowables of the material selected. The parameters evaluated include yield and ultimate allowables and percentage elongation. The tests were performed in two grain directions, namely, longitudinal and transverse directions. A summary of the average tensile properties for 2024-T3 and 7075-T6 aluminum alloy is provided in Table 3.1-1.

TABLE 3.1-1. AVERAGE TENSILE PROPERTIES

PRODUCT FORM	YIELD STRENGTH (KSI)		ULTIMATE STRENGTH (KSI)		ELONGATION (%)		YOUNG'S MODULUS (KSI 10 ³)	
	LONG.	TRAN.	LONG.	TRAN.	LONG.	TRAN.	LONG.	TRAN.
2024-T3 0.19" Sheet	53.1	45.0	67.4	67.2	14.8	18.0	10.7	11.0
2024-T3 0.09" Sheet	52.9	42.5	69.0	67.5	17.0	19.2	11.4	10.2
2024-T351 0.25" Plate	51.1	45.4	70.0	67.0	20.2	18.8	10.5	11.0
2024-T3511 0.19" Tee	53.3	50.5	67.4	62.6	17.8	7.5	11.0	10.7
2024-T3511 0.25" Angle	47.6	43.2	62.3	58.9	21.3	10.7	11.1	10.3
7075-T651 0.31" Plate	77.9	75.4	82.7	84.1	13.5	12.8	10.1	10.2
7075-T6 0.16" Sheet	77.2	73.8	81.6	84.3	15.0	13.3	10.4	10.8
7075-T651 0.4" Plate	77.2	72.6	79.6	79.4	13.8	11.5	11.1	10.7
7075-T6511 0.31" Tee	78.9	69.7	86.2	76.6*	12.8	9.3	10.9	10.3
7075-T6511 0.31" Angle	82.7	77.2	89.2	85.2	11.8	11.0	10.4	10.2

*Below A-allowable, i.e. 78.0

3.2 CRACK INITIATION TEST PROGRAM

The purpose of the crack initiation test program was to provide fatigue initiation allowables for the product form used during the structural test program.

The method of predicting crack initiation ($a_0 = 0.050$ inch corner flaw) was derived during Phase 1 of the program. The crack initiation was postulated to be a function of damage accumulation which is determined by the strain energy density at the edge of a notch $S = 0.5 (\sigma K)^2 / E$. The stress severity

factor ($K = \alpha \beta \gamma K_t$) was selected as a measure of the elastic stress concentration at the edge of a fastener hole subjected to both fastener load transfer and bypass stresses generated by loads away from the hole. The parameters $\alpha \beta \gamma$ were determined experimentally to characterize the effect of fastener/hole interference fit, clamp-up, and the presence of faying surface sealant, respectively. The technique for predicting crack initiation and the initiation parameters associated with it are described in Volume II of the report. The relation between the strain energy density and the number of cycles needed to crack initiation was established experimentally (Volume II) for 2024-T3XX, and 7075-T6XX aluminum alloys as being:

$$S = 10.4261 (N_t)^{-0.3660} \text{ for 2024-T3XX} \quad 3.2.1A$$

$$S = 20.4257 (N_t)^{-0.4516} \text{ for 7075-T6XX} \quad 3.2.1B$$

An effort to establish distinct values for α , β , and γ to characterize the effect of interference fit, clamp-up and sealant considered seperately was not successful because of insufficient test specimens. However, the combined effects of the three parameters were experimentally established as being:

$$\alpha \beta \gamma = 0.8503 \text{ for 2024-T3XX} \quad 3.2.2A$$

$$= 0.8126 \text{ for 7075-T6XX} \quad 3.2.2B$$

The crack growth lives N_g from $a_o = .050$ inch for all specimens were predicted using the "DAMGRO" computer program. The life required to initiate a 0.05 inch crack is defined as $(N_p - N_g)$ where N_p is the total life (initiation and growth). The damage index d_i for the initiation of a 0.05 inch quarter-circular corner crack is defined as $d_i = (N_p - N_g)/N_p$. The calculated value of d_i is then curve-fitted into the following equations. For Group A there was no interference fit, clamp-up, or sealant between the faying surface.

$$d_i = 1.0 - 0.629S_{\max} \text{ for 2024-T3} \quad 3.3.3$$

$$d_i = 0.873 - 0.795S_{\max} \text{ for 7075-T651} \quad 3.3.4$$

For the specimens of Groups B, C and D, where one or more of the parameters existed, the damage index was obtained in the same manner as outlined above. The data points were curve-fitted into the following equations:

$$d_i = 1.0 - 0.540S_{\max} \quad \text{for 2024-T3} \quad 3.3.5$$

$$d_i = 0.958 - 0.619S_{\max} \quad \text{for 7075-T651} \quad 3.3.6$$

It should be reiterated that Equations 3.3.3, 3.3.4, 3.3.5 and 3.3.6 represent the damage index for the initiation of a 0.05 inch quarter-circular corner crack for the specimens subjected to constant amplitude fatigue loading. For the case of spectrum loading, the damage index 'd_f' to initiate an 0.05 inch quarter-circular corner crack was determined using the weighted average. Equations 3.3.3 through 3.3.6 and the A-10A and AMAVS spectra were used as input data for determining the values of d_f which are given in Table 3.2-1.

TABLE 3.2-1. DAMAGE INDEX "d_f"

<u>LOADING SPECTRUM</u>	<u>MATERIAL</u>	<u>σ_{max} (KSI)</u>	<u>GROUP A</u>	<u>GROUP B, C, D</u>
A-10A	2024-T3XX	35.75	0.8868	0.9028
A-10A	2024-T3XX	37.75	0.873	0.8917
AMAVS	7075-T6XX	21.48	0.8056	0.9050
AMAVS	7075-T6XX	30.35	0.7448	0.8522
AMAVS	7075-T6XX	37.75	0.6750	0.7944
Const. Amplit.	2024-T3XX	17.10	0.8725	0.8925
Const. Amplit.	2024-T3XX	28.0	0.6581	0.7065

3.3 FRACTURE TOUGHNESS TEST PROGRAM

The purpose of the fracture toughness test program was to establish fracture toughness allowables for the material form used during the structural test program defined in Task IV. The test included evaluation of the critical fracture toughness factor ' K_{IC} ' and the construction of the resistance curves 'R-Curves'.

3.3.1 Data Reduction

The critical fracture toughness for the product form was evaluated using:

$$K_{APP} = \frac{P_{max}}{Wt} \sqrt{\pi a_o \text{ Sec } \frac{\pi a_o}{W}} \quad (3.3.7)$$

$$K_{IC} = \frac{P_{max}}{Wt} \sqrt{\pi a_f \text{ Sec } \frac{\pi a_f}{W}} \quad (3.3.8)$$

Where a_o and a_f are the initial crack and the final crack size respectively, and P_{max} is the failure load. The average values of the fracture toughness allowables are listed in Table 4-1.

The procedure used in determining the R-Curves is defined in ASTM standard E561. The standard provides the means for defining the material toughness ' K_R ' in term of effective crack length at the time of slow crack extension. The R-Curves give a measure of the material resistance to cracking. The compliance method was chosen in constructing the R-Curves. Figures 3.3-1 through 3.3-10 present the R-Curves for 2024-T3XX and 7075-T6XX generated during the Basic Test Program.

TABLE 3.3-1. AVERAGE FRACTURE TOUGHNESS PROPERTIES

MATERIAL FORM	THICKNESS (IN)	WIDTH (IN)	K_{app} (Ksi \sqrt{in})	K_{IC} (Ksi \sqrt{in})
2024-T3 Sheet	0.193	12.0	83.00	116.00
2025-T3 Sheet	0.088	18.0	98.95	155.90
2024-T351 Plate	0.253	8.0	75.92	100.00
2024-T3511 Ext. (TEE)	0.188	2.75	43.88	58.00
2024-T3511 Ext. (ANGLE)	0.238	2.25	43.85	62.40
7075-T651 Plate	0.324	3.0	47.37	61.34
7075-T651 Plate	0.406	3.0	41.07	53.45
7075-T6 Sheet	0.157	12.0	82.25	97.62
7075-T6511 Ext. (TEE)	0.300	2.75	55.68	77.56
7075-T6511 Ext. (ANGLE)	0.310	2.75	51.72	67.33

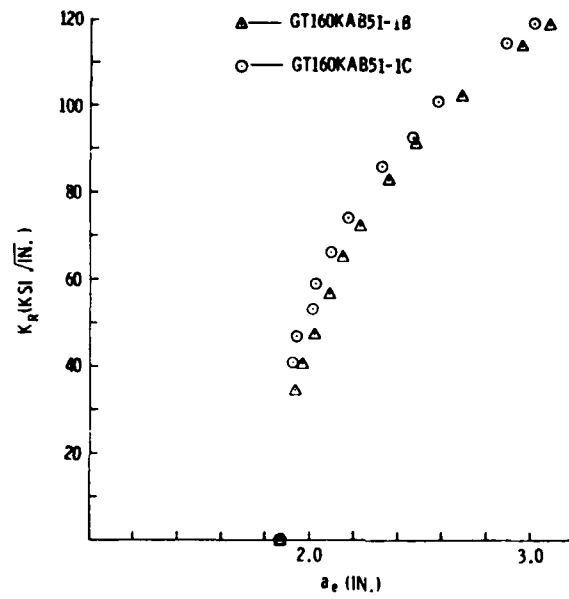


Figure 3.3-1. R Curve for 2024-T3 Sheet ($W = 12.0$ in.)

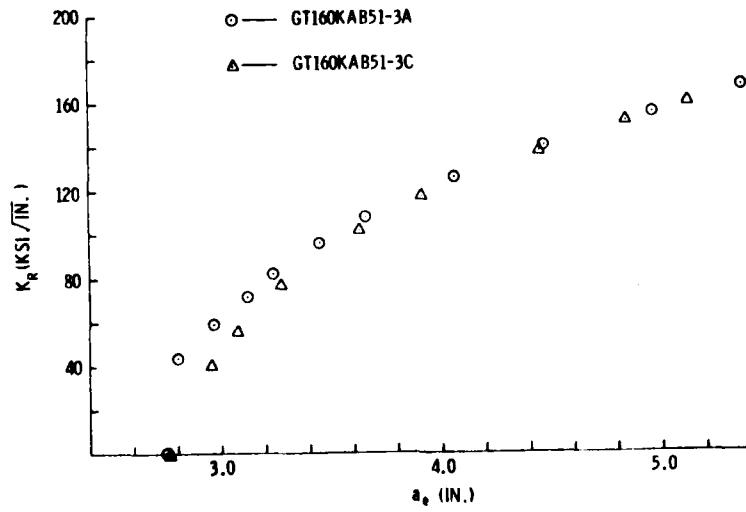


Figure 3.3-2. R Curve for 2024-T3 Sheet ($W = 18.0$ in.)

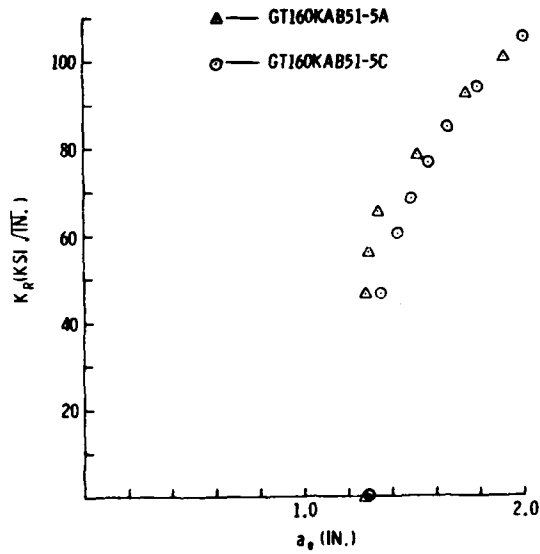


Figure 3.3-3. R Curve for 2024-T351 Plate ($W = 8.0$ in.)

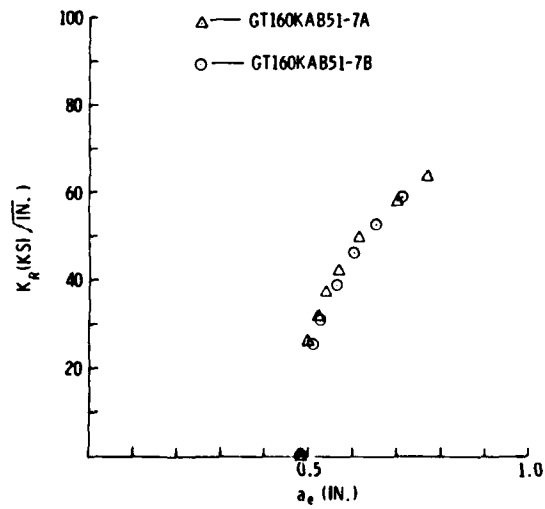


Figure 3.3-4. R Curve for 2024-T351 Tee Extrusion ($W = 2.75$ in.)

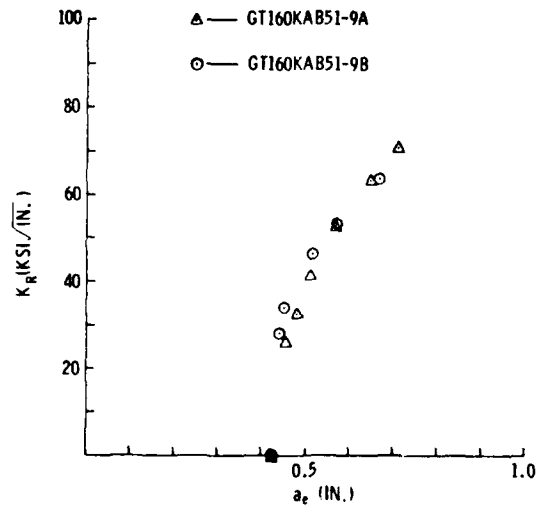


Figure 3.3-5. R Curve for 2024-T3511 Angle Extrusion
($W = 2.25$ in.)

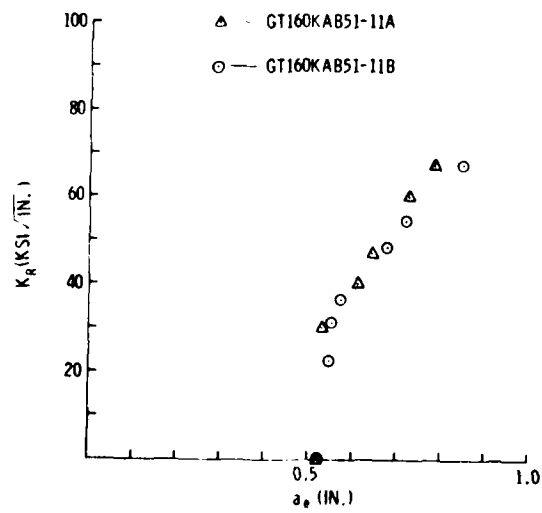


Figure 3.3-6. R Curve for 7075-T651 Plate
($W = 3.0$ in., $t = 0.324$)

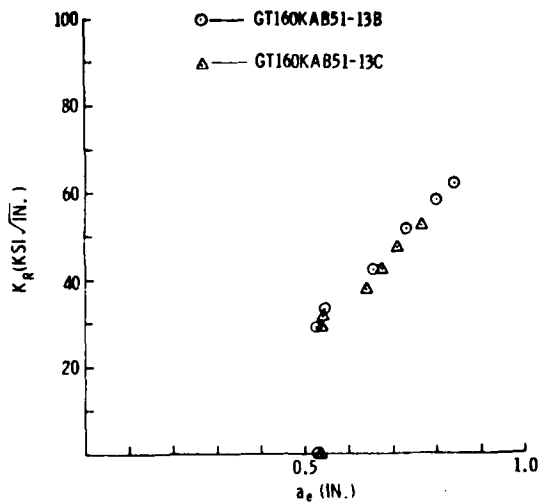


Figure 3.3-7. R Curve for 7075-T651 Plate
(W = 3.0 in., t = 0.406 in.)

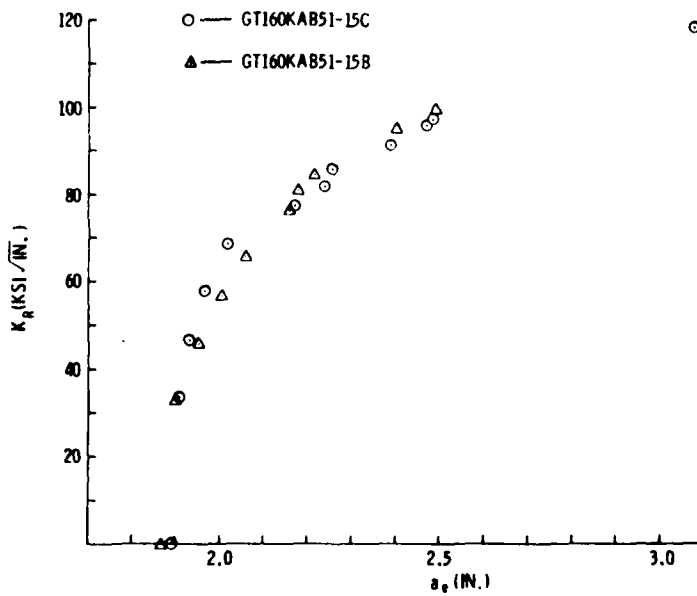


Figure 3.3-8. R Curve for 7075-T6 Sheet (W = 12.0 in.)

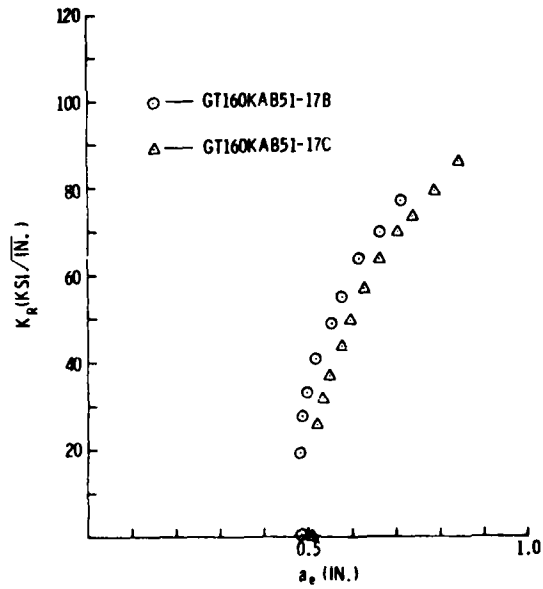


Figure 3.3-9. R Curve for 7075-T6511 Tee Extrusion
($W = 2.75$ in.)

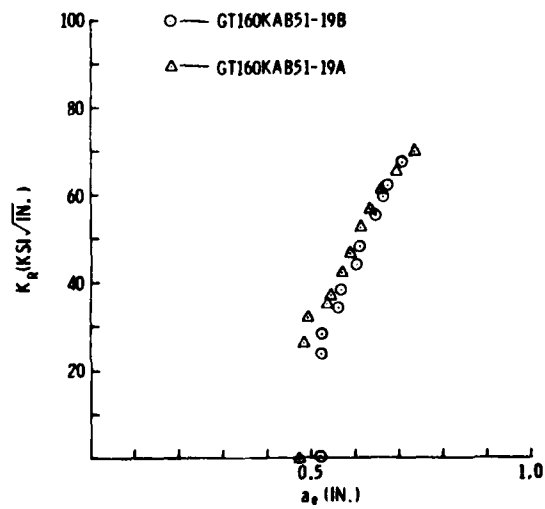


Figure 3.3-10. R Curve for 7075-T6511 Angle Extrusion
($W = 2.75$ in.)

3.4 CONSTANT AMPLITUDE CRACK GROWTH RATE TEST PROGRAM

The purpose of the constant amplitude crack growth rate test program was to establish crack growth allowables for the material form used during the structural test program. The test data were fit into the "Modified Walker Equation" in term of da/dN vs K_{max} .

The raw test data for each specimen was reduced to da/dN vs. K_{max} using a seven point polynomial scheme. The crack growth rate, ' da/dN vs. K_{max} ' was plotted on log-log scale for each product form, which included either positive or negative stress ratios. The data was then fitted into the Modified Walker Equation:

$$\frac{da}{dN} = c \left((1-R)^m K_{max} \right)^n \quad (3.4.1)$$

where K_{max} and R are the maximum stress intensity and the stress ratio, respectively. The constant c , m and n , were evaluated from the test data in the following manner:

- 1) The da/dN vs. $(1-R)^m K_{max}$ plots were constructed for various values of m .
- 2) The value of m which produced the narrowest band of data points was chosen for equation (1) evaluation.
- 3) After the selection of ' m ', the constant ' c ' and ' N ' were evaluated using a least source curve fitting procedure.

The constants c , m and n determined in this manner are given in Table 3.4-1 for eight product forms. From Table 3.4-1 it can be seen that for positive stress ratios, the value of ' m ' for 2024-T3XX varies between 0.60 and 0.70, while for 7075-T6XX it varies between 0.50 and 0.55. At negative stress ratios, the value of m is equal to 0.00 for all but two product forms. The 2024 extruded tee and angle product forms both have a value of m equal to

1.00. Furthermore, the slope of the log-log plot for the Walker equation, which is denoted by coefficient n and which is defined as the change in the crack growth rate divided by the change in $(1-R)^m K_{max}$, is larger for all product forms of 2024 under positive stress ratios than for the corresponding product forms under negative stress ratios. This observation implies that the crack growth rate for 2024-T3XX is more sensitive to changes in the stress intensity factor under positive stress ratios than under negative stress ratios. However, from the test results a similar conclusion for 7075-T6XX cannot be made.

For the majority of the test, an excellent fit was obtained when the Modified Walker's Equation was used. An exception was the test results from specimens No. 2 made of 2024-T3511 tee tested at $R > 0$, and No. 3 made of 7075-T6511 tested at $R > 0$. The test results of these two (2) specimens were not included in the curve fitting because of large deviations. The Walker's constant C for 7075-T651 plate (Figure 3.4-6) was re-evaluated subsequent to the crack growth predictions because of large discrepancies in the predicted life. The updated value of c is 1.70×10^{-8} . The updated constant reduced the deviations somewhat, however, this was not sufficient to yield accurate predictions. A list of the Walker's constants is provided in Table 3.4-1.

TABLE 3.4-1. MODIFIED WALKER'S EQUATION
COEFFICIENTS

PRODUCT FORM	STRESS RATIO	c	m	n
2024-T3 Sheet	positive	2.2374E-09	0.70	3.3386
2024-T3 Sheet	negative	6.2126E-09	0.00	2.9783
2024-T351 Plate	positive	7.7269E-09	0.65	2.8180
2024-T351 Plate	negative	4.5865E-8	0.00	2.2338
2024-T3511 Angle	positive	7.6198E-11	0.60	4.5667
2024-T3511 Angle	negative	4.3322E-11	1.00	4.0093
2024-T3511 Tee	positive	1.5998E-10	0.65	4.5545
2024-T3511 Tee	negative	2.3033E-09	1.00	3.1154
7075-T6 Sheet	positive	1.3579E-07	0.50	1.9752
7075-T6 Sheet	negative	1.0654E-07	0.00	2.0950
7075-T651 Plate	positive	1.0454E-08	0.50	2.8033
7075-T651 Plate (1)	positive	1.7000E-08	0.50	2.8033
7075-T651 Plate	negative	2.6409E-08	0.00	2.4962
7075-T6511 Angle	positive	1.9047E-08	0.50	2.6640
7075-T6511 Angle	negative	3.1758E-08	0.00	2.5814
7075-T6511 Tee	positive	9.7285E-08	0.55	2.0369
7075-T6511 Tee	negative	5.8669E-08	0.00	2.4602

(1) Updated fit test data

2024-T3 SHEET
 GT160KAB49-01, 0.19" THICK, $R \geq 0$
 WALKER CNSTS: $c = 2.2374E-09$, $m = 0.7$, $n = 3.3386$

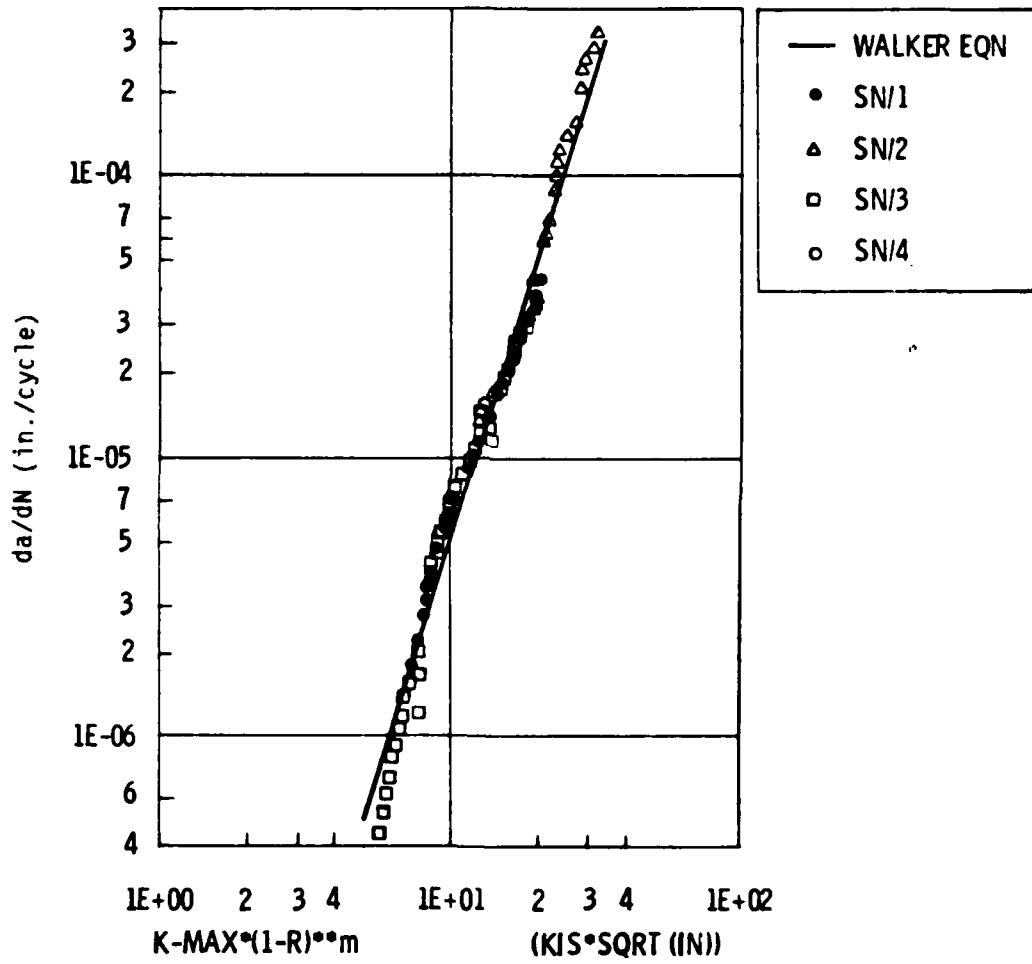


Figure 3.4-1. Constant Amplitude Crack Growth Rate for 2024-T3 Sheet $R \geq 0$

2024-T351 PLATE
 GT160KAB49-03, 0.25" THICK, R_z0
 WALKER CNSTS: c = 7.7269E-09, m = .65, n = 2.8180

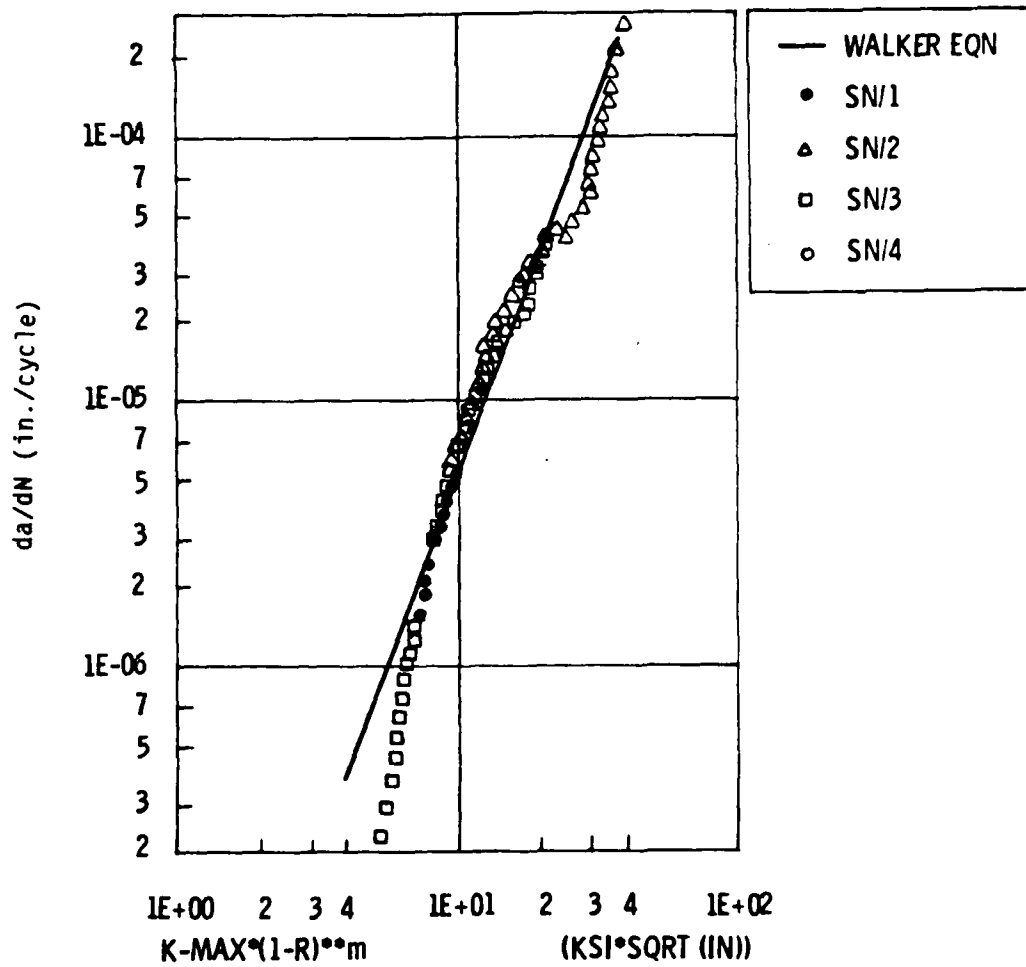


Figure 3.4-2. Constant Amplitude Crack Growth Rate for 2024-T351 Plate R_z0

2024-T3511 TEE
 GT160KAB49-05, 0.19" THICK, R ≥ 0
 WALKER CNSTS: c = 7.6198E-11, m = 0.6, n = 4.5667

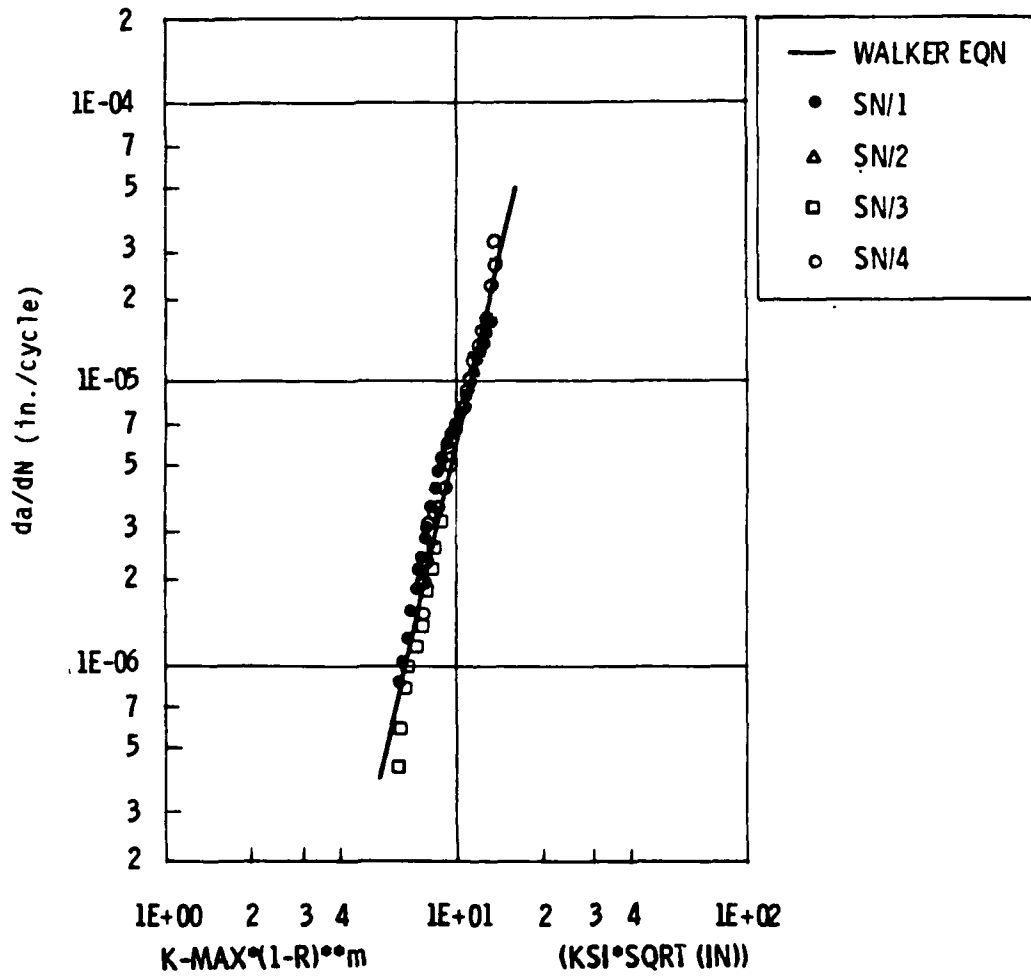


Figure 3.4-3. Constant Amplitude Crack Growth Rate for 2024-T3511 Tee $R \geq 0$

2024-T3511 ANGLE
 GT160KAB49-07, 0.25" THICK, $R \geq 0$
 WALKER CNSTS: $c = 7.6198E-11$, $m = 0.6$, $n = 4.5667$

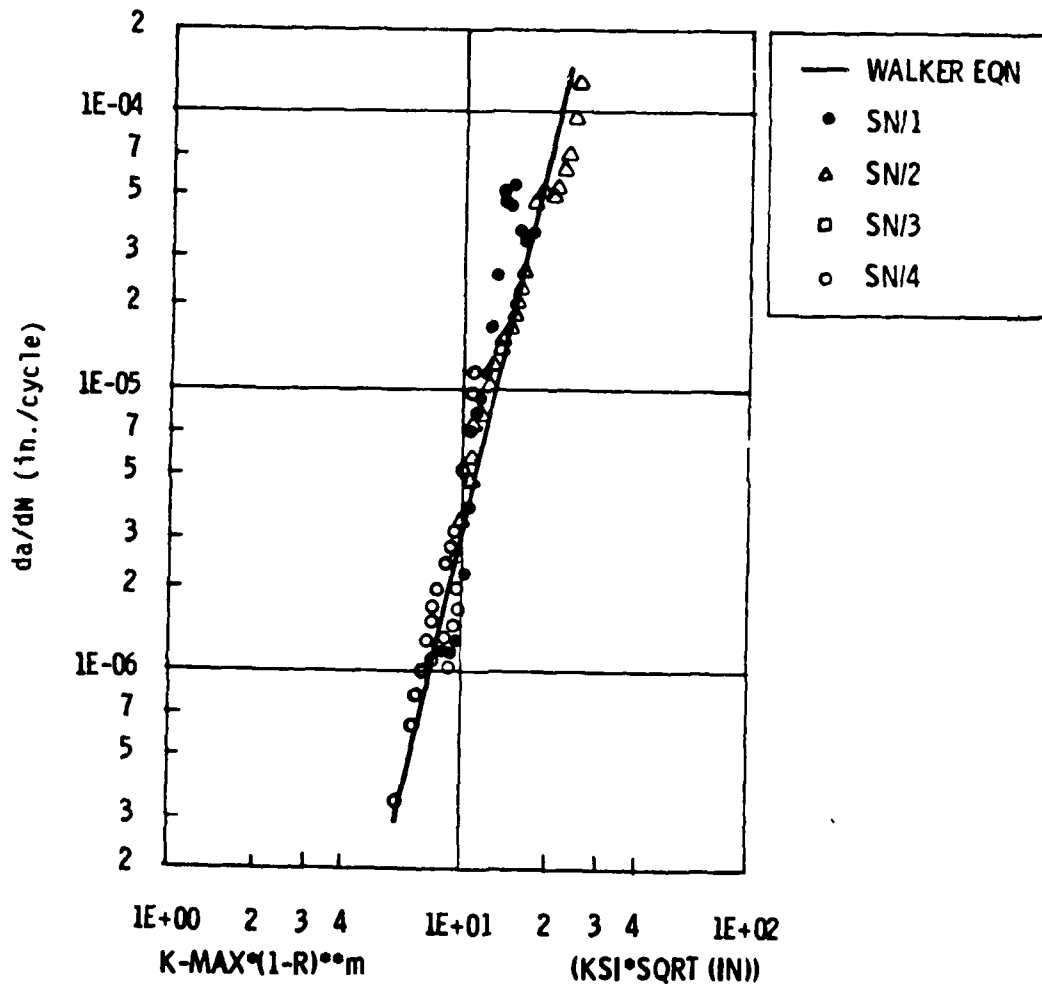


Figure 3.4-4. Constant Amplitude Crack Growth Rate for 2024-T3511 Angle $R \geq 0$

7075-T6 SHEET
 CT160KAB49-11, 0.16" THICK, $R \geq 0$
 WALKER CNSTS: $c = 1.3579E-07$, $m=0.5$, $n=1.9752$

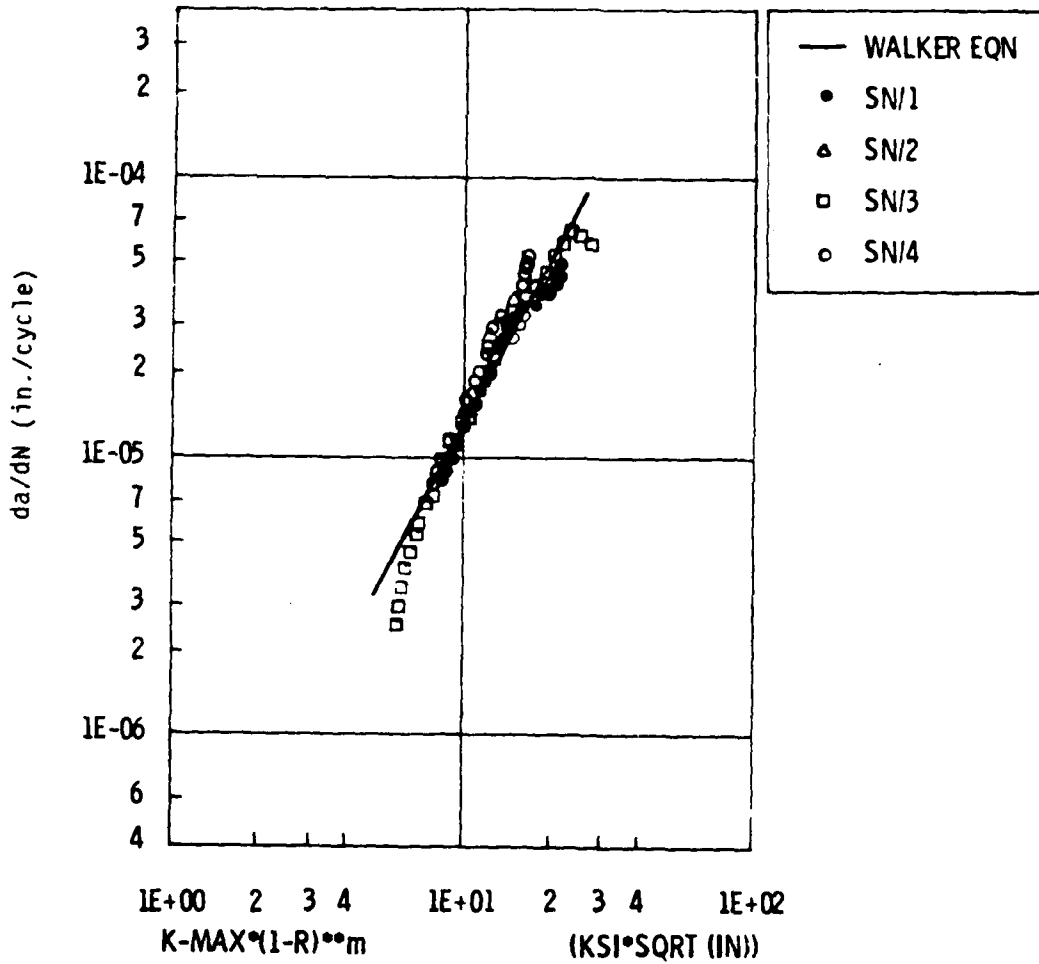


Figure 3.4-5. Constant Amplitude Crack Growth Rate for 7075-T6 Sheet $R \geq 0$

7075-T651 PLATE
 GT160DAB49-13, 0.31" THICK, R \geq 0
 WALKER CNSTS: $c = 1.054E-08$, $m = 0.5$, $n = 2.8033$

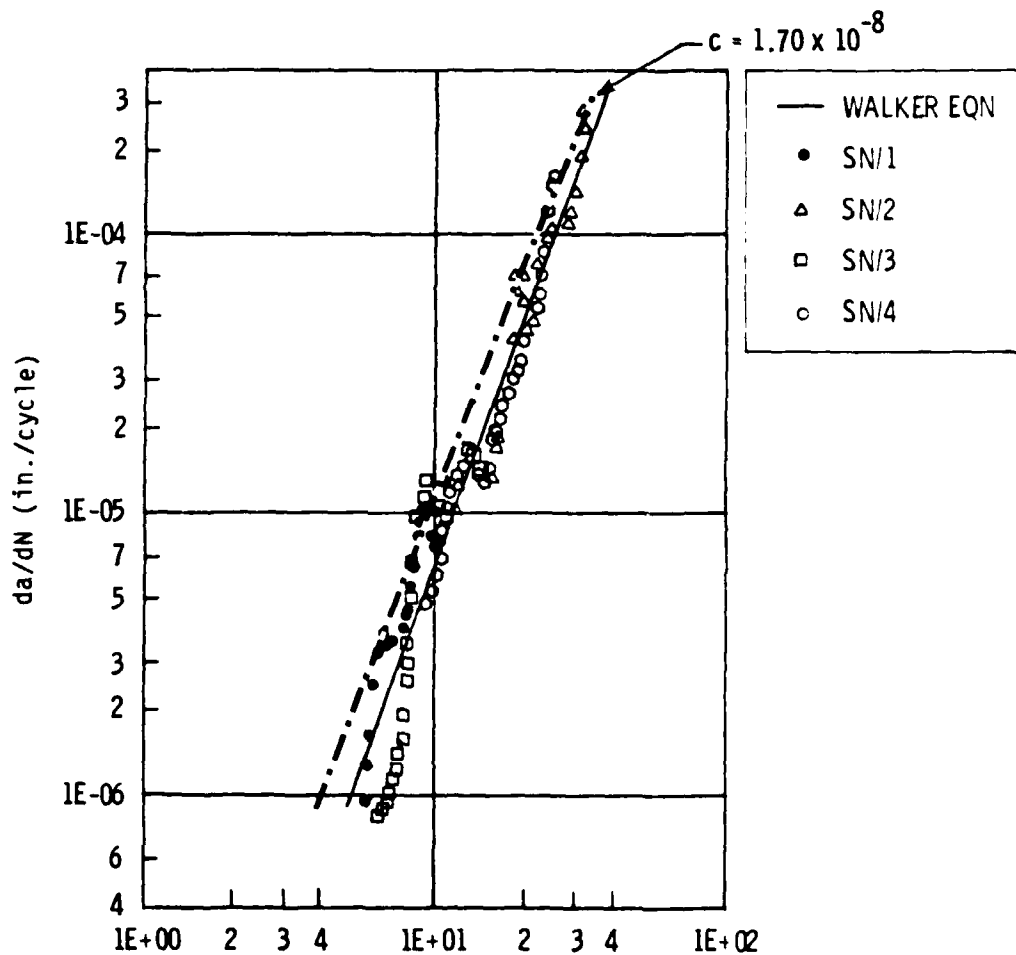


Figure 3.4-6. Constant Amplitude Crack Growth Rate for 7075-T651 Plate R \geq 0

7075-T6511 TEE
 GT160KAB49-15, 0.30" THICK, R≥0
 WALKER CNSTS: c = 9.7285E-08, m = .55, n = 2.0369

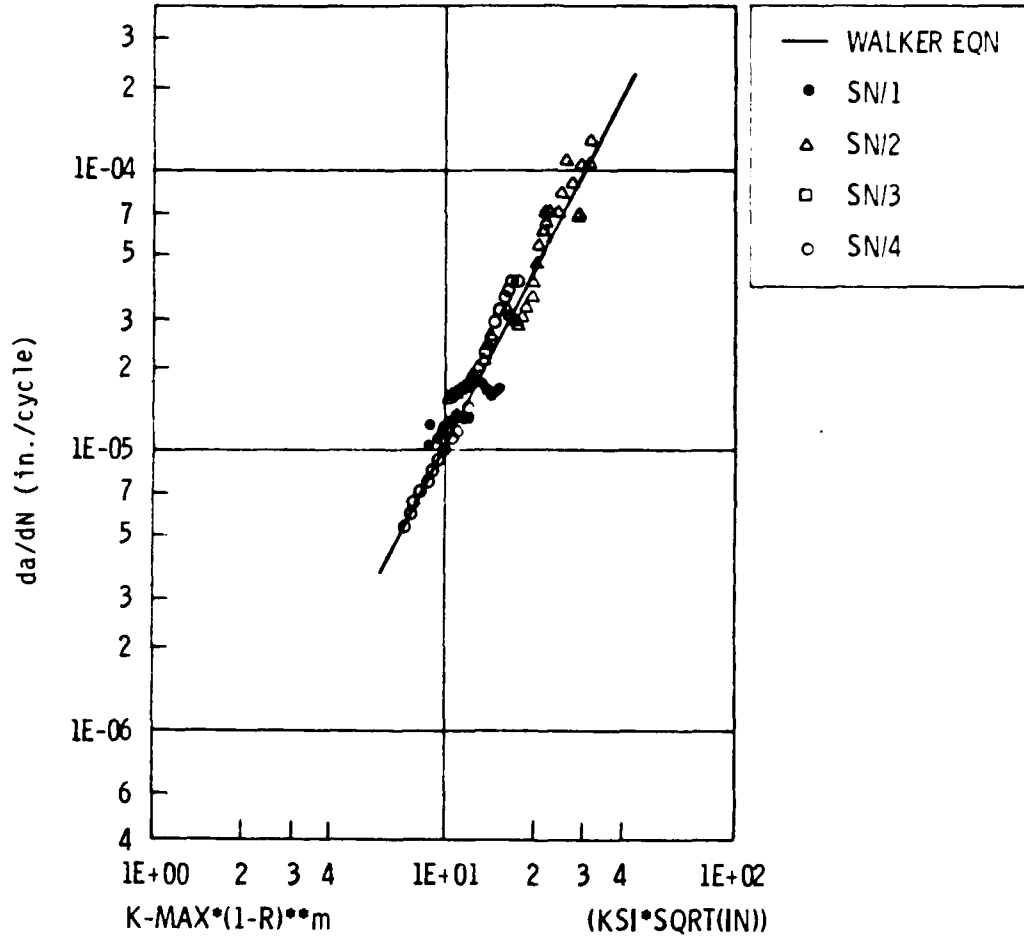


Figure 3.4-7. Constant Amplitude Crack Growth Rate for 7075-T6511 Tee R≥0

7075-T6511 ANGLE
 GT160KAB49-17, 0.31" THICK, $R \geq 0$
 WALKER CNSTS: $c = 1.9047E-08$, $m = 0.5$, $n = 2.6640$

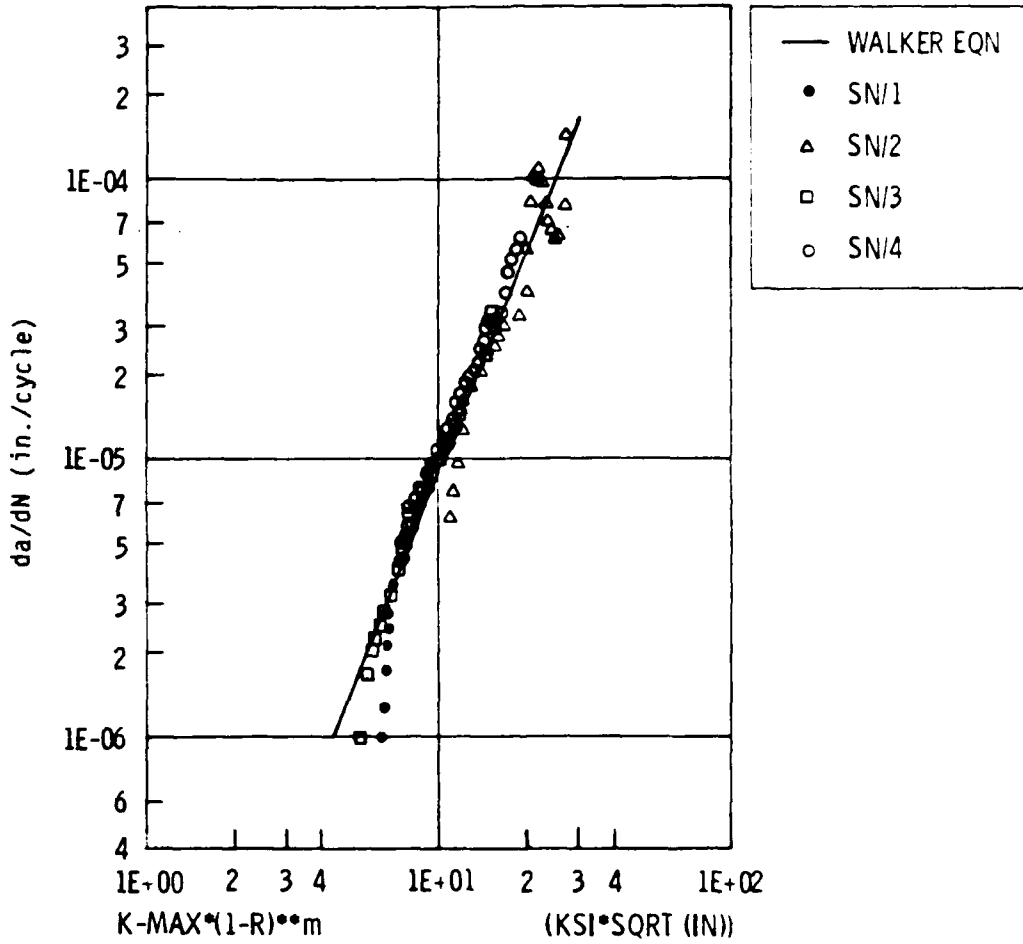


Figure 3.4-8. Constant Amplitude Crack Growth Rate for 7075-T6511 Angle $R \geq 0$

2024-T3 SHEET
 GT160KAB49-21, 0.19" THICK, R<0
 WALKER CNSTS: $c = 6.2126E-09$, $m = 0.0$, $n = 2.9783$

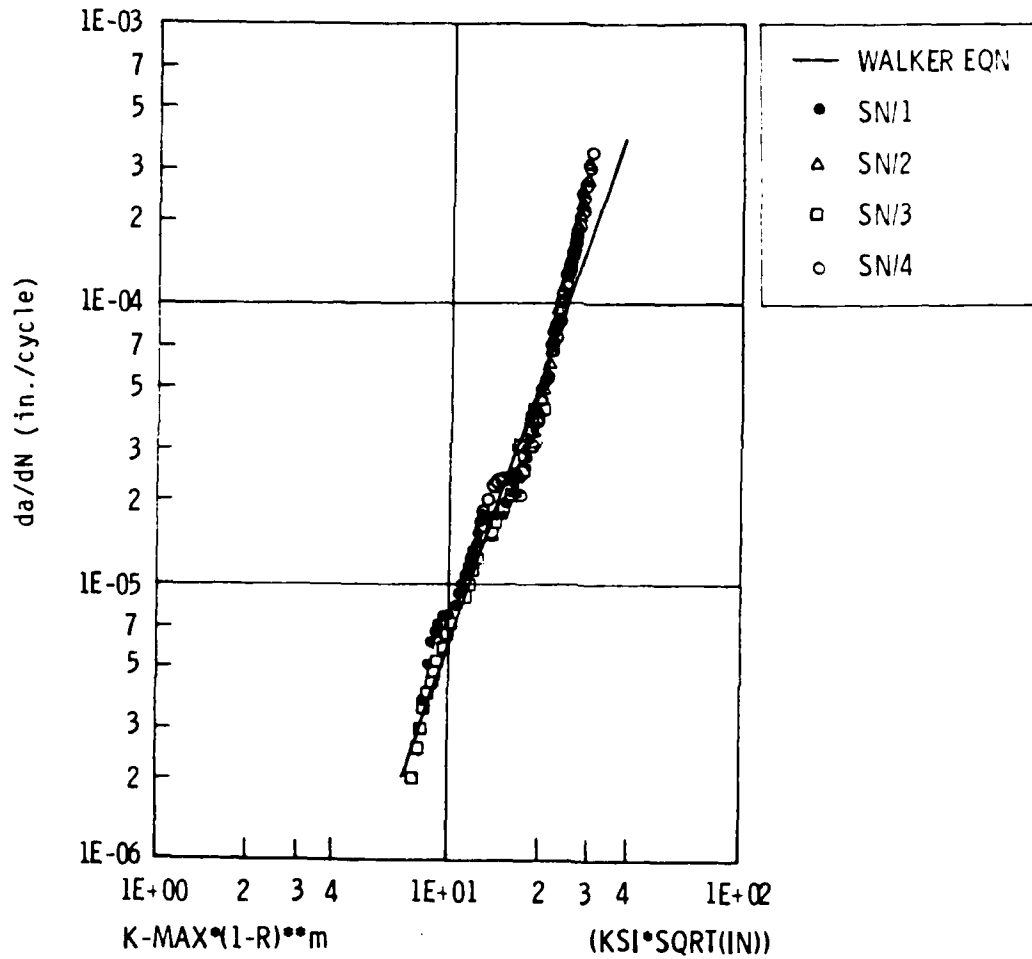


Figure 3.4-9. Constant Amplitude Crack Growth Rate for 2024-T3 Sheet R<0

2024-T351 PLATE
 GT160KAB49-23, 0.25" THICK, R<0
 WALKER CNSTS: $c = 4.5865E-08$, $m = 0.0$, $n = 2.2338$

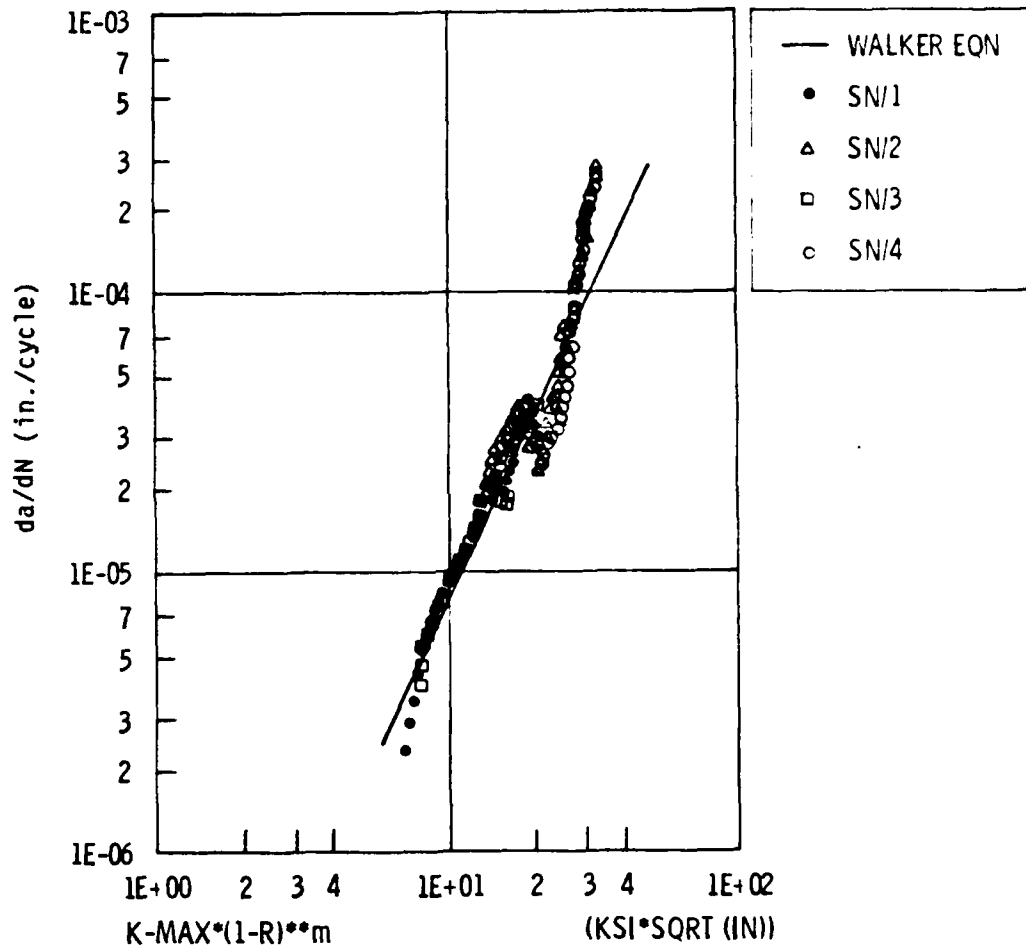


Figure 3.4-10. Constant Amplitude Crack Growth Rate for 2024-T351 Plate R<0

2024-T3511 TEE
 GT160KAB49-25, 0.19" THICK, R<0
 WALKER CNSTS: $c = 2.3033E-09$, $m = 1.0$, $n = 3.1154$

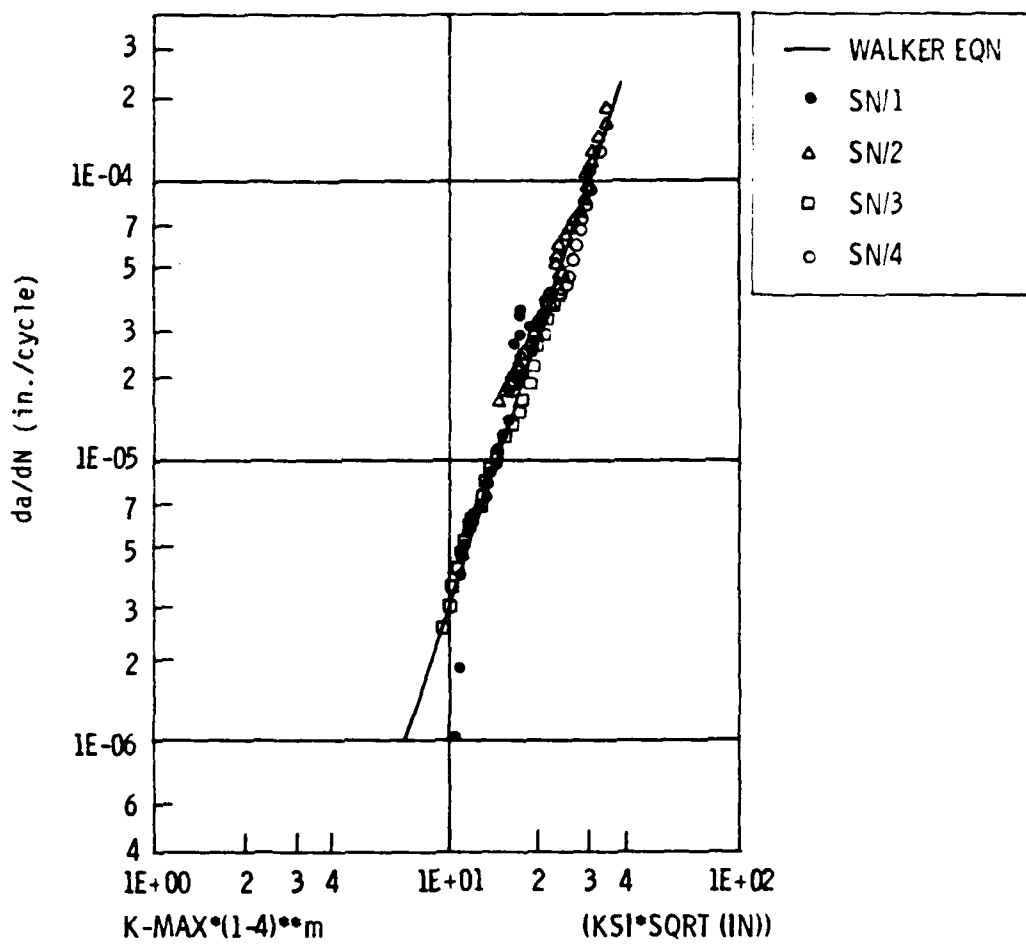


Figure 3.4-11. Constant Amplitude Crack Growth Rate for 2024-T3511 Tee $R < 0$

2024-T3511 ANGLE
 GT160KAB49-27, 0.25" THICK, R < 0
 WALKER CNSTS: $c = 4.3322E-11$, $m = 1.0$, $n = 4.0093$

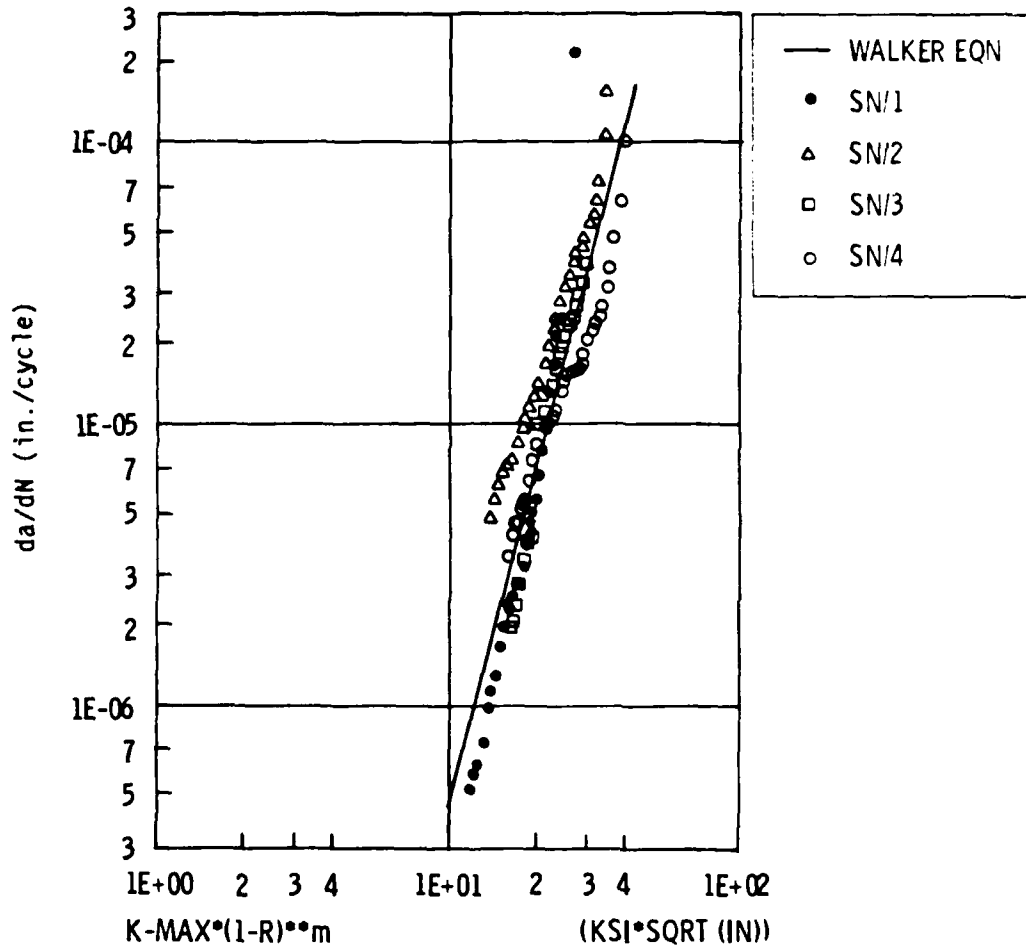


Figure 3.4-12. Constant Amplitude Crack Growth Rate for 2024-T3511 Angle R < 0

7075-T6 SHEET
 GT160KAB49-31, 0.16" THICK, R<0
 WALKER CNSTS: $c = 1.0654E-07$, $m = 0.0$, $n = 2.0950$

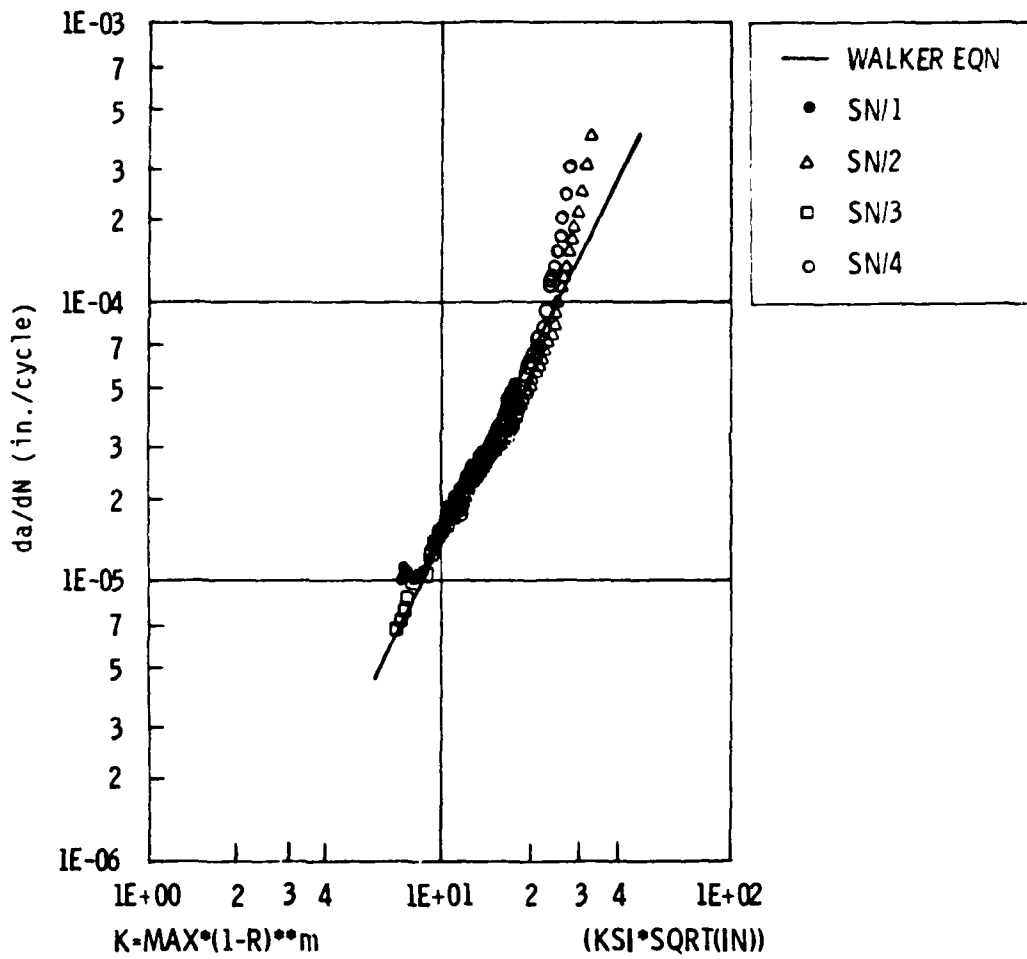


Figure 3.4-13. Constant Amplitude Crack Growth Rate for 7075-T6 Angle R<0

7075-T651 PLATE
 GT160KAB49-33, 0.31" THICK, R<0
 WALKER CNSTS: c = 2.6409E-08, m = 0.0, n = 2.4962

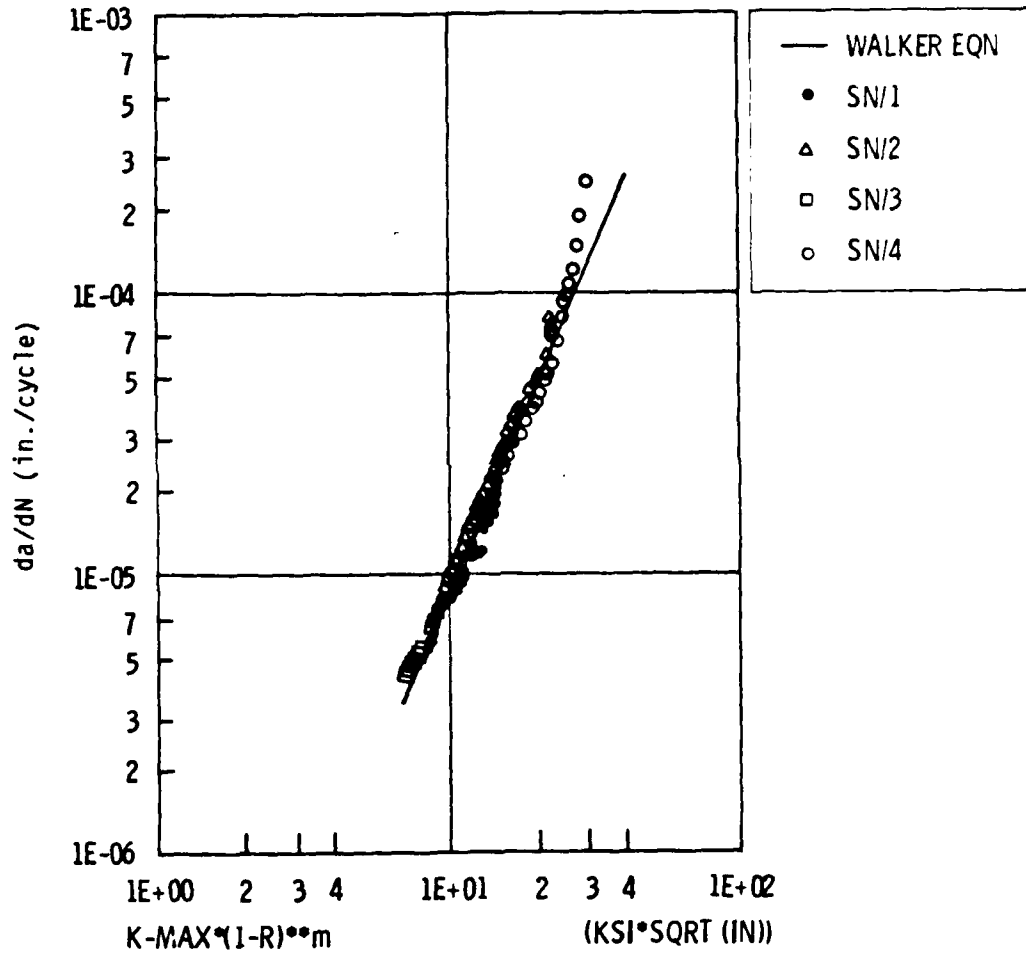


Figure 3.4-14. Constant Amplitude Crack Growth Rate for 7075-T651 Plate R<0

7075-T6511 TEE
 GT160KAB49-35, 0.30" THICK, R<0
 WALKER CNSTS: $c = 5.8669E-08$, $m = 0.0$, $n = 2.4602$

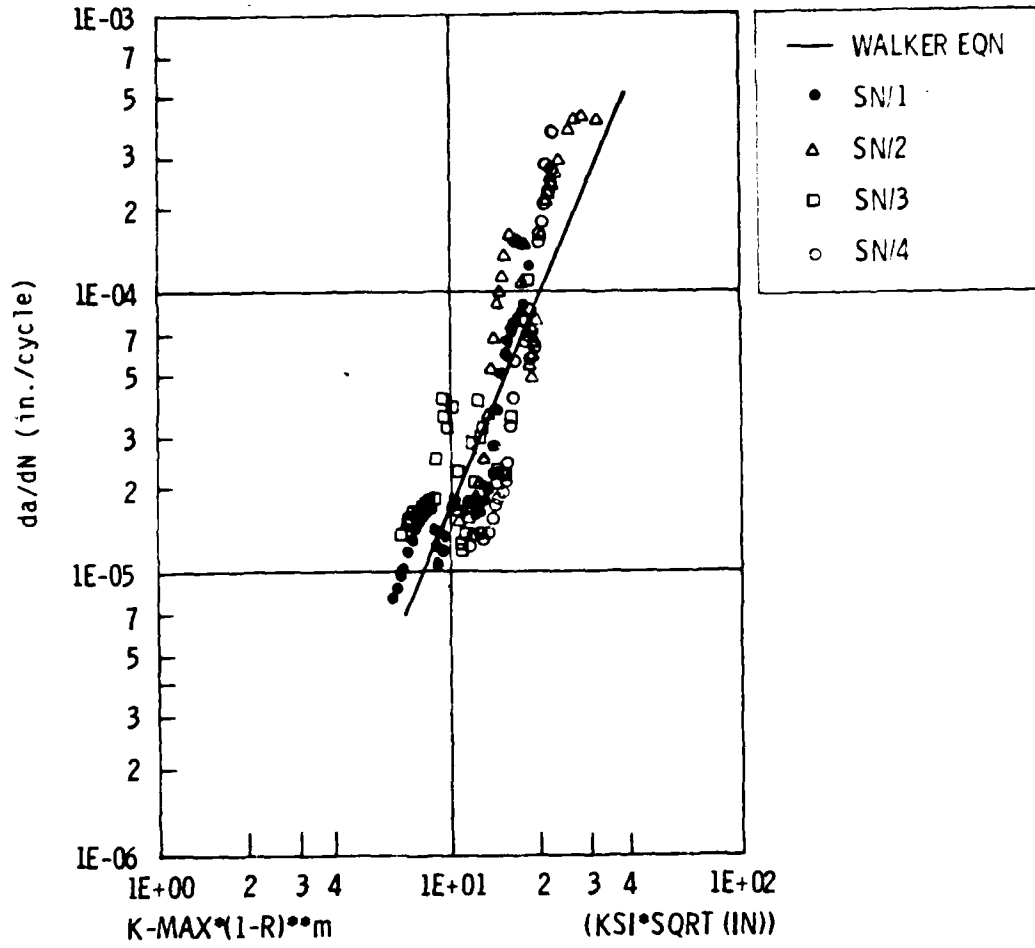


Figure 3.4-15. Constant Amplitude Crack Growth Rate for 7075-T6511 Tee R<0

7075-T6511 ANGLE
 GT160KAB49-37, 0.31" THICK, R<0
 WALKER CNSTS: $c = 3.1758E-08$, $m = 0.0$, $n = 2.5814$

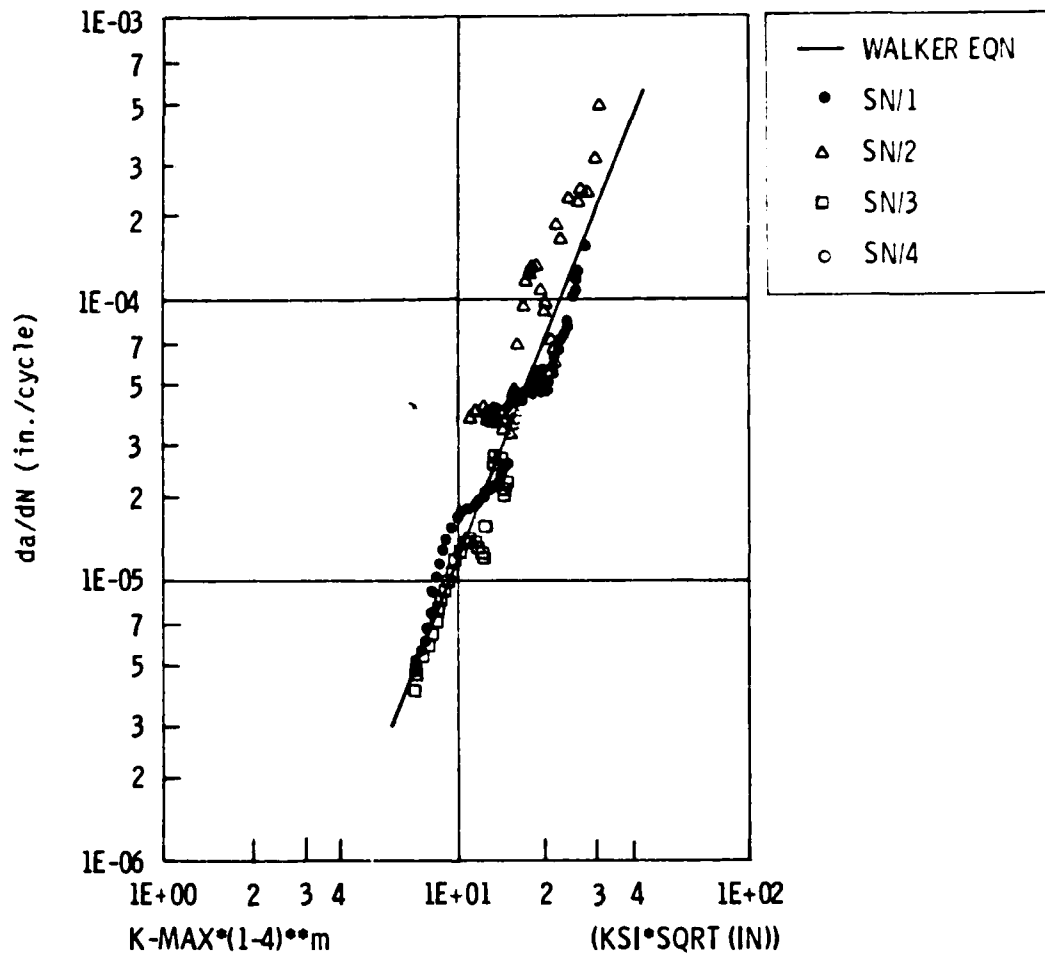


Figure 3.4-16. Constant Amplitude Crack Growth Rate for 7075-T6511 Angle R<0

4.0 STRUCTURAL TEST PROGRAM

The purpose of the structural test program was to assess the analytical capabilities for predicting crack growth lives using two methods, namely, the standard crack growth method, 'Method 1' and the combined method, 'Method 2'. It also provides a guideline for selecting critical crack locations on structural element typical to airframe construction. The results of the tests and analyses are used to provide an assessment of the current damage tolerance criterion defined in MIL-A-83444.

The structural test program included the testing of thirty-six (36) lap-joint specimens and thirty-six (36) stringer-reinforced specimens as listed in Table 4-1. The specimens were subjected to flight-by-flight randomized loading spectra derived from fighter/trainer (A-10A) and bomber/cargo (AMAVS) type aircrafts, and to a constant amplitude loading spectrum (C.A.). Listings of the loading spectra are provided in Volume IV of the report. All specimens contained an initially induced fatigue crack of $a_0 = 0.050$ inch. In order to simulate this fatigue crack, flaws were initially introduced by means of a sawcut, followed by a constant amplitude cycling until the desired flaw size was achieved.

TABLE 4-1. STRUCTURAL TEST PROGRAM

Specimen Configuration	No. of Specimen	Material	Applied Spectrum Loading
Lap-Joint Single-Shear	6	2024-T3XX	C.A.
Lap-Joint Single-Shear	6	2024-T3XX	A-10A
Lap-Joint Single-Shear	6	7075-T6XX	AMAVS
Lap-Joint Double-Shear	6	2024-T3XX	C.A.
Lap-Joint Double-Shear	6	2024-T3XX	A-10A
Lap-Joint Double-Shear	6	7075-T6XX	AMAVS
Skin/Stringer 'TEE' Center	4	2024-T3XX	C.A.
Skin/Stringer 'TEE' Center	4	2024-T3XX	A-10A
Skin/Stringer 'TEE' Center	4	2024-T3XX	C.A.
Skin/Stringer 'L' Edge	4	2024-T3XX	A-10A
Skin/Stringer 'L' Edge	4	2024-T3XX	C.A.
Skin/Stringer 'L' Edge	4	2024-T3XX	A-10A
Skin/Stringer 'L' Edge	4	7075-T6XX	AMAVS
Skin/Stringer Split Skin 'TEE'	4	7075-T6XX	AMAVS

The analytical predictions were performed using the 'DAMGRO' computer program (Ref. Section 2.0). The loading spectra for the analyses were simplified to a block loadings. Listings of the analytical loading spectra are provided in Appendix A.

4.1 LAP-JOINT SPECIMEN STRUCTURAL TEST PROGRAM

The lap-joint specimen structural test program included three (3) groups of specimens as listed below:

- a. Base line specimen configuration was without fastener interference fit, clamp-up, and sealant.
- b. Specimens containing fastener clamp-up and hole interference fit.
- c. Specimens containing clamp-up, interference fit, and sealant.

Total of thirty-six (36) specimens were tested covering two (2) types of specimen splice joint configurations; the single-shear lap-joint and the double-shear lap-joint specimens. The specimens were subjected to randomized flight-by-flight spectra and constant amplitude loading. The specimens contained an initial flaw of 0.050 inch common to the splice plates and the skin.

4.1.1 Single-Shear Lap-Joint Specimens Test Program

A total of eighteen (18) single-shear lap-joint specimens were tested. The specimen configuration consisted of split skin parts spliced at mid section through two rows of Hi-Loks. The splice was made from a plate and extruded tee sections. A typical specimen photo is shown in Figure 4.1.1-1. All specimens contained an initial flaw located at the mid hole of the 1st row of attachments common to the splice plate and the skin. The flaw size was 0.050 inch corner crack, located close to the faying surface. The flaw was introduced by mean of a saw-cut followed by application of constant amplitude loading. The introduction of the flaw was made prior to the specimen assembly and drilling of the remaining holes. It should be noted that the initial flaw always existed at a fastener hole with clearance fit.

The specimens were subjected to constant amplitude loading with a maximum stress level of 17.0 Ksi at R=0.10, and to A-10A and AMAVS loading spectra with maximum stress level of 37.75 Ksi. The test program coverage is provided in Table 4.1.1-1.

In performing the analytical prediction, various parameters were used, such as load transfer fraction through the cracked hole and the adjacent holes. Also, the friction stress through the faying surface and the hole stress concentration due to pin deflection were used. All these parameters were evaluated during Phase 1 of the program and presented in Volume II of the report. For single-shear lap-joint specimens the load transfer used is given by:

$$P = 0.08699 - 0.00150 (a/R) \qquad 0 \leq a/R \leq 6 \qquad (4.1.1)$$

$$P = 0.07745 + 0.00072 (a/R) \qquad 8 \leq a/R \leq 14 \qquad (4.1.2)$$

The load transfer at the adjacent holes to the cracked hole, is given by:

$$P = 0.08805 + 0.00015 (a/R) \qquad 0 \leq a/R \leq 6 \qquad (4.1.3)$$

$$P = 0.07821 - 0.00501 (a/R) \qquad 8 \leq a/R \leq 14 \qquad (4.1.4)$$

The faying surface frictional forces were determined using the equations previously derived and are listed in Volume II of the report. The values used were 3.8 Ksi and 3.1 Ksi for the 2024-T3XX and 7075-T6XX specimens, respectively.

The frictional forces induced by clamp-up was also determined during Phase 1 and are listed in Volume II of the report. They were determined to be 5.0 Ksi and 4.2 Ksi for the 2024-T3XX and 7075-T6XX specimens, respectively. Both the faying surface frictional forces and the clamp-up frictional forces were used in Method 2 only.

4.1.1.1 Analytical Prediction vs. Test Results of Single-Shear Lap-Joint Specimens.

The life predictions of the single-shear lap-joint specimens were accomplished using the computer program 'DAMGRO'. The predictions which were performed using "Method 1" and "Method 2" were correlated against the experimental data, as shown in Figures 4.1.1-2 through 4.1.1-19. A summary of predicted life vs. experimental life, and the corresponding standard deviation is shown in Tables 4.1.1-2 through 4.1.1-4 for specimens subjected to constant amplitude, A-10A and AMAVS loading spectra, respectively.

The life predictions obtained for the specimens which were subjected to a constant amplitude loading reflect conservative results for both Method 1 and Method 2. Since Method 1 did not account for fastener interference fit, clamp-up or sealant, the predicted lives are identical. Method 2 accounts for these parameters during the crack initiation phase. The test results indicate that life to failure was highest for specimens with interference fit and clamp-up but without presence of sealant. The same trend occurred with Method 2 predictions. However, the overall standard deviation is about the same for Method 1 and Method 2, being 35%.

The life predictions for specimens subjected to A-10A loading spectra is summarized in Table 4.1.1-3. The result indicate better accuracy for Method 1 than Method 2. Again Group B of the test seems to have the highest number of cycles to failure. The overall standard deviation for Method 1 is 32.7% against 42.6% for Method 2. For Group A, the life prediction using Method 2 is off by a factor of 3. For Group A specimens the lives predicted using Method 2 analysis were more conservative and less accurate than Method 1 predictions. The reason being, Method 2 predicts early crack initiation at the diagonally opposite side of the cracked hole, causing two (2) cracks at the same hole to propagate simultaneously. Method 1 assumption of secondary flaw of 0.005 in. at adjacent holes is not as severe as two (2) cracks at the same hole. This phenomenon is not the same when using some of the benefits due to specimens configuration for Groups B and C.

The life predictions for specimens subjected to AMAVS loading spectrum is summarized in Table 4.1.1-4. The results were unconservative both for Method 1 and Method 2. The test results were consistent with specimens subjected to C.A. or A-10A loading spectra, indicating highest life for Group B. In this series of specimens, Method 2 yielded closer correlation to test, but was on the unconservative side. Although the constant amplitude da/dN curve for 7075-T6XX plate was corrected (Ref. Figure 3.4-6), the prediction was not accurate. It is therefore, concluded that the retardation model (Modified Willenborg) was not adequate to account for the AMAVS spectrum.

The C group test results indicate that the presence of sealant in the faying surface tends to reduce the fatigue life, while both the B and C group results indicate that interference fit tends to increase the fatigue life.

TABLE 4.1.1-1. SINGLE-SHEAR LAP-JOINT SPECIMENS TEST PROGRAM

GROUP	MATERIAL FORM	SPECIMEN CONFIGURATION			SPECIMEN ID	APPLIED SPECTRUM	MAXIMUM STRESS (KSI)
		INTERFER	CLAMP-UP	SEALANT			
A	2024-T3XX	No	No	No	LJ- 1, LJ- 2	C.A.	17.0
	2024-T3XX	No	No	No	LJ- 3, LJ- 4	A-10A	37.75
	7075-T6XX	No	No	No	LJ-25, LJ-26	AMAVS	37.75
B	2024-T3XX	Yes	Yes	No	LJ- 5, LJ- 6	C.A.	17.0
	2024-T3XX	Yes	Yes	No	LJ- 7, LJ- 8	A-10A	37.75
	7075-T6XX	Yes	Yes	No	LJ-27, LJ-28	AMAVS	37.75
C	2024-T3XX	Yes	Yes	Yes	LJ- 9, LJ-10	C.A.	17.0
	2024-T3XX	Yes	Yes	Yes	LJ-11, LJ-12	A-10A	37.75
	7075-T6XX	Yes	Yes	Yes	LJ-29, LJ-30	AMAVS	37.75

TABLE 4.1.1-2. ANALYTICAL VS. EXPERIMENTAL CRACK GROWTH FOR SINGLE-SHEAR LAP-JOINT SPECIMENS SUBJECTED TO CONSTANT AMPLITUDE LOADING SPECTRUM

GROUP (REF. TABLE 4.1.1-1)	MAXIMUM* STRESS (KSI)	AVERAGE** TEST RESULTS TO FAILURE (CYCLES)	ANALYTICAL PREDICTIONS			
			METHOD 1		METHOD 2	
			LIFE (CYCLES)	% DEV	LIFE (CYCLES)	% DEV
A	17.0	45,250	40,730	9.9	30,555	32.5
B	17.0	96,700	40,730	46.2	67,724	30.0
C	17.0	79,105	40,730	49.2	41,289	41.8
EXPERIMENTAL/ANALYTICAL AVERAGE DEV.				35.1	34.7	

*R=0.10

**Average of two specimens

TABLE 4.1.1-3. ANALYTICAL VS. EXPERIMENTAL CRACK GROWTH FOR SINGLE-SHEAR LAP-JOINT SPECIMENS SUBJECTED TO A-10A LOADING SPECTRUM

GROUP (REF. TABLE 4.1.1-1)	MAXIMUM STRESS (KSI)	AVERAGE* TEST RESULTS TO FAILURE (CYCLES)	ANALYTICAL PREDICTIONS			
			METHOD 1		METHOD 2	
			LIFE (CYCLES)	% DEV	LIFE (CYCLES)	% DEV
A	37.75	44,594	24,408	45.2	15,087	66.2
B	37.75	59,798	24,408	-12.8	53,138	11.1
C	37.75	41,365	24,408	40.1	20,473	50.5
EXPERIMENTAL/ANALYTICAL AVERAGE DEV.				32.7	42.6	

* Average of two specimens

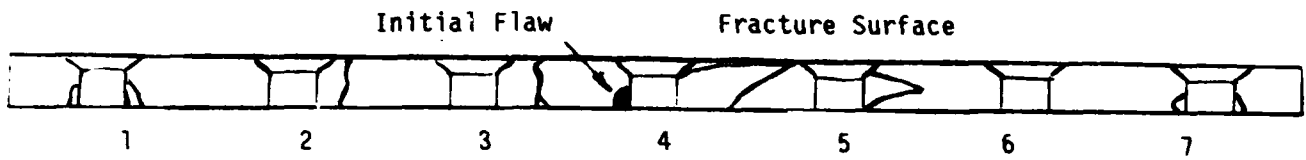
TABLE 4.1.1-4. ANALYTICAL VS. EXPERIMENTAL CRACK GROWTH FOR SINGLE-SHEAR LAP-JOINT SPECIMENS SUBJECTED TO AMAVS LOADING SPECTRUM

GROUP (REF. TABLE 4.1.1-1)	MAXIMUM STRESS (KSI)	AVERAGE* TEST RESULTS TO FAILURE (CYCLES)	ANALYTICAL PREDICTIONS			
			METHOD 1		METHOD 2	
			LIFE (CYCLES)	% DEV	LIFE (CYCLES)	% DEV
A	37.75	5,387	22,189	-310.0	9,132	- 69.5
B	37.75	11,105	22,189	- 99.8	23,343	-110.0
C	37.75	9,980	22,189	-125.0	9,944	0.0
EXPERIMENTAL/ANALYTICAL AVERAGE DEV.				-178.3		- 59.8

* Average of two specimens



Figure 4.1.1.1-1. Photo of Single-Shear Lap-Joint Specimen
Subsequent to Failure



SPECIMEN = LJ-1 (Ref. Table 4.1.1-1)
 MATERIAL = 2024-T3XX
 LOADING = C.A.
 TEST LIFE = 44,200 CYCLES
 METHOD 1 PREDICTED LIFE = 40,730 CYCLES
 METHOD 2 PREDICTED LIFE = 30,555 CYCLES

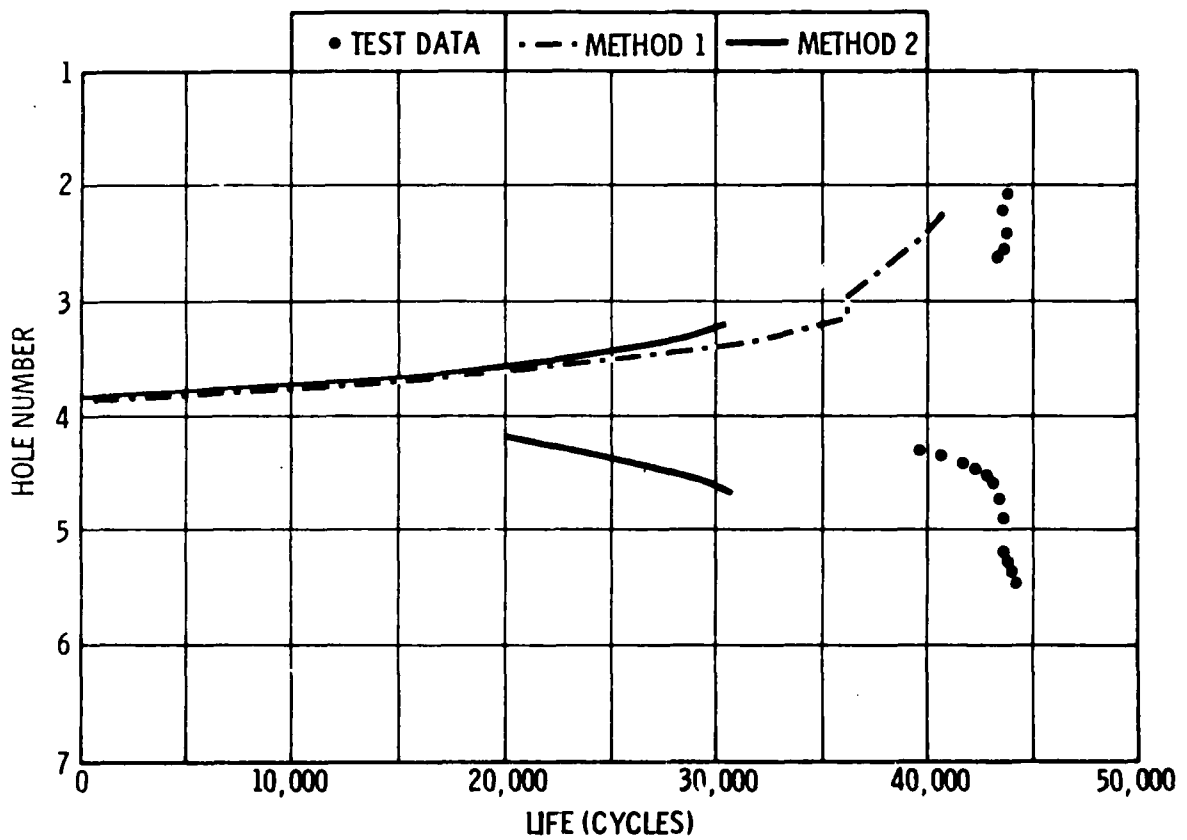
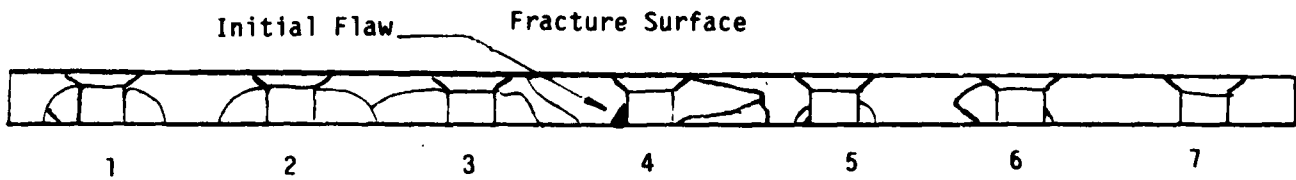


Figure 4.1.1-2. Crack Growth Diagram for Single-Shear Lap-Joint Specimen LJ-1



SPECIMEN = LJ-2 (Ref. Table 4.1.1-1)
 MATERIAL = 2024-T3XX
 LOADING = C.A.
 TEST LIFE = 46,300 CYCLES
 METHOD 1 PREDICTED LIFE = 40,730 CYCLES
 METHOD 2 PREDICTED LIFE = 30,555 CYCLES

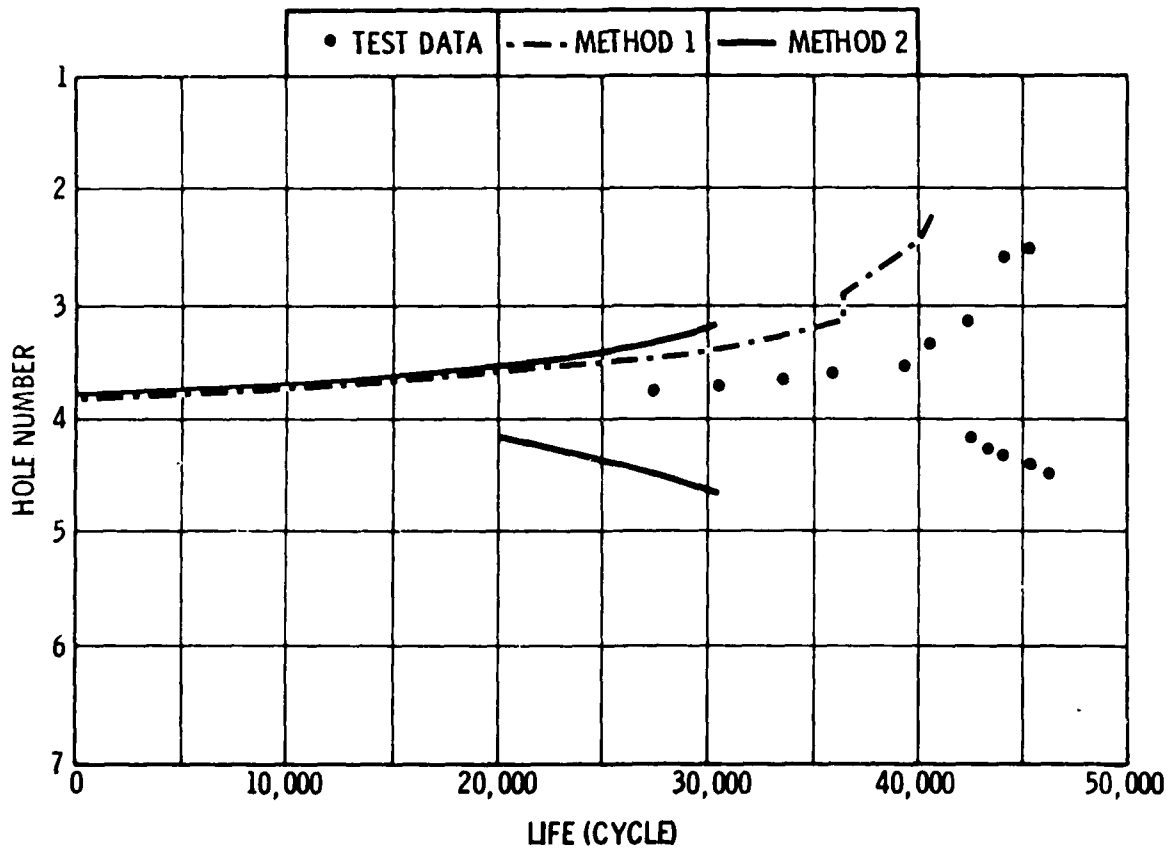
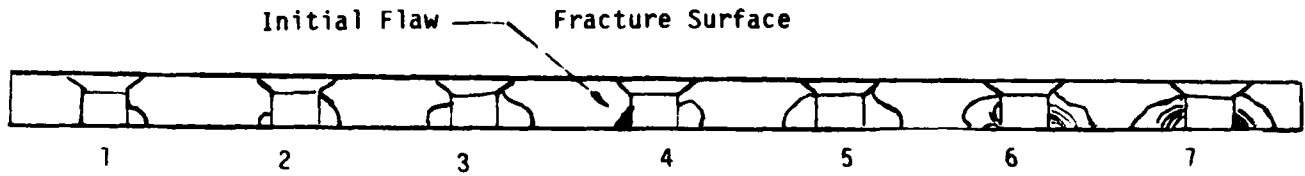


Figure 4.1.1-3. Crack Growth Diagram for Single-Shear Lap-Joint Specimen LJ-2



SPECIMEN = LJ-3 (Ref. Table 4.1.1-1)
 MATERIAL = 2024-T3XX
 LOADING = A-10A
 TEST LIFE = 42,086 CYCLES
 METHOD 1 PREDICTED LIFE = 24,408 CYCLES
 METHOD 2 PREDICTED LIFE = 15,087 CYCLES

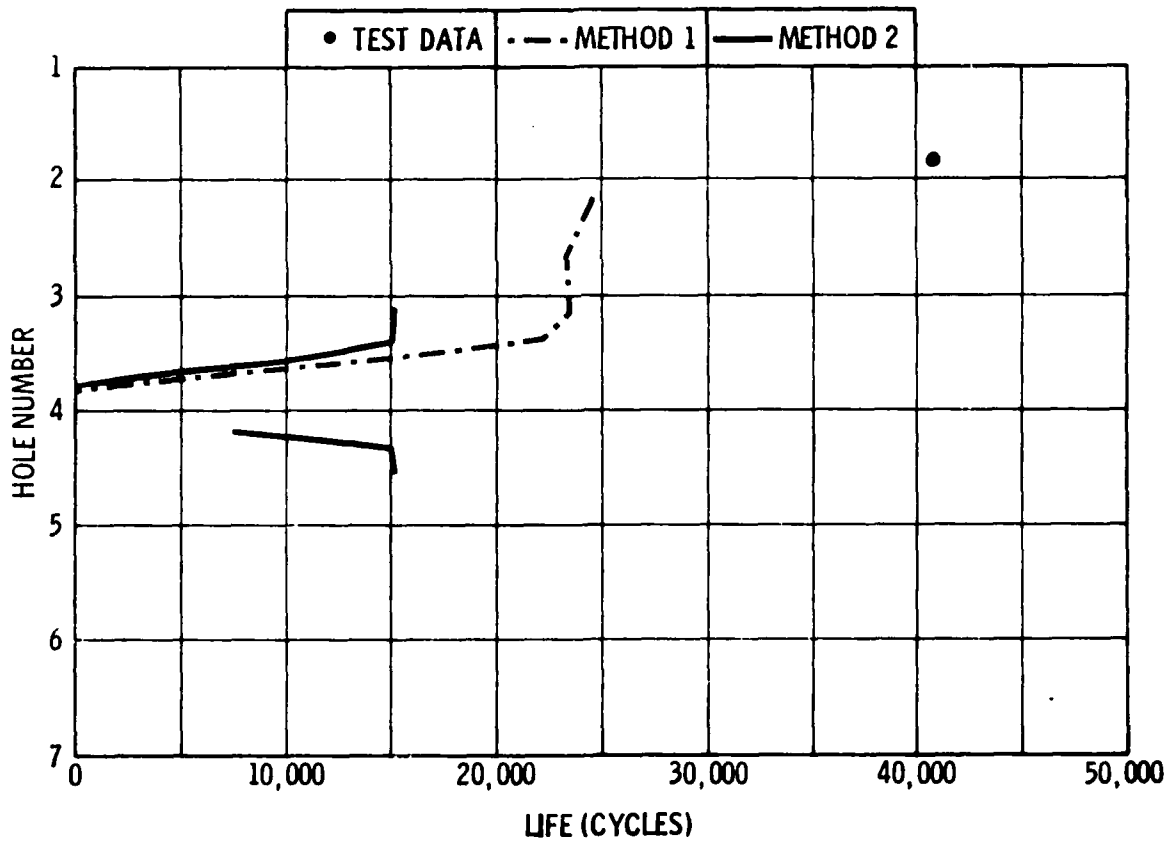
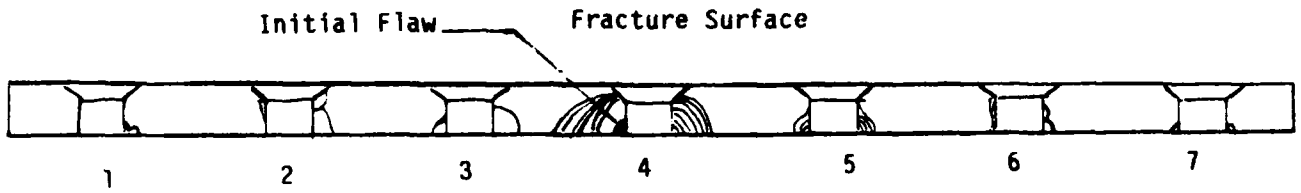


Figure 4.1.1-4. Crack Growth Diagram for Single-Shear Lap-Joint Specimen LJ-3



SPECIMEN = LJ-4 (Ref. Table 4.1.1-1)
 MATERIAL = 2024-T3XX
 LOADING = A-10A
 TEST LIFE = 47,102 CYCLES
 METHOD 1 PREDICTED LIFE = 24,408 CYCLES
 METHOD 2 PREDICTED LIFE = 15,087 CYCLES

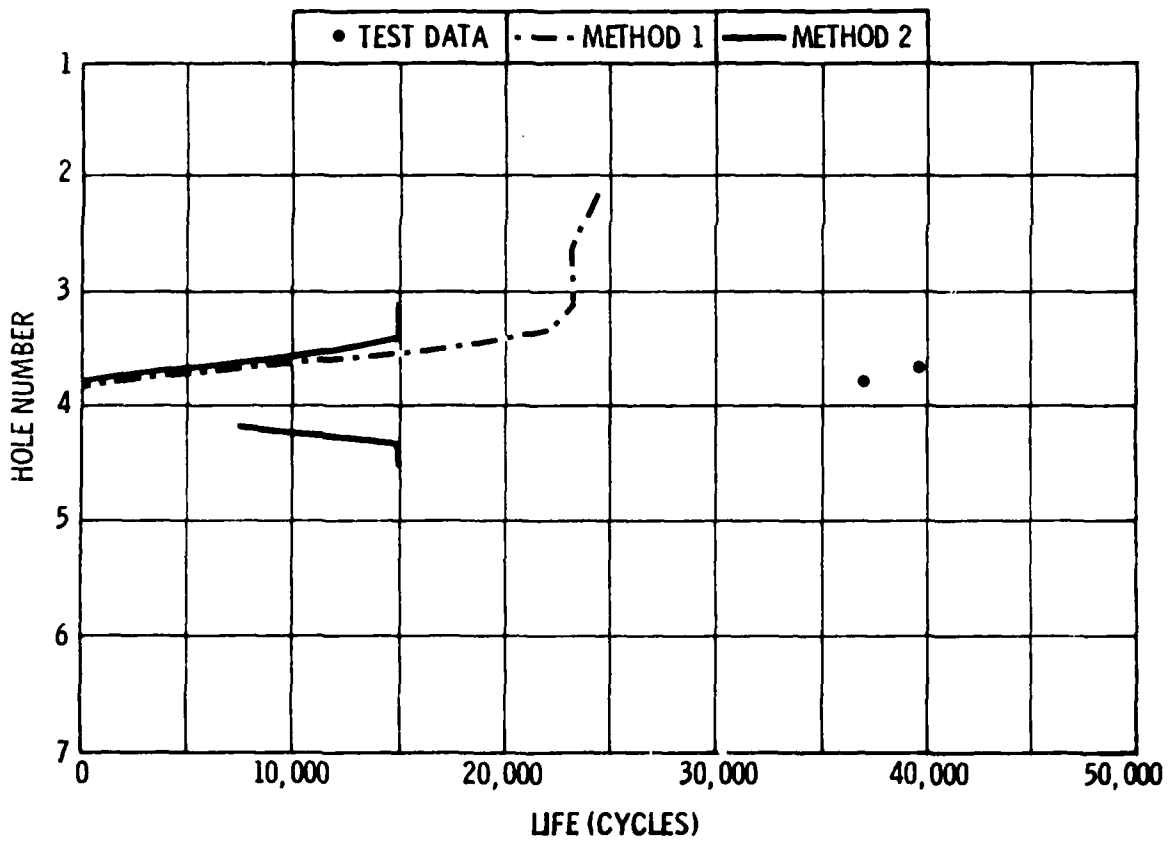
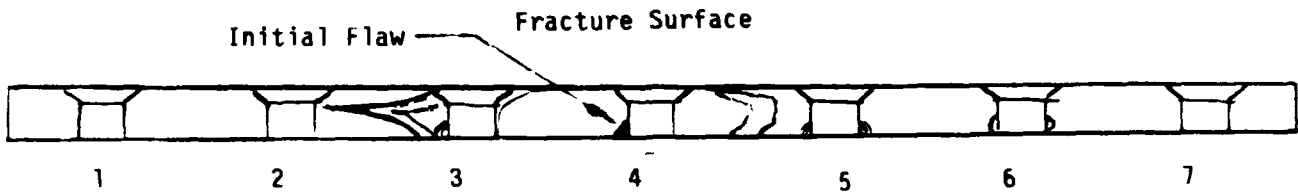


Figure 4.1.1-5. Crack Growth Diagram for Single-Shear Lap-Joint Specimen LJ-4



SPECIMEN = LJ-5 (Ref. Table 4.1.1-1)
 MATERIAL = 2024-T3XX
 LOADING = C.A.
 TEST LIFE = 94,700 CYCLES
 METHOD 1 PREDICTED LIFE = 40,730 CYCLES
 METHOD 2 PREDICTED LIFE = 67,724 CYCLES

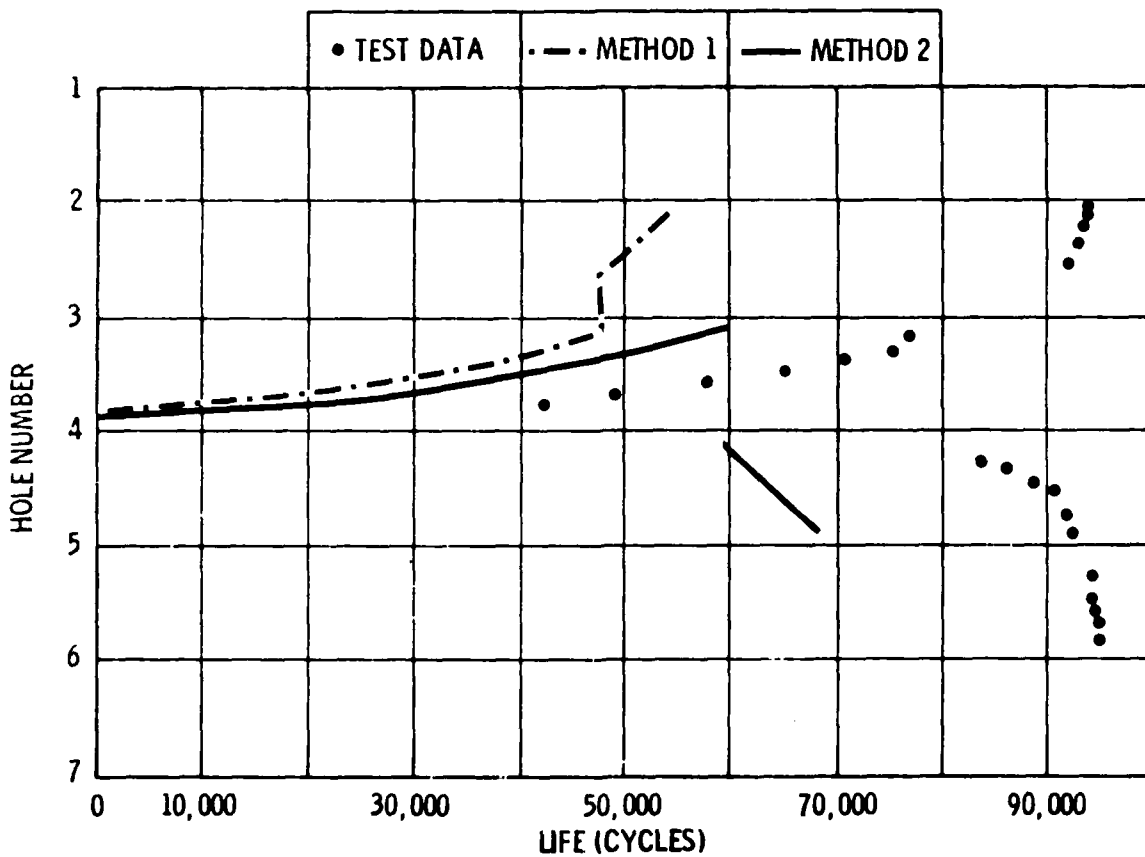
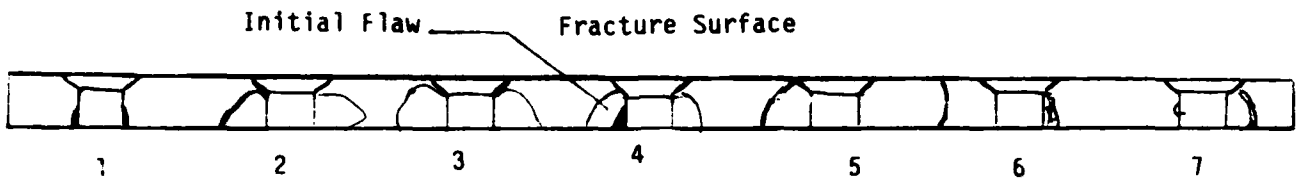


Figure 4.1.1-6. Crack Growth Diagram for Single-Shear Lap-Joint Specimen LJ-5



SPECIMEN = LJ-6 (Ref. Table 4.1.1-1)
 MATERIAL = 2024-T3XX
 LOADING = C.A.
 TEST LIFE = 98,700 CYCLES
 METHOD 1 PREDICTED LIFE = 40,730 CYCLES
 METHOD 2 PREDICTED LIFE = 67,724 CYCLES

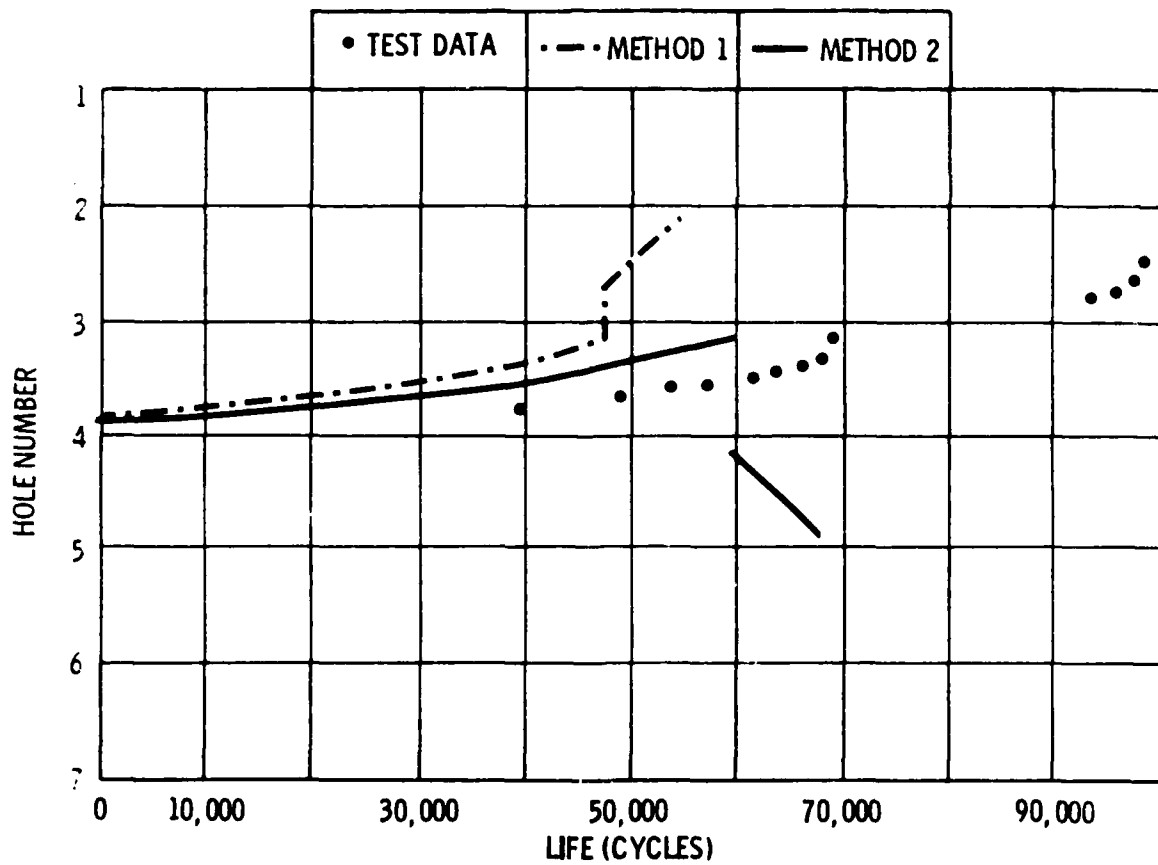
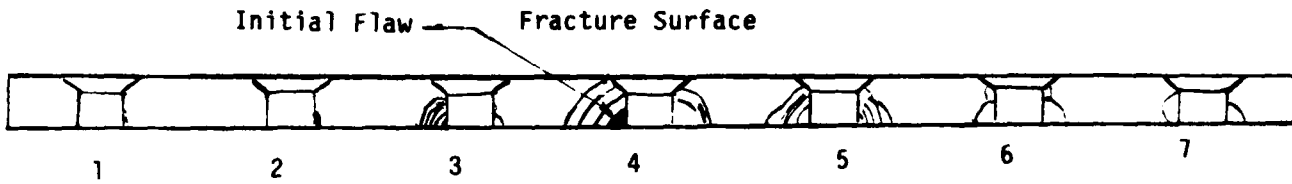


Figure 4.1.1-7. Crack Growth Diagram for Single-Shear Lap-Joint Specimen LJ-6



SPECIMEN = LJ-7 (Ref. Table 4.1.1-1)
 MATERIAL = 2024-T3XX
 LOADING = A-10A
 TEST LIFE = 59,598 CYCLES
 METHOD 1 PREDICTED LIFE = 24,408 CYCLES
 METHOD 2 PREDICTED LIFE = 53,138 CYCLES

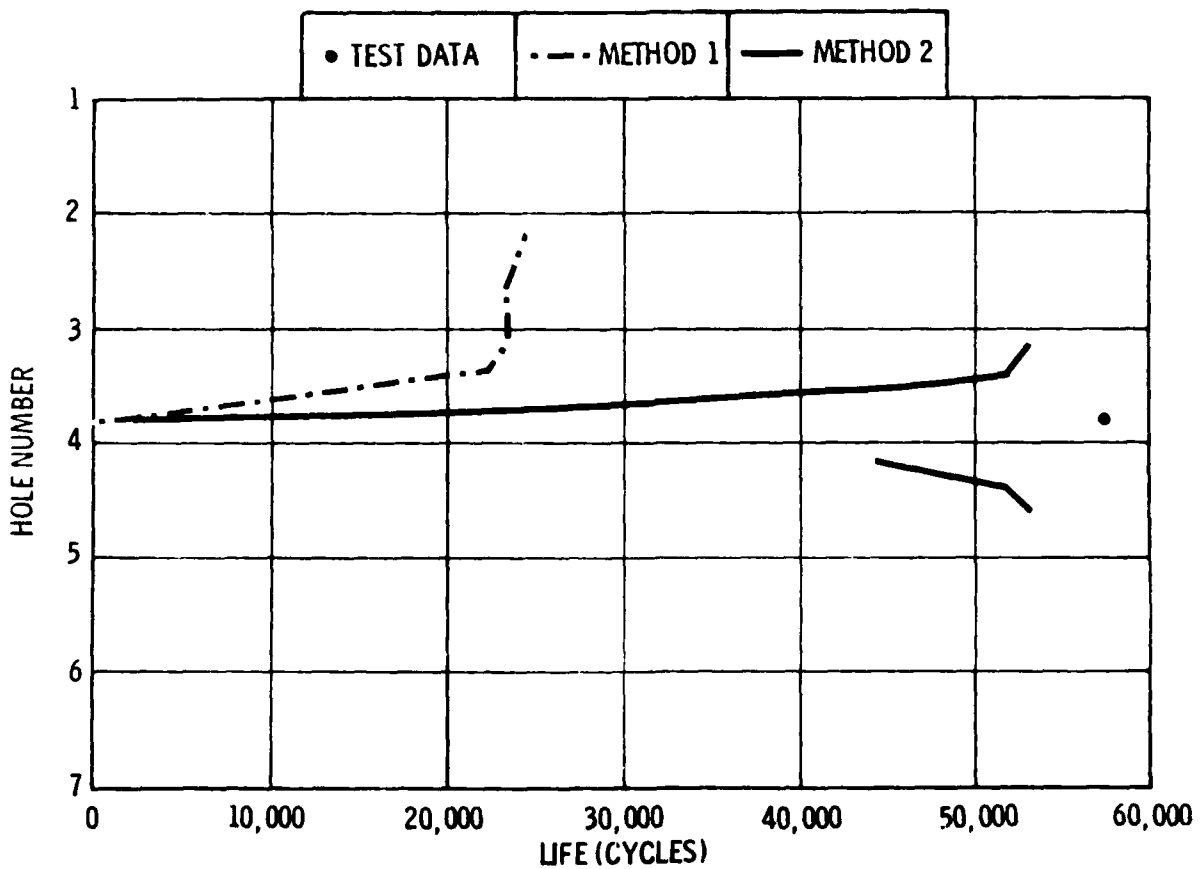
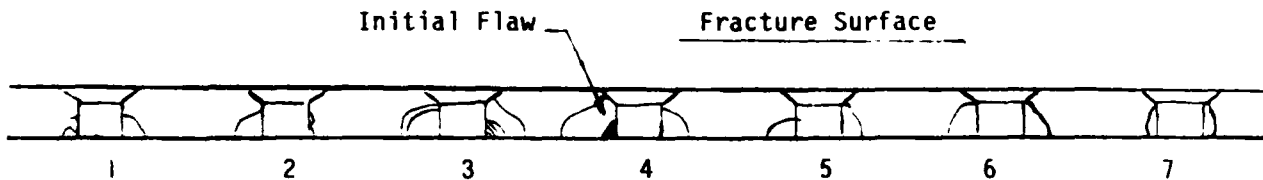


Figure 4.1.1-8. Crack Growth Diagram for Single-Shear Lap-Joint Specimen LJ-7



SPECIMEN = LJ-8 (Ref. Table 4.1.1-1)
 MATERIAL = 2024-T3XX
 LOADING = A-10A
 TEST LIFE = 59,638 CYCLES
 METHOD 1 PREDICTED LIFE = 24,408 CYCLES
 METHOD 2 PREDICTED LIFE = 53,138 CYCLES

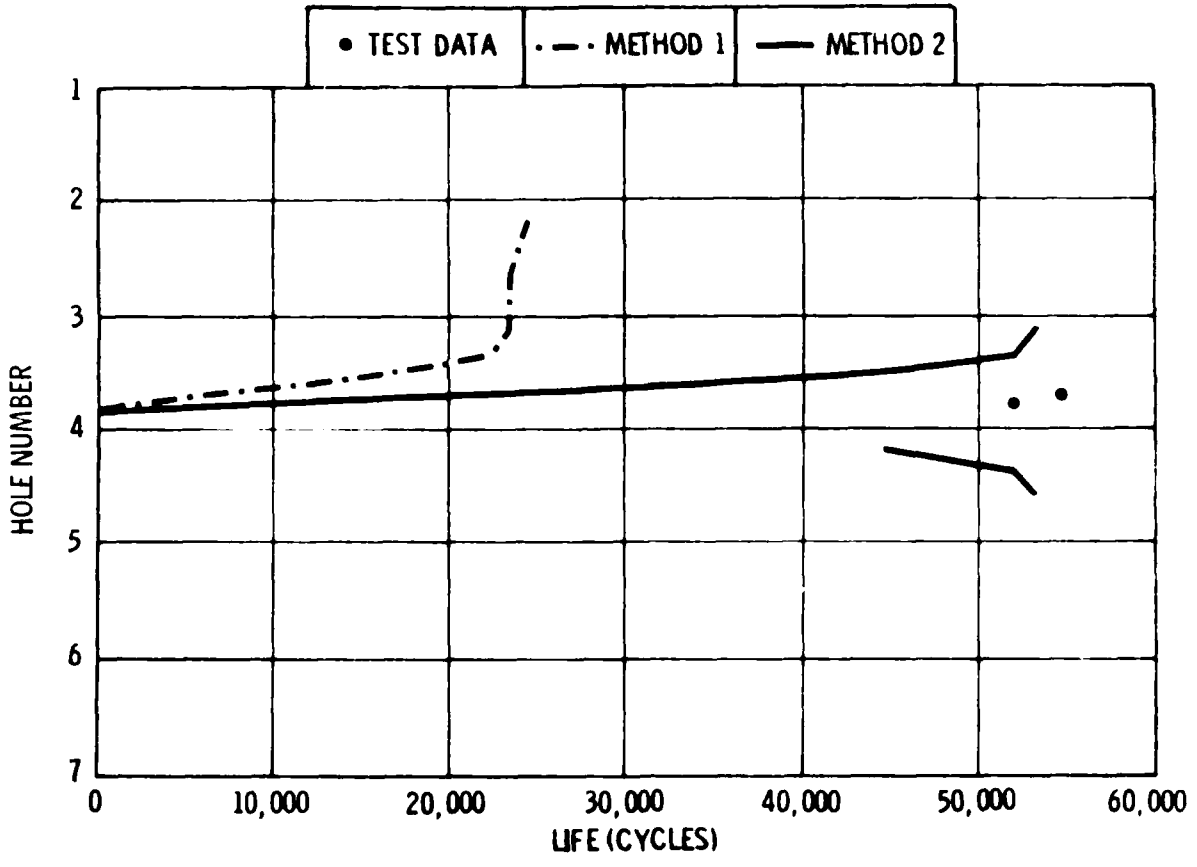
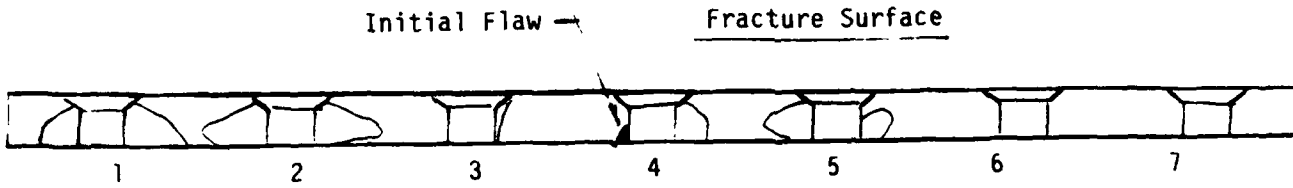


Figure 4.1.1-9. Crack Growth Diagram for Single-Shear Lap-Joint Specimen LJ-8



SPECIMEN = LJ-9 (Ref. Table 4.1.1-1)
 MATERIAL = 2024-T3XX
 LOADING = C.A.
 TEST LIFE = 69,910 CYCLES
 METHOD 1 PREDICTED LIFE = 40,730 CYCLES
 METHOD 2 PREDICTED LIFE = 41,289 CYCLES

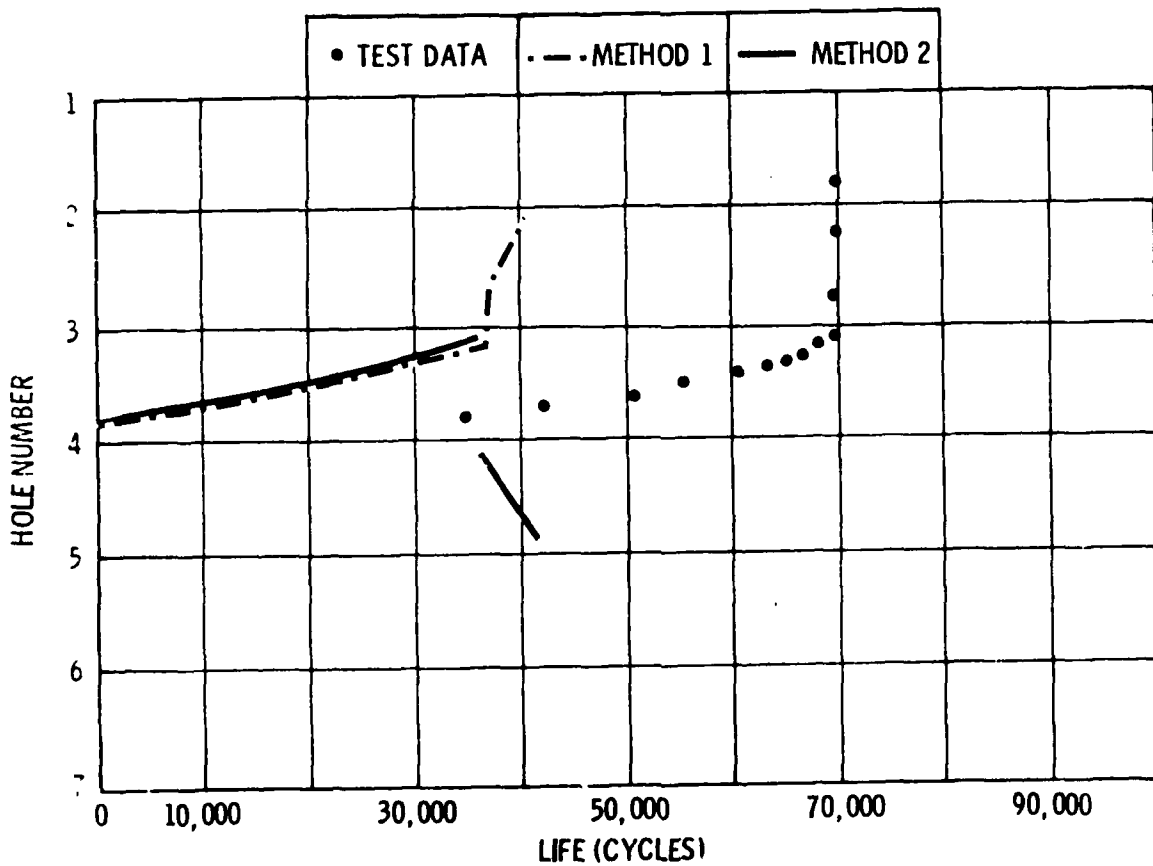
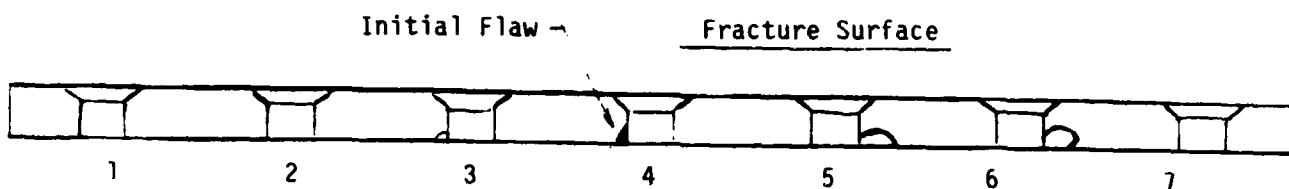


Figure 4.1.1-10. Crack Growth Diagram for Single-Shear Lap-Joint Specimen LJ-9



SPECIMEN = LJ-10 (Ref. Table 4.1.1-1)
 MATERIAL = 2024-T3XX
 LOADING = C.A.
 TEST LIFE = 88,300 CYCLES
 METHOD 1 PREDICTED LIFE = 40,730 CYCLES
 METHOD 2 PREDICTED LIFE = 41,289 CYCLES

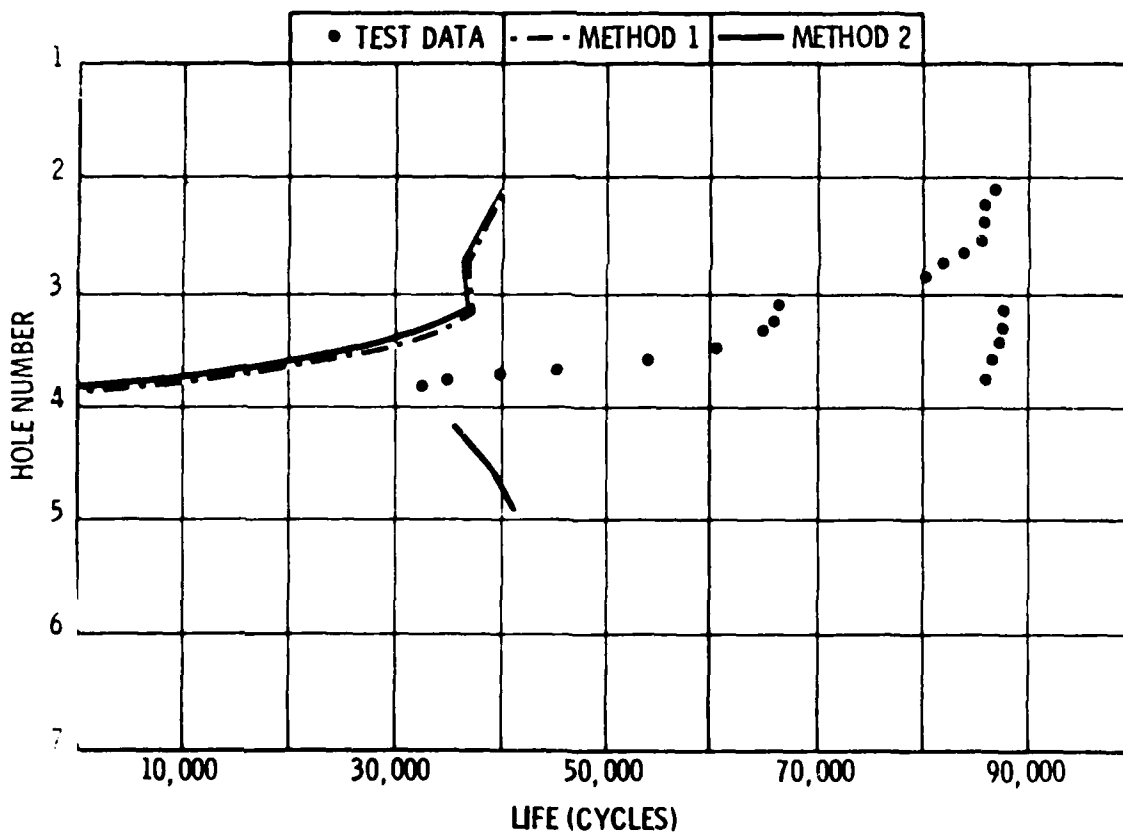
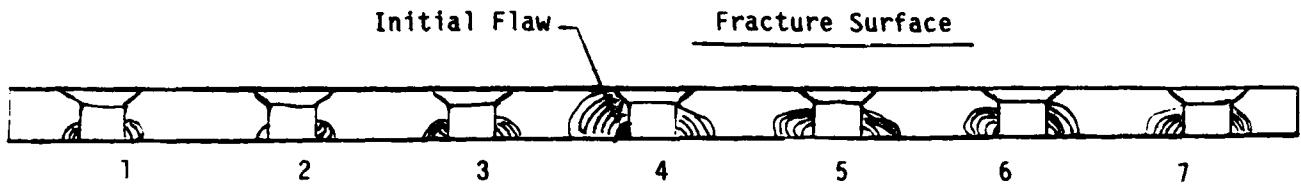


Figure 4.1.1-11. Crack Growth Diagram for Single-Shear Lap-Joint Specimen LJ-10



SPECIMEN = LJ-11 (Ref. Table 4.1.1-1)
 MATERIAL = 2024-T3XX
 LOADING = A-10A
 TEST LIFE = 41,037 CYCLES
 METHOD 1 PREDICTED LIFE = 24,408 CYCLES
 METHOD 2 PREDICTED LIFE = 20,473 CYCLES

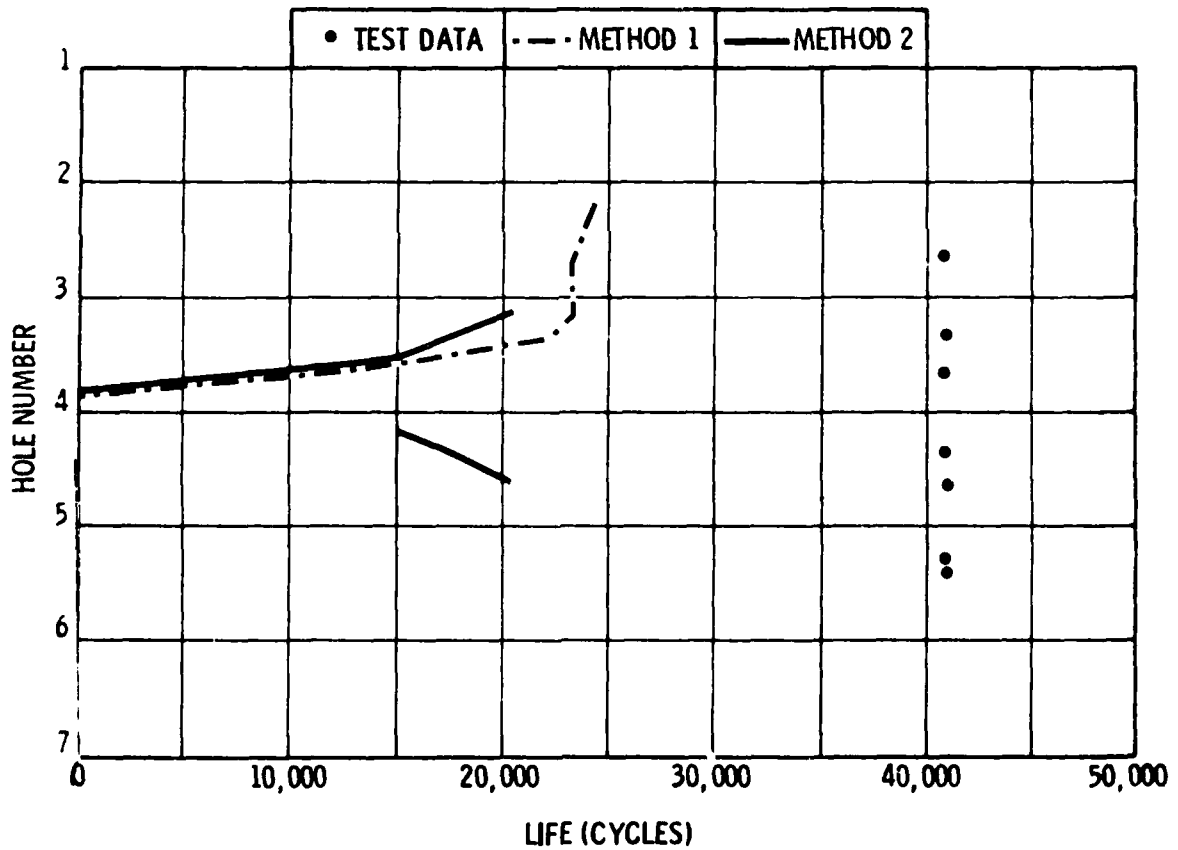
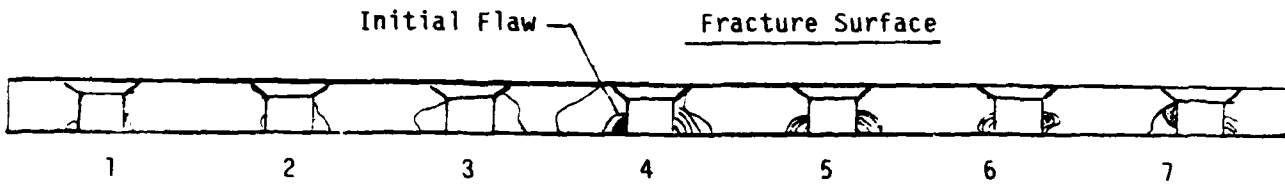


Figure 4.1.1-12. Crack Growth Diagram for Single-Shear Lap-Joint Specimen LJ-11



SPECIMEN = LJ-12 (Ref. Table 4.1.1-1)
 MATERIAL = 2024-T3XX
 LOADING = A-10A
 TEST LIFE = 41,693 CYCLES
 METHOD 1 PREDICTED LIFE = 24,408 CYCLES
 METHOD 2 PREDICTED LIFE = 20,473 CYCLES

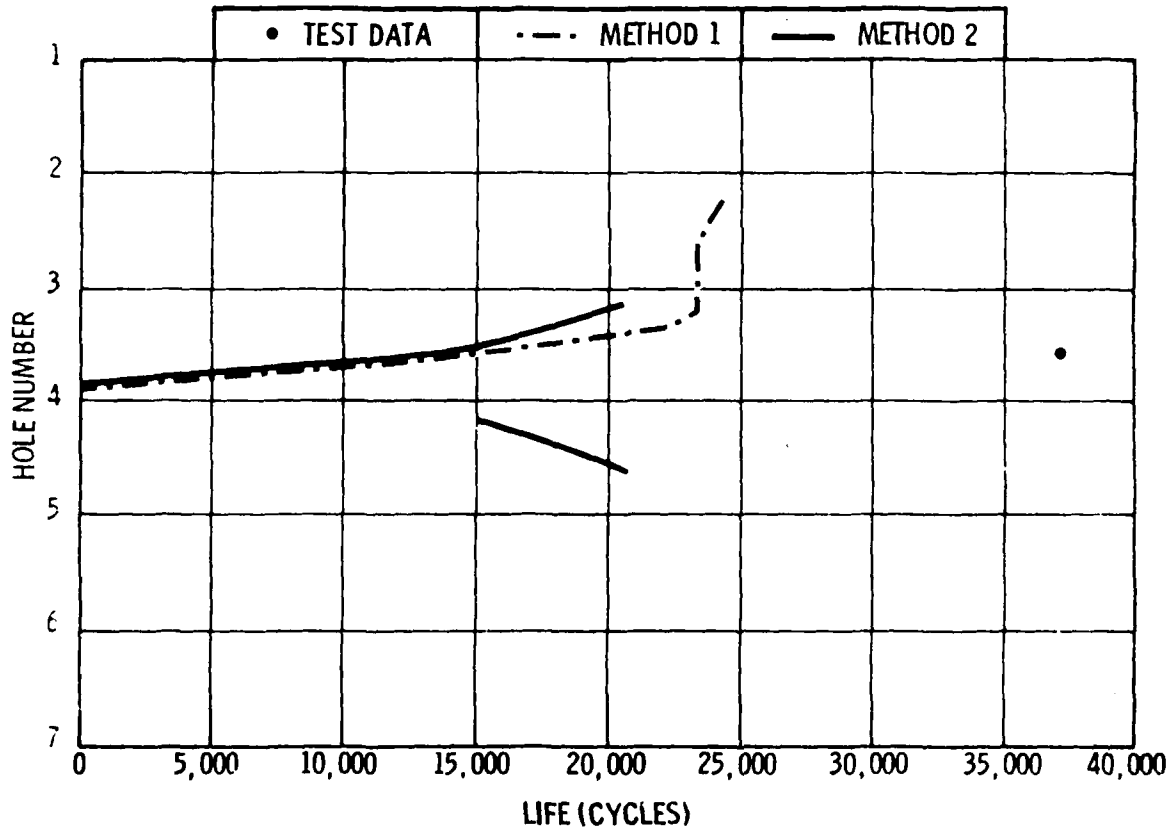
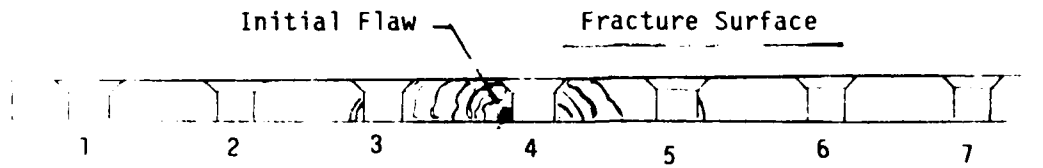


Figure 4.1.1-13. Crack Growth Diagram for Single-Shear Lap-Joint Specimen LJ-12



SPECIMEN = LJ-25 (Ref. Table 4.1.1-1)
 MATERIAL = 7075-T6XX
 LOADING = AMAVS
 TEST LIFE = 3,559 CYCLES
 METHOD 1 PREDICTED LIFE = 22,189 CYCLES
 METHOD 2 PREDICTED LIFE = 9,132 CYCLES

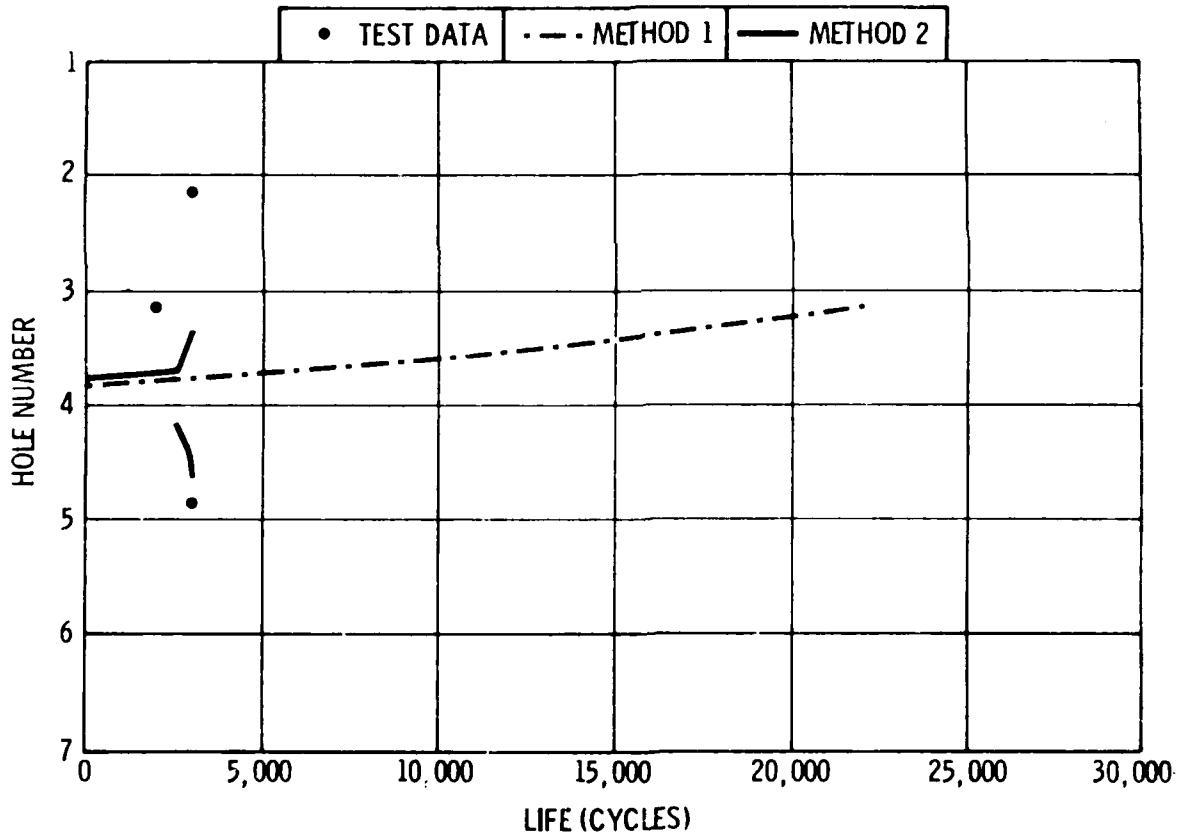
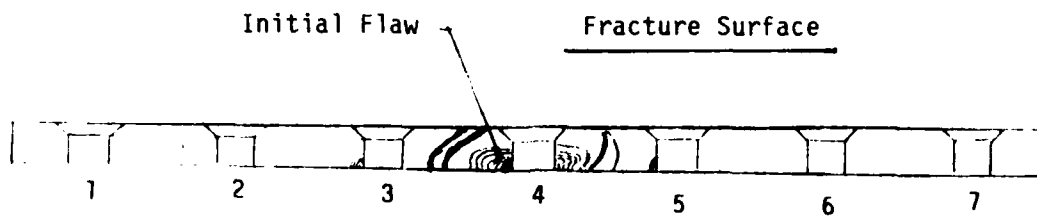


Figure 4.1.1-14. Crack Growth Diagram for Single-Shear Lap-Joint Specimen LJ-25



SPECIMEN = LJ-26 (Ref. Table 4.1.1-1)
 MATERIAL = 7075-T6XX
 LOADING = AMAVS
 TEST LIFE = 7,215 CYCLES
 METHOD 1 PREDICTED LIFE = 22,189 CYCLES
 METHOD 2 PREDICTED LIFE = 9,132 CYCLES

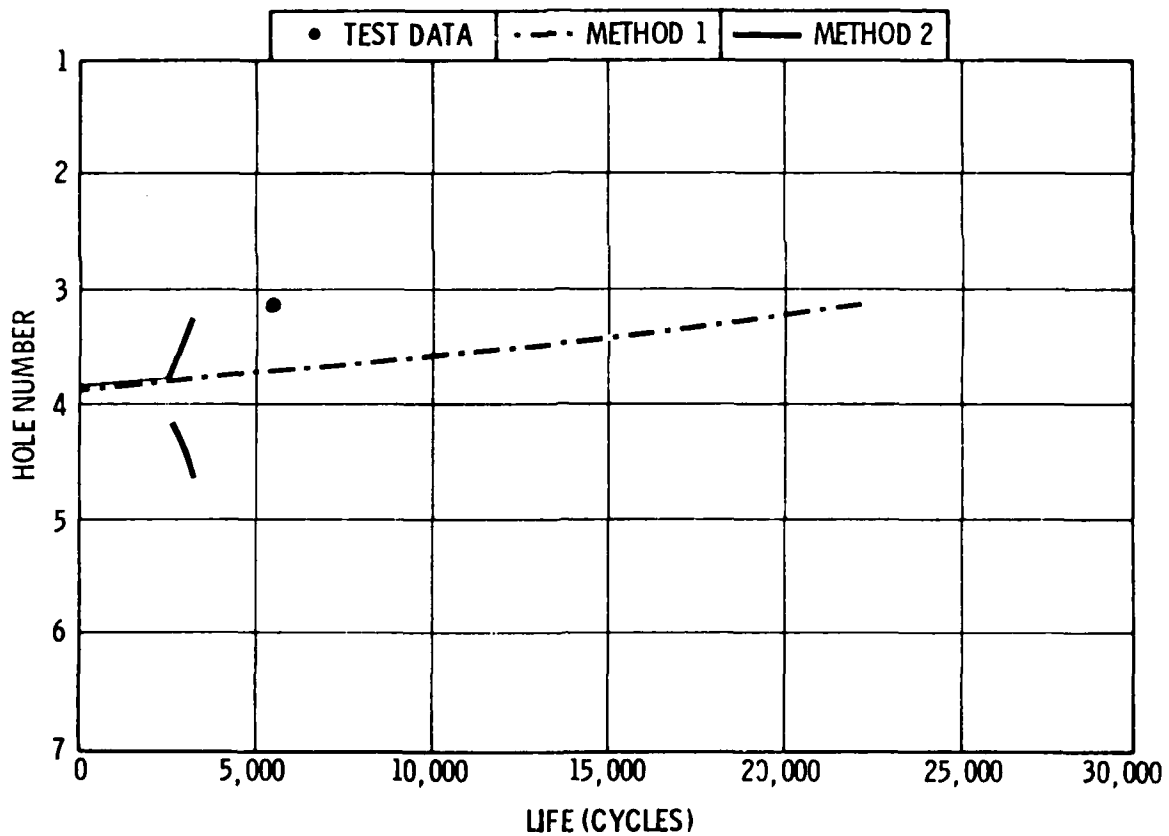
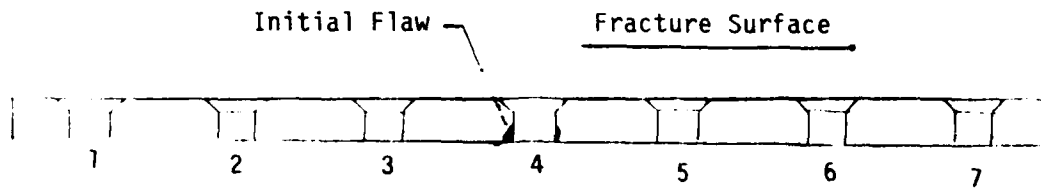


Figure 4.1.1-15. Crack Growth Diagram for Single-Shear Lap-Joint Specimen LJ-26



SPECIMEN = LJ-27 (Ref. Table 4.1.1-1)
 MATERIAL = 7075-T6XX
 LOADING = AMAVS
 TEST LIFE = 11,091 CYCLES
 METHOD 1 PREDICTED LIFE = 22,189 CYCLES
 METHOD 2 PREDICTED LIFE = 23,343 CYCLES

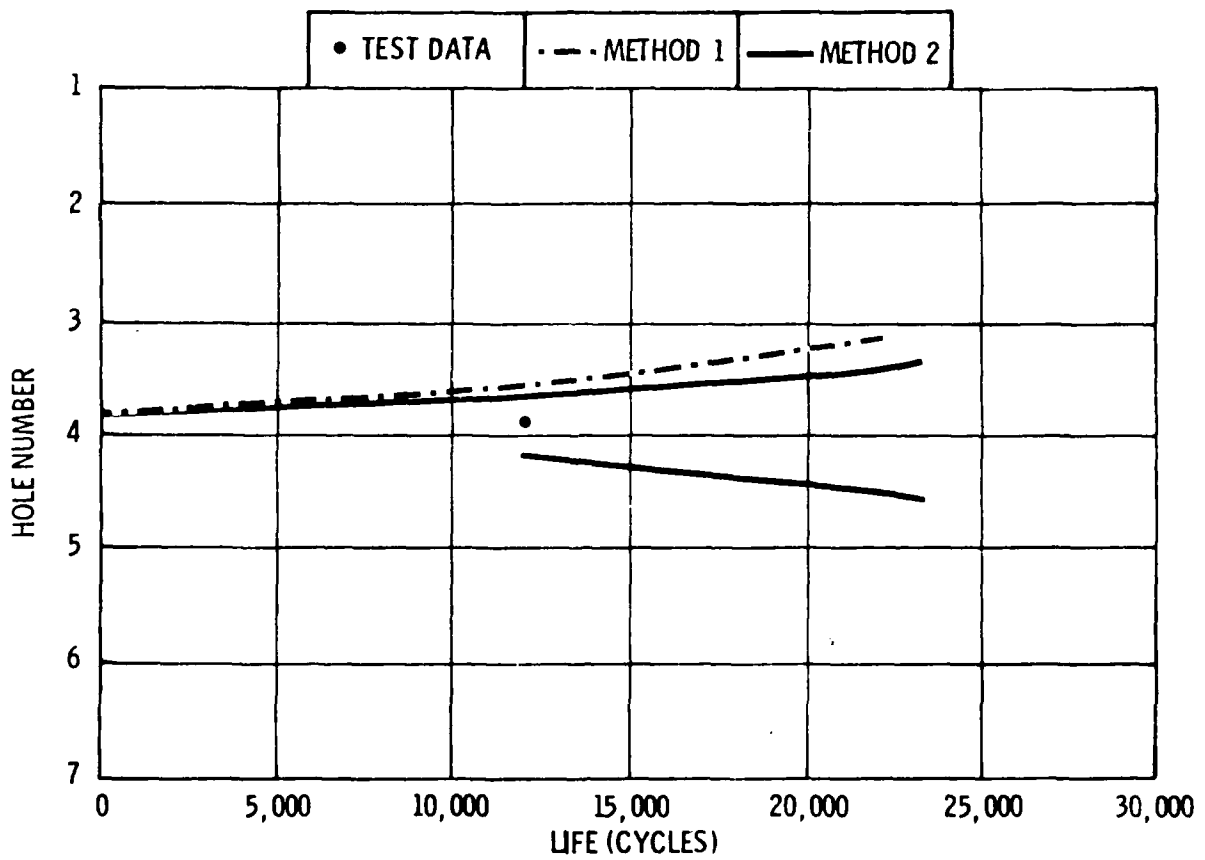
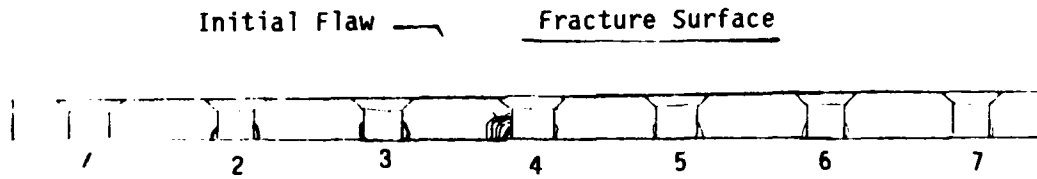


Figure 4.1.1-16. Crack Growth Diagram for Single-Shear Lap-Joint Specimen LJ-27



SPECIMEN = LJ-28 (Ref. Table 4.1.1-1)
 MATERIAL = 7075-T6XX
 LOADING = AMAVS
 TEST LIFE = 11,119 CYCLES
 METHOD 1 PREDICTED LIFE = 22,189 CYCLES
 METHOD 2 PREDICTED LIFE = 23,343 CYCLES

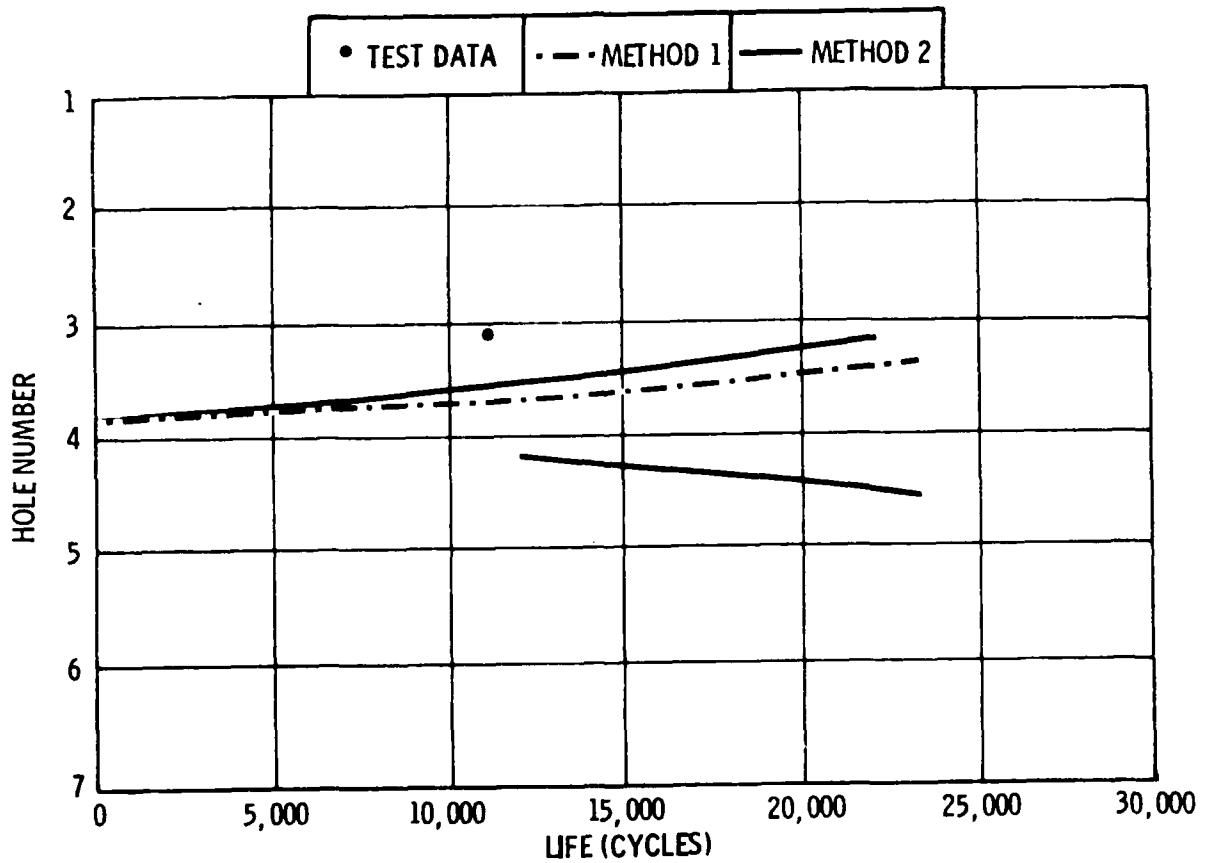
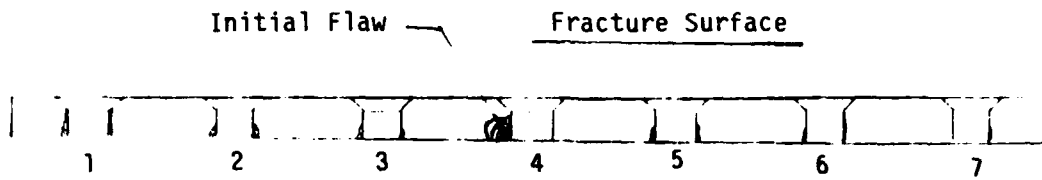


Figure 4.1.1-17. Crack Growth Diagram for Single-Shear Lap-Joint Specimen LJ-28



SPECIMEN = LJ-29 (Ref. Table 4.1.1-1)
 MATERIAL = 7075-T6XX
 LOADING = AMAVS
 TEST LIFE = 11,091 CYCLES
 METHOD 1 PREDICTED LIFE = 22,189 CYCLES
 METHOD 2 PREDICTED LIFE = 9,944 CYCLES

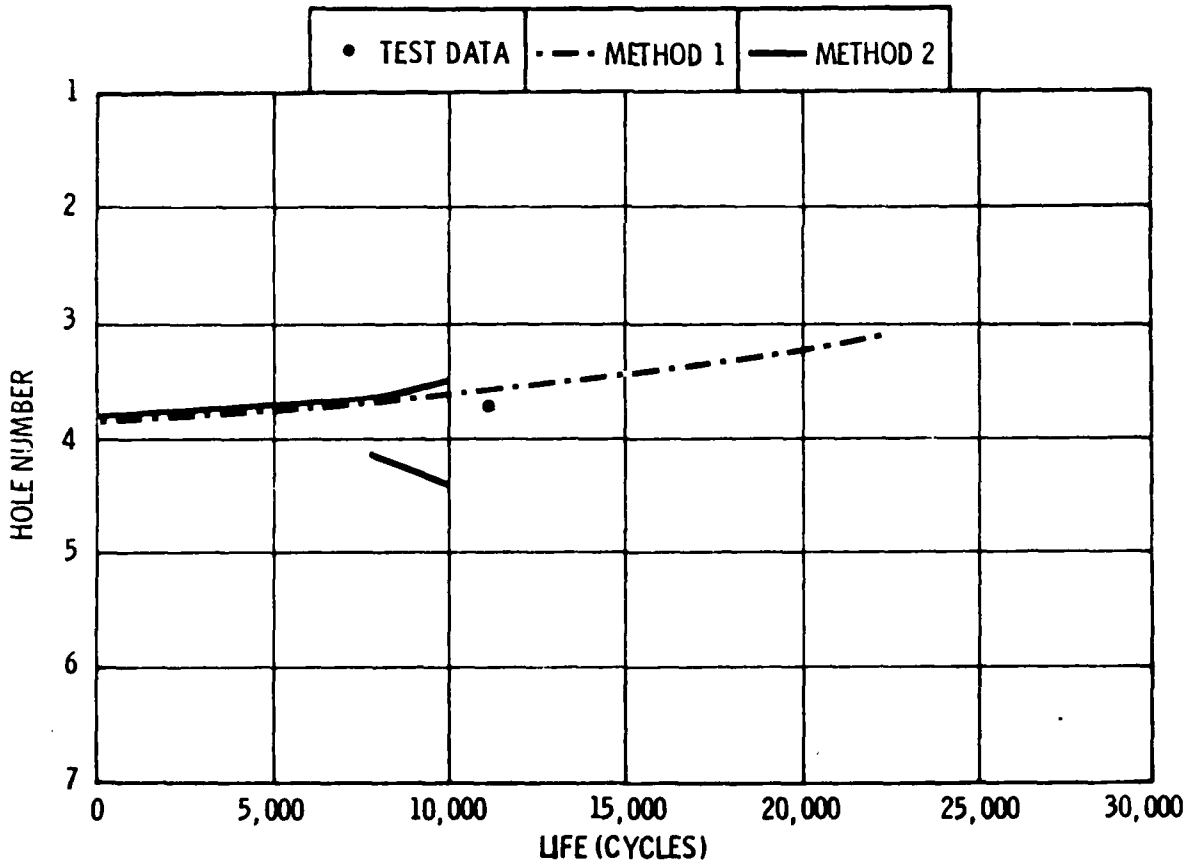
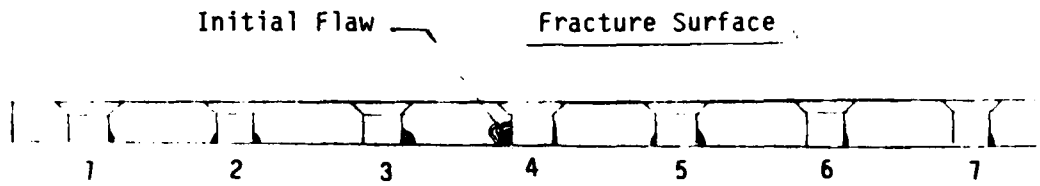


Figure 4.1.1-18. Crack Growth Diagram for Single-Shear Lap-Joint Specimen LJ-29



SPECIMEN = LJ-30 (Ref. Table 4.1.1-1)
 MATERIAL = 7075-T6XX
 LOADING = AMAVS
 TEST LIFE = 8,870 CYCLES
 METHOD 1 PREDICTED LIFE = 22,189 CYCLES
 METHOD 2 PREDICTED LIFE = 9,944 CYCLES

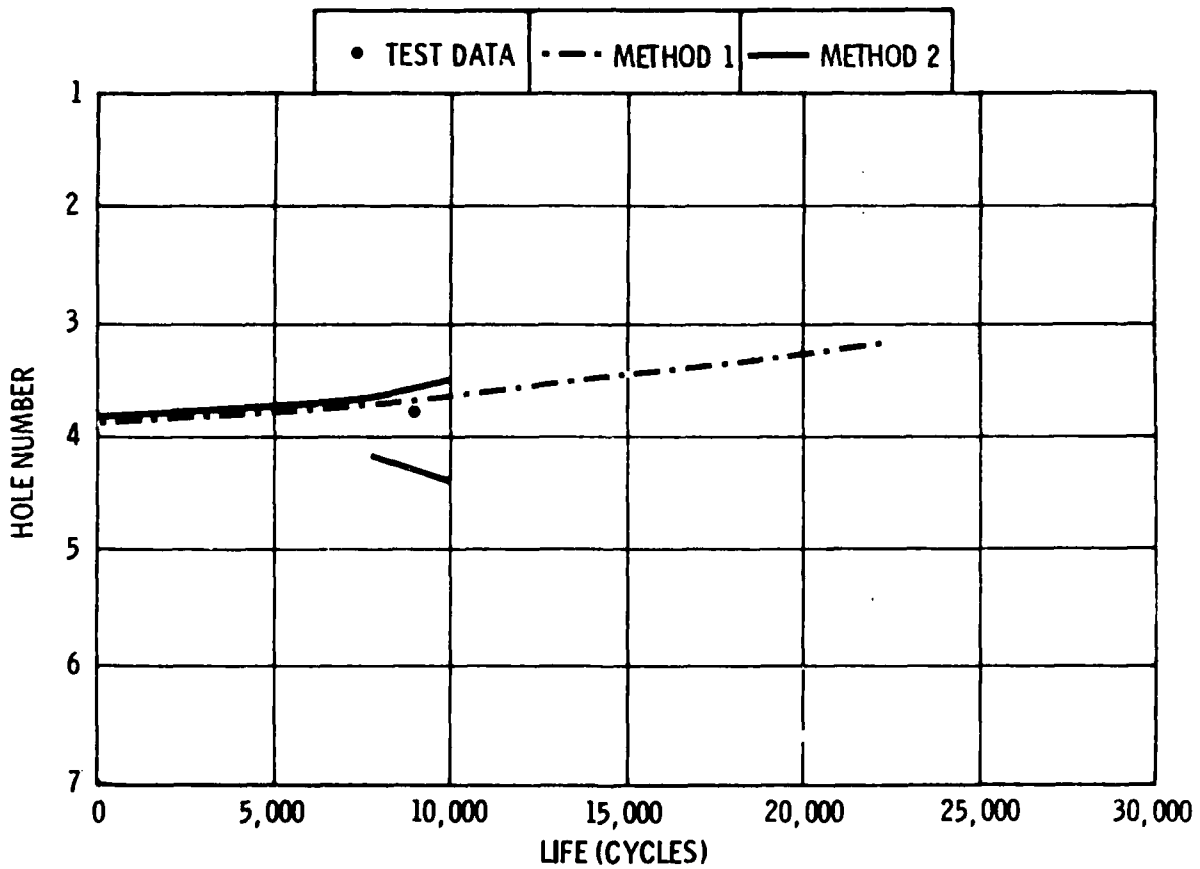


Figure 4.1.1-19. Crack Growth Diagram for Single-Shear Lap-Joint Specimen LJ-30

4.1.2 Double-Shear Lap-Joint Test Program

A total of eighteen (18) double-shear lap-joint specimens were tested. The specimen configuration consisted of a split skin spliced on both sides with splice plates attached using two rows of Hi-Loks. A photo of a test specimen is shown in Figure 4.1.2-1. Due to symmetry, this type of specimen is known to have better structural strength characteristics than the single-shear configuration. All specimens contained an initially induced fatigue crack of 0.050 inch located in the middle hole of the first row of fasteners, and common to the skin and splice plates. The specimens were made of 2024-T3XX or 7075-T6XX aluminum alloys. A list of the test program is provided in Table 4.1.2-1.

TABLE 4.1.2-1. DOUBLE-SHEAR LAP-JOINT SPECIMENS TEST PROGRAM

GROUP	MATERIAL FORM	SPECIMEN CONFIGURATION			SPECIMENS I.D.	APPLIED SPECTRUM	MAXIMUM STRESS LEVEL (Ksi)
		INTER'F	CLAMP-UP	SEALANT			
A	2024-T3XX	No	No	No	LJ-13, LJ-14	C.A.	13.1/4.7
	2024-T3XX	No	No	No	LJ-15, LJ-16	A-10A	37.75
	7075-T6XX	No	No	No	LJ-31, LJ-32	AMAVS	37.75
B	2024-T3XX	Yes	Yes	No	LJ-17, LJ-18	C.A.	13.1/4.7
	2024-T3XX	Yes	Yes	No	LJ-19, LJ-20	A-10A	37.75
	7075-T6XX	Yes	Yes	No	LJ-33, LJ-34	AMAVS	37.75
C	2024-T3XX	Yes	Yes	Yes	LJ-21	C.A.	13.1/4.7
	2024-T3XX	Yes	Yes	Yes	LJ-22, LJ-23 LJ-24	A-10A	37.75
	7075-T6XX	Yes	Yes	Yes	LJ-35, LJ-36	AMAVS	37.75

The specimens were subjected to a constant amplitude loading spectrum and to randomized flight-by-flight loading spectra. The randomized spectra which contained marker band cycles are described in Appendix A of Volume III.

In performing the crack growth and crack initiation analytical predictions, various parameters were used in the analytical equations to reflect the specimen configurations. Both Method 1 and Method 2 contained correction in

the stress intensity function to include % of load transfer. For the hole containing the initial flaw, the load transfer is given by:

$$P = 0.08146 - 0.00282 (a/R) \quad 0 \leq a/R \leq 6 \quad (4.1.5)$$

$$P = 0.07523 - 0.00262 (a/R) \quad 8 \leq a/R \leq 14 \quad (4.1.6)$$

The amount of load transfer at the adjacent holes is given by:

$$P = 0.08104 + 0.00026 a/R \quad 0 \leq a/R \leq 6 \quad (4.1.7)$$

$$P = 0.07548 - 0.00214 a/R \quad 8 \leq a/R \leq 14 \quad (4.1.8)$$

The equations were derived in Phase 1 of the program reflecting the double-shear specimen configuration. In addition to the load transfer, Method 2 used such parameters as the faying surface friction and the attachments clamp-up load. The stress due to the faying surface was determined to be 7.7 Ksi for the 2024-T3XX specimens and 6.2 Ksi for the 7075-T6XX specimens. The stress due to clamp-up of hardware was determined to be 8.45 Ksi for all the double-shear specimens.

4.1.2.1 Test Results vs. Analytical Predictions for Double-Shear Lap-Joint Specimens

The average test results and the analytical predictions of the double-shear lap-joint specimens are summarized in Tables 4.1.2-2 through 4.1.2-4 and presented in Figures 4.1.2-2 through 4.1.2-19 for specimens subjected to constant amplitude, A-10A and AMAVS loading spectra respectively.

4.1.2.1.1 Crack Growth Predictions for Double-Shear Lap-Joint Specimens Subjected to Constant Amplitude Loading Spectrum

The predicted crack growth rates for the specimens subjected to a constant amplitude loading were correlated against the test results. For Group 'A' specimens, which were tested at a maximum stress of 13.1 Ksi and stress ratio of $R = 0.36$, the predicted lives reflect a range of approximately 45% deviation by both Method 1 and Method 2. For Group 'B', no failure occurred at 2×10^6

cycles of testing, Method 1 predicted 121,100 cycles to failure, and Method 2 predicted 1.23×10^6 cycles to failure. Method 1 is extremely conservative mainly due to the assumption of a secondary flaw presence. Method 2, however, needed much more time for secondary flaw initiation. Group 'C' specimens were tested at a maximum stress of 17.1 Ksi and stress ratio of $R = 0.10$. The average life to failure was 129,300 cycles. The predicted 'C' specimen lives, both by Method 1 and Method 2 were much less than the experimental, and had the same order of magnitude difference for both methods. The test results indicate clearly the benefit of interference fit attachment. However, the effect of sealant was not clear due to the variation in stress level. Except for Group B, both methods gave the same accuracy for crack growth prediction. For this group, Method 2 proved to yield a much closer correlation when time to initiation is long due to low stress level. A summary of the experimental vs. analytical results are provided in Table 4.1.2-2.

TABLE 4.1.2-2. ANALYTICAL VS. EXPERIMENTAL CRACK GROWTH LIFE FOR DOUBLE-SHEAR LAP-JOINT SPECIMENS SUBJECTED TO CONSTANT AMPLITUDE LOADING SPECTRUM

GROUP (REF. TABLE 4.1.2-1)	MAXIMUM STRESS (Ksi)	AVERAGE TEST RESULTS	ANALYTICAL PREDICTIONS			
			METHOD 1		METHOD 2	
			LIFE (CYCLES)	% DEV.	LIFE (CYCLES)	% DEV.
A	13.1 $R = 0.36$	214,050	121,100	43.4	115,500	46.0
B	13.1 $R = 0.36$	2×10^6	121,100	N/A	1.23×10^6	N/A
C	17.0 $R = 0.10$	129,300	20,840	83.9	25,514	80.3
EXPERIMENTAL/ANALYTICAL AVERAGE DEV.				63.6	63.1	

4.1.2.1.2 Crack Growth Predictions for Double-Shear Lap-Joint Specimens Subjected to A-10A Loading Spectrum

The predicted crack growth lives for the specimens subjected to the A-10A loading spectrum are summarized in Table 4.1.2-3. For Group 'A', the average life to failure was 39,185 cycles compared to 175,485 cycles and 107,038 cycles for Groups 'B' and 'C' respectively. The test results indicate the benefit of

interference fit fasteners and the negative effect of sealant at the faying surface. Distinction in crack growth lives among the three groups cannot be made using Method 1, however, it can be beneficial for Method 2. The over-all deviations were 56.8% and 44.6% for Method 1 and Method 2, respectively, indicating better results for Method 2.

TABLE 4.1.2-3. ANALYTICAL VS. EXPERIMENTAL CRACK GROWTH LIFE FOR DOUBLE-SHEAR LAP-JOINT SPECIMENS SUBJECTED TO A-10A LOADING SPECTRUM

GROUP (REF. TABLE 4.1.2-1)	MAXIMUM STRESS (Ksi)	AVERAGE TEST RESULTS	ANALYTICAL PREDICTIONS			
			METHOD 1		METHOD 2	
			LIFE (CYCLES)	% DEV.	LIFE (CYCLES)	% DEV.
A	37.75	39,185	31,890	18.6	22,466	42.7
B	37.75	175,485	31,890	81.8	141,196	19.5
C	37.75	107,038	31,890	70.2	30,208	71.7
EXPERIMENTAL/ANALYTICAL AVERAGE DEV.				56.8		44.6

4.1.2.1.3 Crack Growth Predictions for Double-Shear Lap-Joint Specimens Subjected to AMAVS Loading Spectrum

The crack growth lives for the specimens subjected to AMAVS loading spectrum are summarized in Table 4.1.2-4. The test results indicate the same trend as in the case of the constant amplitude and the A-10A spectrum. Namely, better life for specimens with interference fit fasteners and without faying surface sealant. Both Method 1 and Method 2 predicted conservative results, with slightly better correlation in Method 2.

TABLE 4.1.2-4. ANALYTICAL VS. EXPERIMENTAL CRACK GROWTH LIFE FOR DOUBLE-SHEAR LAP-JOINT SPECIMENS SUBJECTED TO AMAVS LOADING SPECTRUM

GROUP (REF. TABLE 4.1.2-1)	MAXIMUM STRESS (Ksi)	AVERAGE TEST RESULTS	ANALYTICAL PREDICTIONS			
			METHOD 1		METHOD 2	
			LIFE (CYCLES)	% DEV.	LIFE (CYCLES)	% DEV.
A	37.75	46,750	30,660	34.4	20,007	57.2
B	37.75	148,917	30,660	79.4	78,014	47.6
C	37.75	120,700	30,660	74.6	33,834	71.9
EXPERIMENTAL/ANALYTICAL AVERAGE DEV.				62.8		58.9

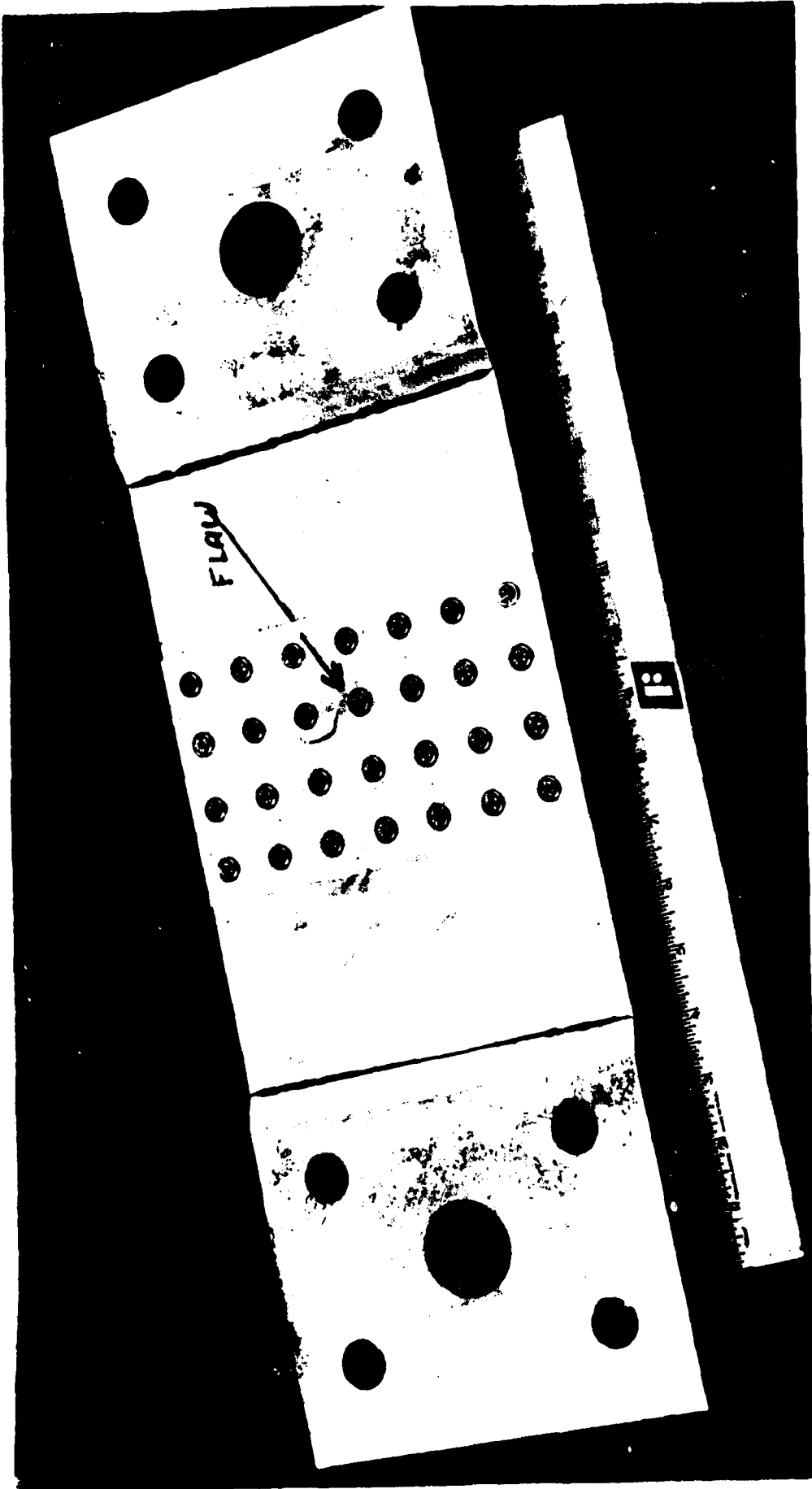


Figure 4.1.2-1. Photo of Double-Shear Lap-Joint Specimen

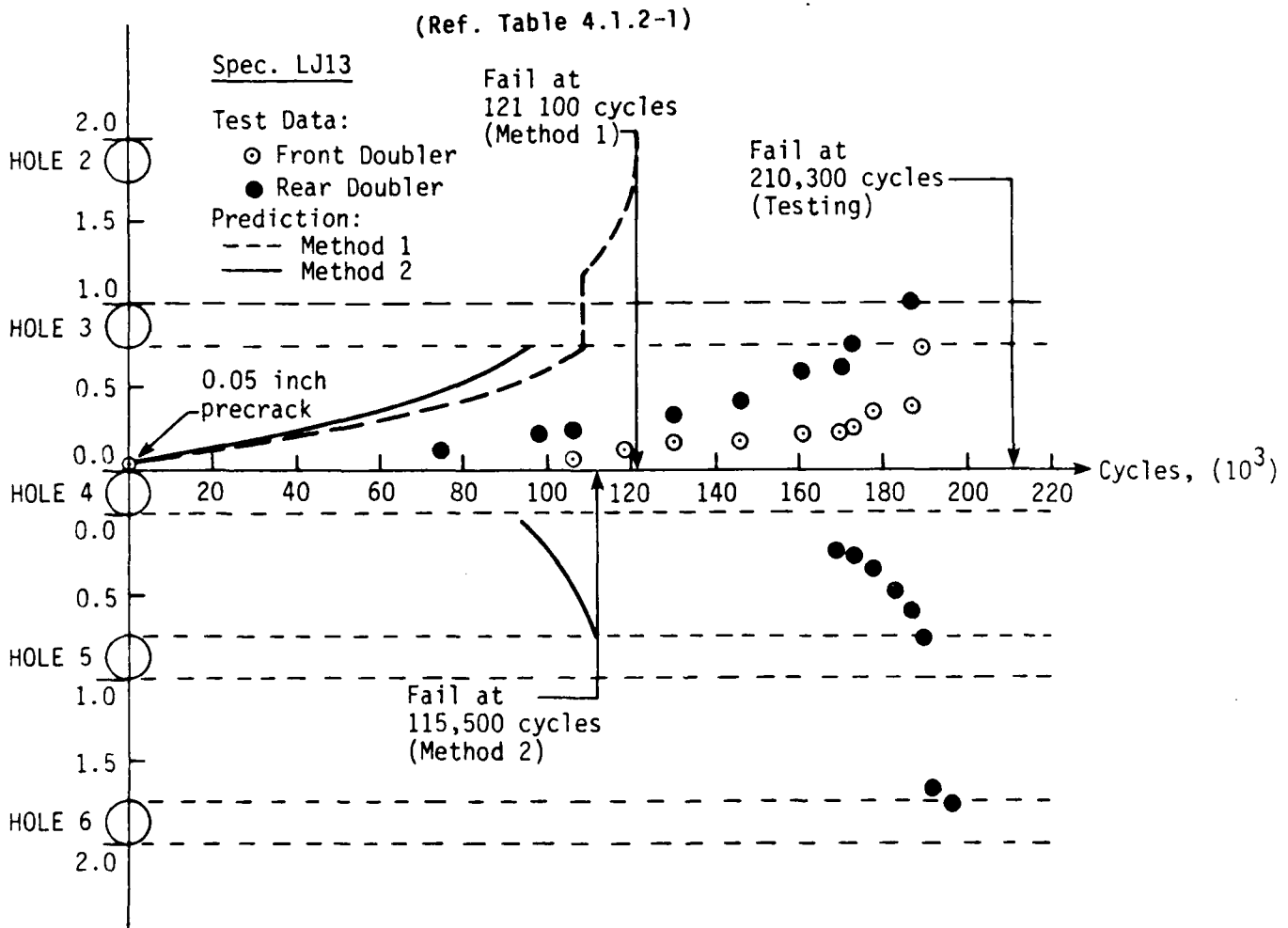


Figure 4.1.2-2. Crack Growth Diagram for Double-Shear Lap-Joint Specimen LJ-13

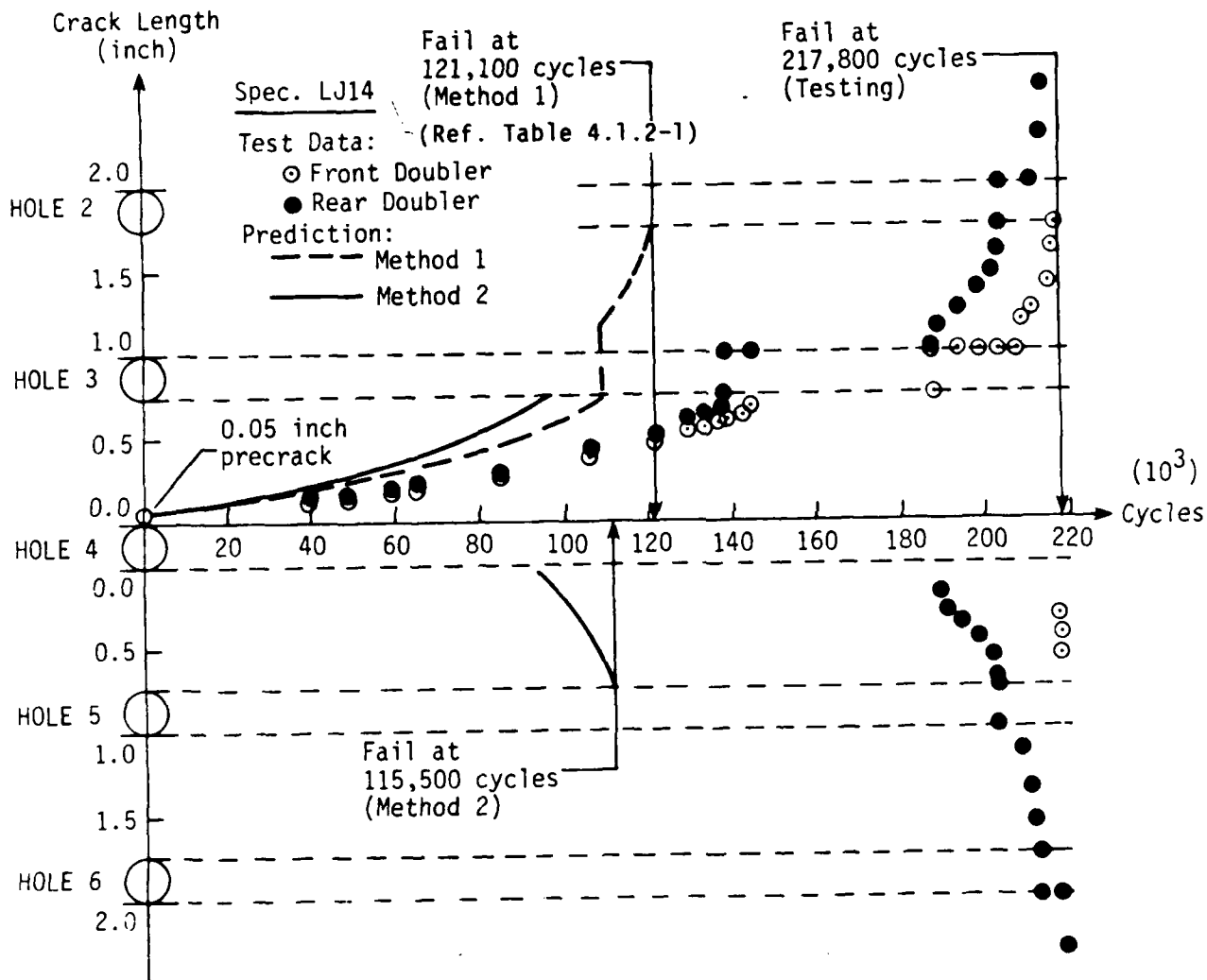


Figure 4.1.2-3. Crack Growth Diagram for Double-Shear Lap-Joint Specimen LJ-14

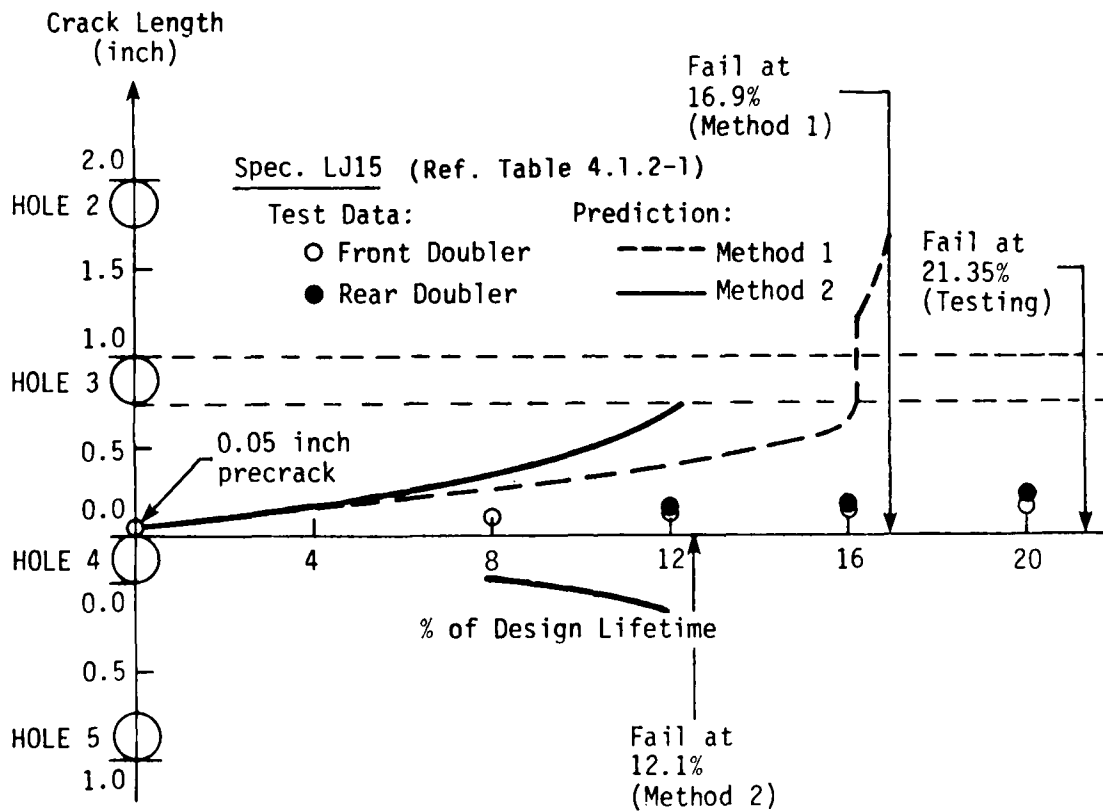


Figure 4.1.2-4. Crack Growth Diagram for Double-Shear Lap-Joint Specimen LJ-15

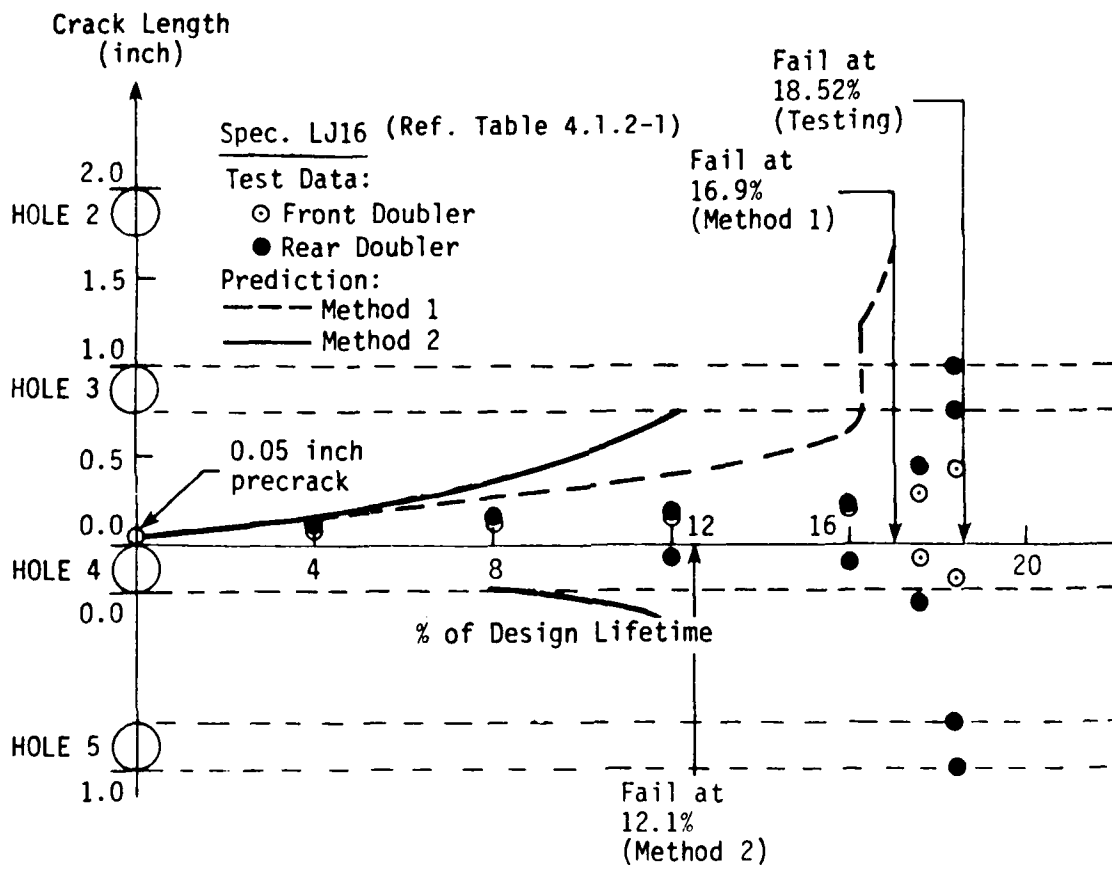


Figure 4.1.2-5. Crack Growth Diagram for Double-Shear Lap-Joint Specimen LJ-16

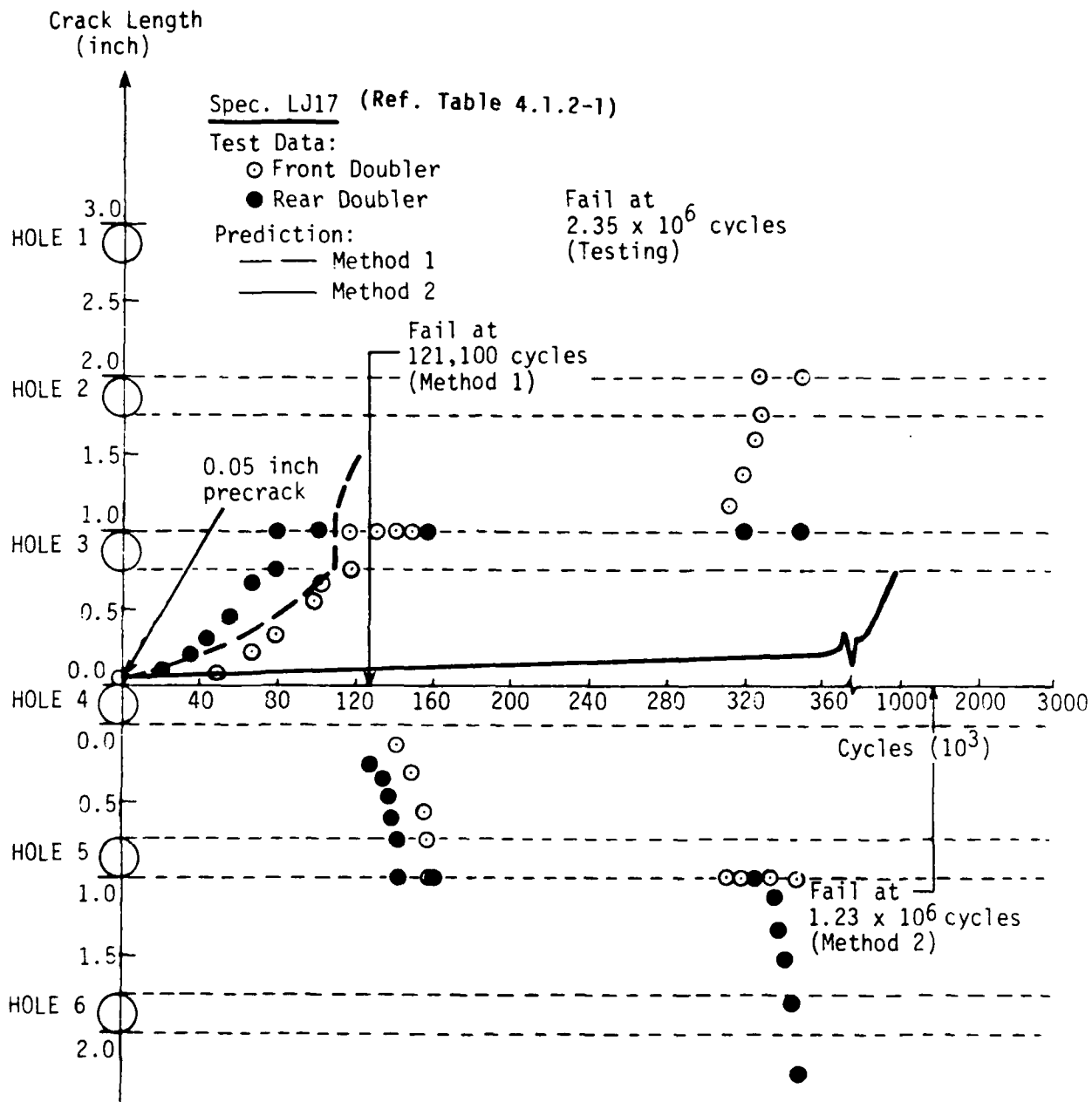


Figure 4.1.2-6. Crack Growth Diagram for Double-Shear Lap-Joint Specimen LJ-17

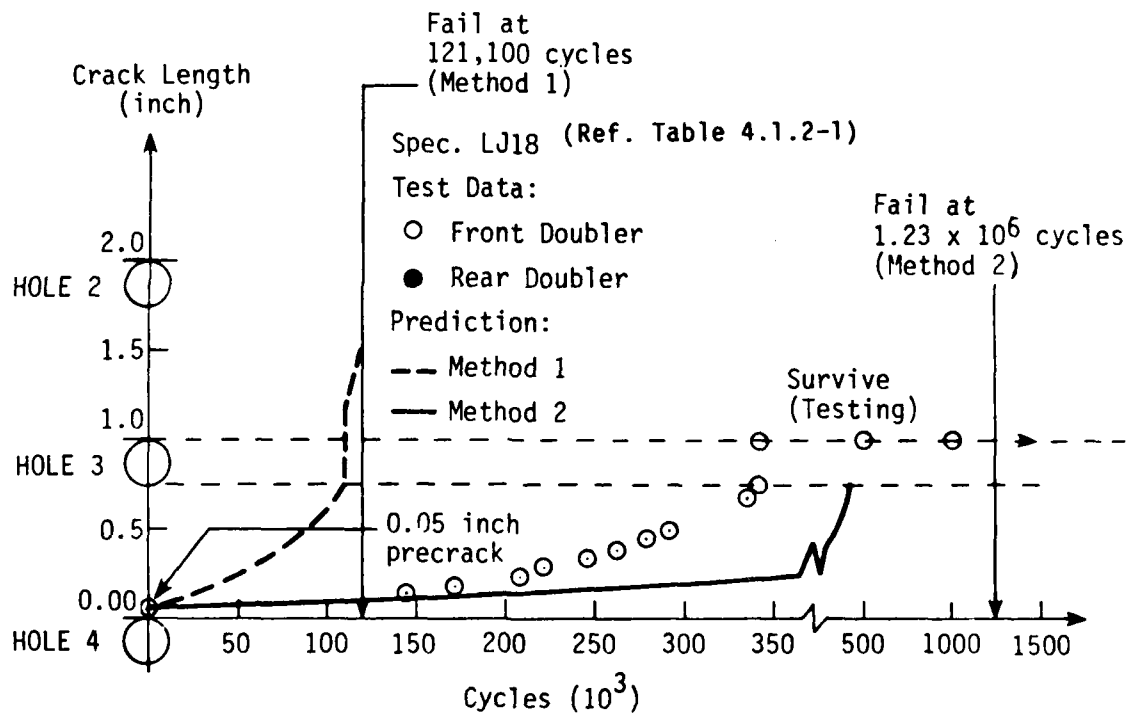


Figure 4.1.2-7. Crack Growth Diagram for Double-Shear Lap-Joint Specimen LJ-18

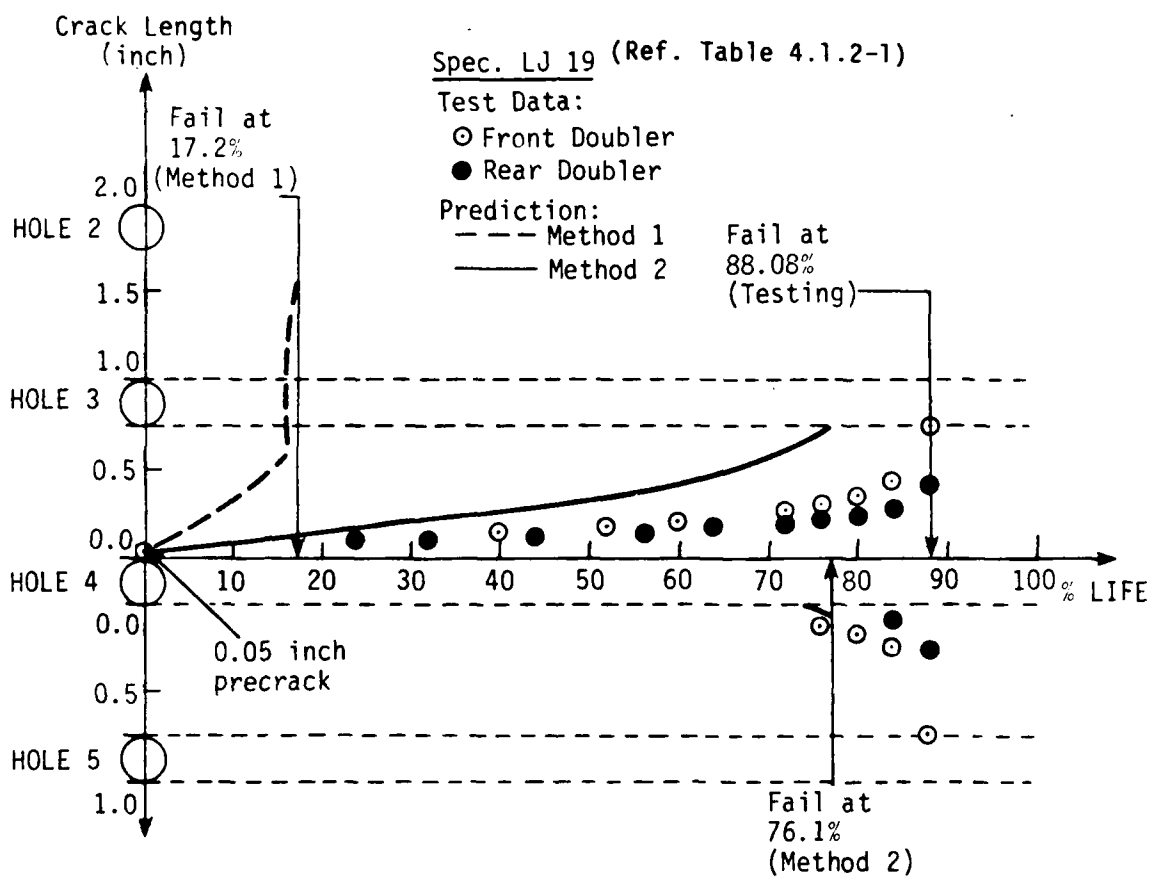


Figure 4.1.2-8. Crack Growth Diagram for Double-Shear Lap-Joint Specimen LJ-19

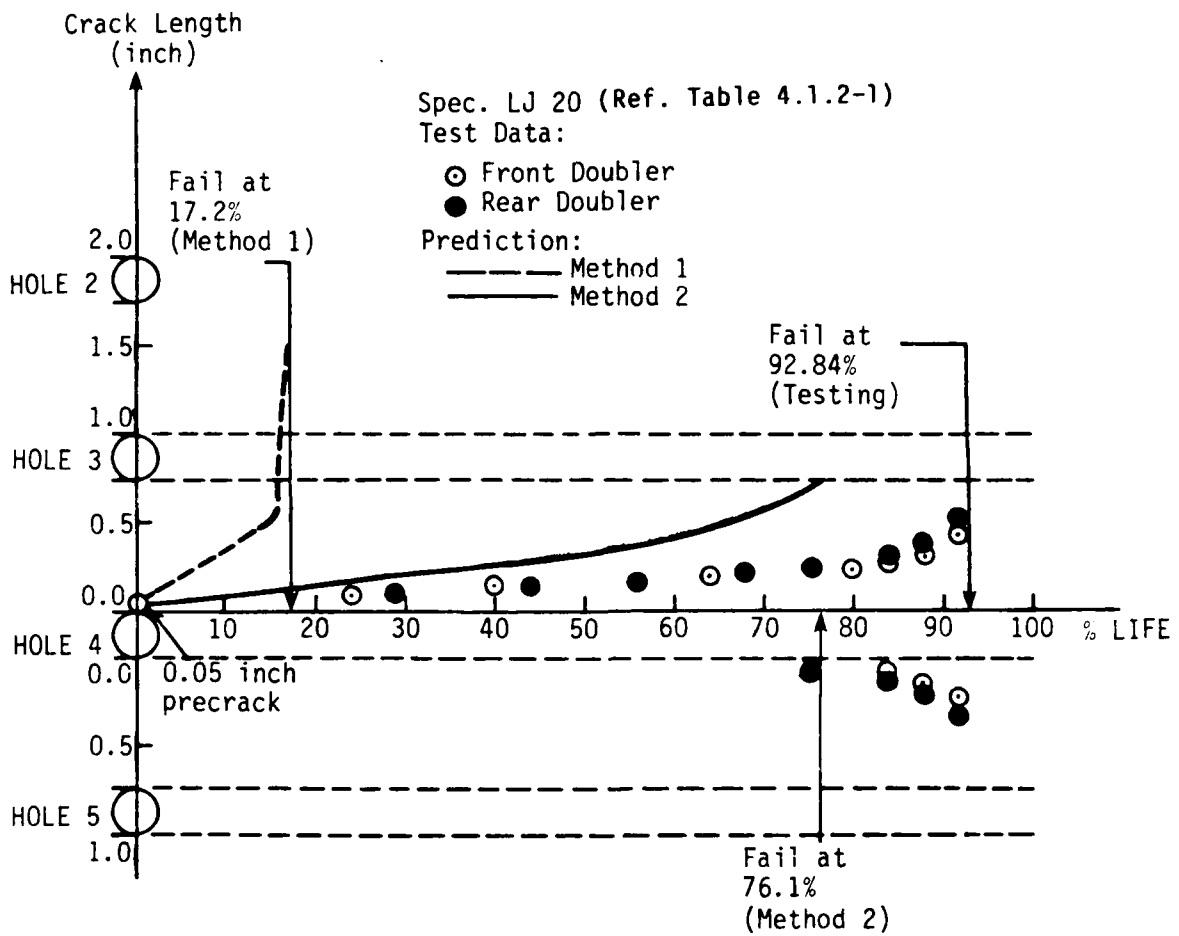


Figure 4.1.2-9. Crack Growth Diagram for Double-Shear Lap-Joint Specimen LJ-20

Spec LJ 21 (Ref. Table 4.1.2-1)

Test Data:

○ Front Doubler

● Rear Doubler

Prediction:

--- Method 1

— Method 2

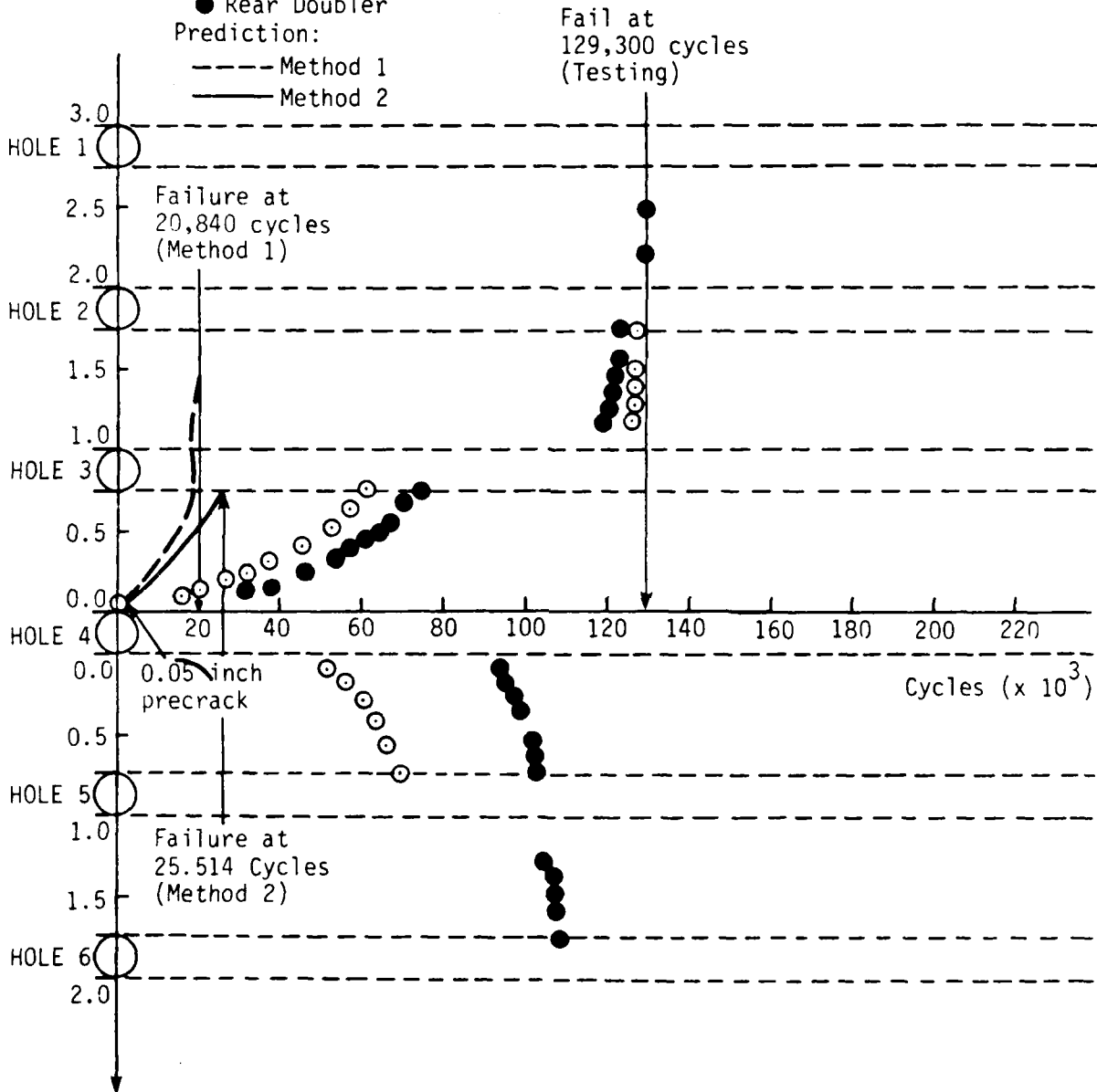


Figure 4.1.2-10. Crack Growth Diagram for Double-Shear Lap-Joint Specimen LJ-21

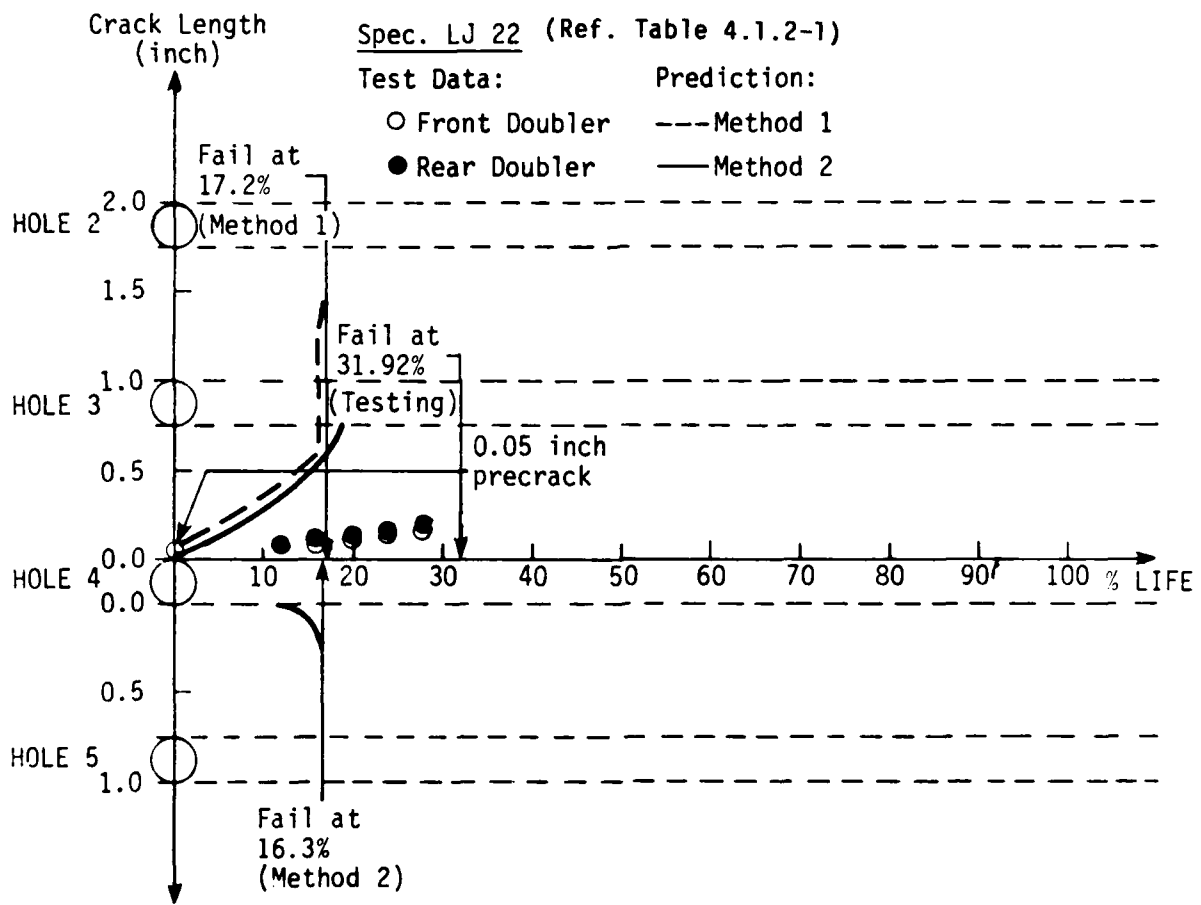


Figure 4.1.2-11. Crack Growth Diagram for Double-Shear Lap-Joint Specimen LJ-22

Spec. LJ 23 (Ref. Table 4.1.2-1)

Test Data:

○ Front Doubler

● Rear Doubler

Prediction:

--- Method 1

— Method 2

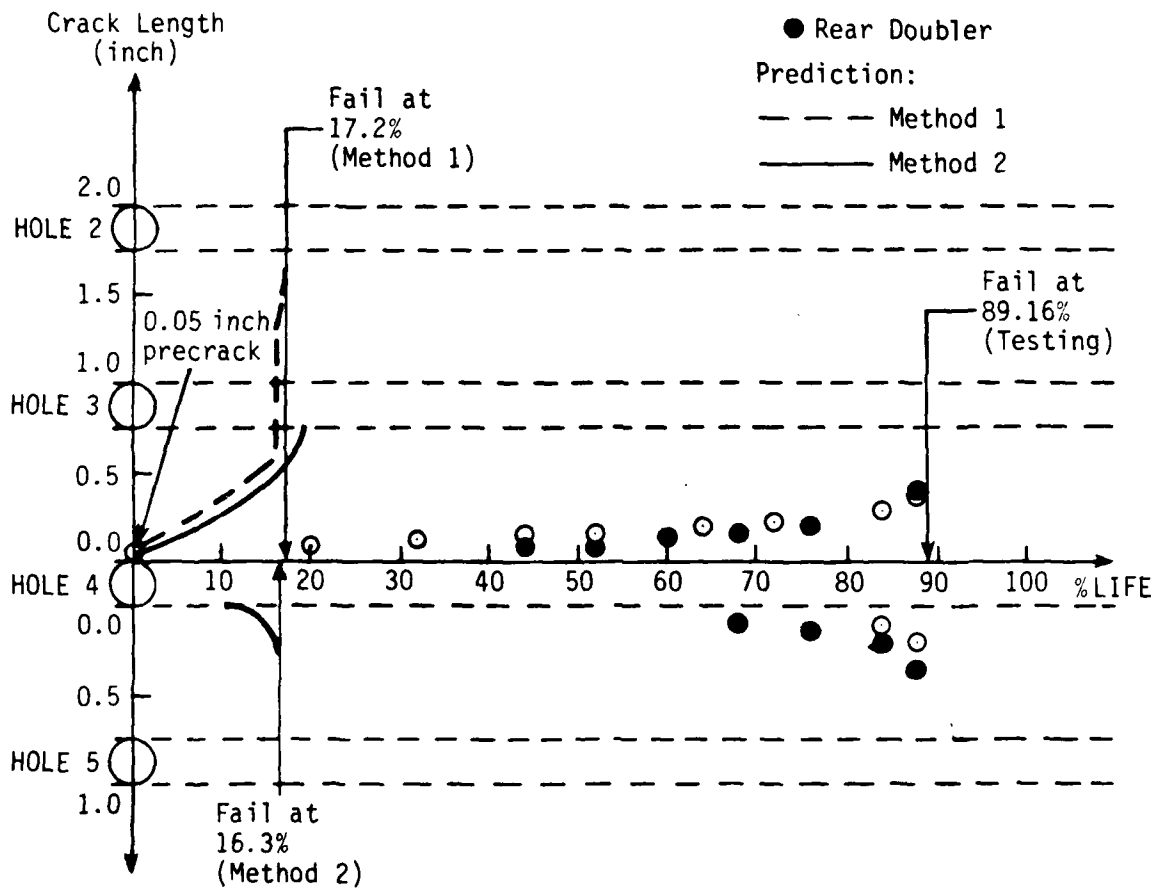


Figure 4.1.2-12. Crack Growth Diagram for Double-Shear Lap-Joint Specimen LJ-23

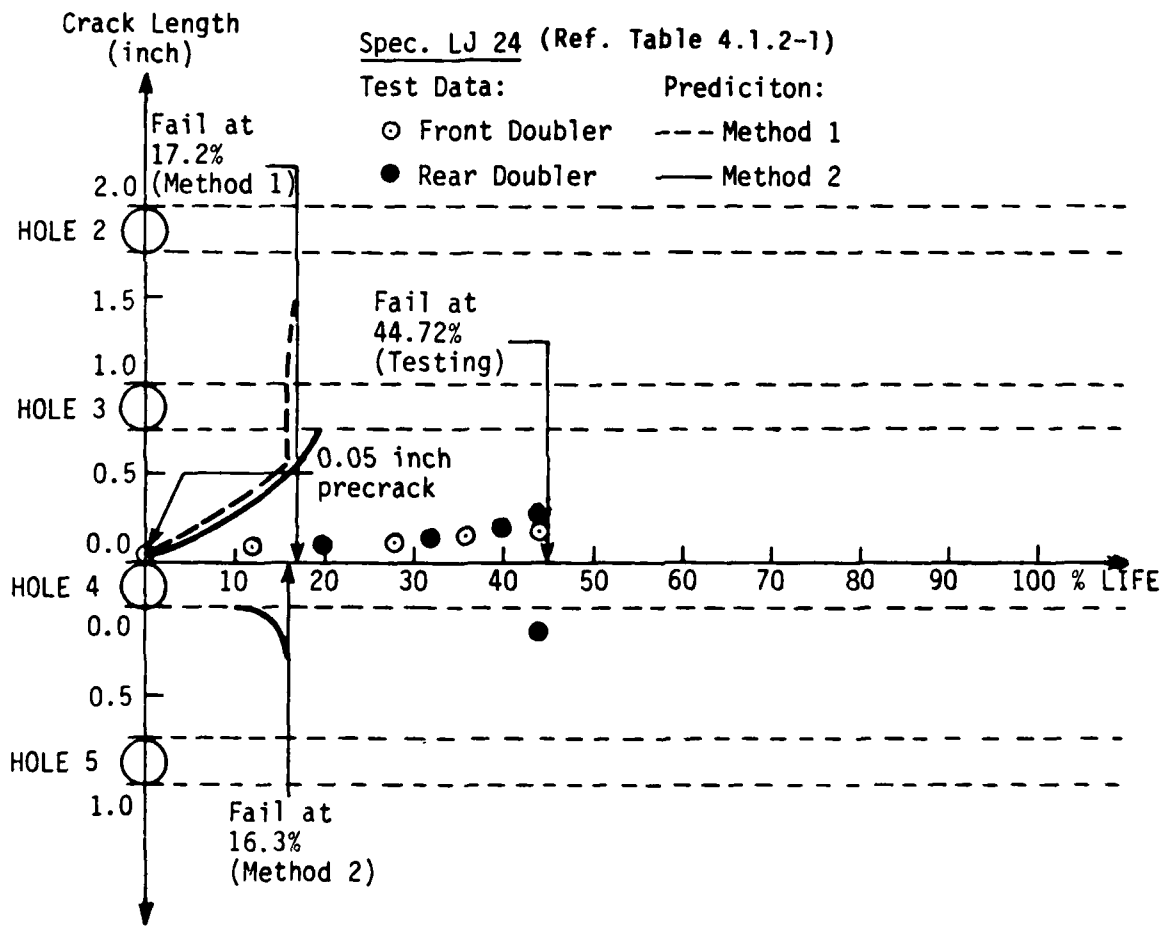


Figure 4.1.2-13. Crack Growth Diagram for Double-Shear Lap-Joint Specimen LJ-24

Spec. LJ 31 (Ref. Table 4.1.2-1)

Test Data:

○ Front Doubler

● Rear Doubler

Prediction:

--- Method 1

— Method 2

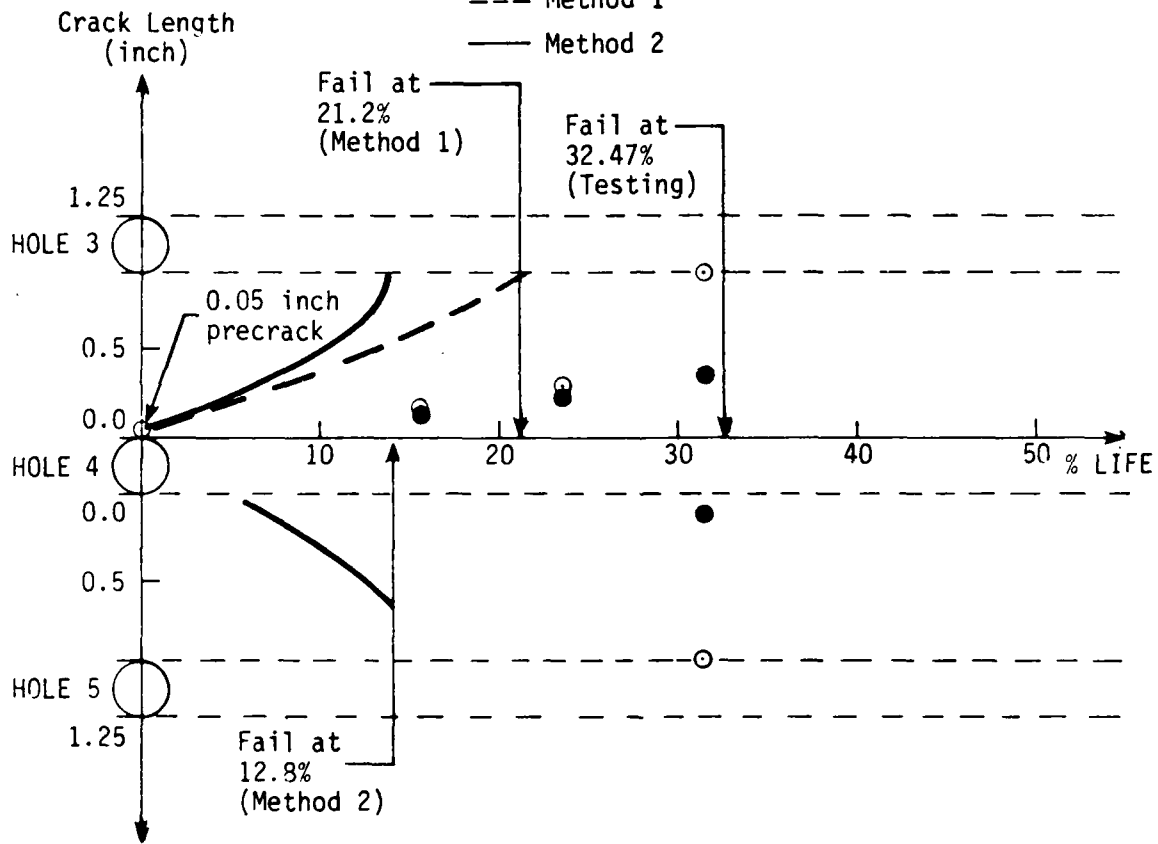


Figure 4.1.2-14. Crack Growth Diagram for Double Shear Lap-Joint Specimen LJ-31

(Ref. Table 4.1.2-1) Spec. LJ 32

Test Data:

○ Front Doubler

● Rear Doubler

Prediction:

--- Method 1

— Method 2

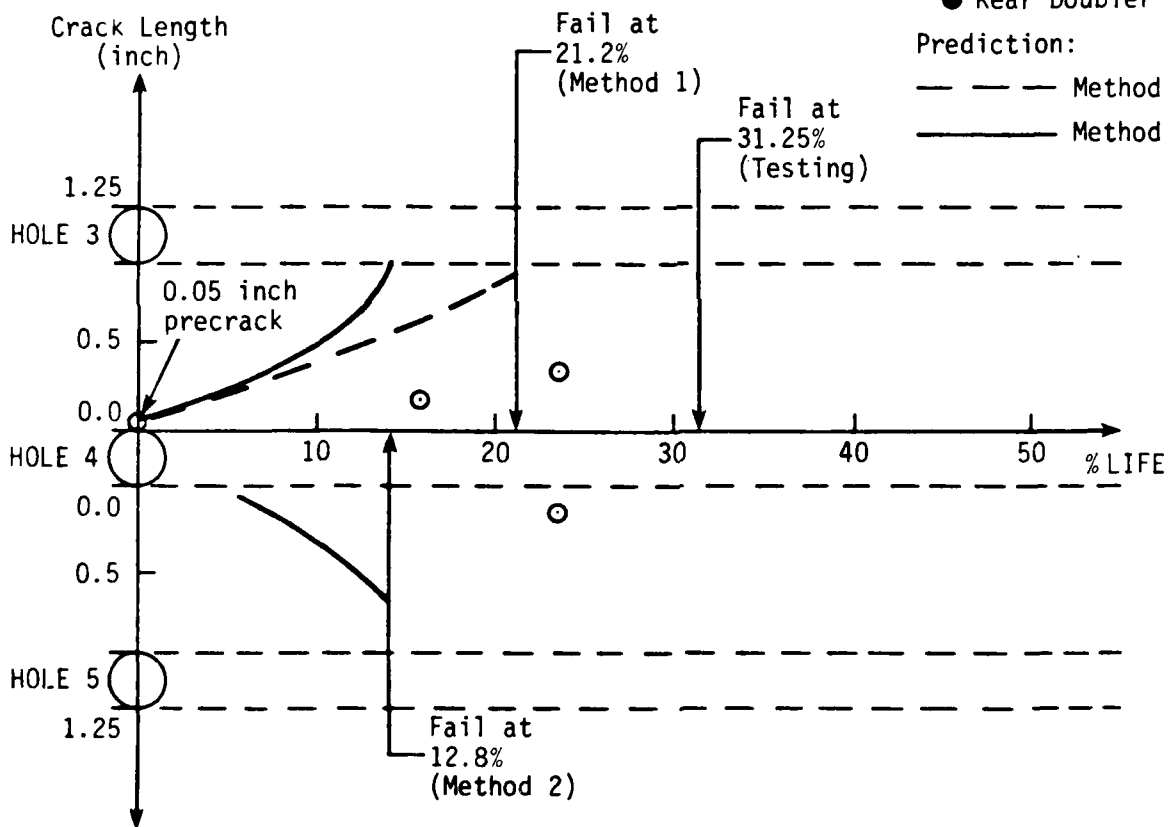


Figure 4.1.2-15. Crack Growth Diagram for Double-Shear Lap-Joint Specimen LJ-32

Spec. LJ 33 (Ref. Table 4.1.2-1)

Test Data:
 ○ Front Doubler
 ● Rear Doubler

Prediction:
 - - - Method 1
 ——— Method 2

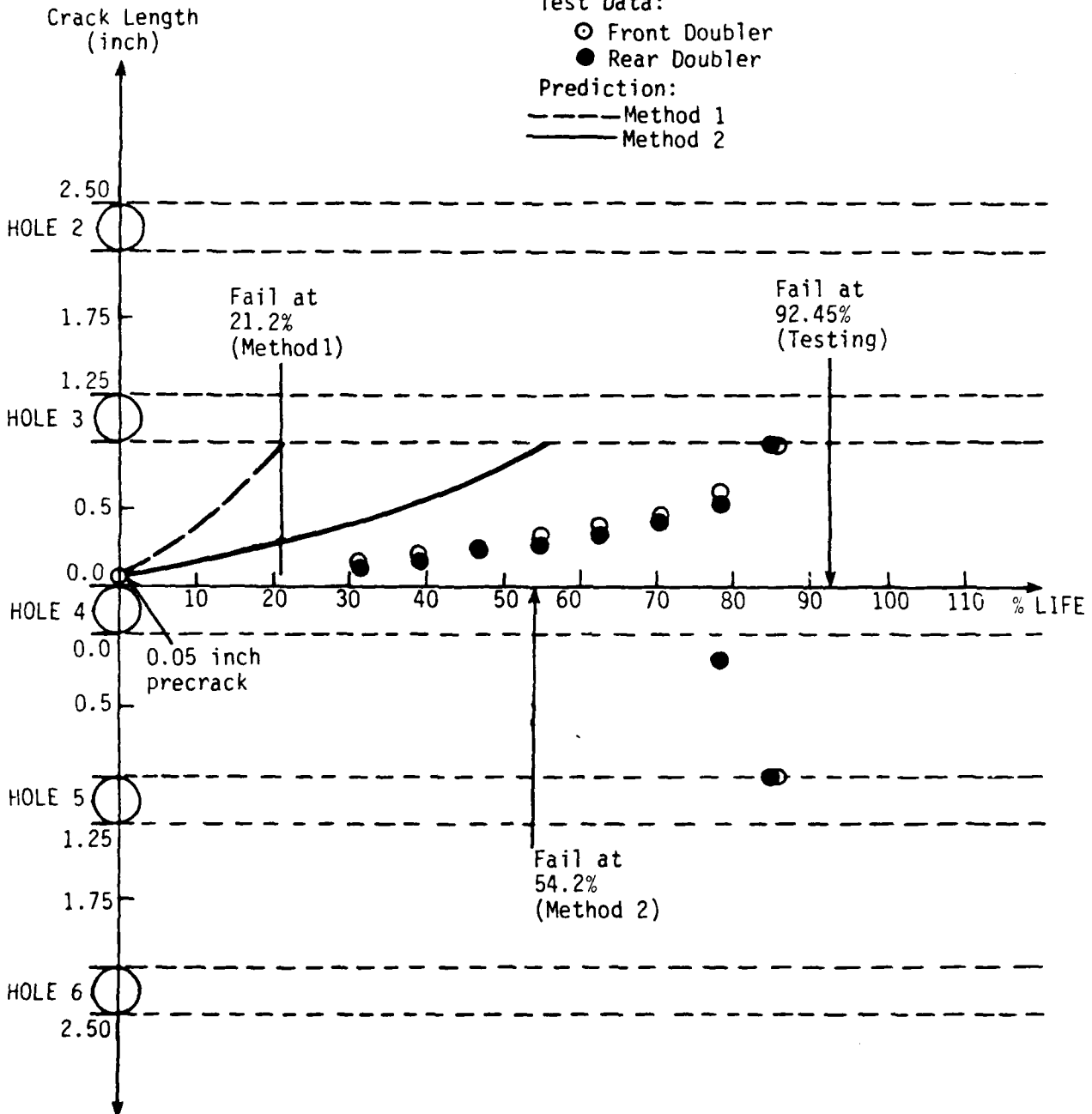


Figure 4.1.2-16. Crack Growth Diagram for Double-Shear Lap-Joint Specimen LJ-33

Spec. LJ 34 (Ref. Table 4.1.2-1)

Test Data:

○ Front Doubler

● Rear Doubler

Prediction:

--- Method 1

— Method 2

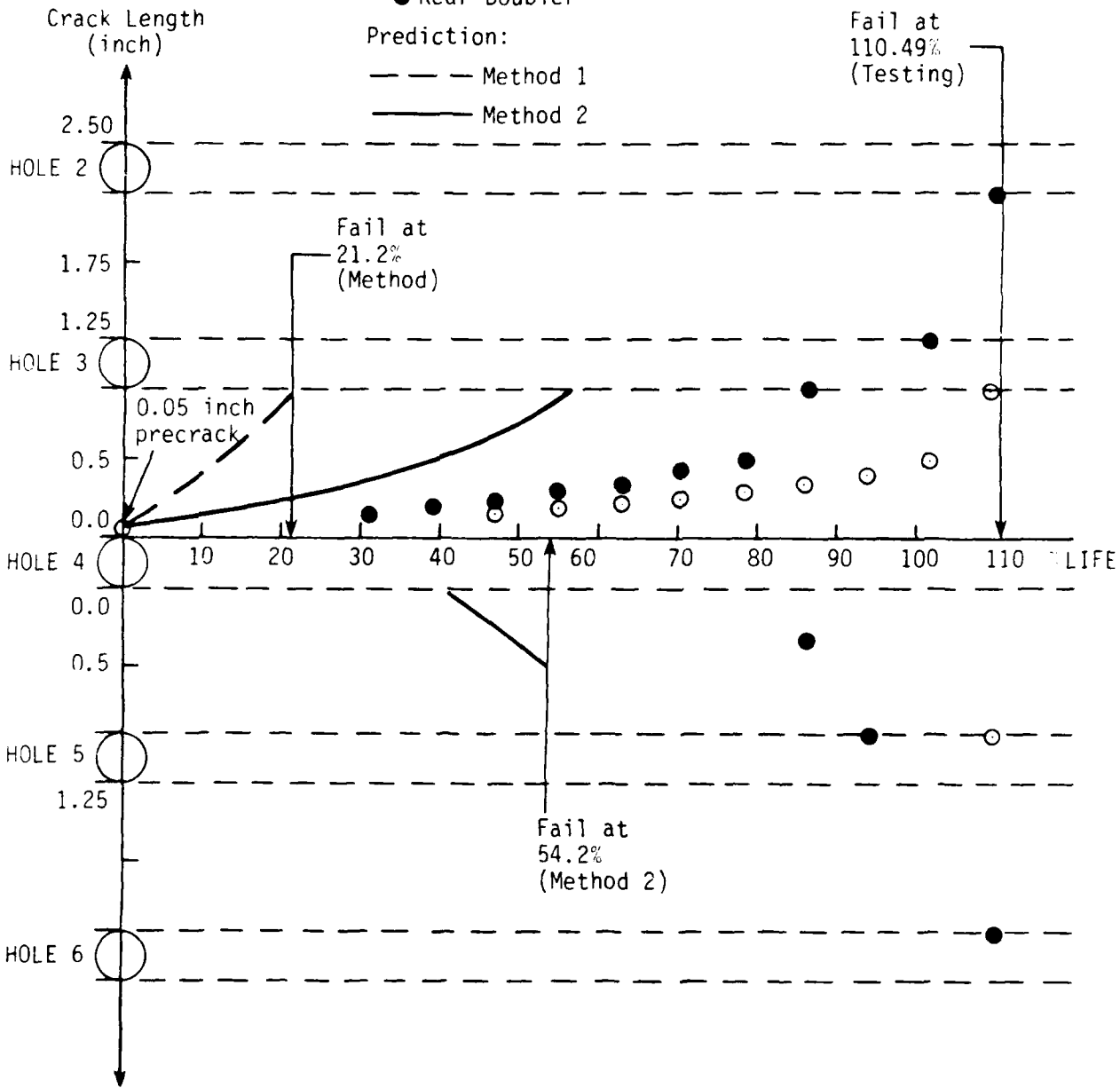


Figure 4.1.2-17. Crack Growth Diagram for Double-Shear Lap-Joint Specimen LJ-34

Spec. LJ 35 (Ref. Table 4.1.2-1)

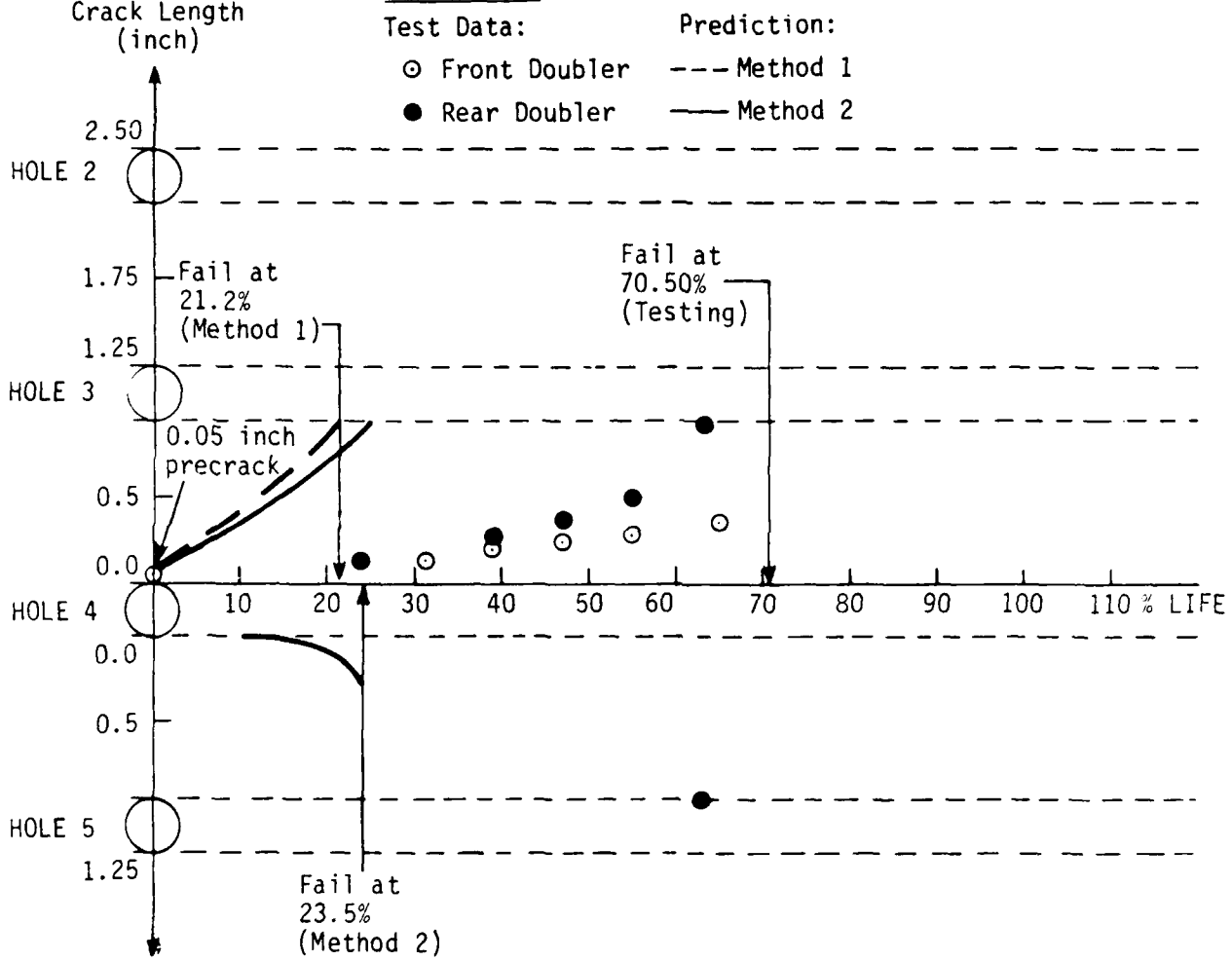


Figure 4.1.2-18. Crack Growth Diagram for Double-Shear Lap-Joint Specimen LJ-35

Spec LJ 36 (Ref. Table 4.1.2-1)

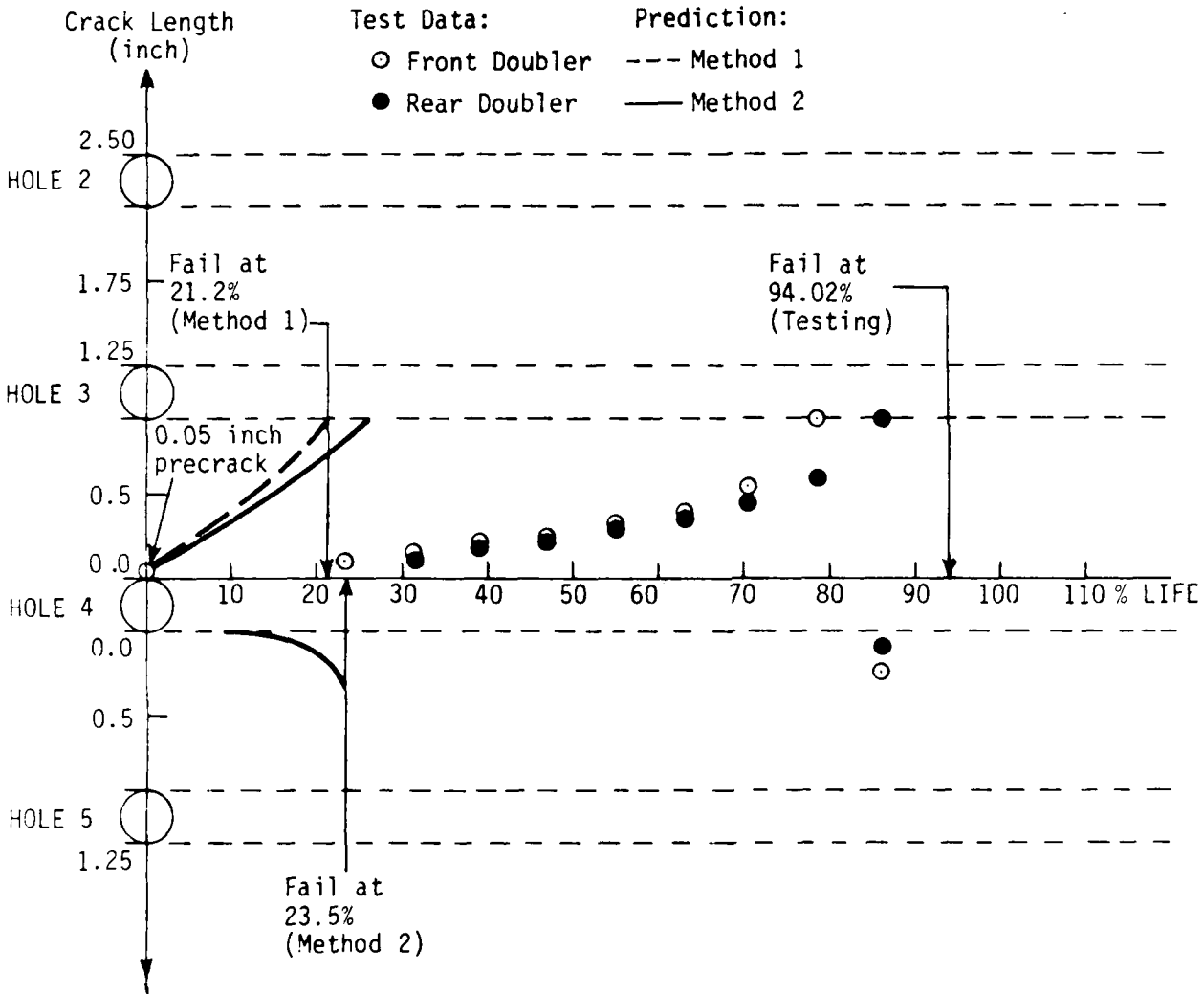


Figure 4.1.2-19. Crack Growth Diagram for Double-Shear Lap-Joint Specimen LJ-36

4.2 STRINGER-REINFORCED SPECIMENS TEST PROGRAM

The purpose of the stringer-reinforced specimen test program was to evaluate the effectiveness of the analytical methods in predicting crack growth and crack initiation of structural components typical of that used in airframe construction. It also provides a guideline in selecting critical initial flaw locations for damage tolerance analyses.

A total of thirty-six (36) specimens were tested. They included four (4) different specimen configurations as listed below:

- a. Center T-stringer with continuous skin,
- b. Center L-stringer with continuous skin,
- c. Edge L-stringer with continuous skin,
- d. Center T-stringer with split skin.

The specimens measured 48.0 inches in length and 18.0 inches in width. The thicknesses varied between 0.188 inch to 0.312 inch. The specimens were made of 2024-T3XX or 7075-T6XX aluminum alloys which is representative of material used in the lower wing covers of fighter/trainer and bomber/cargo type aircraft, respectively. All specimens contained an initial flaw of 0.050 inch located at the edge of a hole common to the stringer and skin. The initial flaws were introduced by means of a saw-cut followed by application of constant amplitude loading. The introduction of the initial flaw was done prior to the specimen assembly and the drilling of fastener holes other than the one containing the saw-cut.

Two flaw configurations were tested; they included those which were directed toward the upstanding leg of the stringer, and those directed away from the upstanding leg of the stringer. The stringers were mechanically attached to the skin by means of counter-sunk Hi-Loks varying in diameter between 0.188 inch to 0.312 inch.

The specimens were subjected to A-10A, AMAVS and constant amplitude loading until failure was achieved. Table 4.2-1 provides a description of the test program.

4.2.1 Test Results and Analytical Predictions

The test results of thirty-six (36) stringer reinforced specimens are summarized in Tables 4.2-2 through 4.2-4 for specimens subjected to constant amplitude, A-10A and AMAVS loading spectra. The tables present the average test data of two (2) similar test configurations and the corresponding analytical predictions. The analytical methods included predictions using Method 1 and Method 2. The predictions were made for the skin and the stringers from an initial flaw of 0.050 inch for each component independently. In actuality, redistribution of loads may occur when premature failure of stringer element occurs. The life of the specimens is assumed to be achieved when the skin cracking approaches the critical crack length. Figures 4.2-1, 4.2-2 and 4.2-3 present photos of the T-stringer split skin, the L-stringer continuous skin and the L-stringer continuous skin installed in MTS machine, respectively.

4.2.2 Experimental vs. Analytical Predictions of Specimens Subjected to Constant Amplitude Loading Spectrum

Crack Growth predictions for the stringer-reinforced specimens subjected to constant amplitude loading were close to the experimental results, and on the conservative side. The overall standard deviation with respect to the experimental results were 20.5% and 25.13% for Method 1 and Method 2, respectively. The nature of the loading spectrum did not require the use of interaction model, therefore the deviation in predicted life was small. Method 1 shows better accuracy than Method 2 by a small amount. A summary of experimental vs. analytical prediction correlation is provided in Table 4.2-2.

4.2.3 Experimental vs. Analytical Predictions of Specimens Subjected to A-10A Loading Spectrum

Crack growth predictions of stringer-reinforced specimens subjected to A-10A randomized loading spectrum were correlated against the test results. A summary of the correlation is provided in Table 4.2-3. Both Method 1 and Method 2 predictions are more conservative than the experimental results, however,

Method 1 predictions are more accurate than Method 2. The standard deviations for the entire set (12 specimens) were 36.48% and 45.25% for Method 1 and Method 2, respectively. In all cases, Type 'B' specimens survived longer than Type 'A' specimens. However, the analytical predictions do not confirm a similar difference.

4.2.4 Experimental vs. Analytical Predictions of Specimens Subjected to AMAVS Loading Spectrum

Crack growth predictions for stringer-reinforced specimens subjected to AMAVS randomized loading spectrum were correlated against the test results. A summary of the correlation is provided in Table 4.2-4. In most cases the predictions were on the conservative side, except specimen -11A which failed at a life of 259,786 cycles vs. predicted lives of 281,125 cycles and 309,229 cycles for Method 1 and Method 2, respectively. It must be indicated that very conservative analytical predictions were performed prior to testing. The da/dN was subsequently revised to reflect more realistic fit of the test data (Figure 3.4-6). For specimens -9A, and -9B with split skin configuration, specimens failed statically subsequent to crack skin failure although the crack did not initiate in the adjacent skin.

TABLE 4.2-1. TEST MATRIX FOR STRINGER-REINFORCED SPECIMENS

SPECIMEN TYPE	DASH No.	SPECIMEN CONFIGURATION ID	MATERIAL	APPLIED SPECTRUM	MAX. STRESS (ksi)	MIN. STRESS (ksi)
Center T-Stringer	-1A	39,40	2024-T3XX	A-10A	35.75	-8.34
Continuous Skin	-1B	43,44	2024-T3XX	A-10A	35.75	-8.34
Center L-Stringer	-3A	47,48	2024-T3XX	A-10A	35.75	-8.34
Continuous Skin	-3B	50,52	2024-T3XX	A-10A	28.0	-6.54
Edge L-Stringer	-5A	55,56	2024-T3XX	A-10A	35.75	-8.34
Continuous Skin	-5B	59,60	2024-T3XX	A-10A	35.75	-8.34
Center T-Stringer	-7A	61,62	7075-T6XX	AMAVS	30.5	-6.64
Continuous Skin	-7B	63,64	7075-T6XX	AMAVS	30.5	-6.64
Center T-Stringer	-9A	65,66	7075-T6XX	AMAVS	30.5	-6.64
Split Skin	-9B	67,68	7075-T6XX	AMAVS	30.5	-6.64
Edge L-Stringer	-11A	69,70	7075-T6XX	AMAVS	21.50	-4.72
Continuous Skin	-11B	71,72	7075-T6XX	AMAVS	21.50	-4.72
Center T-Stringer	-1A	37,38	2024-T3XX	C.A.	17.0	1.70
Continuous Skin	-1B	41,42	2024-T3XX	C.A.	17.0	1.70
Center L-Stringer	-3A	45,46	2024-T3XX	C.A.	17.0	1.70
Continuous Skin	-3B	49,51	2024-T3XX	C.A.	17.0	1.70
Edge L-Stringer	-5A	53,54	2024-T3XX	C.A.	17.0	1.70
Continuous Skin	-5B	57,58	2024-T3XX	C.A.	17.0	1.70

TABLE 4.2-2. EXPERIMENTAL VS. PREDICTED LIFE FOR STRINGER-REINFORCED SPECIMENS SUBJECTED TO CONSTANT AMPLITUDE LOADING SPECTRUM

SPECIMEN TYPE	DASH NO.	MAXIMUM GROSS STRESS (ksi)	EXPERIMENTAL LIFE TO FAILURE (CYCLES)	ELEMENT	ANALYTICAL PREDICTION			
					METHOD 1		METHOD 2	
					LIFE (CYCLES)	%DEV	LIFE (CYCLES)	%DEV
Center T-Stringer	-1A	17.0	65,820	Skin	56,198	14.6	59,629	9.6
				St'r	26,659		26,659	
Continuous Skin	-1B	17.0	65,142	Skin	57,894	11.1	48,632	25.3
				St'r	21,754		17,047	
Center L-Stringer	-3A	17.0	76,025	Skin	64,021	15.8	60,881	19.9
				St'r	38,434		38,369	
Continuous Skin	-3B	17.0	72,900	Skin	64,021	12.2	60,881	16.5
				St'r	45,000		45,000	
Edge L-Stringer	-5A	17.0	67,136	Skin	59,579	11.3	51,158	23.8
				St'r	25,578		33,341	
Continuous Skin	-5B	17.0	87,647	Skin	36,812	58.0	38,806	55.7
				St'r	39,933		51,202	
EXPERIMENTAL/ANALYTICAL AVERAGE DEV.						20.3		25.13

TABLE 4.2-3. EXPERIMENTAL VS. PREDICTED LIFE FOR STRINGER-REINFORCED SPECIMENS SUBJECTED TO A-10A LOADING SPECTRUM

SPECIMEN TYPE	DASH NO.	MAXIMUM GROSS STRESS (ksi)	EXPERIMENTAL LIFE TO FAILURE (CYCLES)	ELEMENT	ANALYTICAL PREDICTION			
					METHOD 1		METHOD 2	
					LIFE (CYCLES)	%DEV	LIFE (CYCLES)	%DEV
Center T-Stringer	-1A	35.75	191,290	Skin	111,954	41.4	103,871	45.7
				St'r	44,774		52,093	
Continuous Skin	-1B	35.75	202,143	Skin	127,195	37.1	104,000	48.6
				St'r	37,220		37,220	
Center L-Stringer	-3A	35.75	240,210	Skin	144,182	40.0	119,452	50.3
				St'r	119,341		118,948	
Continuous Skin	-3B	28.0	574,875	Skin	341,174	40.6	297,818	48.2
				St'r	496,942		474,693	
Edge L-Stringer	-5A	35.75	130,860	Skin	119,372	8.8	94,235	28.0
				St'r	82,292		89,139	
Continuous Skin	-5B	35.75	151,970	Skin	74,447	51.0	74,885	50.7
				St'r	112,448		141,660	
EXPERIMENTAL/ANALYTICAL AVERAGE DEV.						36.48		45.25

TABLE 4.2-4. EXPERIMENTAL VS. PREDICTED LIFE FOR STRINGER-REINFORCED SPECIMENS SUBJECTED TO AMAVS LOADING SPECTRUM

SPECIMEN TYPE	DASH NO.	MAXIMUM GROSS STRESS (ksi)	EXPERIMENTAL LIFE TO FAILURE (CYCLES)	ELEMENT	ANALYTICAL PREDICTION			
					METHOD 1		METHOD 2	
					LIFE (CYCLES)	%DEV	LIFE (CYCLES)	%DEV
Center T-Stringer	-7A	30.0	146,742	Skin	128,230	12.6	86,214	41.2
Continuous Skin	-7B	30.0	180,150	St'r	117,621		82,554	
				Skin	107,752	40.2	95,800	46.8
				St'r	55,724		60,910	
Center T-Stringer	-9A	30.0	180,269	Skin	53,865	70.1	61,476	65.9
Split Skin	-9B	30.0	164,362	St'r	117,621		82,554	
				Skin	89,960	45.3	75,061	54.3
				St'r	55,724		60,910	
Edge L-Stringer	-11A	20.0	259,786	Skin	281,125	-8.2	309,229	-19.0
Continuous Skin	-11B	20.0	535,153	St'r	146,185		151,944	
				Skin	200,268	62.6	213,812	60.0
				St'r	187,2371		188,220	
EXPERIMENTAL/ANALYTICAL AVERAGE DEV.						39.83		47.86

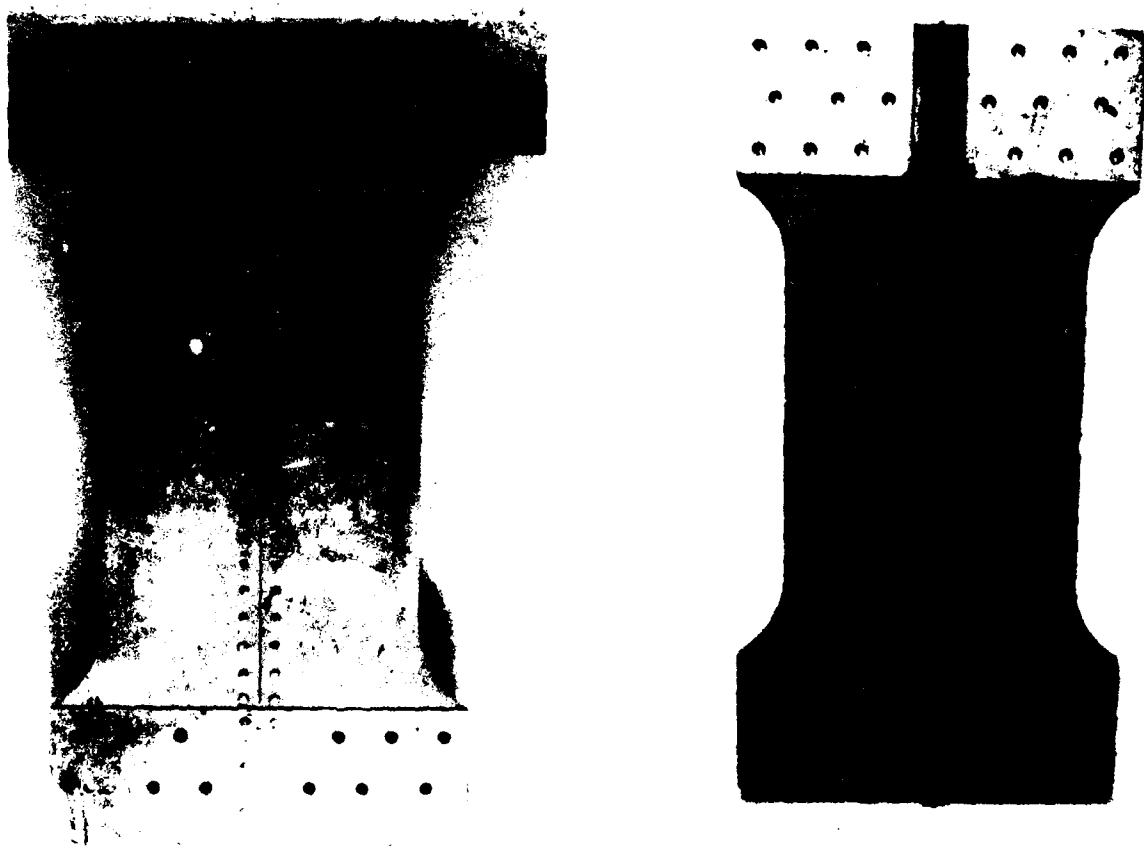


Figure 4.2-1. Stringer Reinforced Specimen Center 'TEE' Split Skin

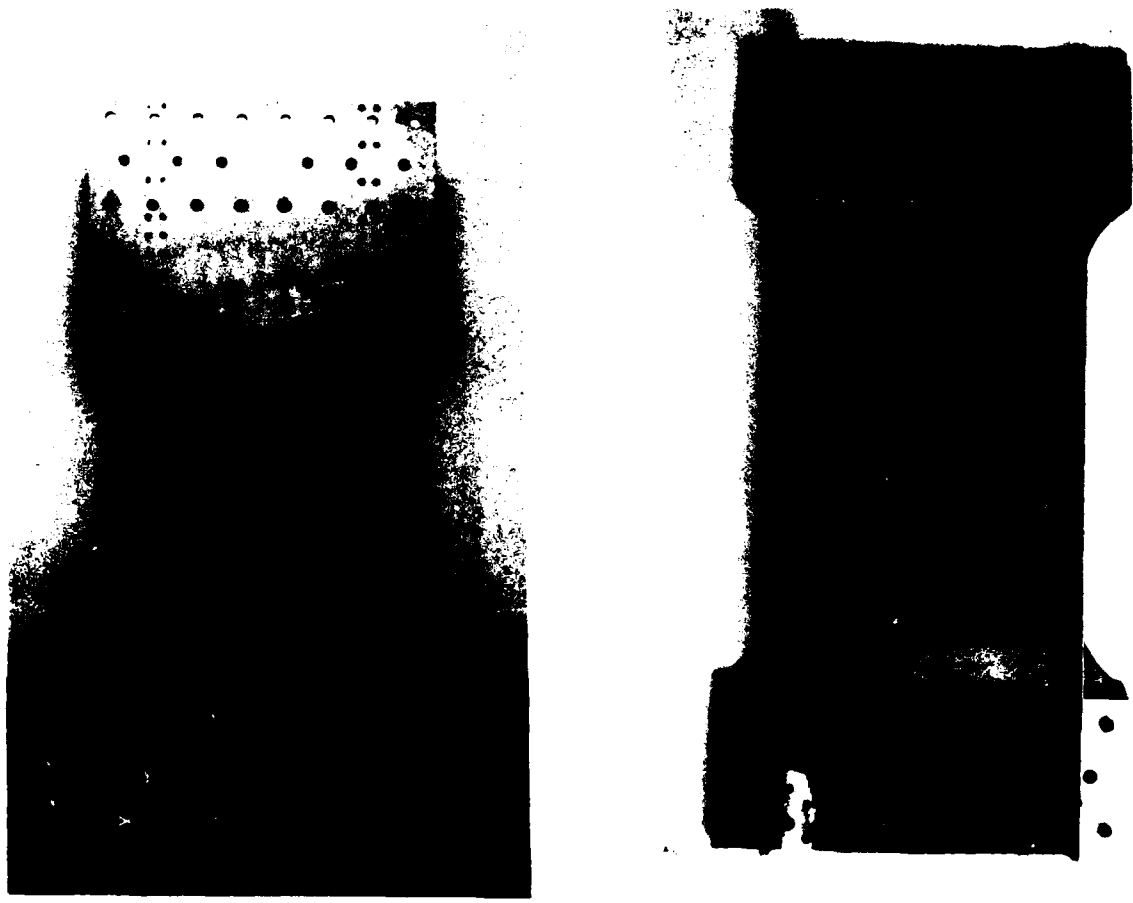


Figure 4.2-2. Stringer Reinforced Specimen Edge 'L' Stringer Continuous Skin



Figure 4.2-3. Stringer Reinforced Specimen Installed on MTS Machine

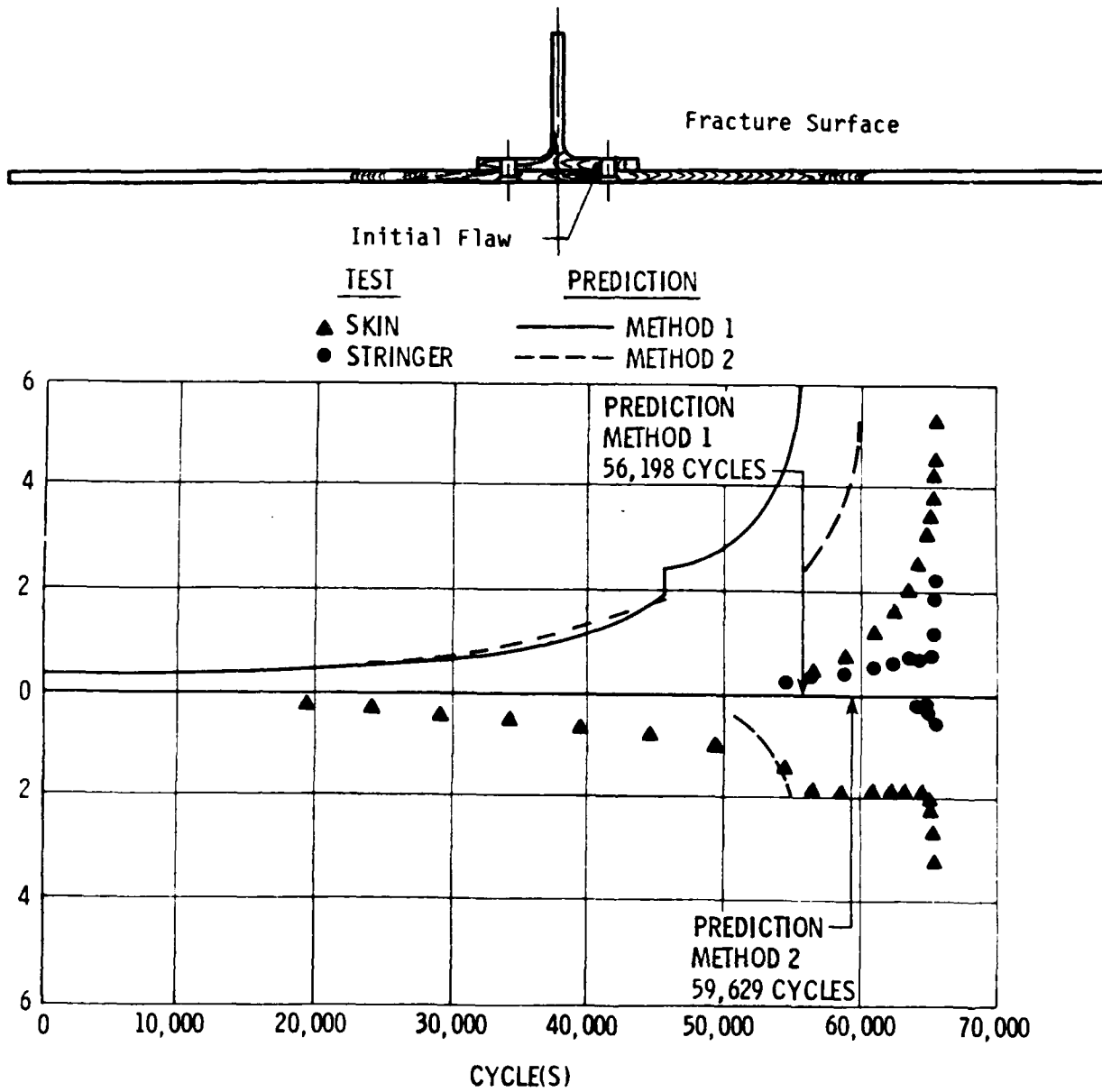


Figure 4.2-4. Crack Growth Diagram for Stringer-Reinforced Specimen No. 37 (-1A) Subjected to C.A. Loading Spectra

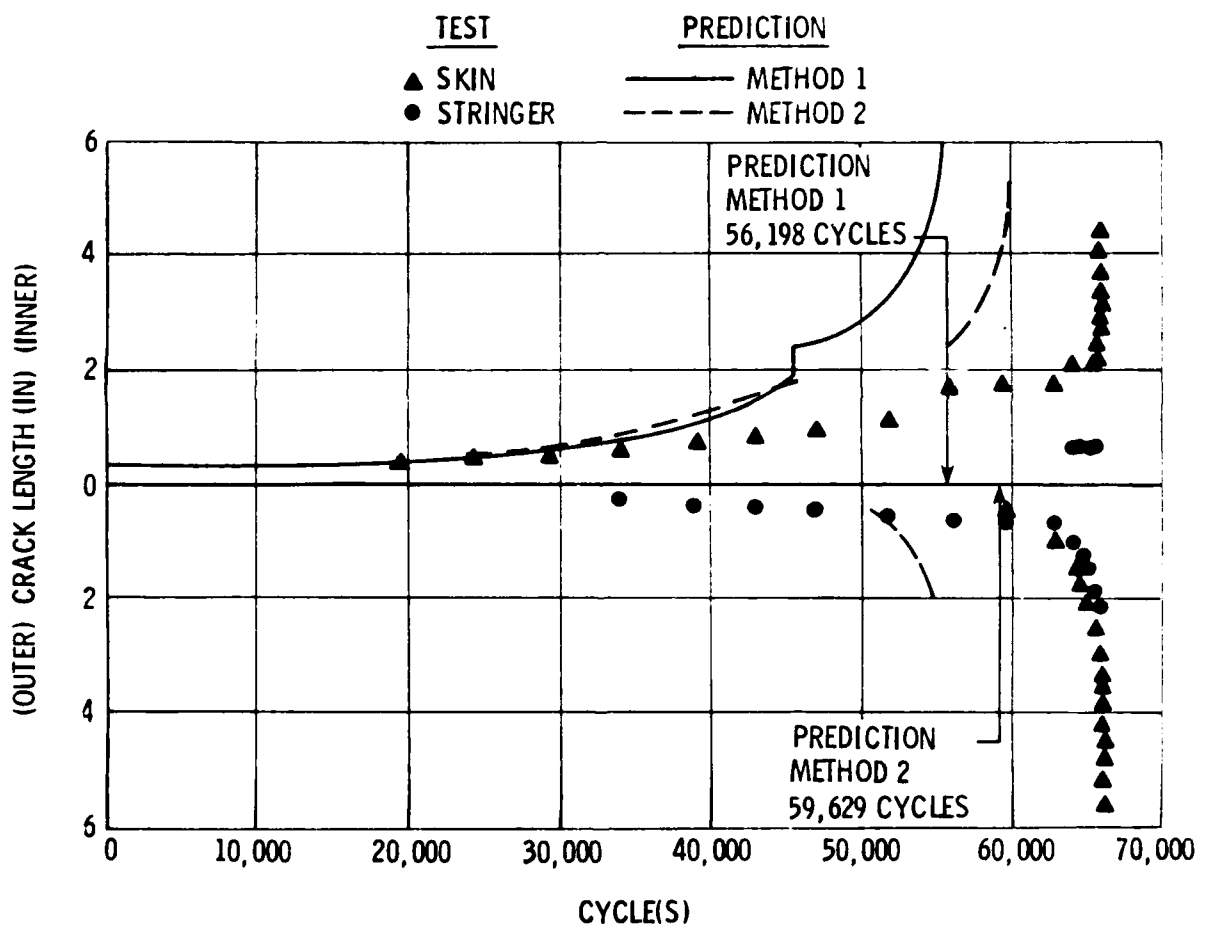
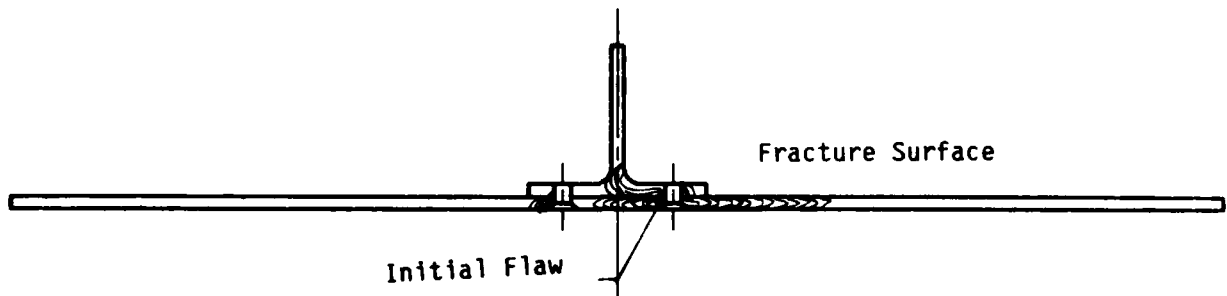
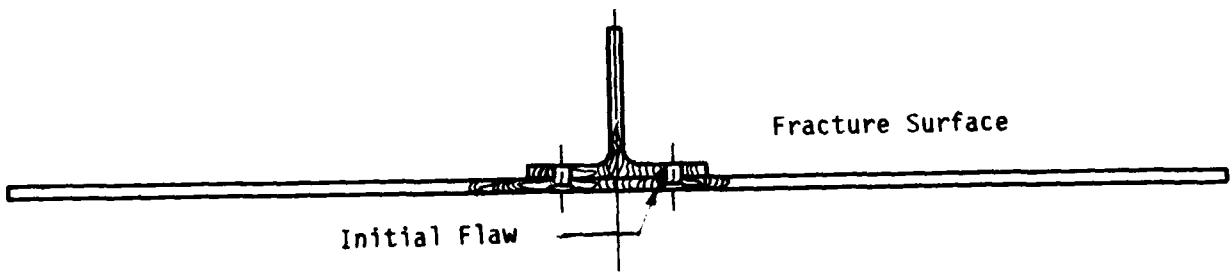


Figure 4.2-5. Crack Growth Diagram for Stringer-Reinforced Specimen No. 38 (-1A) Subjected to C.A. Loading Spectra



TEST
 ▲ SKIN
 ● STRINGER

PREDICTION
 — METHOD 1
 - - - METHOD 2

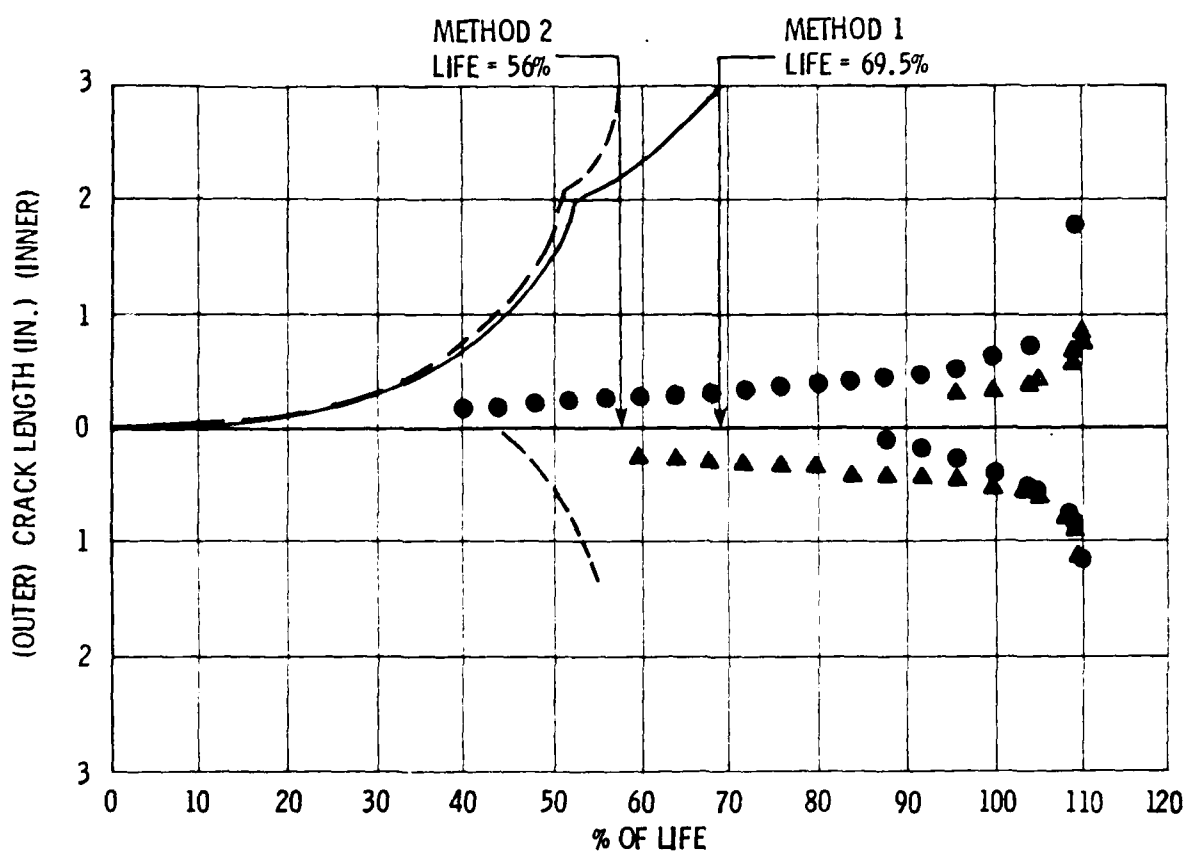


Figure 4.2-6. Crack Growth Diagram for Stringer-Reinforced Specimen No. 39 (-1A) Subjected to A-10A Loading Spectra

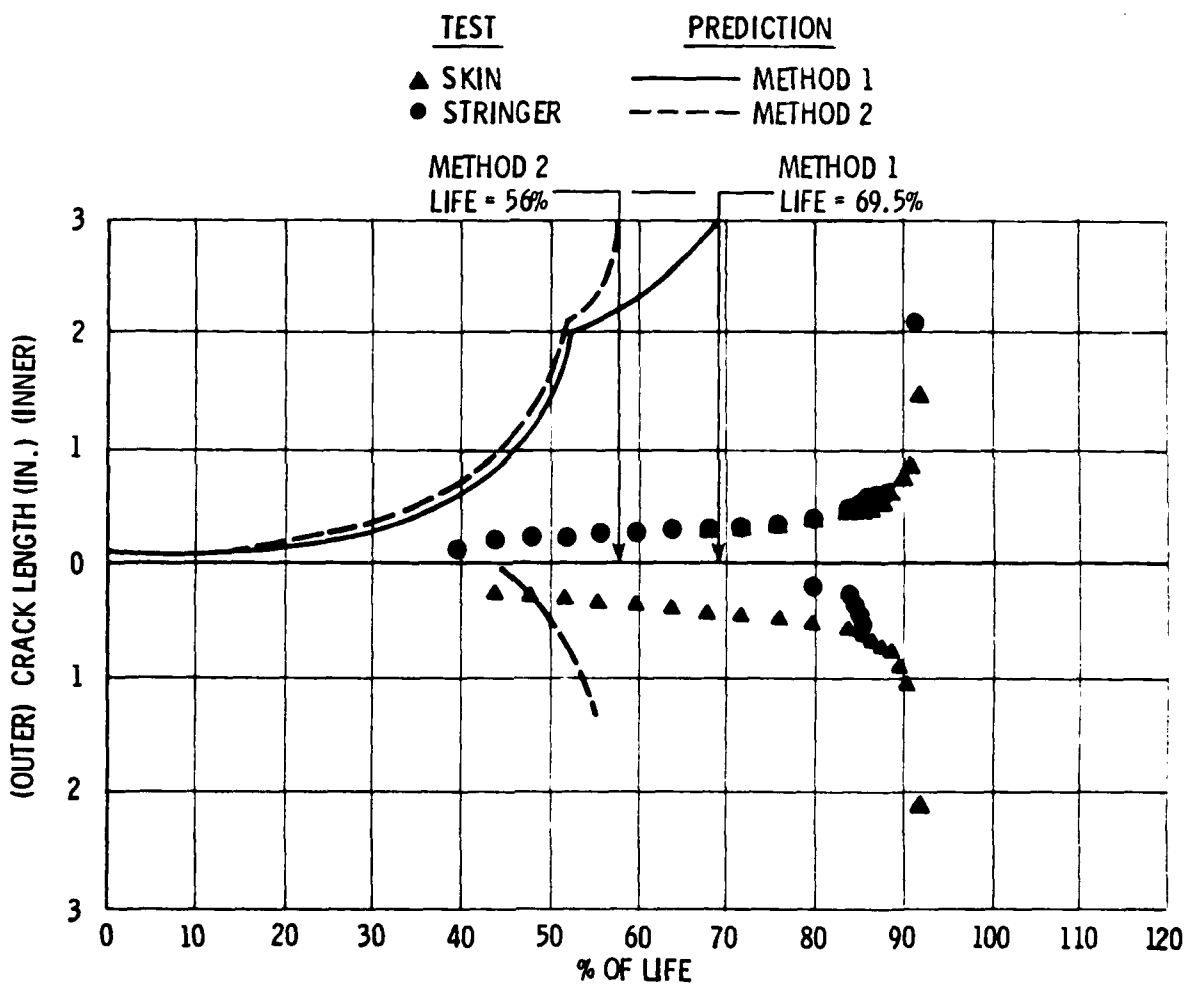
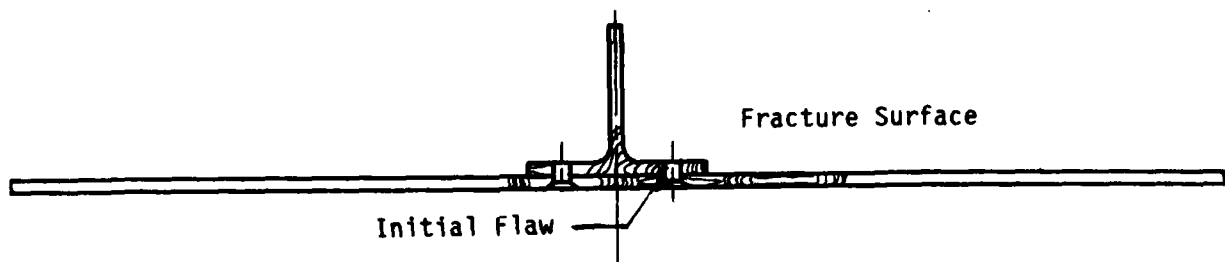


Figure 4.2-7. Crack Growth Diagram for Stringer-Reinforced Specimen No. 40 (-1A) Subjected to A-10A Loading Spectra

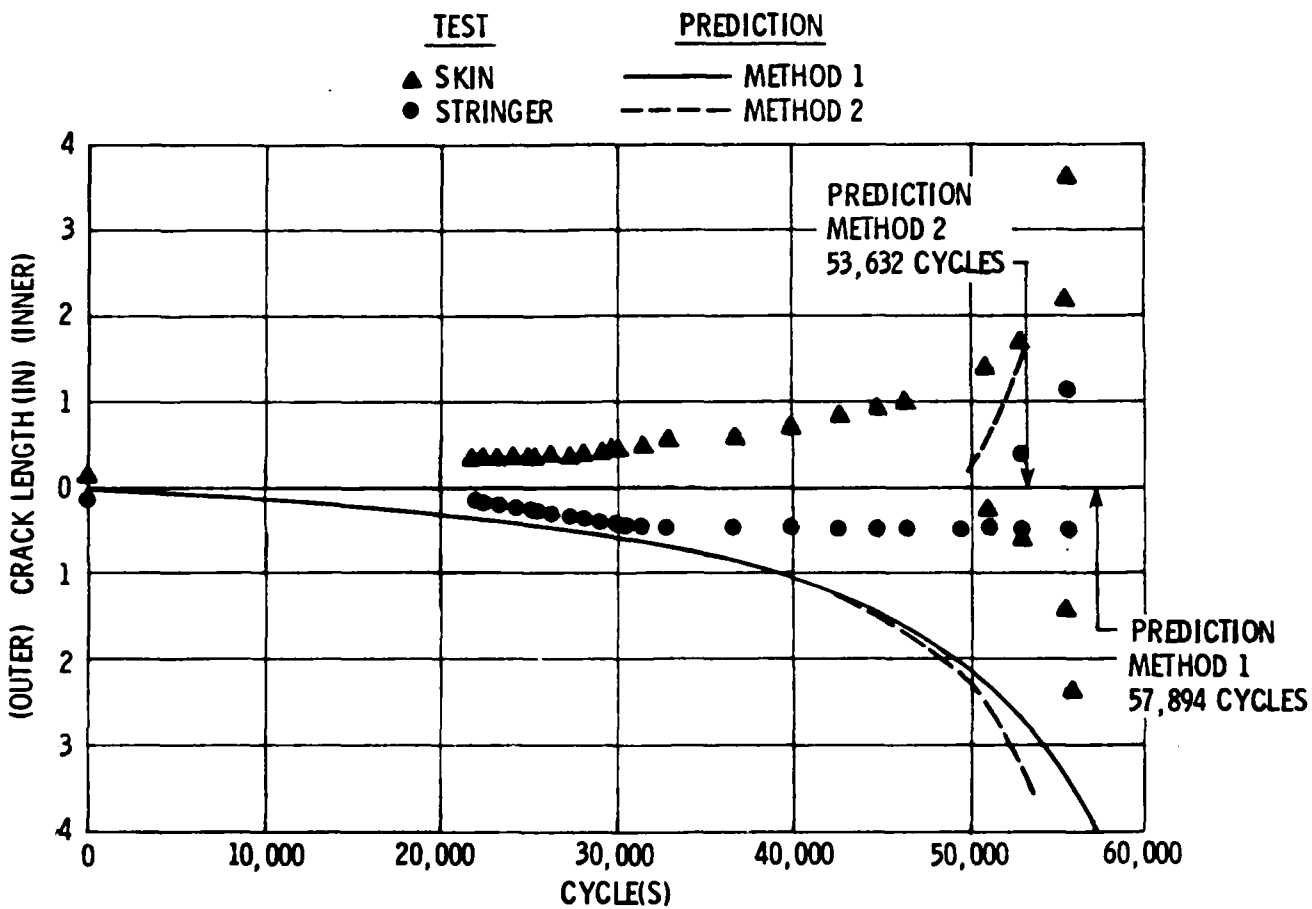
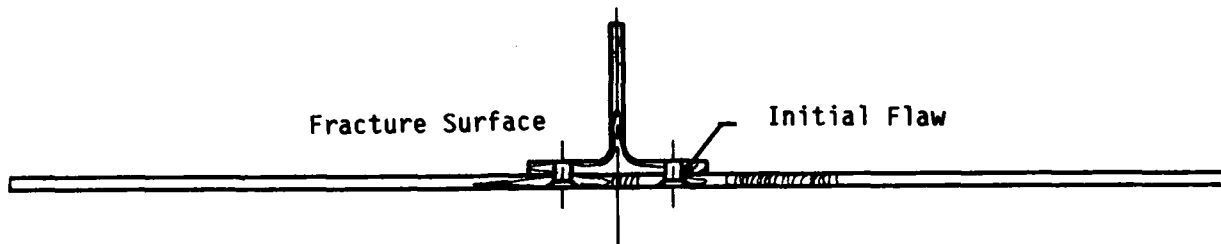


Figure 4.2-8. Crack Growth Diagram for Stringer-Reinforced Specimen No. 41 (-1B) Subjected to C.A. Loading Spectra

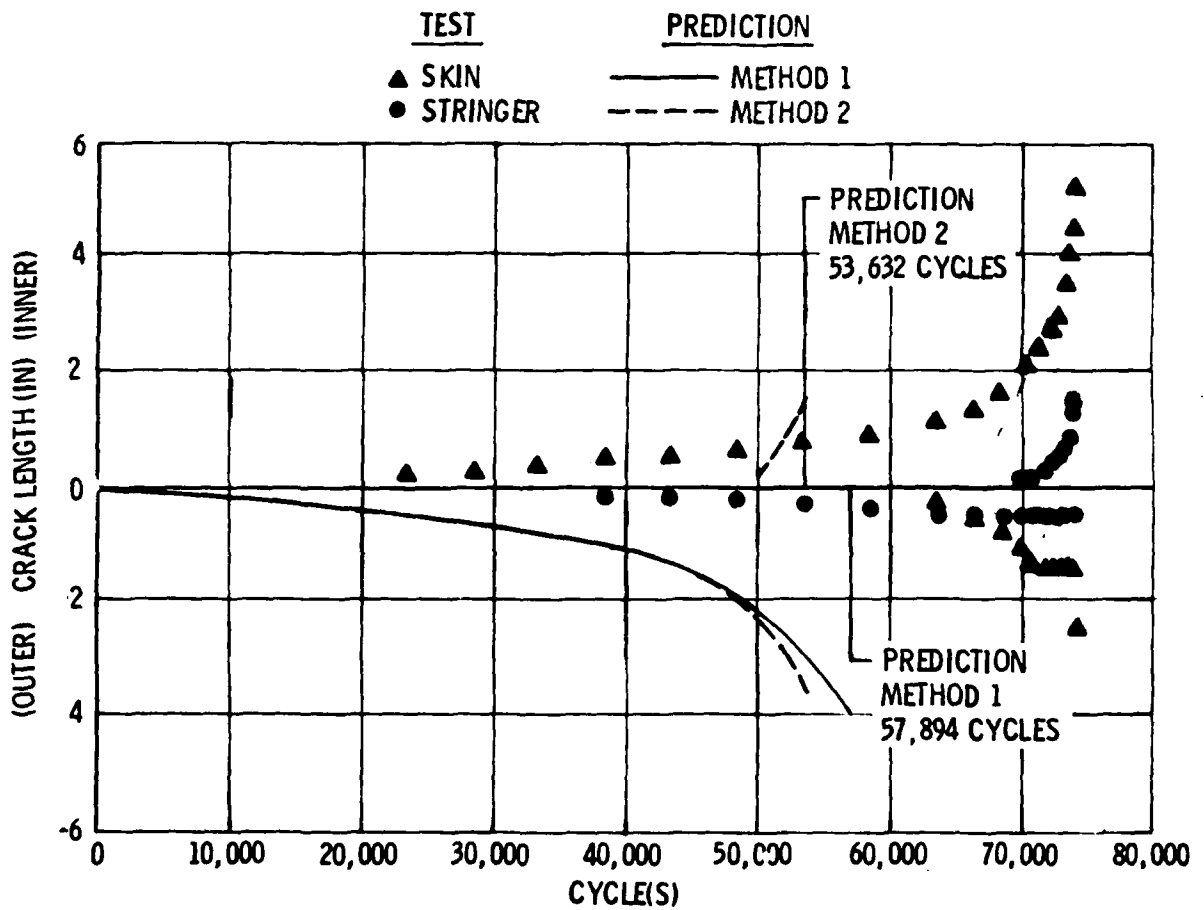
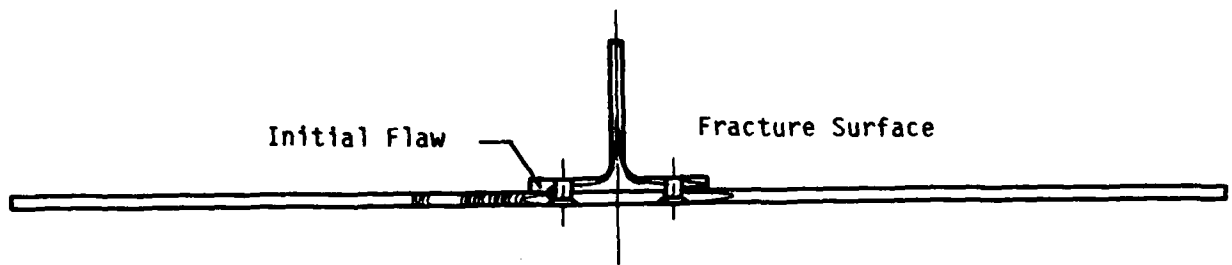


Figure 4.2-9. Crack Growth Diagram for Stringer-Reinforced Specimen No. 42 (-1B) Subjected to C.A. Loading Spectra

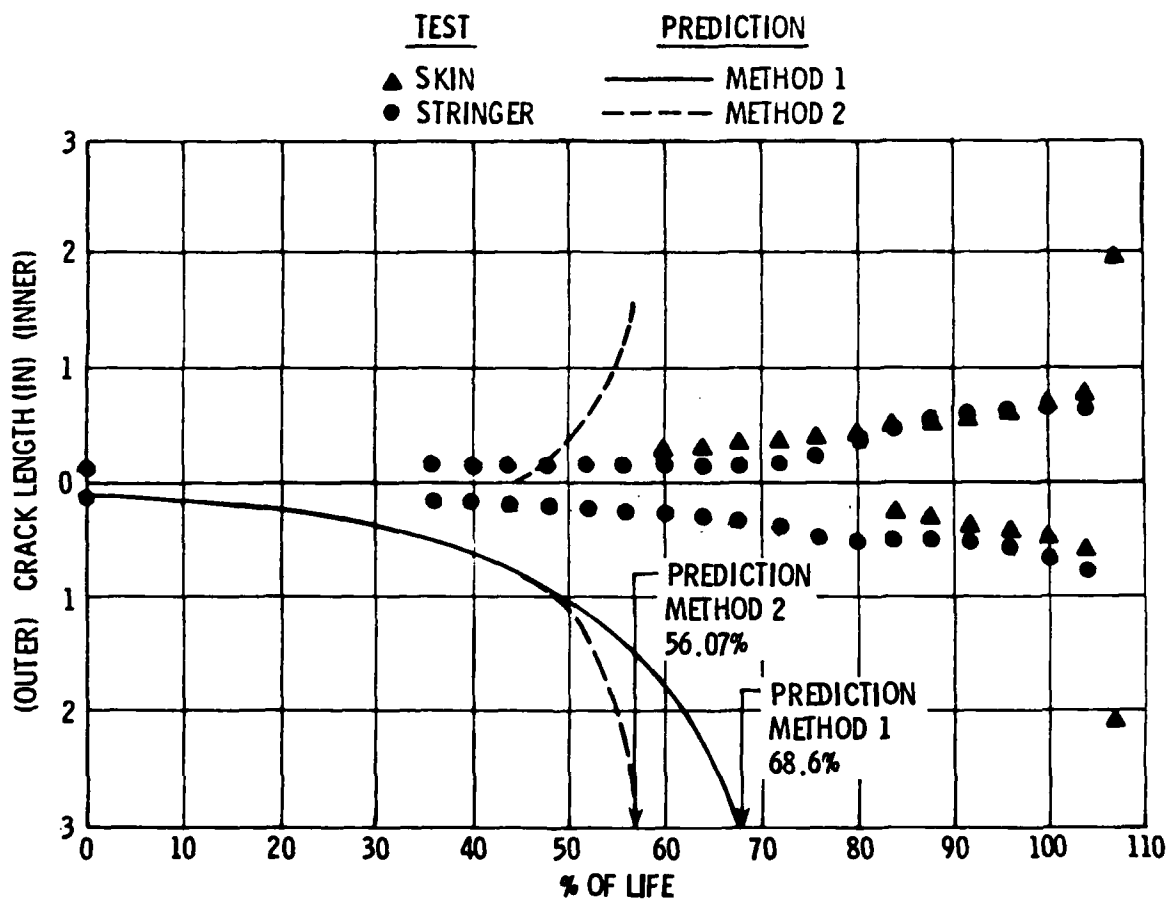
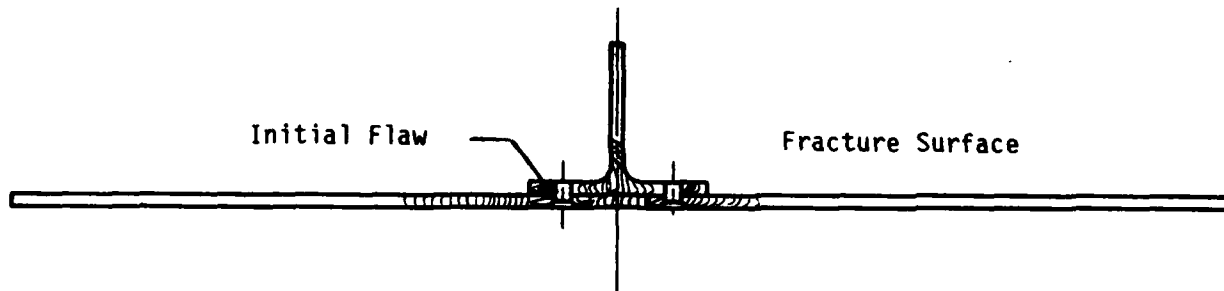


Figure 4.2-10. Crack Growth Diagram for Stringer-Reinforced Specimen No. 43 (-1B) Subjected to A-10A Loading Spectra

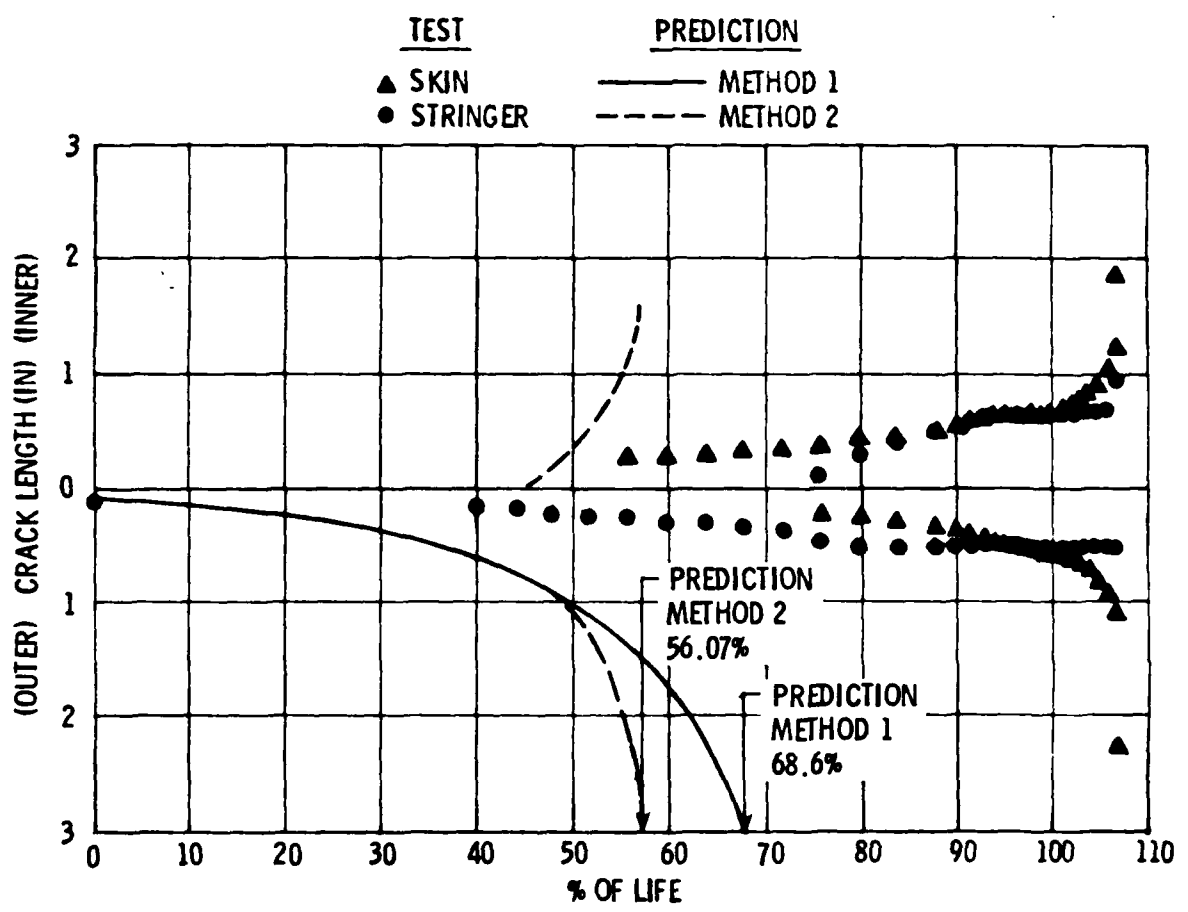
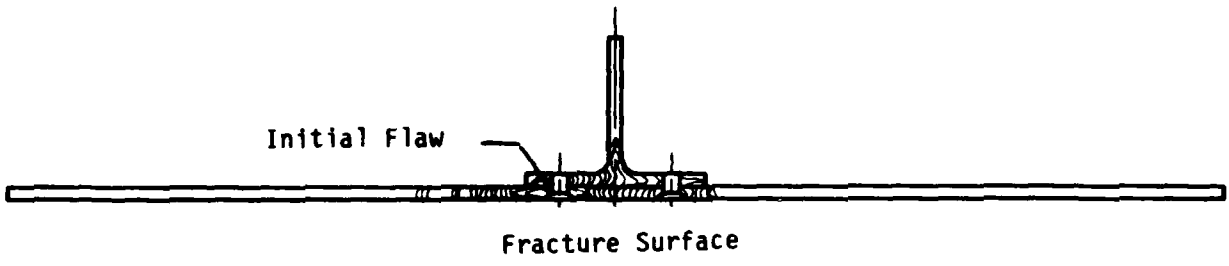


Figure 4.2-11. Crack Growth Diagram for Stringer-Reinforced Specimen No. 44 (-18) Subjected to A-10A Loading Spectra

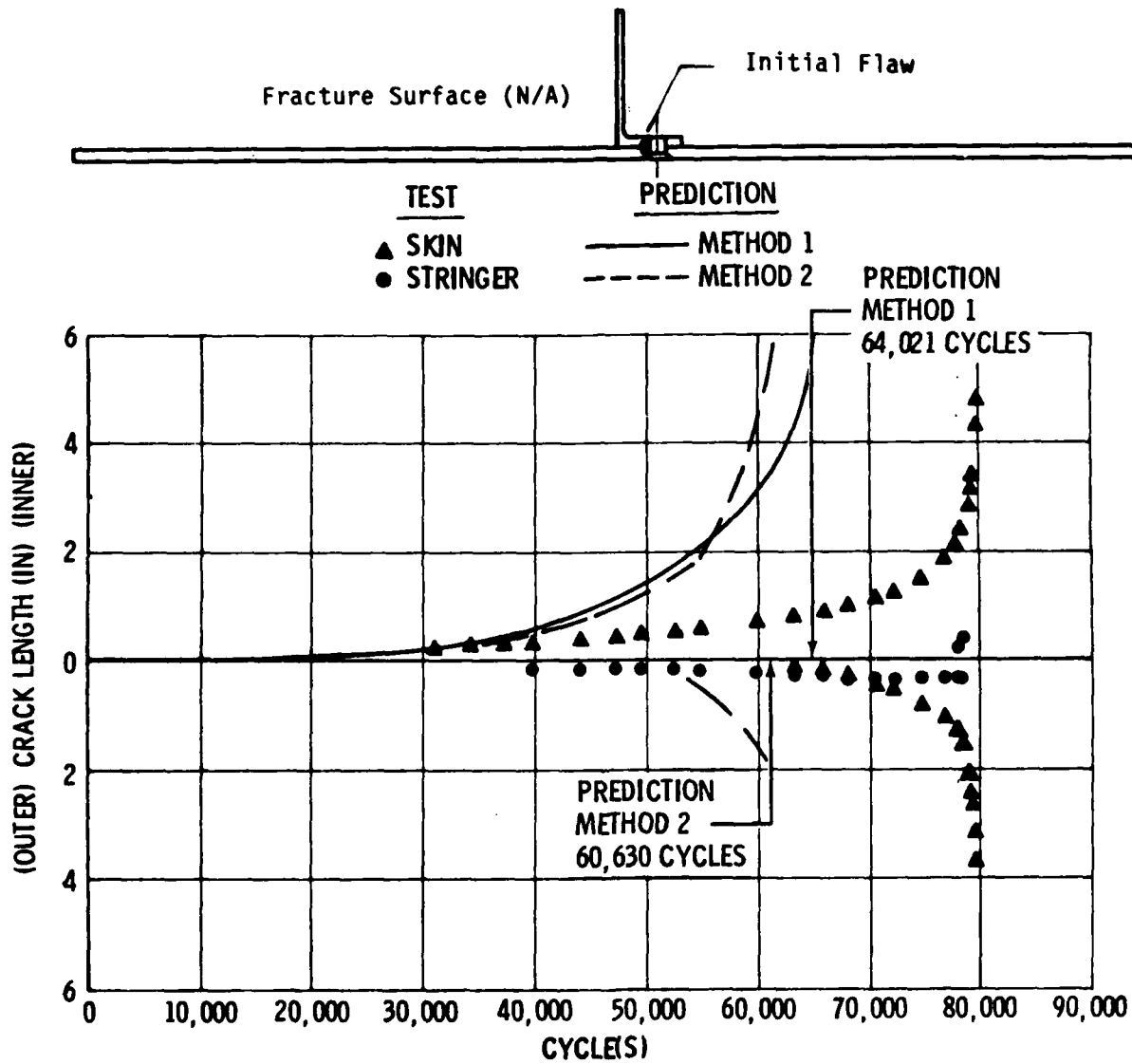


Figure 4.2-12. Crack Growth Diagram for Stringer-Reinforced Specimen No. 45 (-3A) Subjected to C.A. Loading Spectra

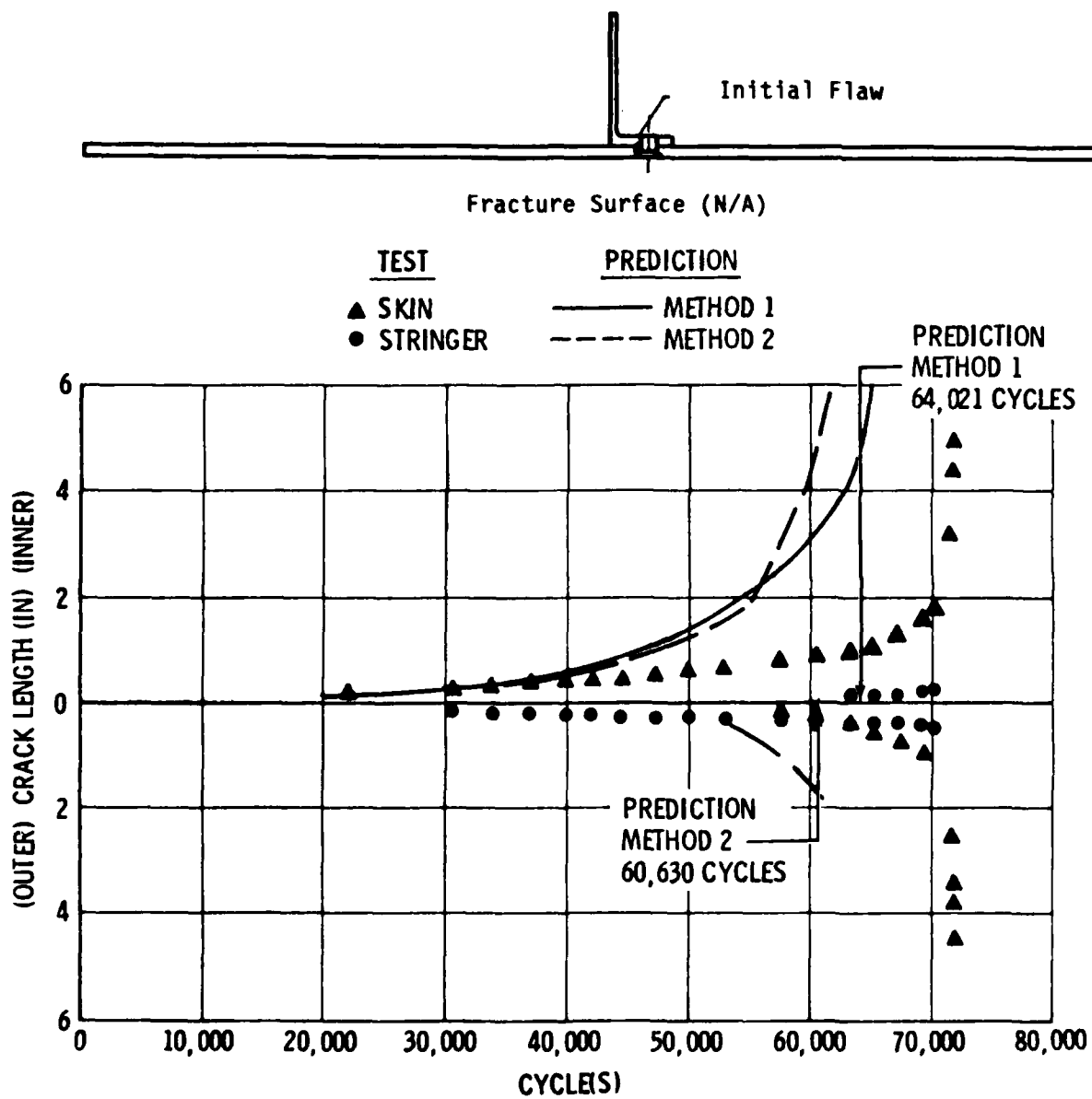


Figure 4.2-13. Crack Growth Diagram for Stringer-Reinforced Specimen No. 46 (-3A) Subjected to C.A. Loading Spectra

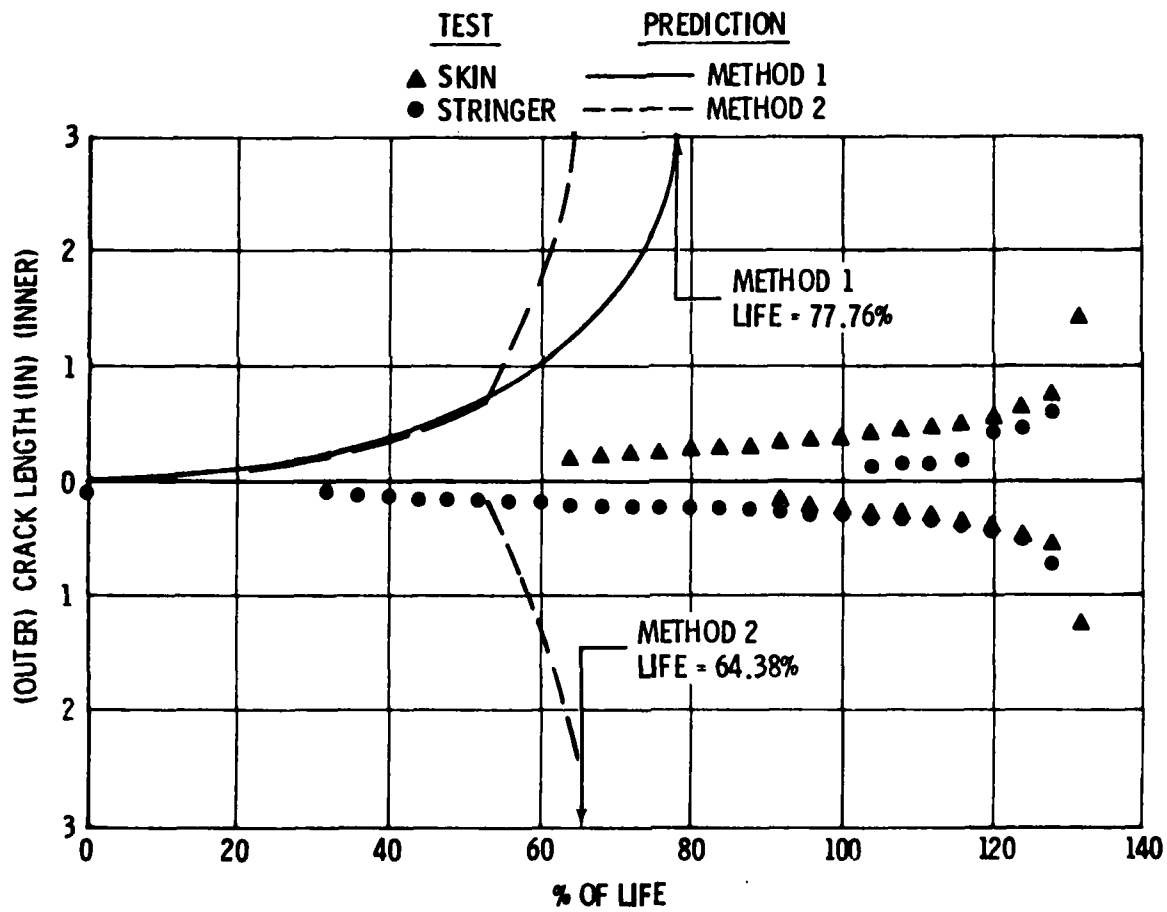
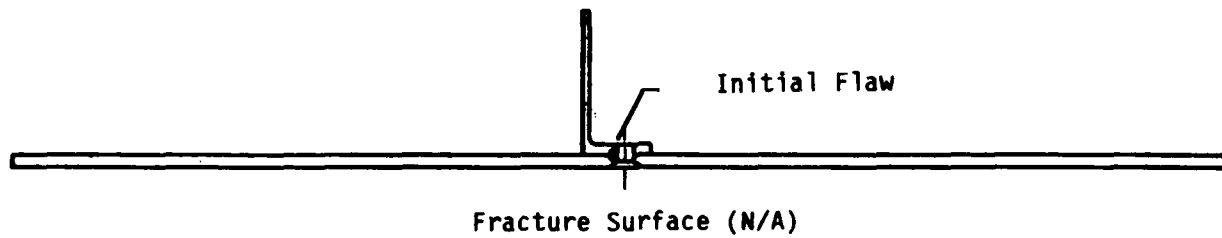


Figure 4.2-14. Crack Growth Diagram for Stringer-Reinforced Specimen No. 47 (-3A) Subjected to A-10A Loading Spectra

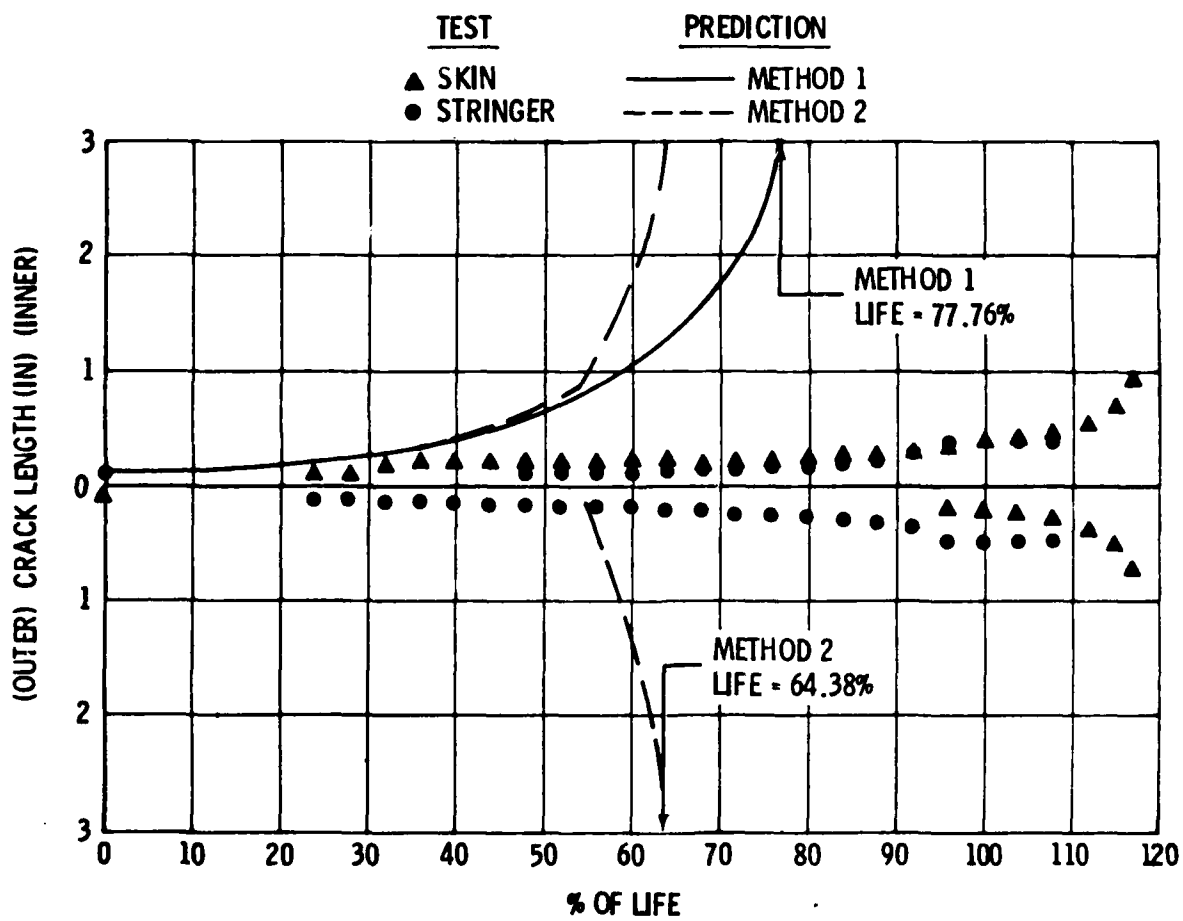
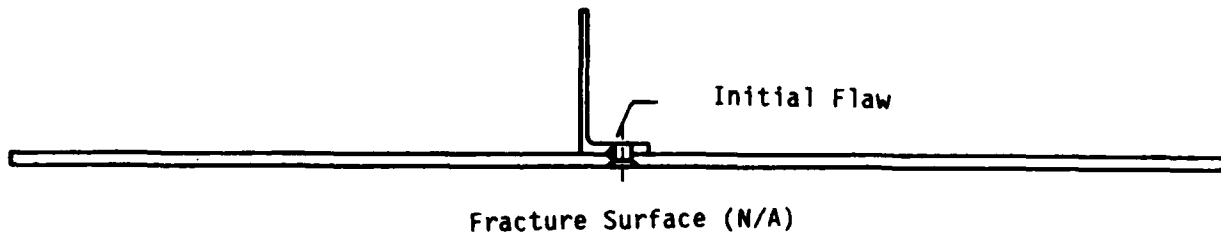


Figure 4.2-15. Crack Growth Diagram for Stringer-Reinforced Specimen No. 48 (-3A) Subjected to A-10A Loading Spectra

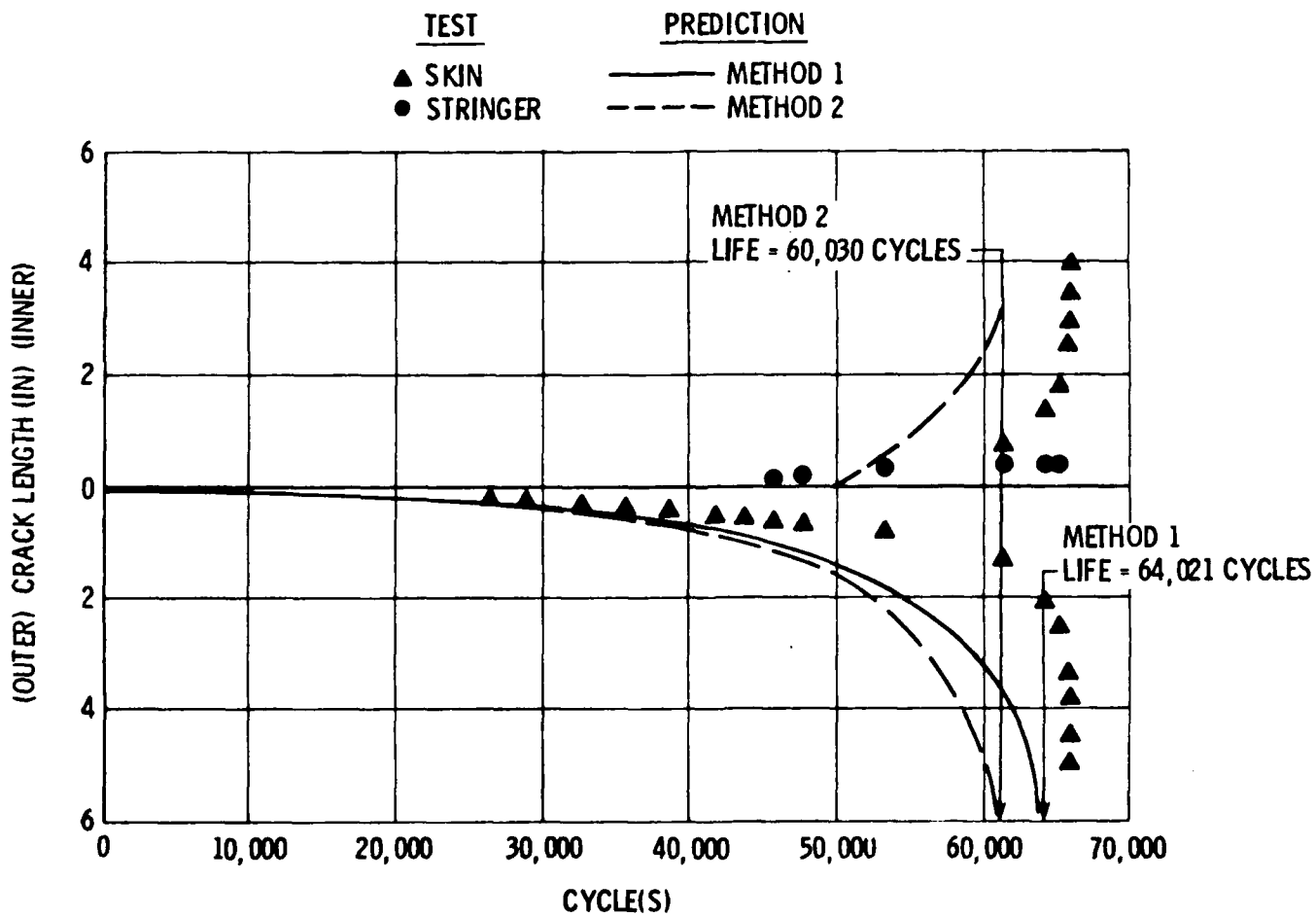
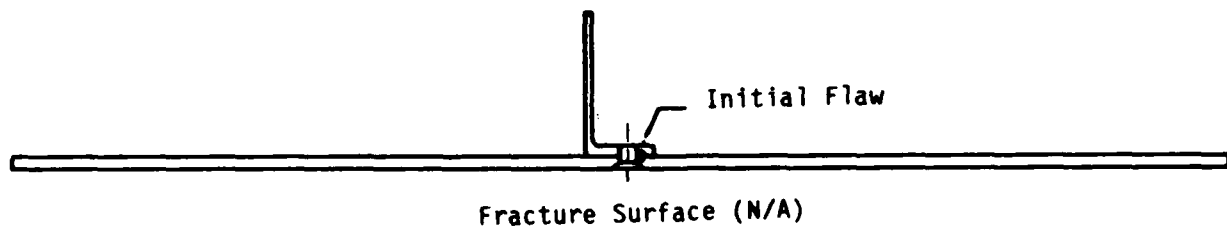


Figure 4.2-16. Crack Growth Diagram for Stringer-Reinforced Specimen No. 49 (-3B) Subjected to C.A. Loading Spectra

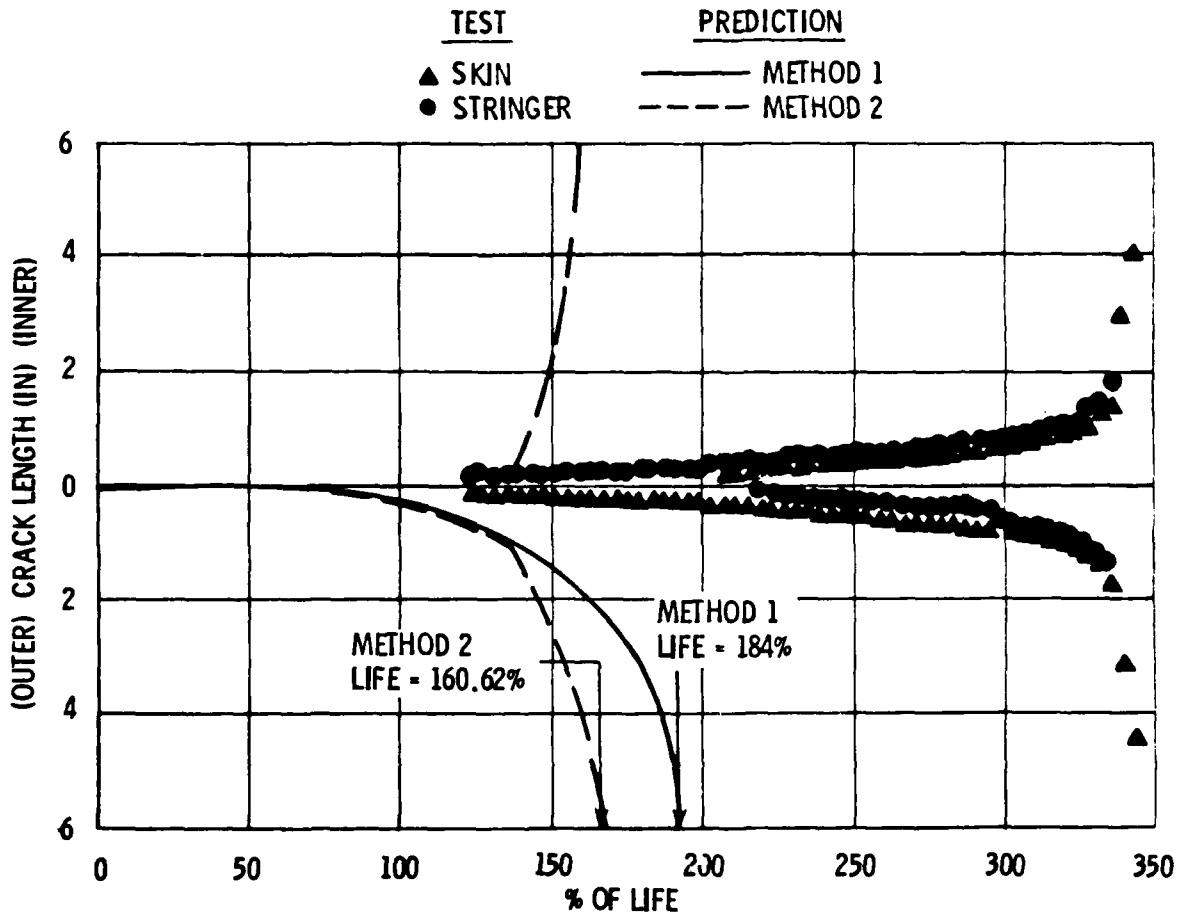
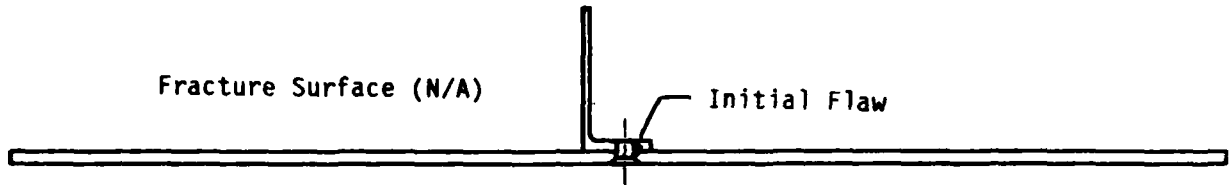


Figure 4.2-17. Crack Growth Diagram for Stringer-Reinforced Specimen No. 50 (-38) Subjected to A-10A Loading Spectra

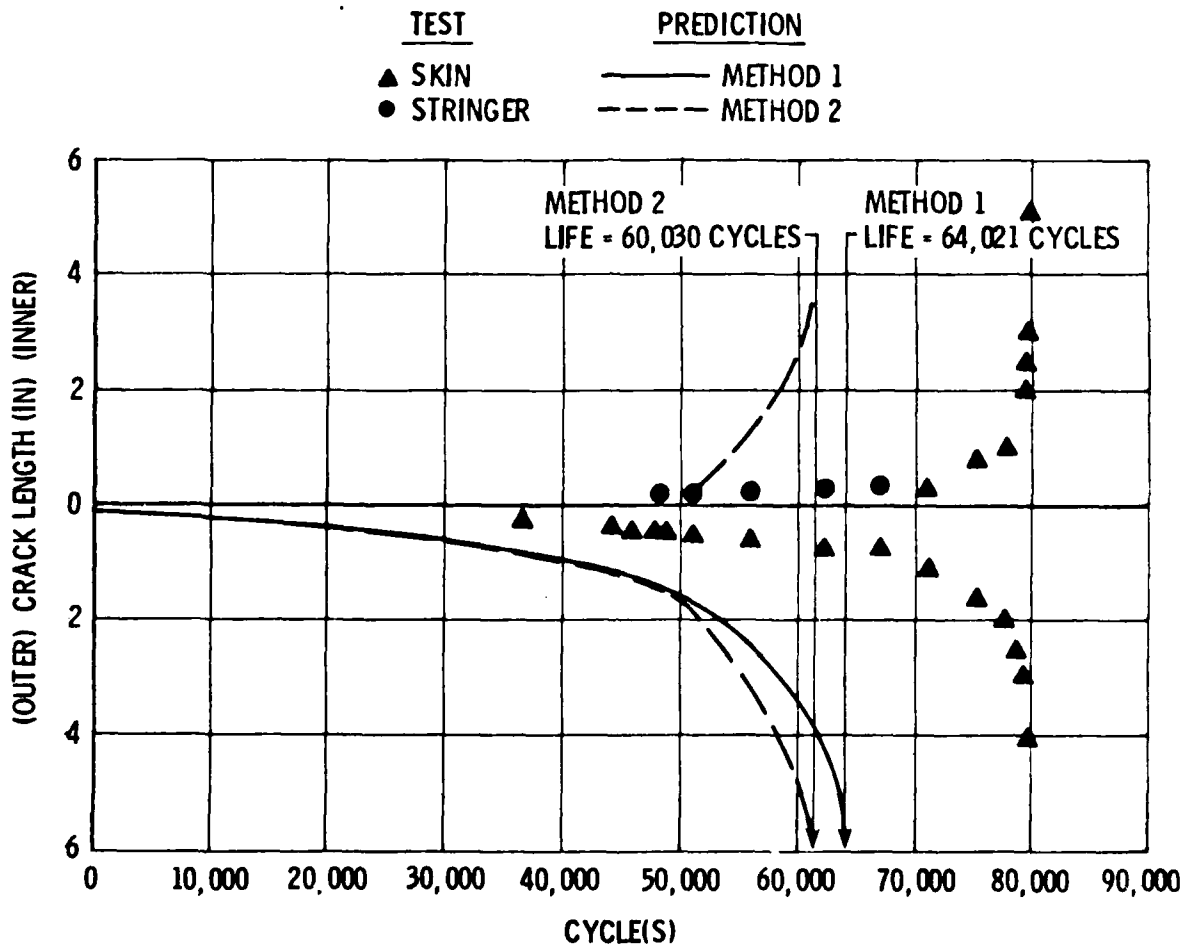
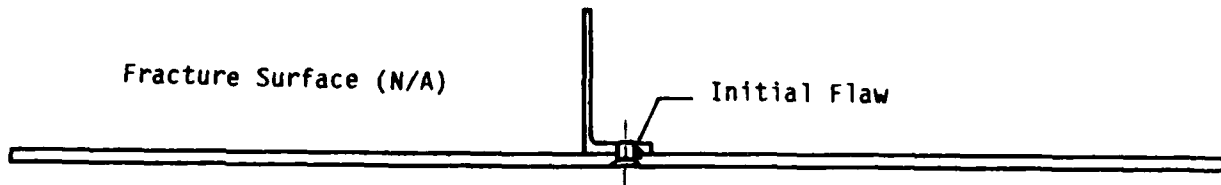


Figure 4.2-18. Crack Growth Diagram for Stringer-Reinforced Specimen No. 51 (-3B) Subjected to C.A. Loading Spectra

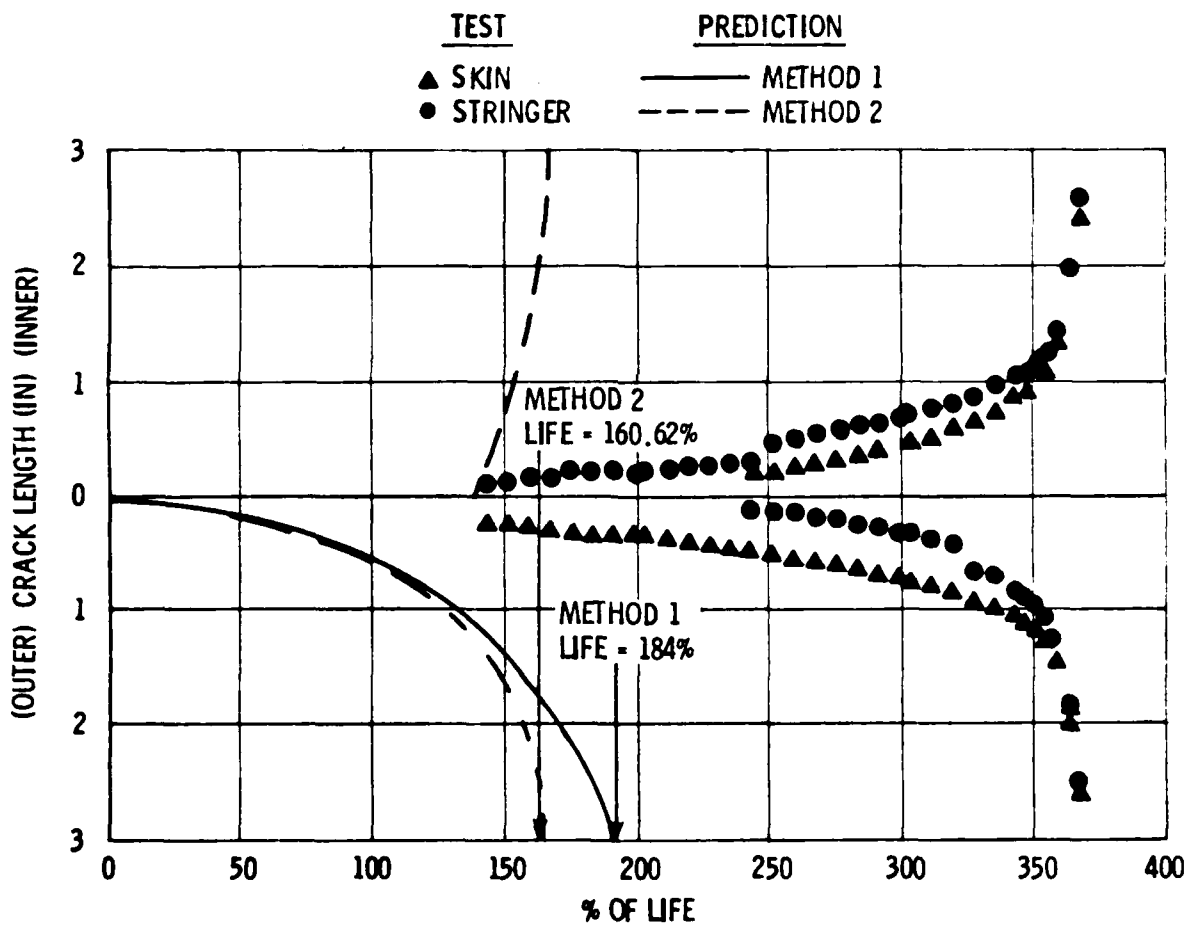
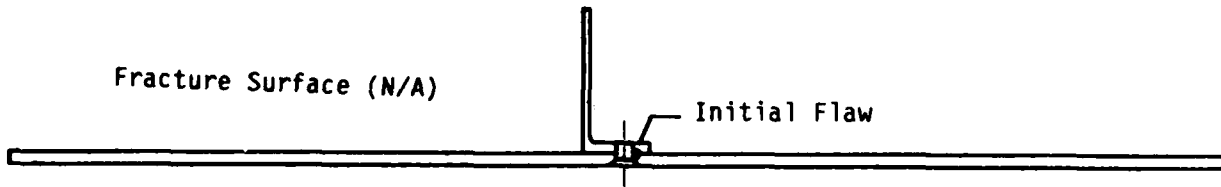


Figure 4.2-19. Crack Growth Diagram for Stringer-Reinforced Specimen No. 52 (-3B) Subjected to A-10A Loading Spectra

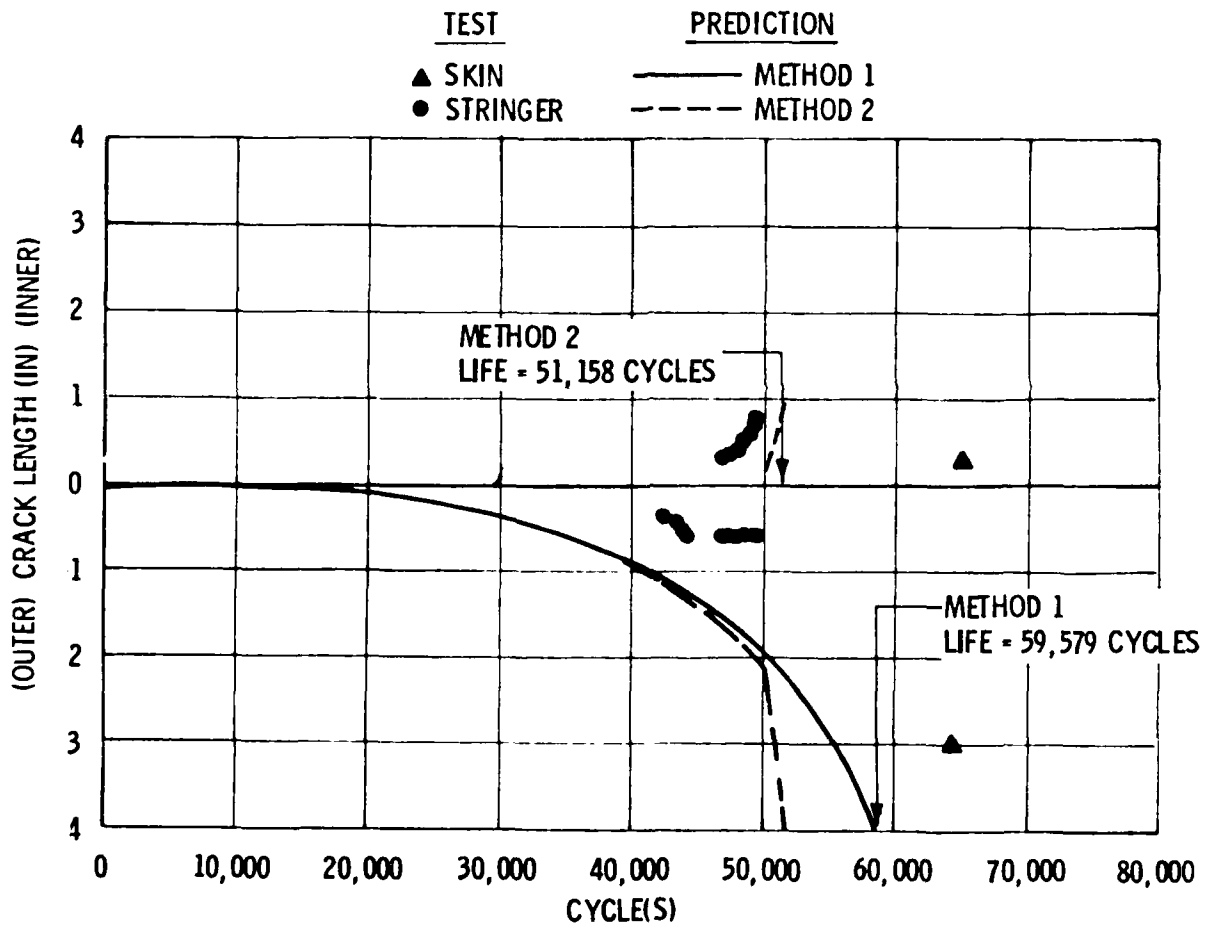
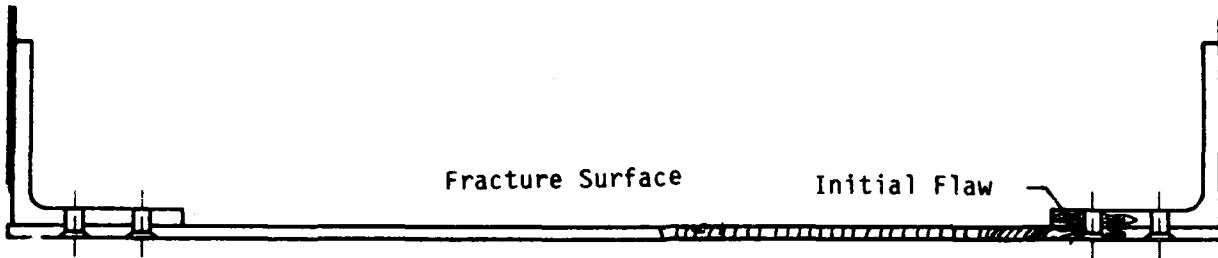


Figure 4.2-20. Crack Growth Diagram for Stringer-Reinforced Specimen No. 53 (-5A) Subjected to C.A. Loading Spectra

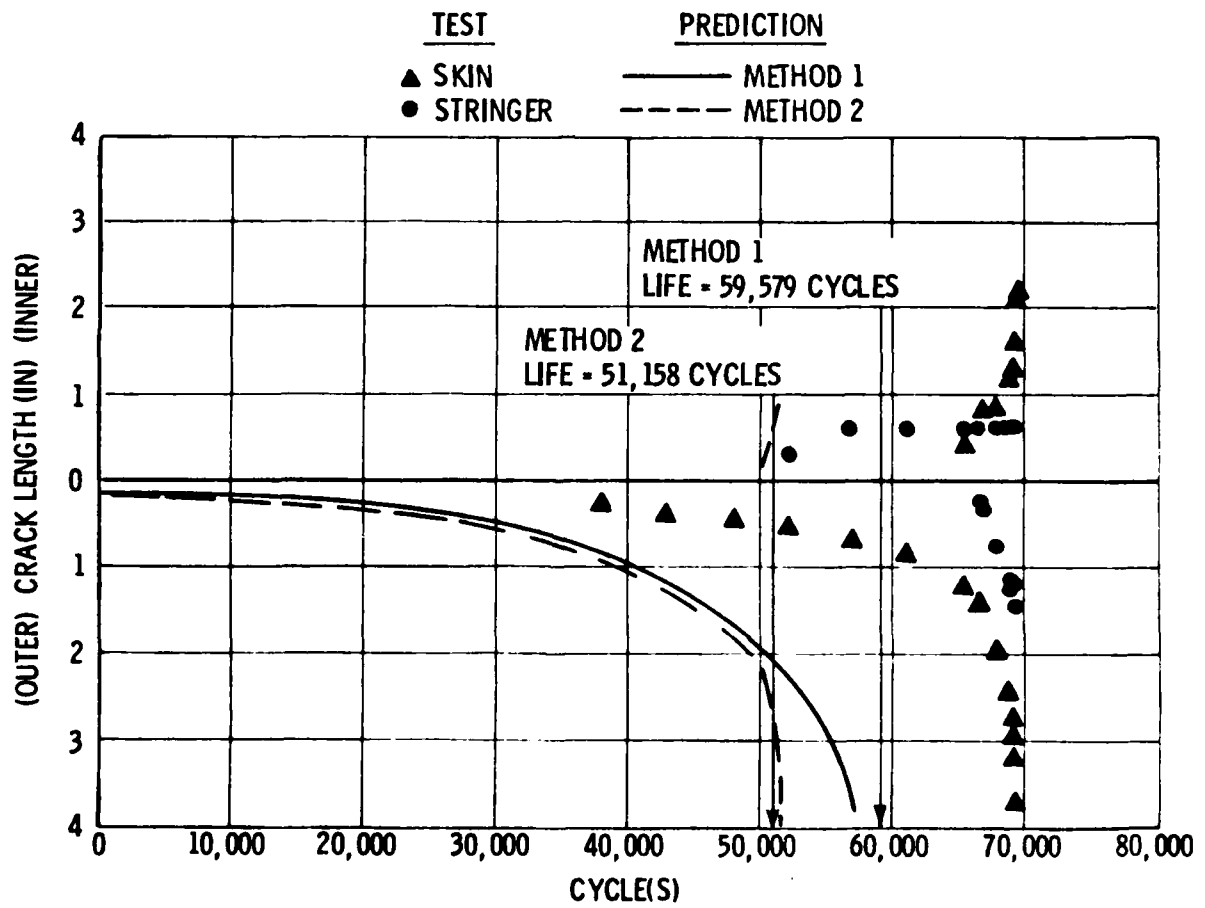
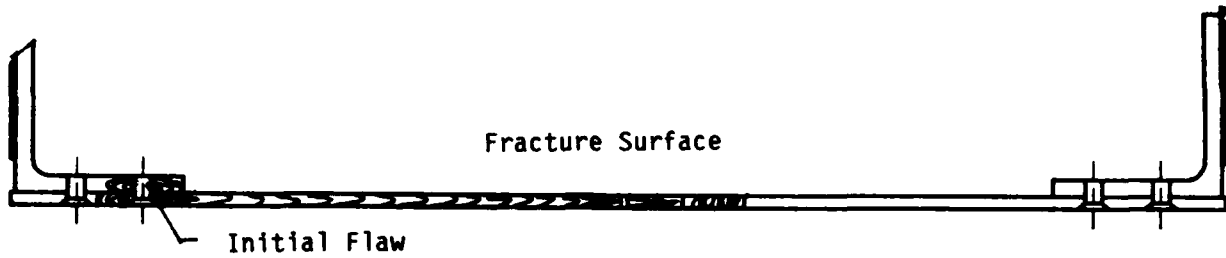


Figure 4.2-21. Crack Growth Diagram for Stringer-Reinforced Specimen No. 54 (-5A) Subjected to C.A. Loading Spectra

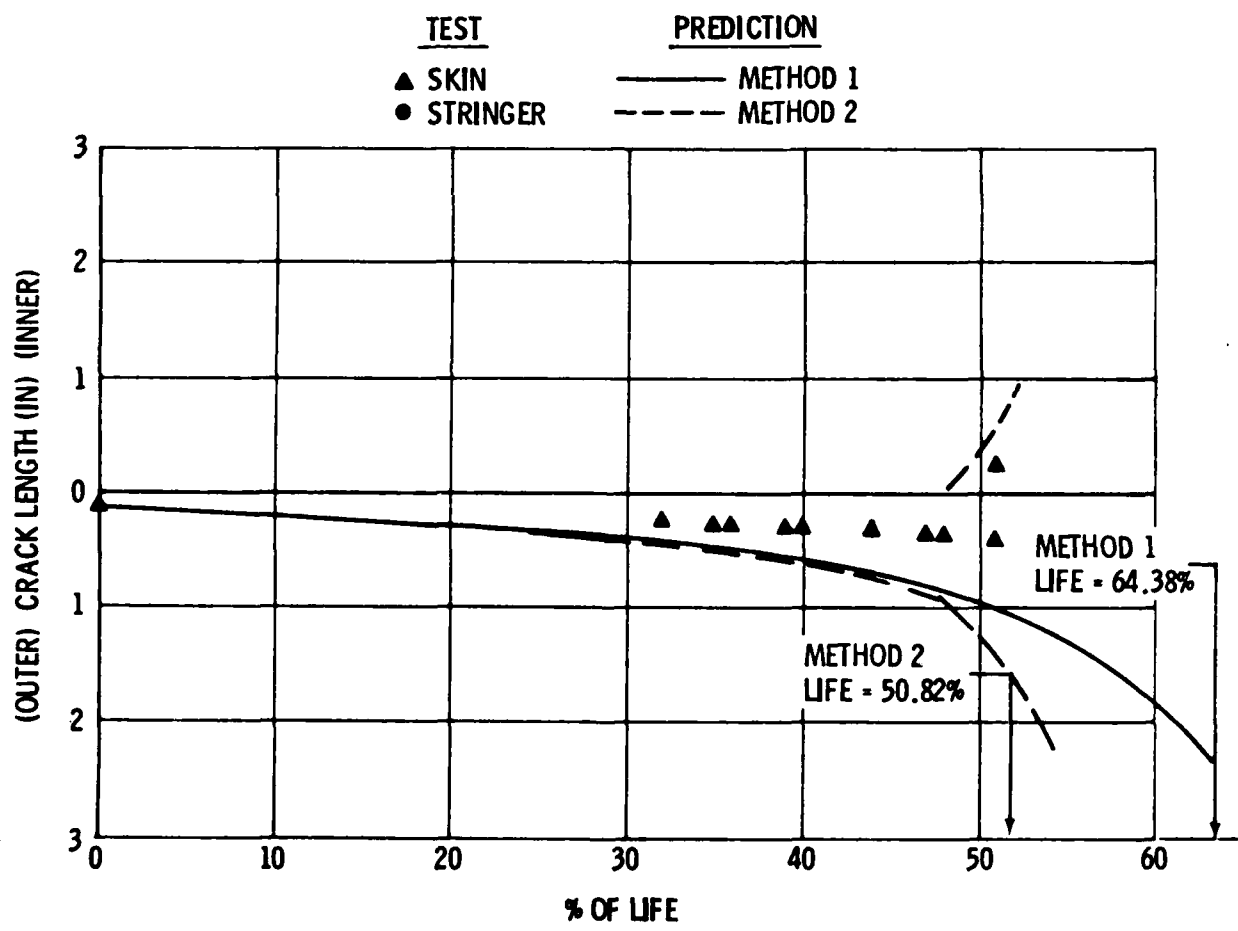
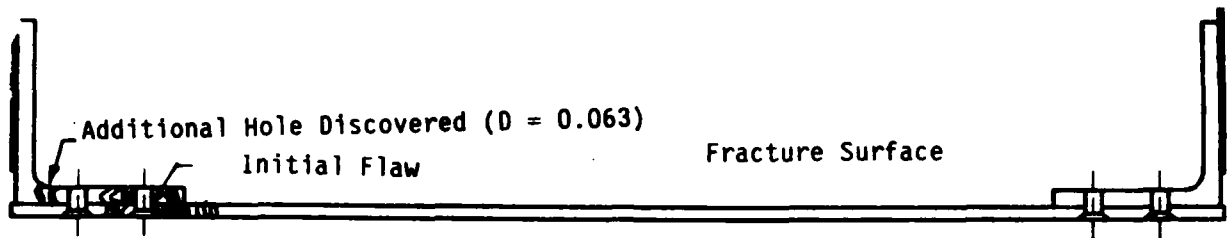


Figure 4.2-22. Crack Growth Diagram for Stringer-Reinforced Specimen No. 55 (-5A) Subjected to A-10A Loading Spectra

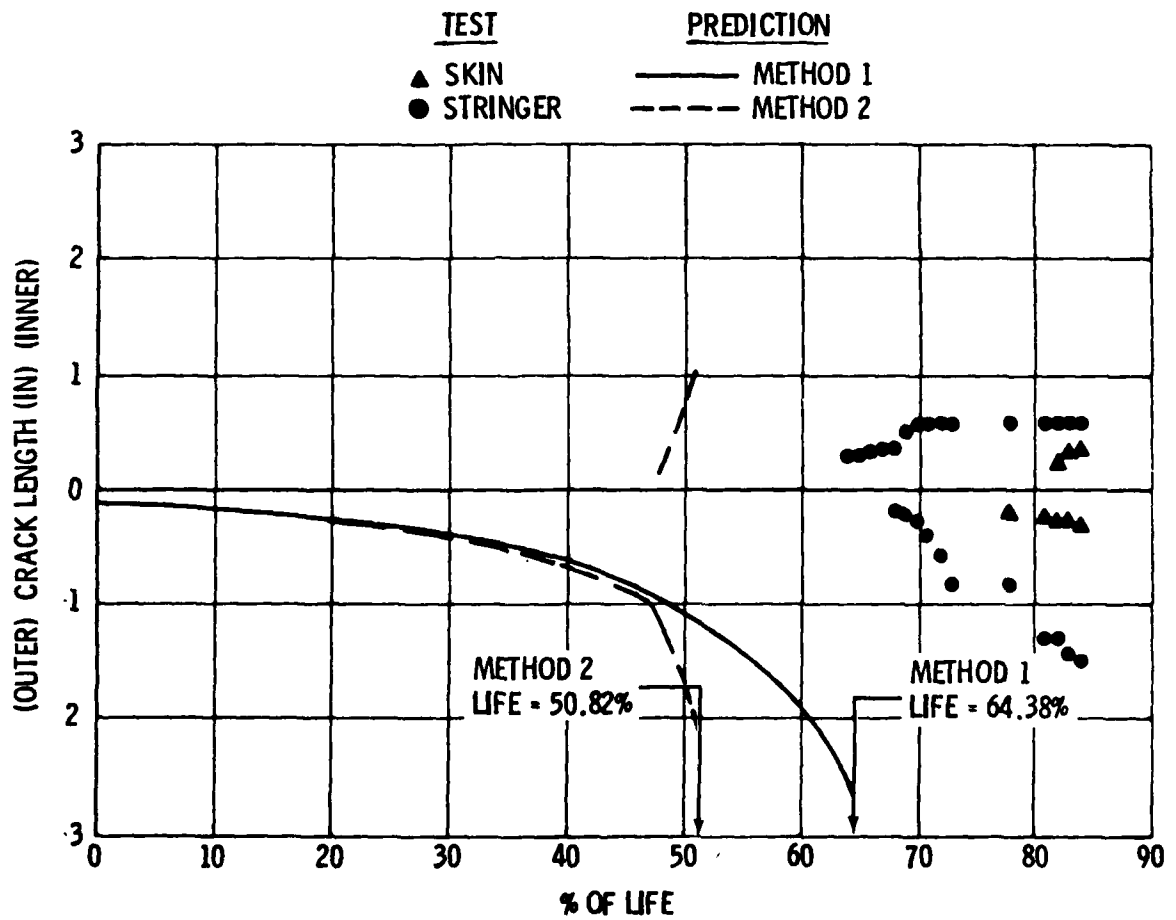
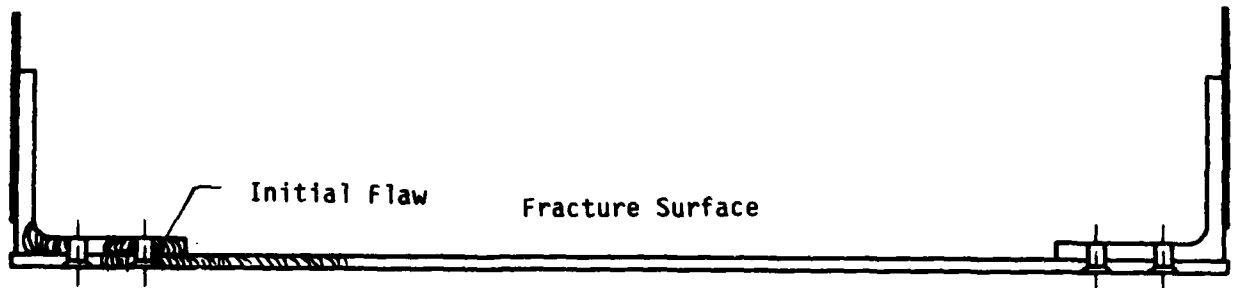


Figure 4.2-23. Crack Growth Diagram for Stringer-Reinforced Specimen No. 56 (-5A) Subjected to A-10A Loading Spectra

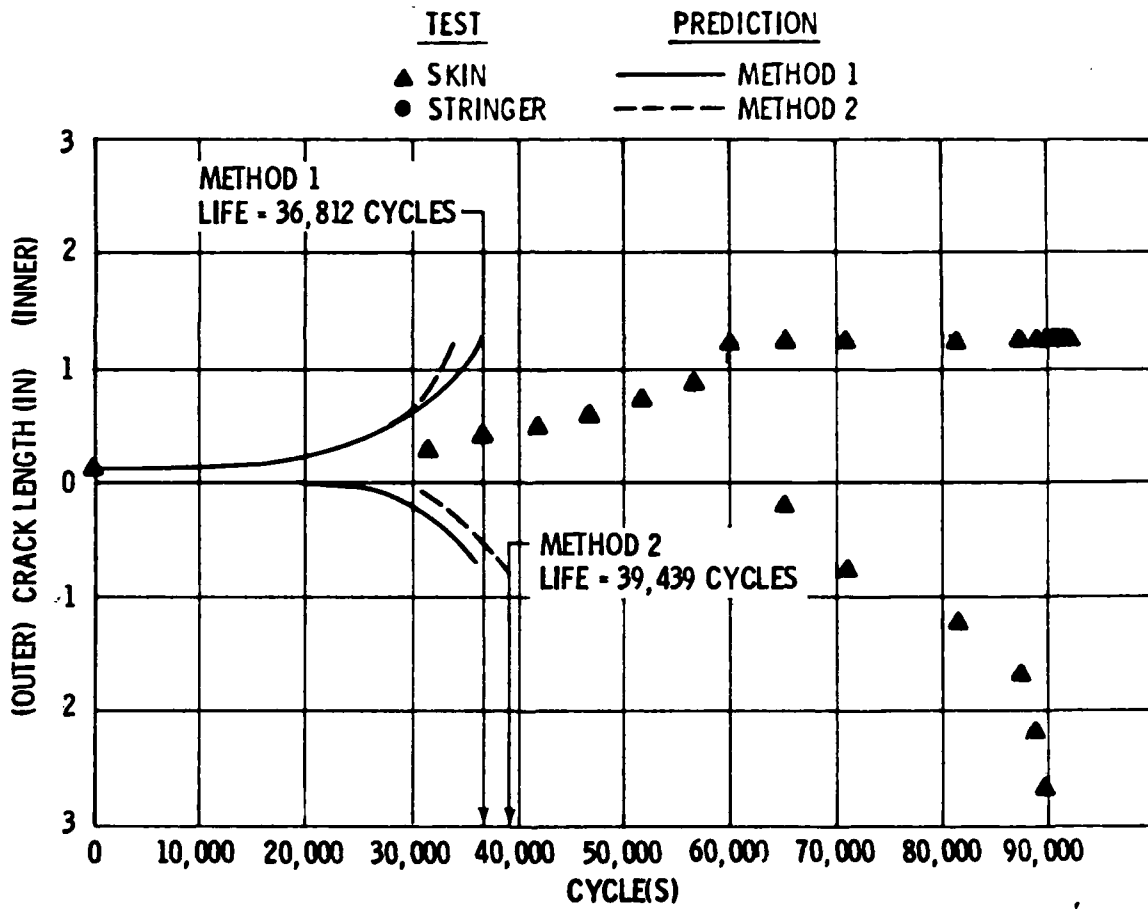
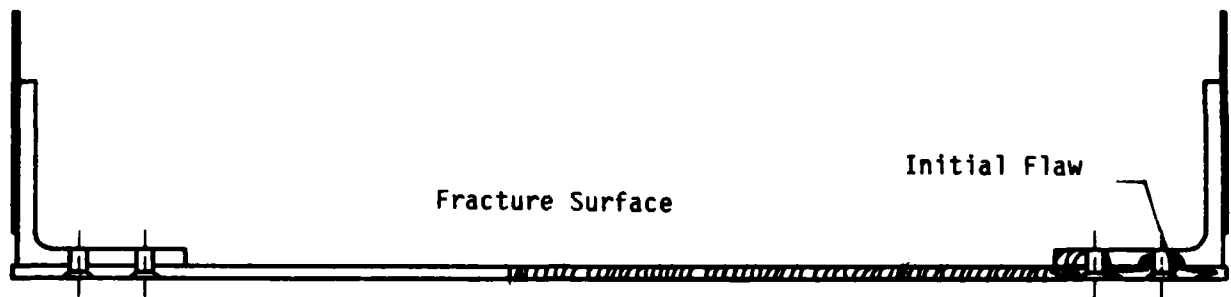


Figure 4.2-24. Crack Growth Diagram for Stringer-Reinforced Specimen No. 57 (-5B) Subjected to C.A. Loading Spectra

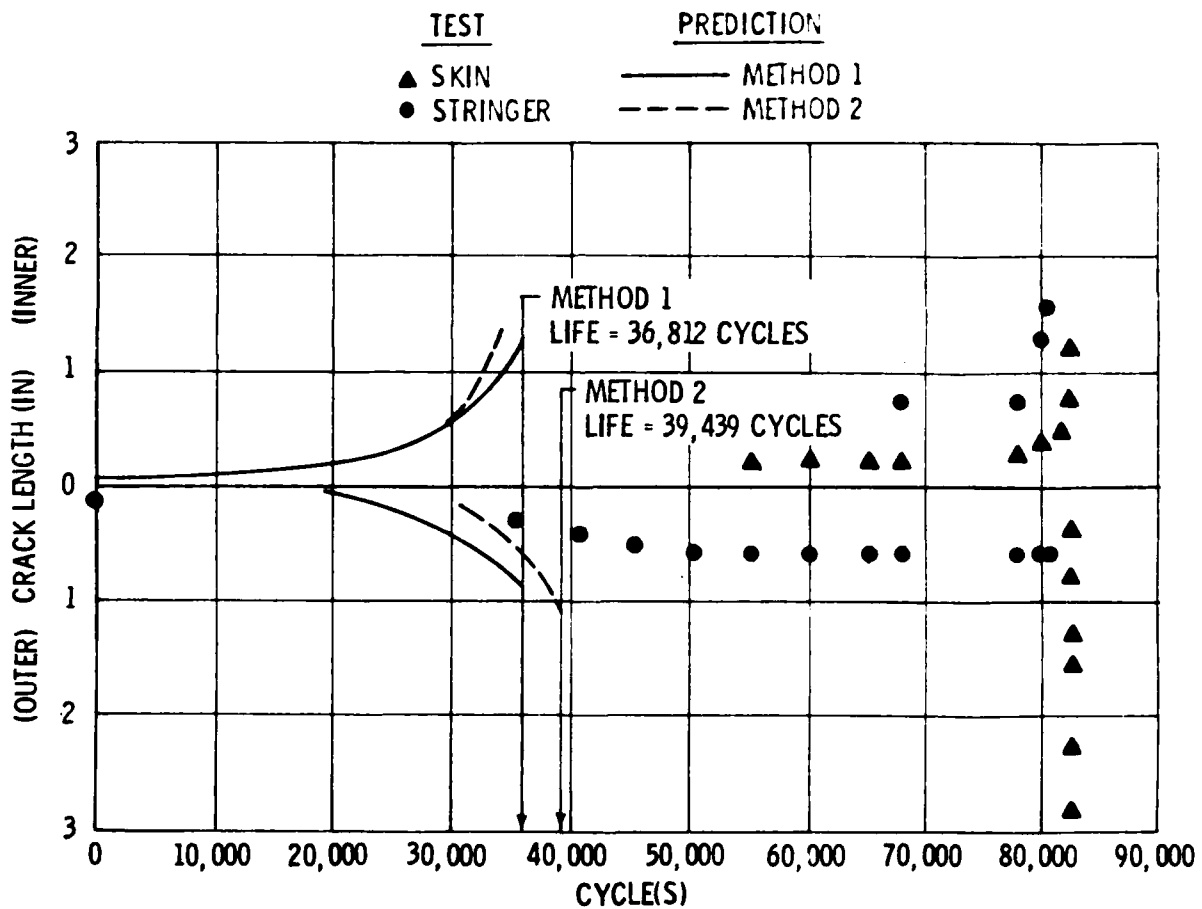
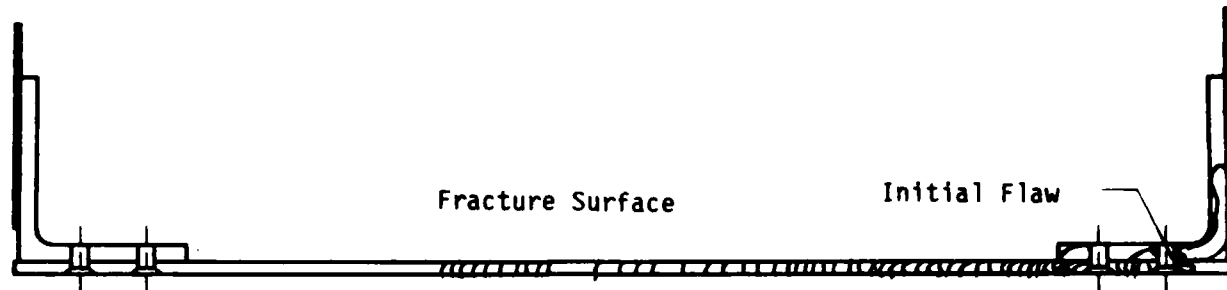


Figure 4.2-25. Crack Growth Diagram for Stringer-Reinforced Specimen No. 58 (-58) Subjected to C.A. Loading Spectra

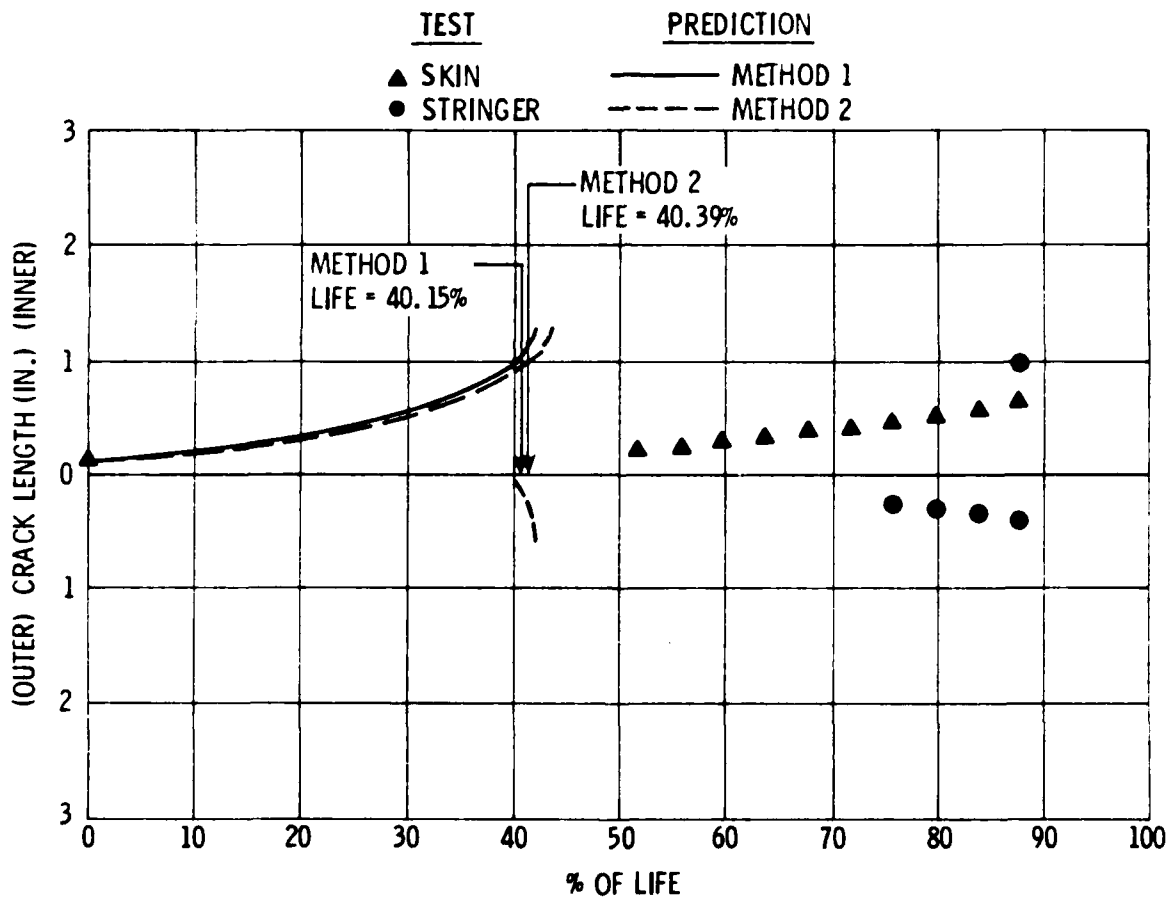
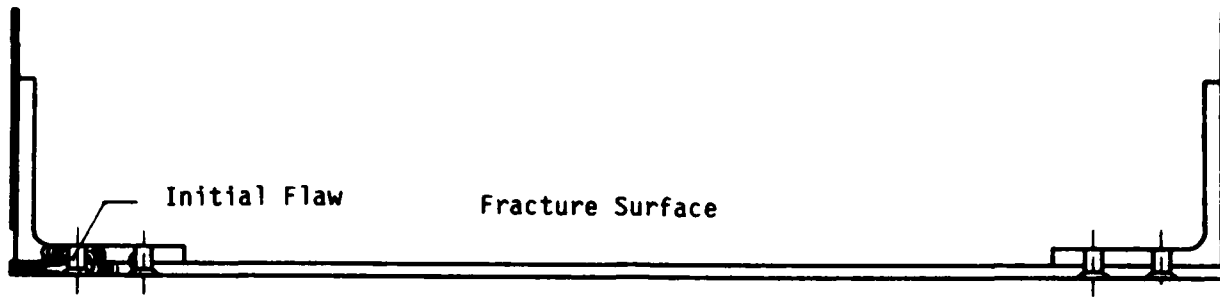


Figure 4.2-26. Crack Growth Diagram for Stringer-Reinforced Specimen No. 59 (-5B) Subjected to A-10A Loading Spectra

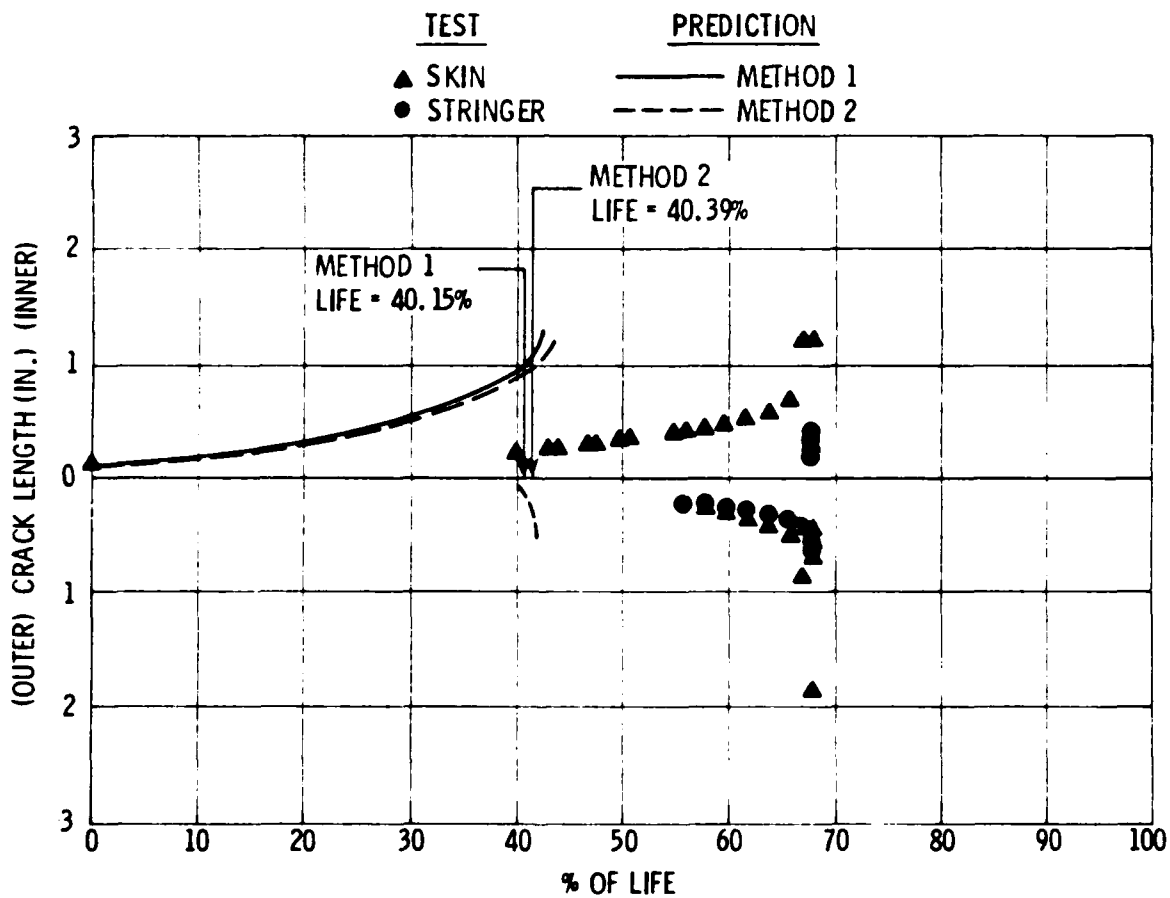
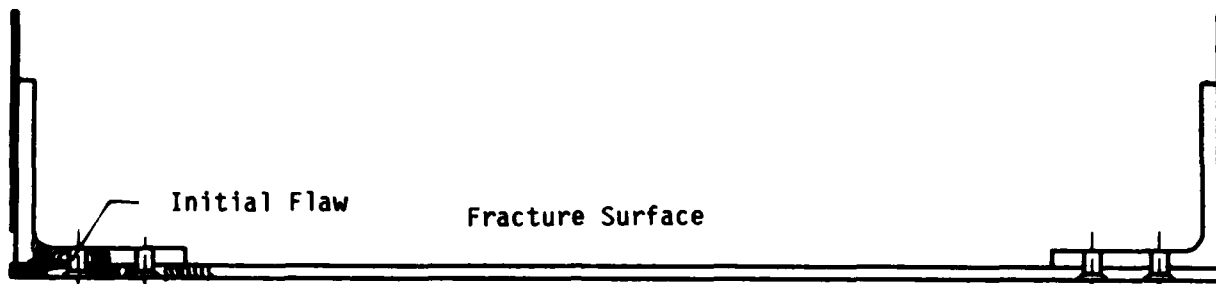


Figure 4.2-27. Crack Growth Diagram for Stringer-Reinforced Specimen No. 60 (-5B) Subjected to A-10A Loading Spectra

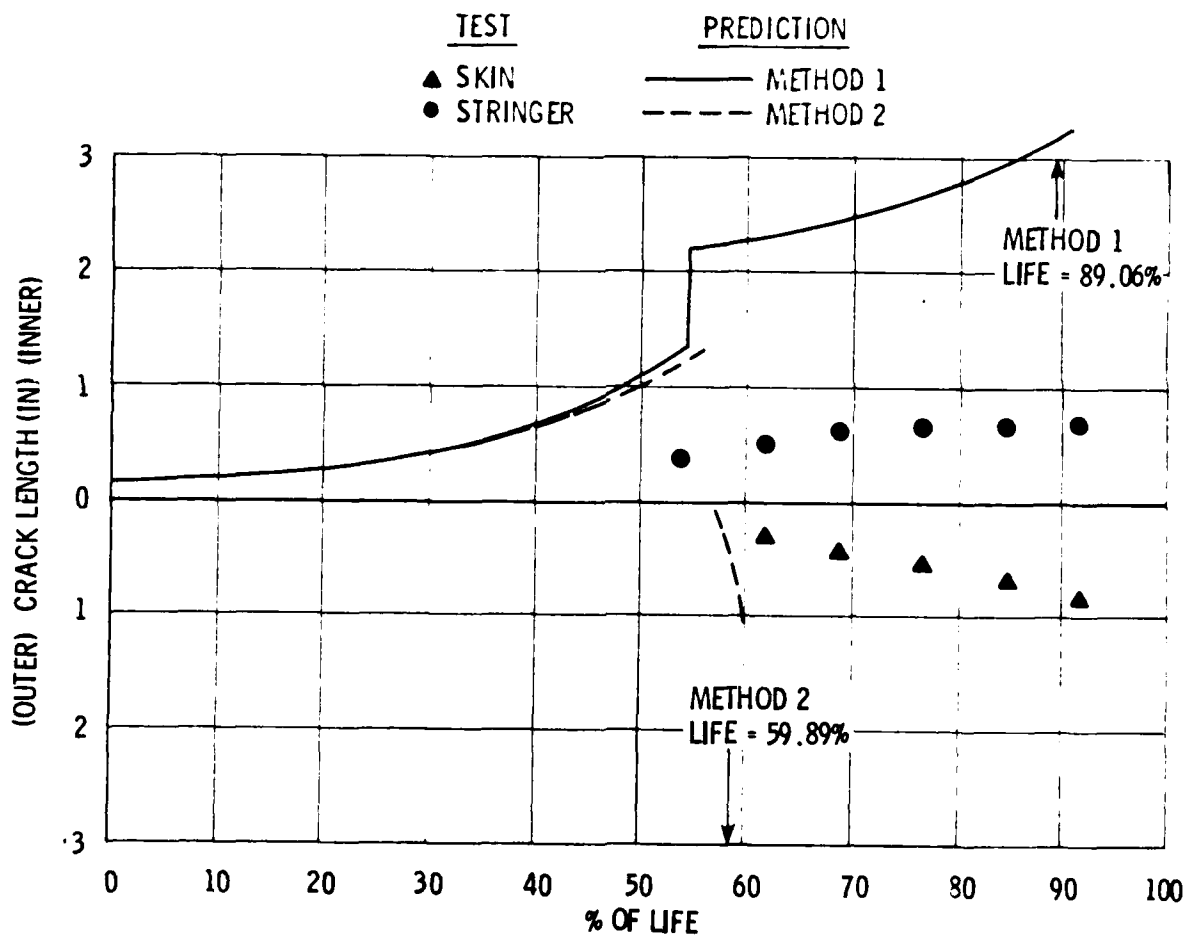
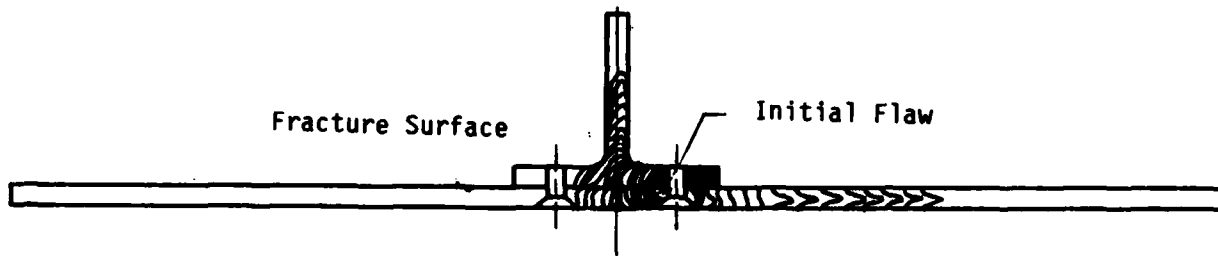


Figure 4.2-28. Crack Growth Diagram for Stringer-Reinforced Specimen No. 61 (-7A) Subjected to AMAVS Loading Spectra

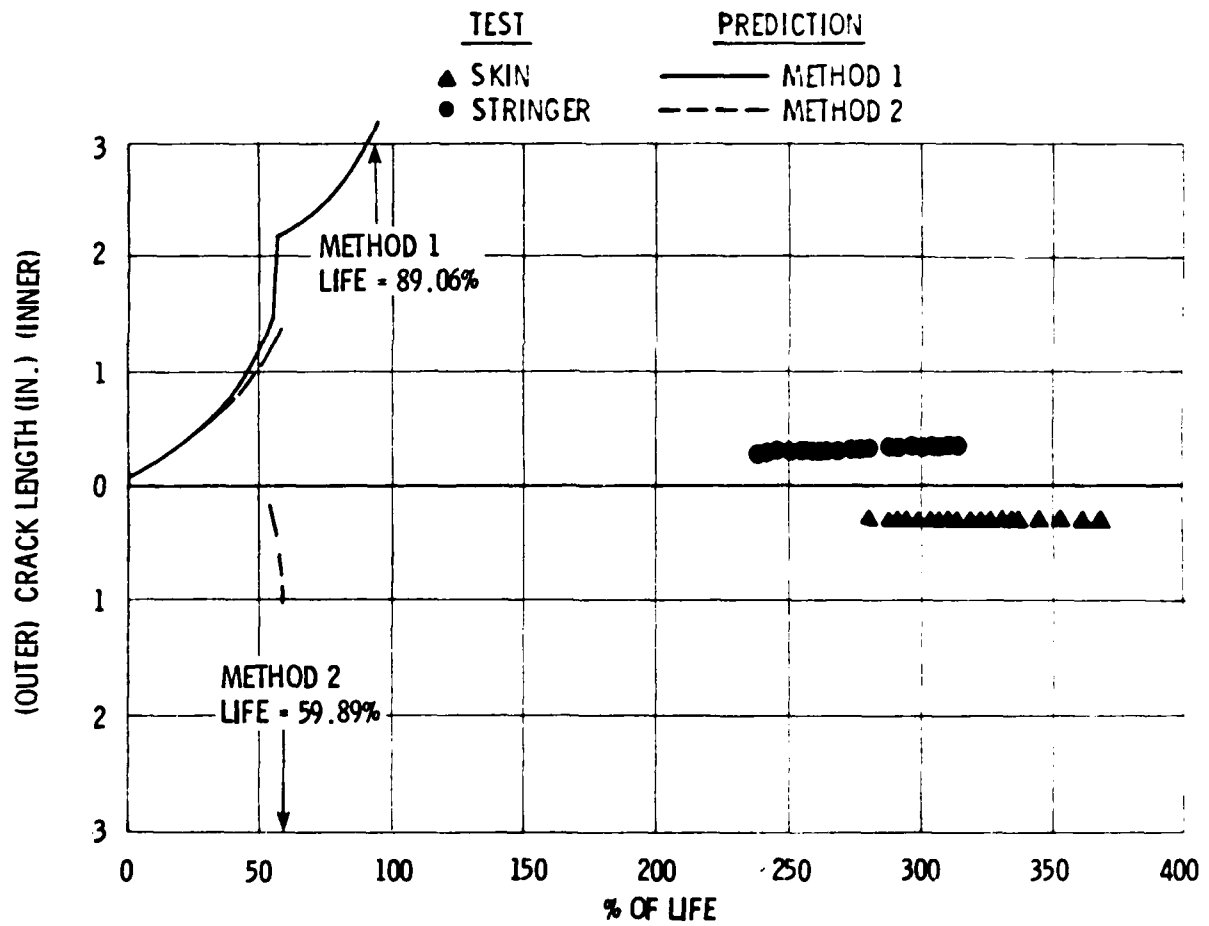
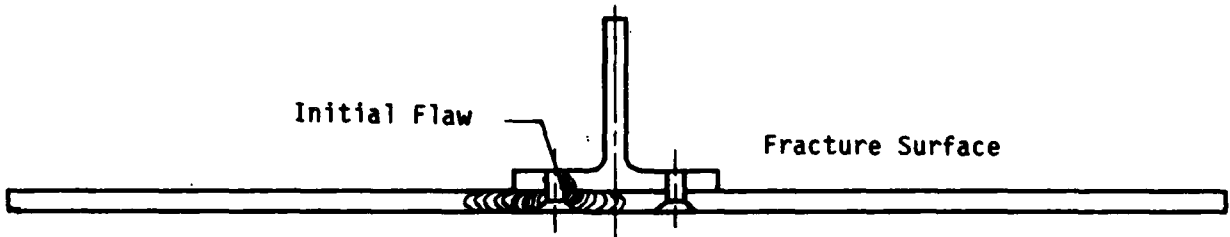


Figure 4.2-29. Crack Growth Diagram for Stringer-Reinforced Specimen No. 62 (-7A) Subjected to AMAVS Loading Spectra

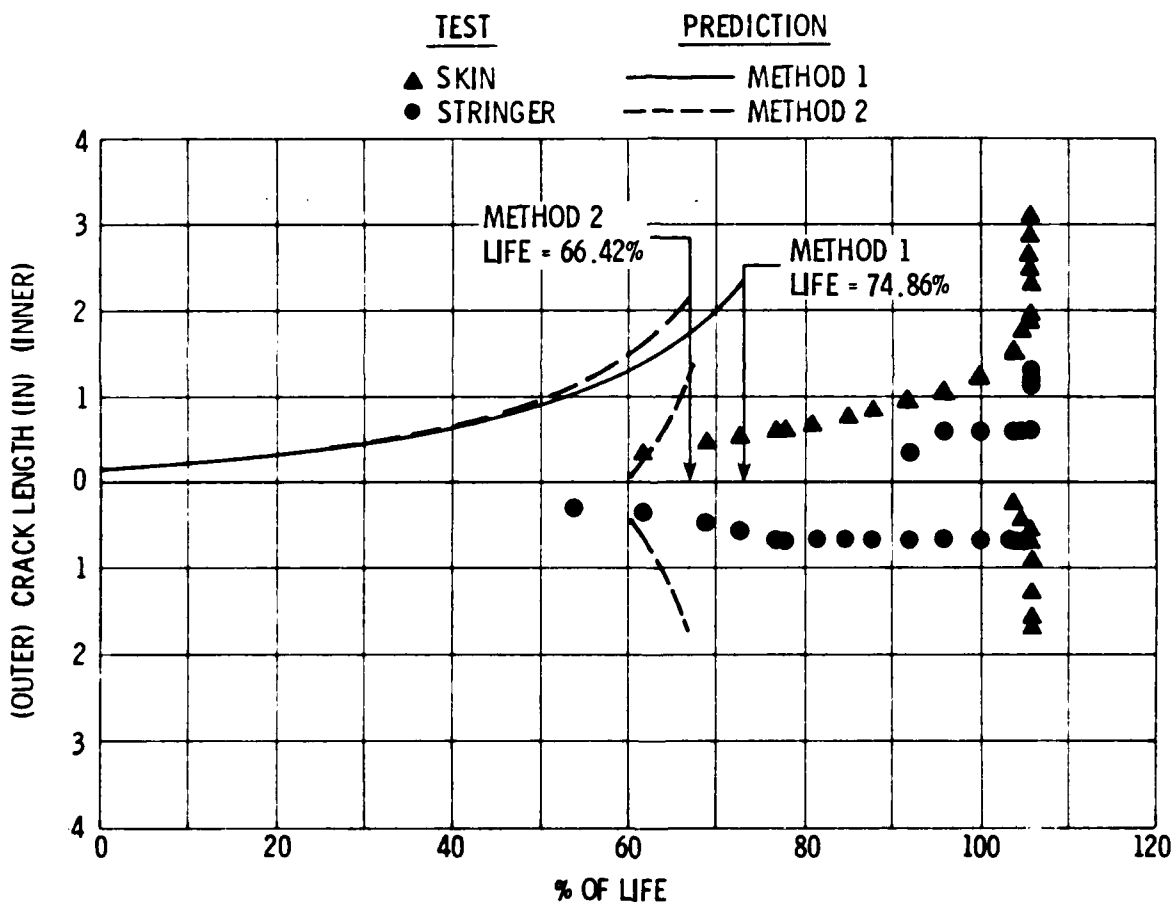
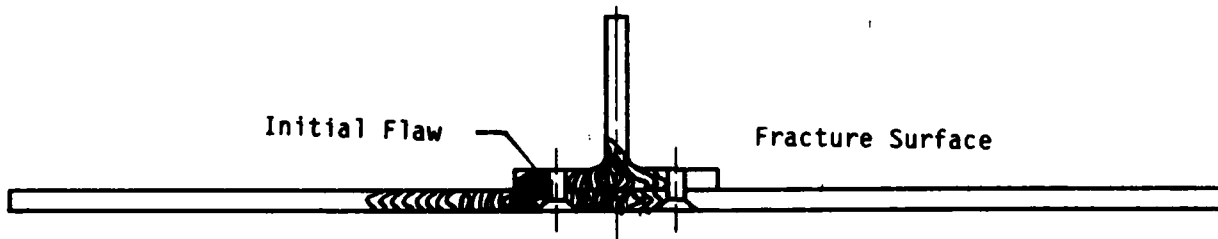


Figure 4.2-30. Crack Growth Diagram for Stringer-Reinforced Specimen No. 63 (-7B) Subjected to AMAVS Loading Spectra

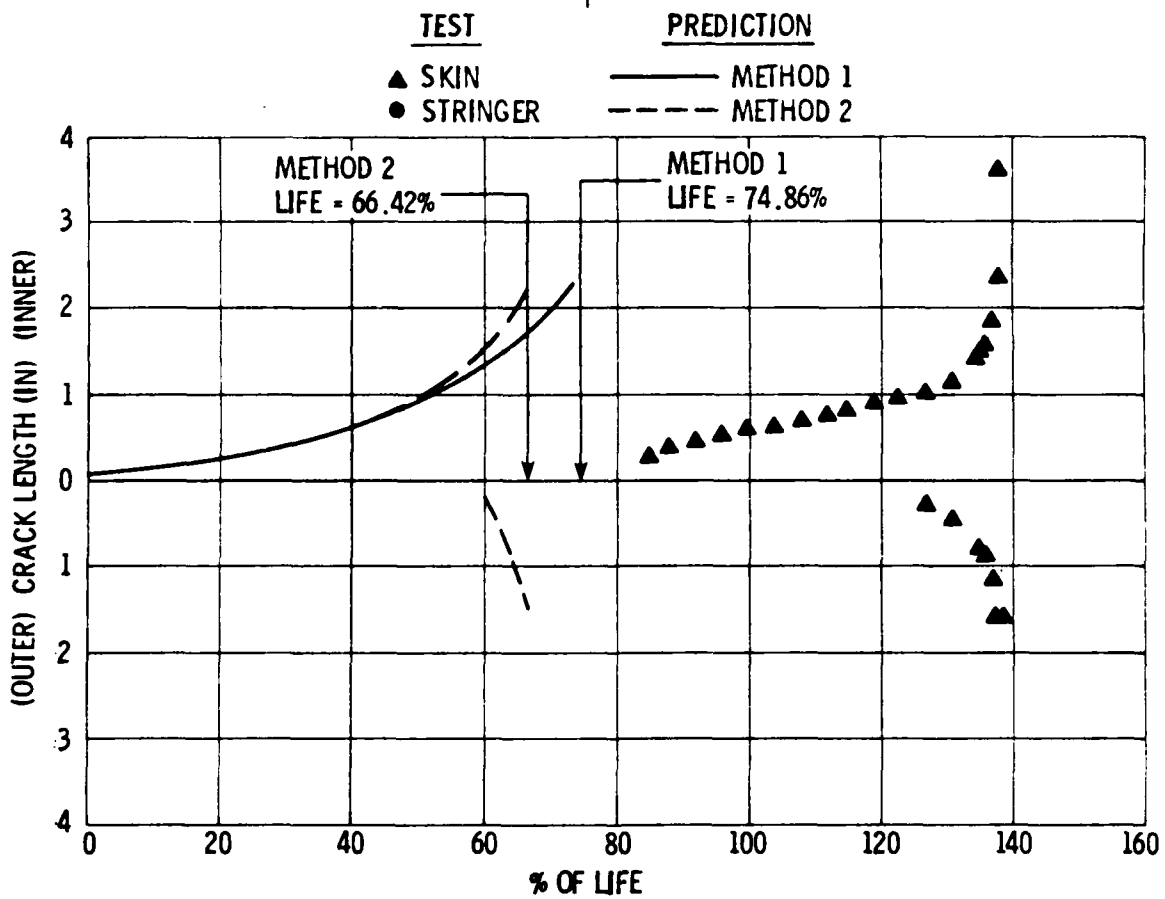
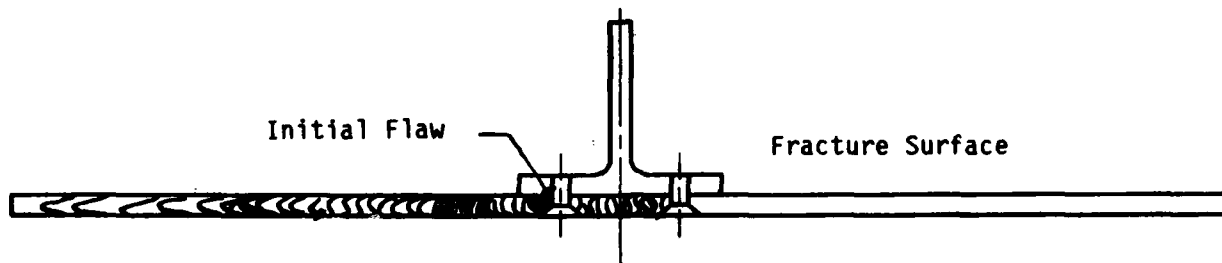


Figure 4.2-31. Crack Growth Diagram for Stringer-Reinforced Specimen No. 64 (-7B) Subjected to AMAVS Loading Spectra

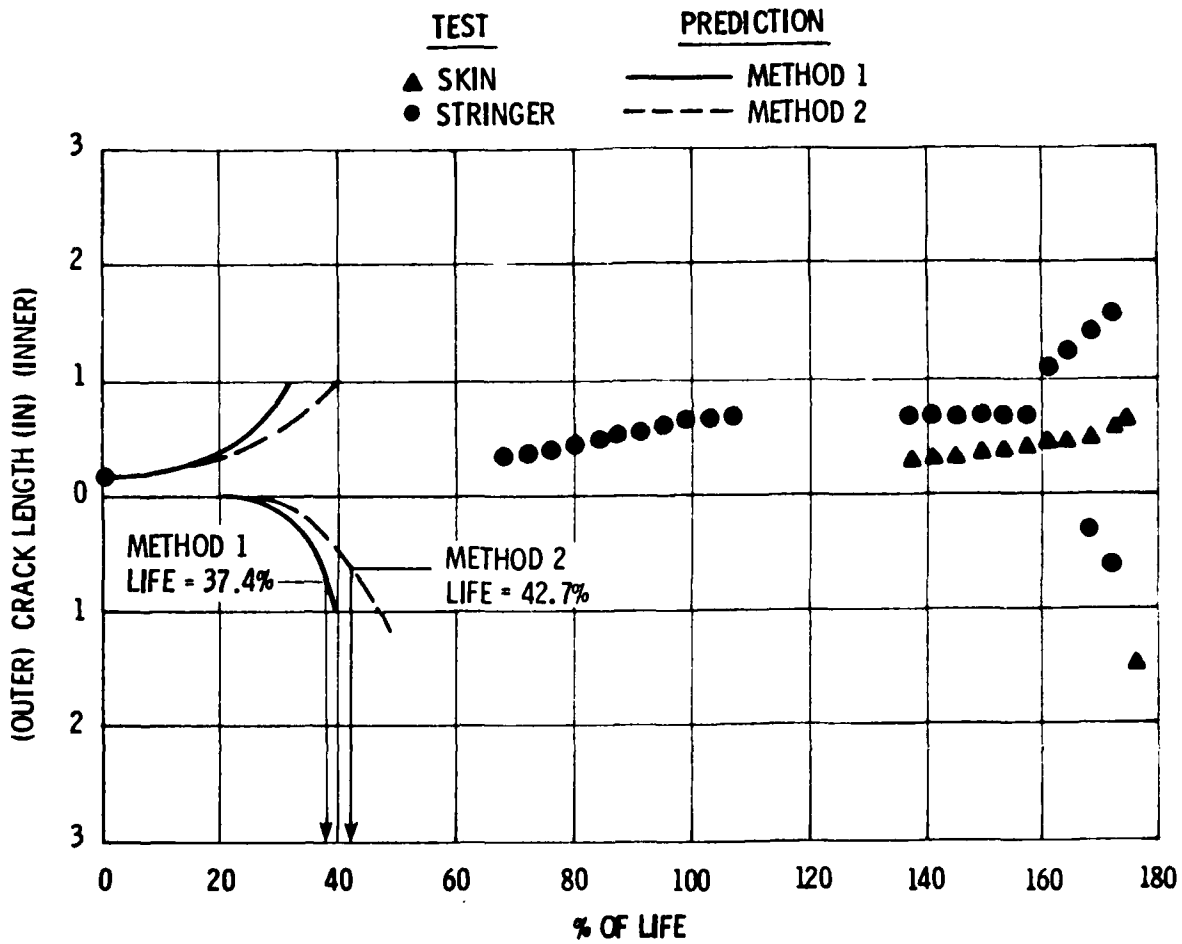
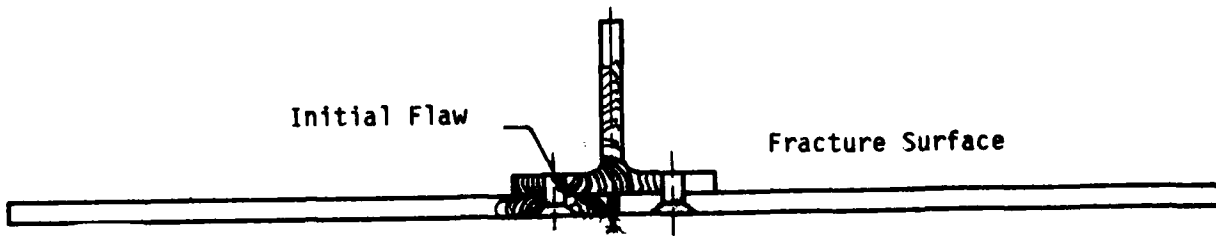


Figure 4.2-32. Crack Growth Diagram for Stringer-Reinforced Specimen No. 65 (-9A) Subjected to AMAVS Loading Spectra

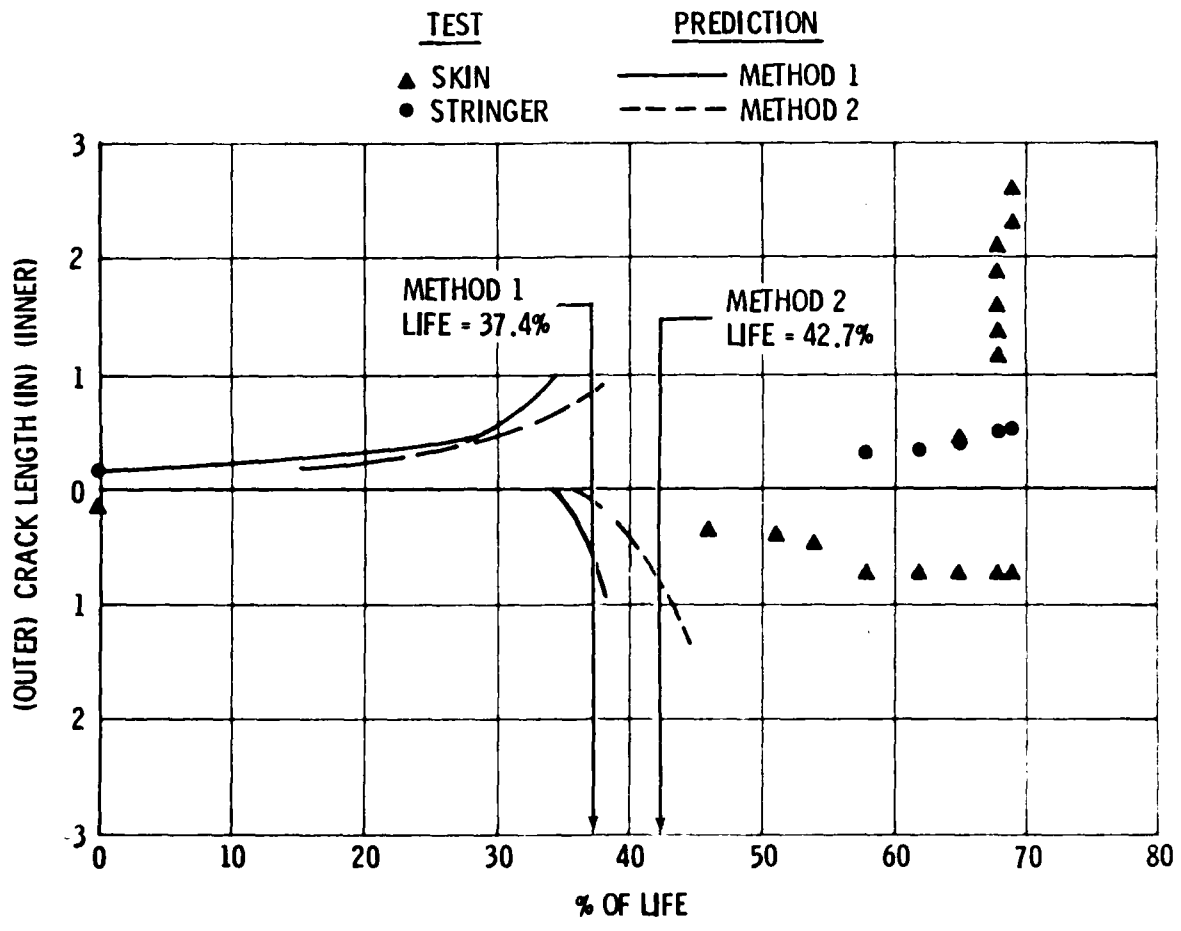
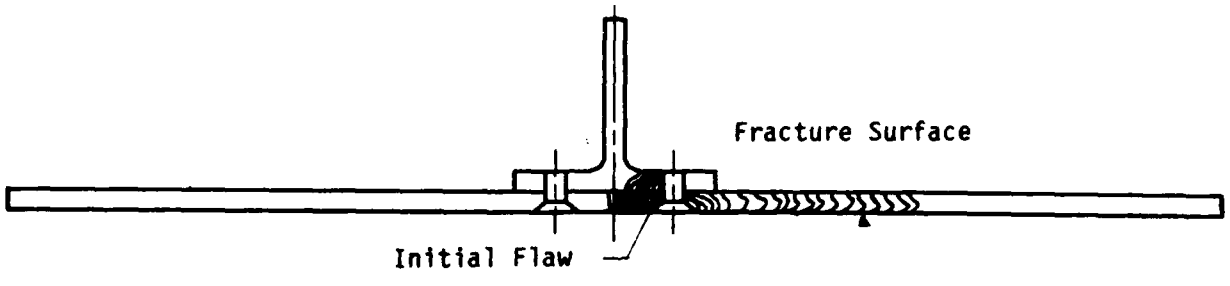


Figure 4.2-33. Crack Growth Diagram for Stringer-Reinforced Specimen No. 66 (-9A) Subjected to AMAVS Loading Spectra

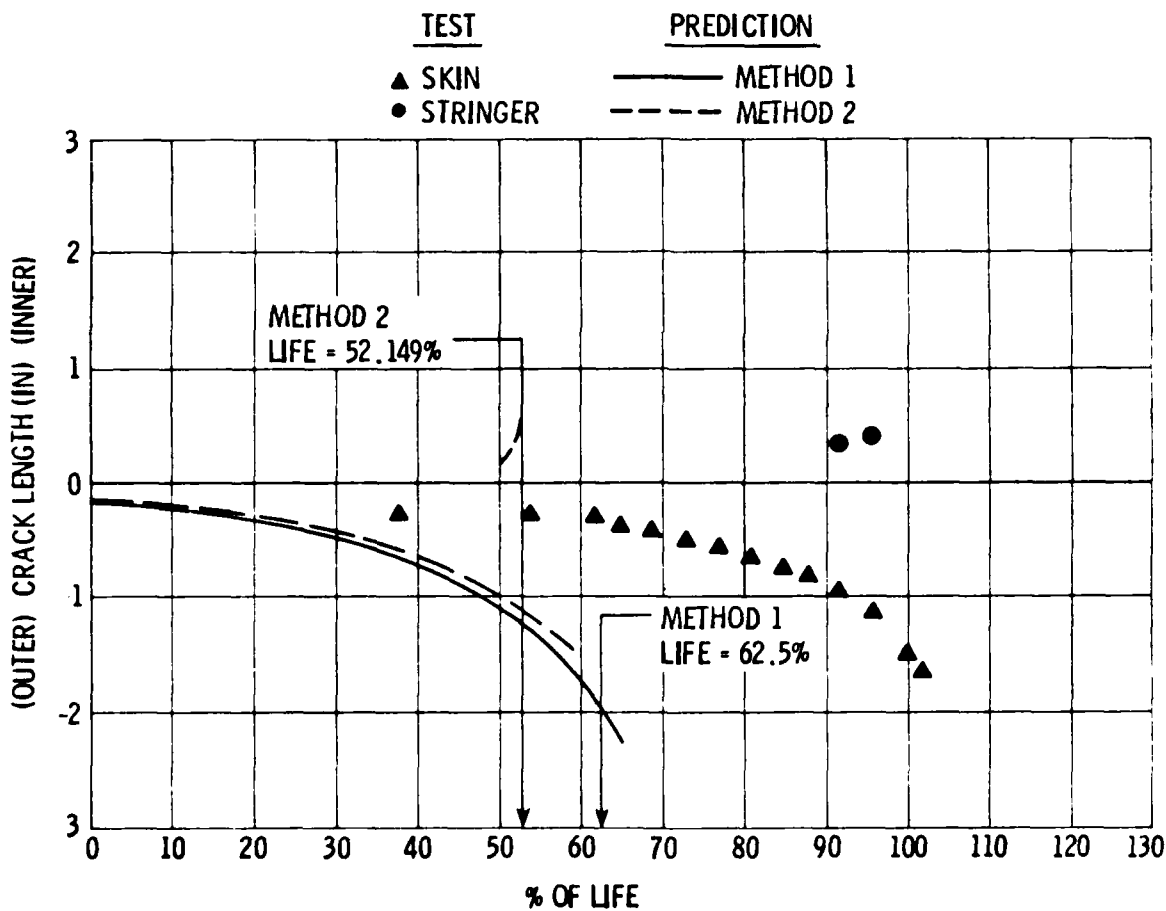
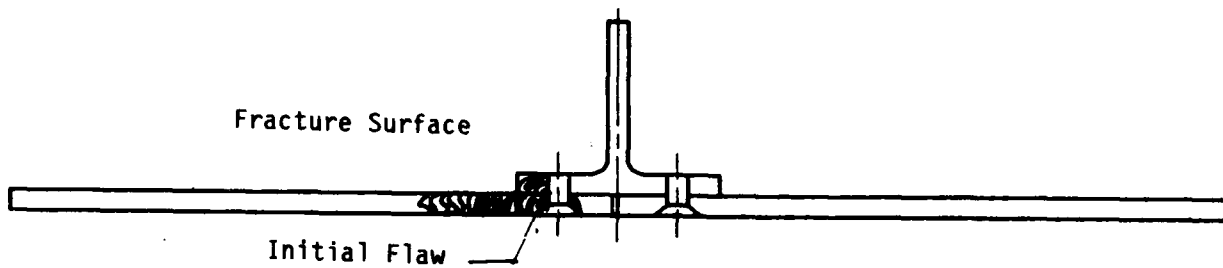


Figure 4.2-34. Crack Growth Diagram for Stringer-Reinforced Specimen No. 67 (-9B) Subjected to AMAVS Loading Spectra

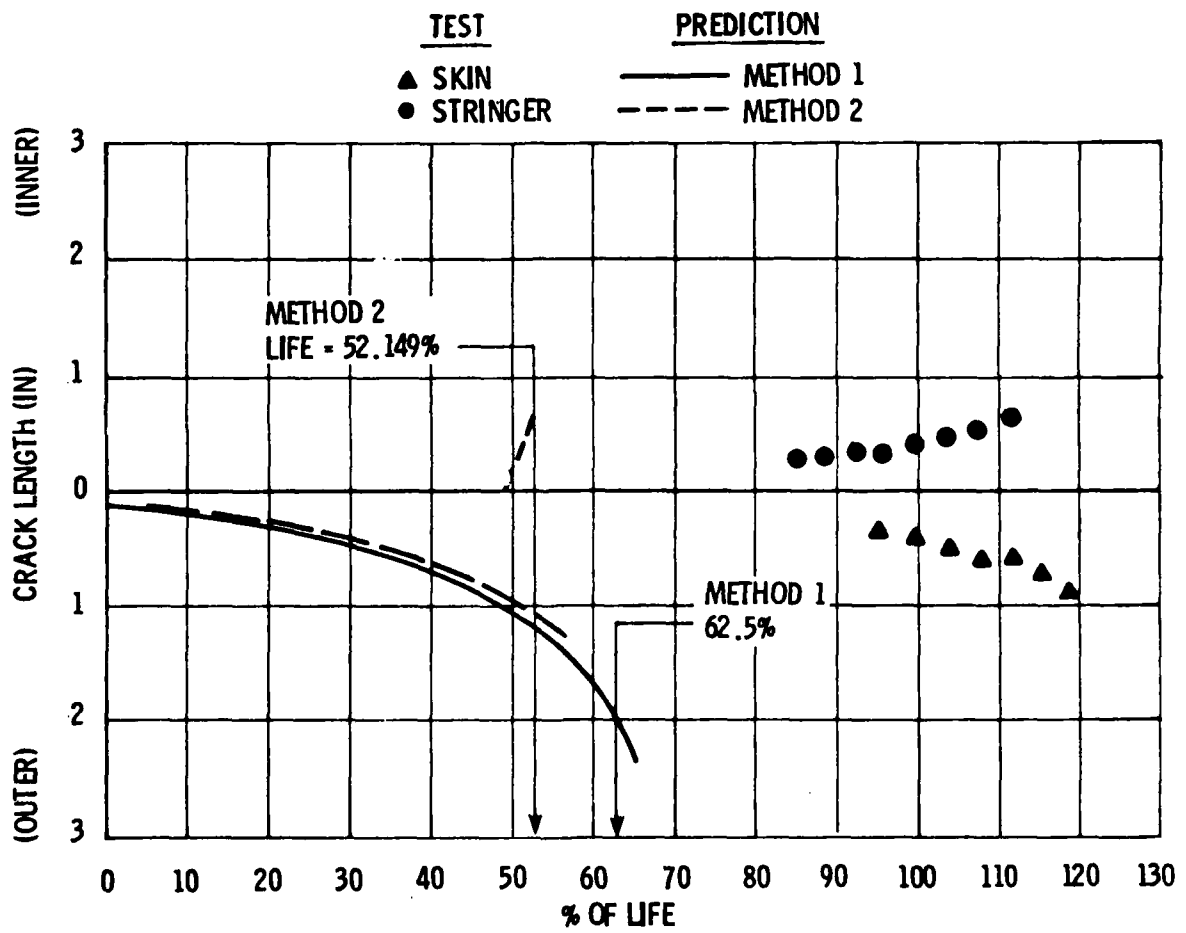
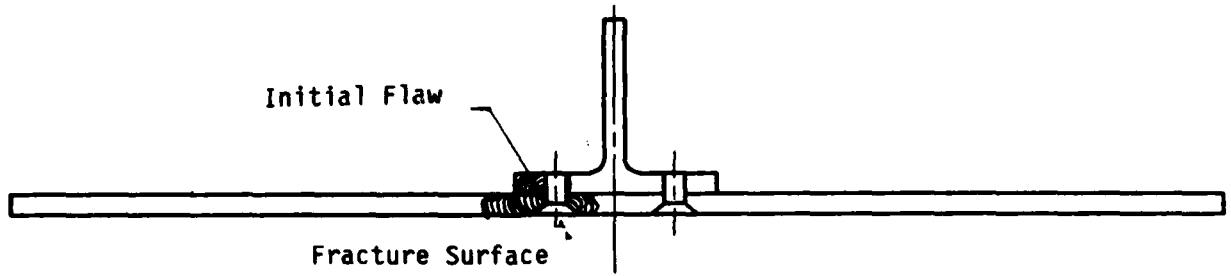


Figure 4.2-35. Crack Growth Diagram for Stringer-Reinforced Specimen No. 68 (-98) Subjected to AMAVS Loading Spectra

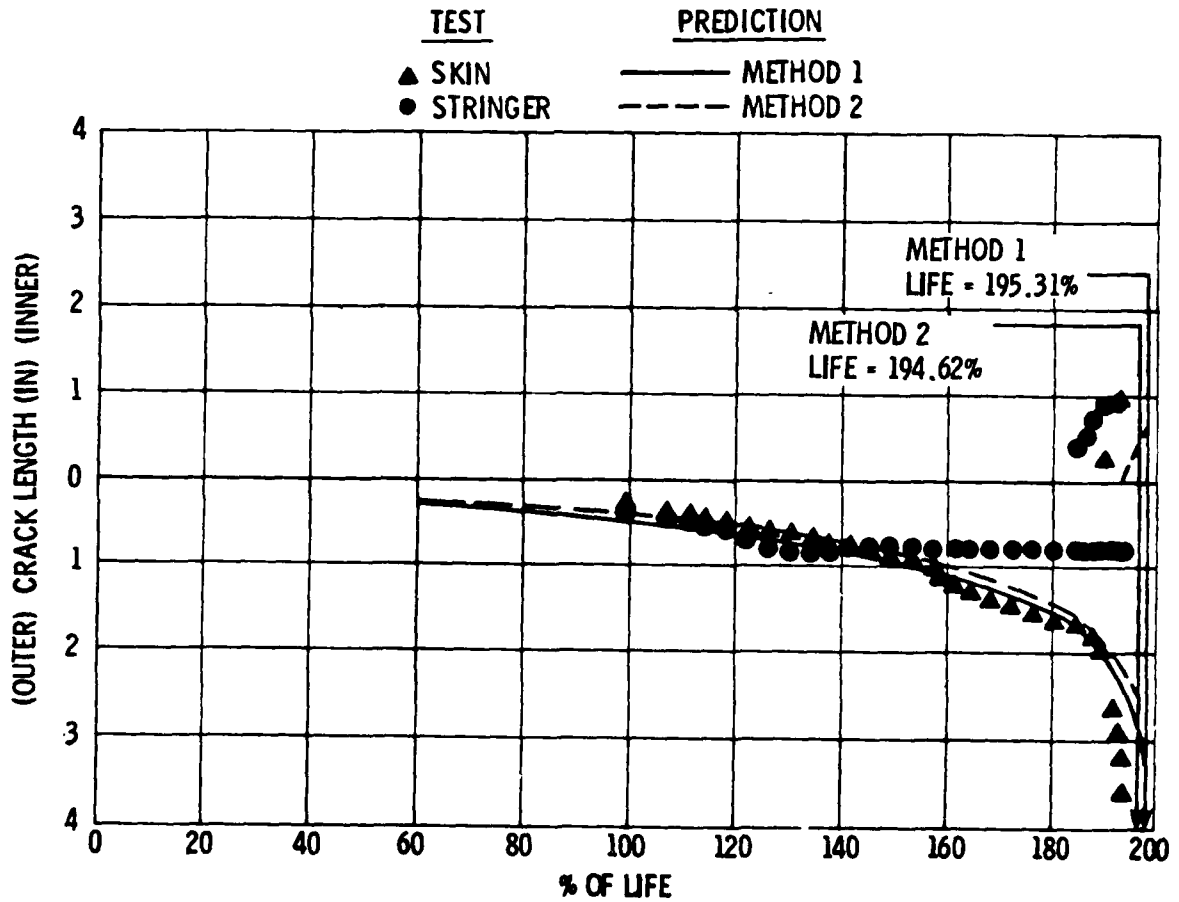
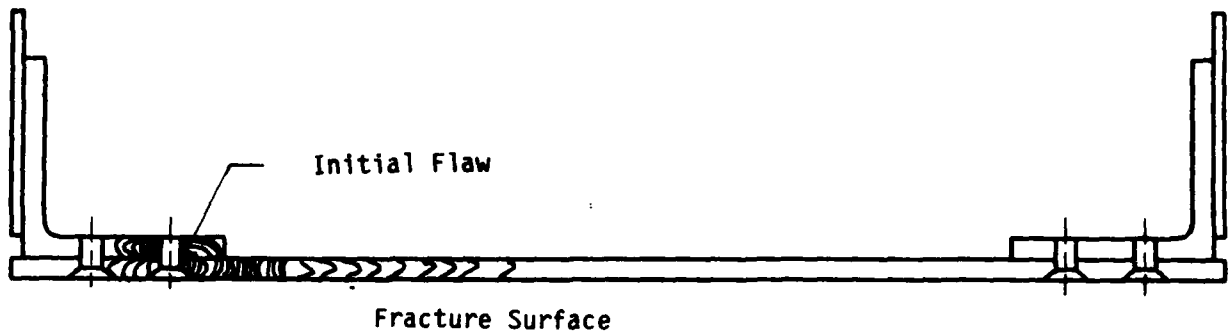


Figure 4.2-36. Crack Growth Diagram for Stringer-Reinforced Specimen No. 69 (-11A) Subjected to AMAVS Loading Spectra

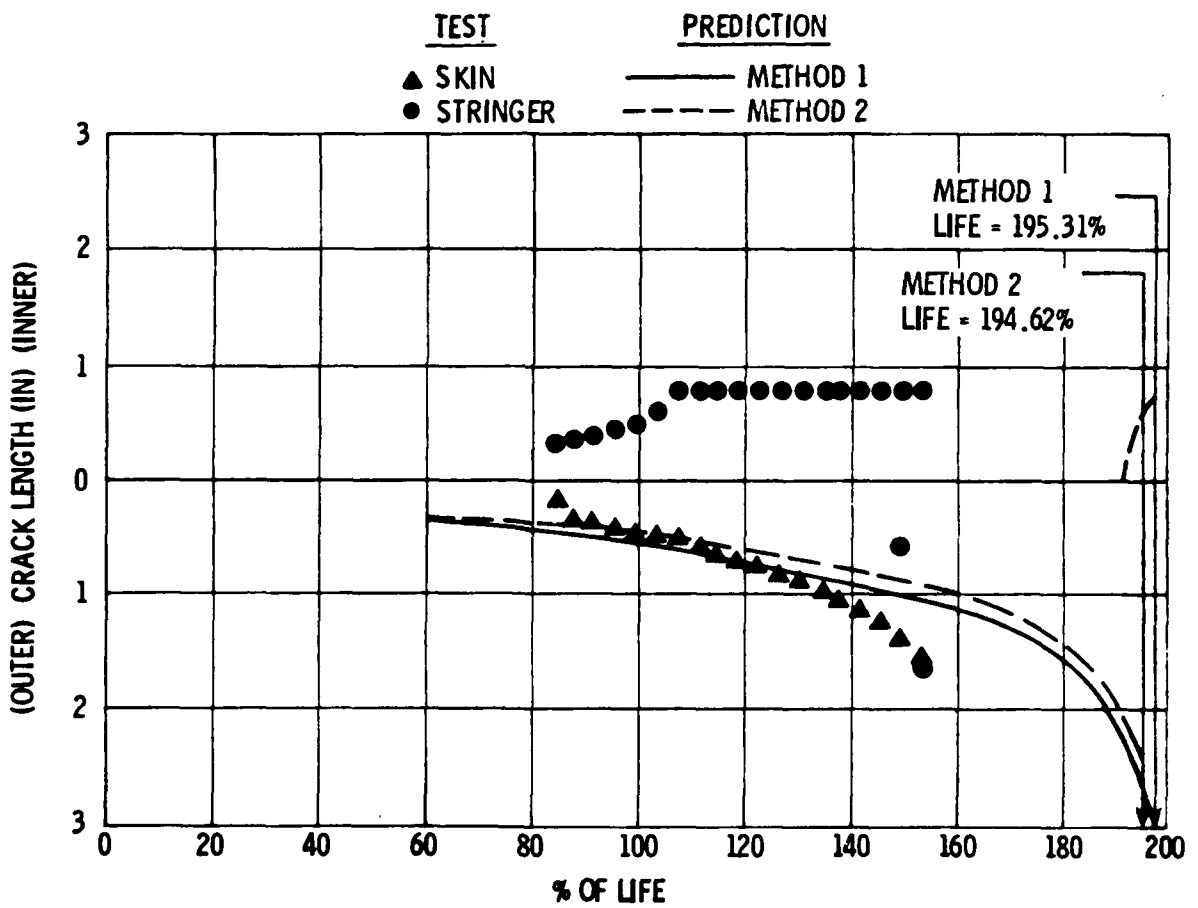
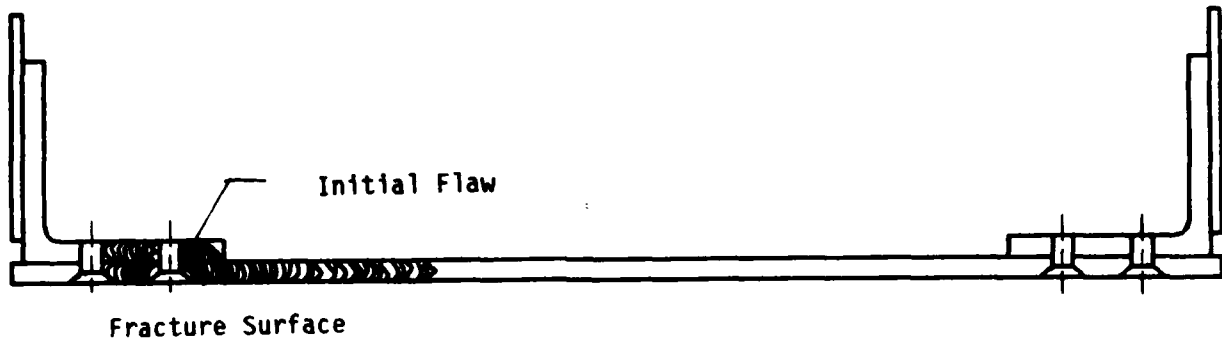


Figure 4.2-37. Crack Growth Diagram for Stringer-Reinforced Specimen No. 70 (-11A) Subjected to AMAVS Loading Spectra

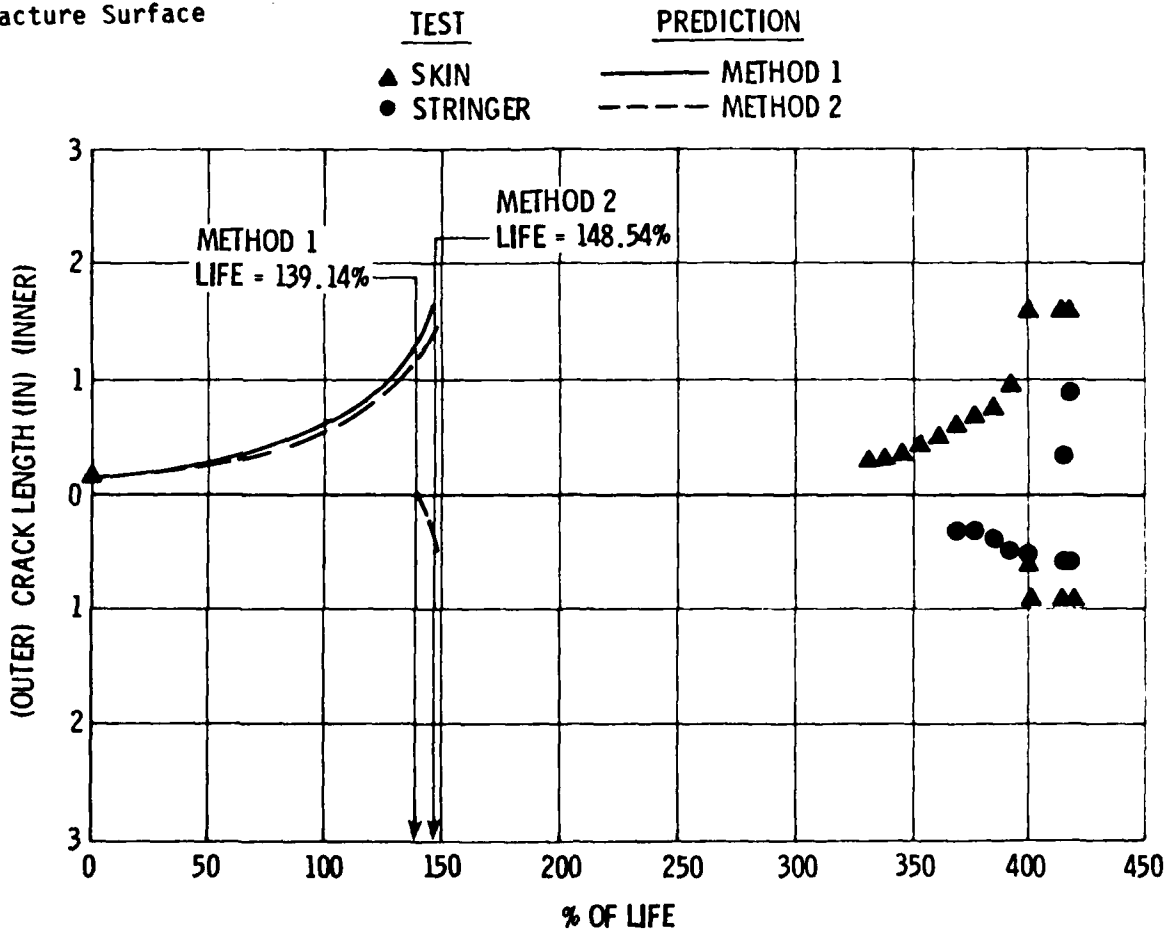
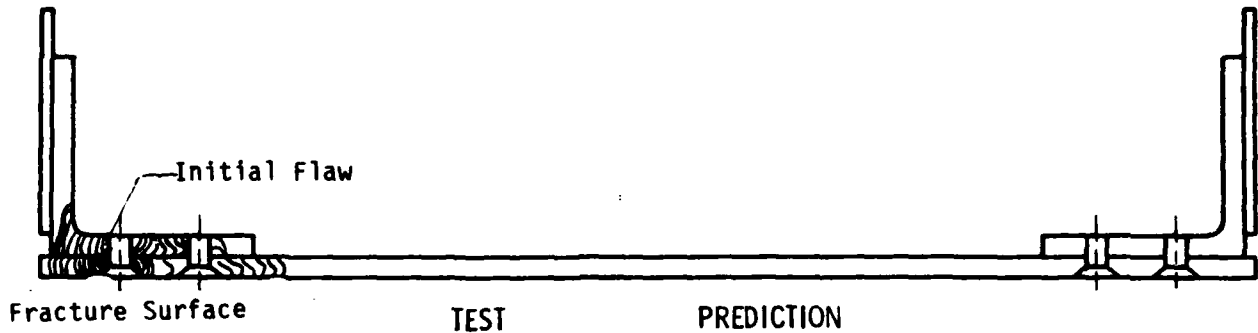


Figure 4.2-38. Crack Growth Diagram for Stringer-Reinforced Specimen No. 71 (-118) Subjected to AMAVS Loading Spectra

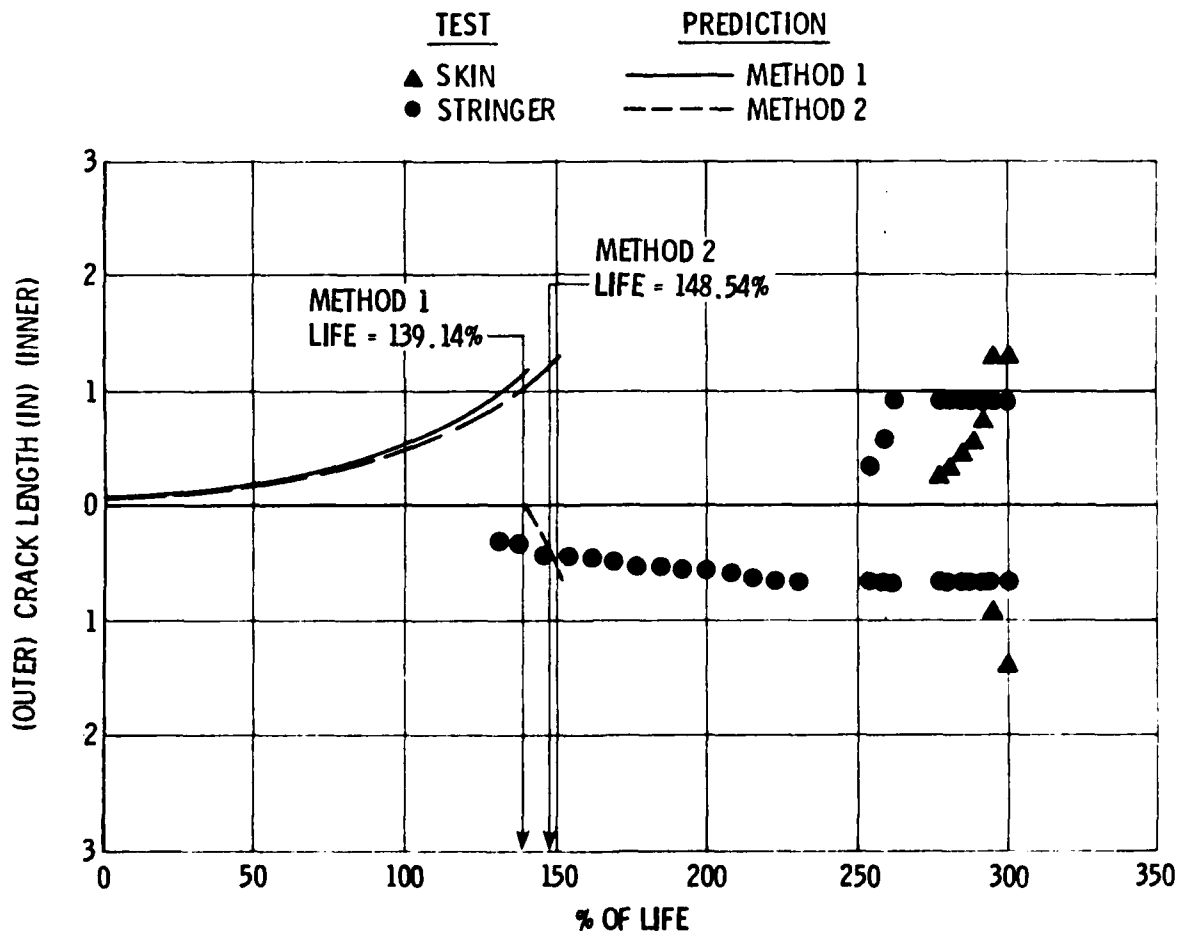
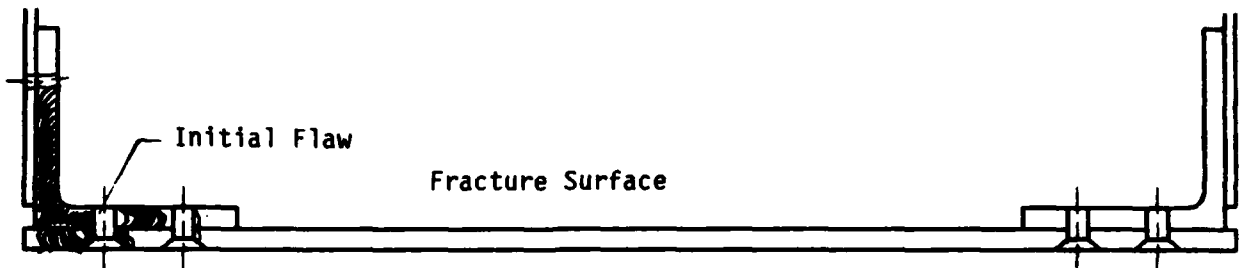


Figure 4.2-39. Crack Growth Diagram for Stringer-Reinforced Specimen No. 72 (-11B) Subjected to AMAVS Loading Spectra

APPENDIX A

Appendix A presents the loading spectra used to perform the crack growth predictions of the structural test specimens. Identical blocks were applied repeatedly until failure occurred. The computer program, 'DAMGRO', is constructed in such a way as to apply each cycle within the load condition separately. In this way, better accuracy is achieved.

A-1. A-10A ANALYTICAL LOADING SPECTRUM

The A-10A Analytical Spectrum represents 4% of the block loading. Each block consists of 204 stress layers in terms of maximum stress followed by minimum stress and the number of cycles associated with it. There are 7,416 cycles in each block. One life of the A-10A consists of 185,400 cycles or 25 repeated blocks. Table A-1 provides a listing of the A-10A Analytical Loading Spectrum. Each condition is presented as a percentage of the maximum stress level in the spectrum (condition No. 37). For maximum stress level of 35.75 Ksi, for example, multiply each condition by 0.3575.

A-2. AMAVS ANALYTICAL LOADING SPECTRUM

The AMAVS Analytical Spectrum represents approximately 7.8% of one life. One life of the AMAVS, was set to be 13,500 hours or 12.8 block loading. Each block consists of 112 stress layers totaling 11,245 cycles. Table A-2 provides a listing of the AMAVS Analytical Loading Spectrum. Each condition is presented as a percentage of the maximum stress level in the spectrum (condition No. 17).

TABLE A-1. A-10A ANALYTICAL LOADING SPECTRUM
(NORMALIZED ABOUT 100 KSI)

STEP	σ_{max} (Ksi)	σ_{min} (Ksi)	CYCLES	STEP	σ_{max} (Ksi)	σ_{min} (Ksi)	CYCLES
1	94.01	-65.79	1.00	2	100.00	-65.01	4.00
3	46.00	-6.88	1.00	4	90.01	-8.99	1.00
5	100.00	-10.01	1.00	6	66.00	-3.29	1.00
7	78.00	-3.90	1.00	8	83.99	-4.19	1.00
9	94.01	-4.68	4.00	10	100.00	-5.00	2.00
11	80.00	0.00	4.00	12	82.00	0.00	1.00
13	83.00	0.00	3.00	14	90.01	0.00	12.00
15	94.01	0.00	9.00	16	100.00	0.00	1.50
17	46.00	2.28	2.50	18	48.00	2.40	2.00
19	50.00	2.48	5.00	20	51.99	2.60	3.00
21	54.02	2.69	1.00	22	56.01	2.80	1.00
23	58.01	2.89	1.00	24	60.01	3.00	6.00
25	62.00	3.09	2.00	26	64.00	3.21	1.00
27	66.00	3.29	11.00	28	72.02	3.58	6.00
29	74.01	3.70	6.00	30	76.01	3.79	2.00
31	80.00	3.99	4.00	32	82.00	4.10	3.00
33	83.99	4.19	2.00	34	88.02	4.39	1.00
35	90.01	4.51	18.00	36	94.01	4.68	11.00
37	100.00	5.00	0.50	38	30.06	3.00	1.00
39	37.99	3.79	2.00	40	40.01	3.99	1.00
41	60.01	5.99	12.00	42	62.00	6.19	4.00
43	64.00	6.39	9.00	44	66.00	6.59	21.00
45	67.99	6.80	4.00	46	70.02	7.00	1.00
47	72.02	6.20	18.00	48	74.01	7.40	7.00
49	76.01	7.61	4.00	50	78.00	7.81	1.00
51	80.00	8.01	24.50	52	82.00	8.18	6.00
53	83.99	8.39	32.00	54	88.02	8.79	2.00
55	90.01	8.99	3.00	56	94.01	9.40	1.00
57	40.01	5.00	1.00	58	46.00	6.88	10.00
59	48.00	7.20	4.00	60	50.00	7.49	7.00
61	54.02	8.10	4.00	62	56.01	8.39	14.00
63	58.01	8.70	5.00	64	60.01	8.99	3.00
65	62.00	9.28	4.00	66	64.00	9.60	4.00
67	66.00	9.89	18.00	68	67.99	10.21	1.00
69	70.02	10.50	2.00	70	72.02	10.79	11.00
71	74.01	11.11	10.00	72	76.01	11.40	8.00
73	78.00	11.60	1.00	74	80.00	12.00	11.50
75	82.00	12.29	1.00	76	83.99	12.61	7.00
77	94.01	14.09	1.00	78	16.00	3.21	5.00
79	19.99	3.99	1.00	80	35.99	7.20	1.00
81	37.99	7.60	2.00	82	40.01	8.01	4.00
83	42.01	8.39	2.00	84	50.00	10.01	12.00
85	51.99	10.38	8.00	86	54.22	10.79	6.00
87	56.01	11.19	22.00	88	58.01	11.60	17.00
89	60.01	12.00	58.00	90	62.00	12.41	24.00
91	64.00	12.78	11.00	92	66.00	13.19	38.00
93	67.99	13.60	6.00	94	70.02	14.00	5.00
95	72.02	14.41	28.00	96	80.00	16.00	28.00
97	82.00	16.40	4.00	98	83.99	16.81	9.00
99	90.01	17.99	10.00	100	94.01	18.80	1.00
101	30.00	7.49	2.00	102	33.99	8.50	2.00

TABLE A-1. A-10A ANALYTICAL LOADING SPECTRUM (Continued)
(NORMALIZED ABOUT 100 KSI)

STEP	σ_{max} (Ksi)	σ_{min} (Ksi)	CYCLES	STEP	σ_{max} (Ksi)	σ_{min} (Ksi)	CYCLES
103	35.99	8.99	2.00	104	37.99	9.49	1.00
105	40.01	10.01	2.00	106	42.01	10.50	3.00
107	46.00	11.48	8.50	108	48.00	12.00	27.00
109	50.00	12.50	134.00	110	51.99	12.99	6.00
111	54.02	13.51	13.00	112	56.01	14.00	111.00
113	60.01	14.98	1.00	114	62.00	15.50	3.00
115	64.00	16.00	1.00	116	66.00	16.49	89.00
117	67.99	17.01	20.00	118	70.02	17.50	3.00
119	62.02	17.99	61.00	120	74.01	18.49	17.00
121	76.01	19.01	13.00	122	80.00	19.99	5.00
123	83.99	21.00	3.00	124	12.00	3.58	1.00
125	14.00	4.19	2.00	126	33.99	10.21	1.00
127	35.99	10.79	5.00	128	37.99	11.40	32.00
129	42.01	12.61	23.00	130	44.01	13.19	17.00
131	46.00	13.80	111.00	132	48.00	14.41	4.00
133	50.00	14.98	1.00	134	51.99	15.59	6.00
135	54.02	16.20	1.00	136	56.01	16.81	209.00
137	58.01	17.39	43.00	138	60.01	17.99	134.00
139	62.00	18.60	13.00	140	64.00	19.21	32.00
141	67.99	20.39	5.00	142	32.00	11.19	7.00
143	33.99	11.89	49.00	144	35.99	12.61	6.00
145	37.99	13.31	10.00	146	40.01	14.99	258.00
147	42.01	14.69	3.00	148	46.00	16.08	14.00
149	48.00	16.81	8.00	150	50.00	17.50	402.00
151	51.99	18.20	1.00	152	54.02	18.89	65.00
153	58.01	20.31	11.00	154	21.99	8.79	1.00
155	30.00	12.00	94.00	156	33.99	13.60	19.00
157	35.99	14.41	434.00	158	37.99	15.19	19.00
159	40.01	16.00	1.00	160	42.01	16.81	19.00
161	44.01	17.59	2.00	162	46.00	18.40	494.00
163	48.00	19.21	92.00	164	51.99	20.80	4.00
165	54.02	21.61	19.00	166	17.99	8.10	2.00
167	19.99	8.99	19.00	168	26.01	11.69	238.00
169	30.00	13.51	534.00	170	33.99	15.30	1.00
171	35.99	16.20	54.00	172	37.99	17.10	5.00
173	40.01	17.99	716.00	174	42.01	18.89	130.00
175	46.00	20.68	11.00	176	48.00	21.61	36.00
177	21.99	10.99	8.00	178	32.00	16.00	5.00
179	33.99	17.01	31.00	180	35.99	17.99	363.00
181	37.99	19.01	93.00	182	42.01	21.00	63.00
183	21.99	12.09	3.00	184	30.00	16.49	37.00
185	33.99	18.69	278.00	186	35.99	19.79	128.00
187	37.00	20.89	38.00	188	19.99	12.00	3.00
189	32.00	19.21	1.00	190	19.99	12.99	7.00
191	21.99	14.29	67.00	192	17.99	12.61	12.00
193	19.99	14.00	212.50	194	16.00	12.00	2.00
195	21.99	16.49	1.00	196	14.00	11.89	1.00
197	16.00	13.60	1.00	198	19.99	17.01	17.00
199	21.99	18.69	293.00	200	19.99	17.99	7.00
201	14.00	13.31	22.00	202	17.99	17.10	4.00
203	19.99	19.01	52.00	204	21.99	20.89	2.00

TABLE A-2. AMAVS ANALYTICAL LOADING SPECTRUM
(NORMALIZED ABOUT 100 KSI)

STEP	σ_{\max} (KSI)	σ_{\min} (KSI)	CYCLES	STEP	σ_{\max} (KSI)	σ_{\min} (KSI)	CYCLES
1	1.30	-12.00	10.00	2	1.30	-11.00	10.00
3	2.90	-15.00	100.00	4	3.00	-14.00	10.00
5	2.50	-11.00	100.00	6	1.60	-7.00	210.00
7	2.70	-10.00	10.00	8	1.70	-6.00	10.00
9	3.20	-11.00	1.00	10	1.70	-5.00	1.00
11	2.90	-8.00	1.00	12	5.20	-11.00	110.00
13	8.10	-17.00	100.00	14	76.70	-22.00	90.00
15	87.30	-22.00	9.00	16	46.00	-11.00	90.00
17	100.00	-22.00	1.00	18	45.00	-7.00	10.00
19	66.80	-11.00	110.00	20	42.30	1.10	1.00
21	50.10	1.40	10.00	22	27.60	1.10	1.00
23	50.00	5.60	10.00	24	74.50	8.60	1.00
25	35.20	4.90	10.00	26	39.10	5.50	100.00
27	88.10	12.60	2.00	28	24.80	3.80	10.00
29	98.90	14.70	1.00	30	40.20	6.60	100.00
31	78.60	12.50	1.00	32	83.10	13.20	1.00
33	92.10	15.10	1.00	34	78.90	14.50	1.00
35	85.50	15.10	1.00	36	86.60	15.70	1.00
37	71.00	13.70	1.00	38	25.70	5.10	10.00
39	36.60	7.30	1.00	40	61.60	12.10	1.00
41	65.50	14.70	10.00	42	47.80	11.10	100.00
43	50.90	11.60	100.00	44	38.80	9.70	1.00
45	22.50	5.80	100.00	46	45.80	12.10	1100.00
47	61.40	15.80	1.00	48	47.80	12.80	600.00
49	69.50	18.70	10.00	50	75.70	20.70	10.00
51	83.30	22.50	10.00	52	88.70	23.90	10.00
53	77.60	21.40	10.00	54	33.60	9.90	10.00
55	57.50	16.60	100.00	56	63.70	18.60	10.00
57	78.10	22.90	10.00	58	78.10	23.00	10.00
59	33.80	10.10	1.00	60	42.20	12.70	2900.00
61	42.00	13.20	10.00	62	23.00	7.70	100.00
63	61.50	20.50	100.00	64	70.10	23.20	10.00
65	28.40	9.60	100.00	66	66.80	23.40	10.00
67	35.70	12.80	10.00	68	38.20	13.80	100.00
69	42.40	15.40	800.00	70	66.80	24.00	90.00
71	73.90	26.70	10.00	72	87.30	33.30	1.00
73	61.50	24.00	10.00	74	61.50	24.10	100.00
75	66.80	26.10	200.00	76	74.50	29.20	100.00
77	30.90	12.30	100.00	78	79.40	31.80	100.00
79	38.90	16.10	100.00	80	69.40	28.20	100.00
81	56.40	23.90	100.00	82	52.00	23.00	100.00
83	69.40	30.30	200.00	84	29.60	13.40	1.00
85	33.30	15.00	100.00	86	54.20	24.20	100.00
87	63.10	29.60	100.00	88	51.60	24.70	1.00
89	20.80	10.10	199.00	90	29.00	14.30	10.00
91	55.50	28.70	1.00	92	27.90	15.30	100.00
93	76.70	42.30	10.00	94	48.90	27.30	10.00
95	64.40	36.20	100.00	96	44.00	27.00	100.00
97	52.40	31.80	10.00	98	46.70	29.60	100.00
99	52.00	35.10	100.00	100	49.70	34.50	100.00
101	50.30	34.90	100.00	102	59.40	41.20	100.00
103	51.20	36.40	100.00	104	31.80	23.60	100.00
105	52.60	38.70	100.00	106	68.30	52.60	100.00
107	64.40	50.30	100.00	108	26.00	21.00	100.00
109	63.90	52.00	100.00	110	57.00	46.60	100.00
111	61.60	51.20	200.00	112	2.60	2.50	1.00